O_2 AND ROS METABOLISMS IN PHOTOSYNTHETIC ORGANISMS

EDITED BY: Chikahiro Miyake, Kentaro Ifuku, Anja Liszkay, Ko Noguchi, Mikko Tikkanen and Yuji Suzuki

PUBLISHED IN: Frontiers in Plant Science

frontiers Research Topics

frontiers

ISSN 1664-8714
ISBN 978-2-88966-363-7
DOI 10.3389/978-2-88966-363-7

About Frontiers

Frontiers is more than just an open-access publisher of scholarly articles: it is a pioneering approach to the world of academia, radically improving the way scholarly research is managed. The grand vision of Frontiers is a world where all people have an equal opportunity to seek, share and generate knowledge. Frontiers provides immediate and permanent online open access to all its publications, but this alone is not enough to realize our grand goals.

Frontiers Journal Series

The Frontiers Journal Series is a multi-tier and interdisciplinary set of open-access, online journals, promising a paradigm shift from the current review, selection and dissemination processes in academic publishing. All Frontiers journals are driven by researchers for researchers; therefore, they constitute a service to the scholarly community. At the same time, the Frontiers Journal Series operates on a revolutionary invention, the tiered publishing system, initially addressing specific communities of scholars, and gradually climbing up to broader public understanding, thus serving the interests of the lay society, too.

Dedication to Quality

Each Frontiers article is a landmark of the highest quality, thanks to genuinely collaborative interactions between authors and review editors, who include some of the world's best academicians. Research must be certified by peers before entering a stream of knowledge that may eventually reach the public - and shape society; therefore, Frontiers only applies the most rigorous and unbiased reviews.
Frontiers revolutionizes research publishing by freely delivering the most outstanding research, evaluated with no bias from both the academic and social point of view. By applying the most advanced information technologies, Frontiers is catapulting scholarly publishing into a new generation.

What are Frontiers Research Topics?

Frontiers Research Topics are very popular trademarks of the Frontiers Journals Series: they are collections of at least ten articles, all centered on a particular subject. With their unique mix of varied contributions from Original Research to Review Articles, Frontiers Research Topics unify the most influential researchers, the latest key findings and historical advances in a hot research area! Find out more on how to host your own Frontiers Research Topic or contribute to one as an author by contacting the Frontiers Editorial Office: researchtopics@frontiersin.org

O_2 AND ROS METABOLISMS IN PHOTOSYNTHETIC ORGANISMS

Topic Editors:
Chikahiro Miyake, Kobe University, Japan
Kentaro Ifuku, Kyoto University, Japan
Anja Liszkay, UMR9198 Institut de Biologie Intégrative de la Cellule (I2BC), France
Ko Noguchi, Tokyo University of Pharmacy and Life Sciences, Japan
Mikko Tikkanen, University of Turku, Finland
Yuji Suzuki, Iwate University, Japan

Citation: Miyake, C., Ifuku, K., Liszkay, A., Noguchi, K., Tikkanen, M., Suzuki, Y., eds. (2021). O_2 and ROS Metabolisms in Photosynthetic Organisms. Lausanne: Frontiers Media SA. doi: 10.3389/978-2-88966-363-7

Table of Contents

frontiers in Plant Science

EDITORIAL
published: 23 November 2020
doi: 10.3389/fpls.2020.618550

Editorial: O_2 and ROS Metabolisms in Photosynthetic Organisms

Kentaro Ifuku[1]*, *Anja Krieger-Liszkay*[2]*, *Ko Noguchi*[3]* and *Yuji Suzuki*[4]*

[1] Graduate School of Biostudies, Kyoto University, Kyoto, Japan, [2] Université Paris-Saclay, CEA, CNRS, Institute for Integrative Biology of the Cell (I2BC), Gif-sur-Yvette, France, [3] School of Life Sciences, Tokyo University of Pharmacy and Life Sciences, Tokyo, Japan, [4] Faculty of Agriculture, Iwate University, Morioka, Japan

Keywords: photosynthesis, reactive oxygen species, electron transport (photosynthetic), redox regulation, oxidative stress

Editorial on the Research Topic

O_2 and ROS Metabolisms in Photosynthetic Organisms

INTRODUCTION

In photosynthesis, water is oxidized to O_2, producing electrons to reduce CO_2. During this process, reactive oxygen species (ROS) can be concomitantly produced. ROS cause oxidative damages if not scavenged appropriately. ROS also function as signaling molecules that change gene expression to alleviate stress conditions, reconstruct cellular functions, and allow acclimation to diverse environmental conditions. This Research Topic "O_2 and ROS Metabolisms in Photosynthetic Organisms" comprises biochemical and molecular studies on mechanisms that suppress ROS production in photosynthetic organisms, as well as effects of ROS on photosynthesis in various species:

OPTIMIZATION OF ATP SYNTHASE C-RINGS FOR OXYGENIC PHOTOSYNTHESIS

Davis and Kramer examined the potential consequences of an altered c-ring stoichiometry of the chloroplast ATP synthase using their computational model of the photosynthetic light reactions, to which they added the possibility to vary the number of c-rings and thereby the *pmf* requirements to synthesize ATP. According to their results, the current c-ring stoichiometry is optimal; it minimizes detrimental side reactions producing ROS and allows high photosynthetic electron transport under a variety of environmental conditions.

IDENTIFICATION OF THE OPTIMAL LIGHT HARVESTING ANTENNA SIZE FOR HIGH-LIGHT STRESS MITIGATION IN PLANTS

Wu et al. evaluated the effect of light growth intensities on mutant Camelina plants with diminished photosystem II (PSII) antenna sizes. Based on fluorescence yields, ROS and lipid peroxidation measurements, and biomass quantifications, the authors conclude that wild-type Camelina plants are well-suited for low light growth, whilst a reduction in PSII antenna size is beneficial at higher light intensities.

OPEN ACCESS

Edited and reviewed by:
Nicolas Rouhier,
Université de Lorraine, France

***Correspondence:**
Kentaro Ifuku
ifuku.kentaro.2m@kyoto-u.ac.jp
Anja Krieger-Liszkay
anja.liszkay@i2bc.paris-saclay.fr
Ko Noguchi
knoguchi@toyaku.ac.jp
Yuji Suzuki
ysuzuki@iwate-u.ac.jp

Specialty section:
This article was submitted to Plant Physiology, a section of the journal Frontiers in Plant Science

Received: *17 October 2020*
Accepted: *04 November 2020*
Published: *23 November 2020*

Citation:
Ifuku K, Krieger-Liszkay A, Noguchi K and Suzuki Y (2020) Editorial: O_2 and ROS Metabolisms in Photosynthetic Organisms. Front. Plant Sci. 11:618550. doi: 10.3389/fpls.2020.618550

NEW LIGHT ON CHLOROPLAST REDOX REGULATION: MOLECULAR MECHANISM OF PROTEIN THIOL OXIDATION

Yoshida et al. give a comprehensive and critical view of the light/dark redox regulation in chloroplasts. They highlight the recent evidence for regulatory disulfide bonds in oxidative pathways in the dark–a regulatory mechanism that has remained elusive since the discovery of the plant thioredoxin system. The newly uncovered "dark side" of chloroplast redox regulation provides an insight into how plants rest their photosynthetic activity at night.

SINGLET OXYGEN METABOLISM: FROM GENESIS TO SIGNALING

Dogra and Kim reviewed two distinct spatially separated $^1O_2$ sensors and signaling pathways. The first pathway is triggered by oxidation of β-carotene or reactive electrophile species derived from lipids generated by $^1O_2$ produced in PSII located in the grana region, while the second pathway involves the $^1O_2$ sensor EXECUTER1 (EX1) protein located in non-appressed margins. They hypothesize a $^1O_2$ generation site, likely tetrapyrroles, in margin PSII undergoing degradation after photoinhibition. EX1 is associated with the protease FtsH, and its proteolysis after oxidation is regarded as the essential step in initiating $^1O_2$ signaling.

MINIMIZING AN ELECTRON FLOW TO MOLECULAR OXYGEN IN PHOTOSYNTHETIC TRANSFER CHAIN: AN EVOLUTIONARY VIEW

Kozuleva et al. describe in a comprehensive review the different sites of O_2 reduction to the superoxide anion radical in respect to their importance with photosystem I (PSI) as the main site followed by the reduction of O_2 by semiquinone in the plastoquinone pool. Thermodynamic and kinetics considerations are taken into account. Homologies and differences between anoxygenic and oxygenic photosynthetic complexes are discussed.

PHOTORESPIRATION COUPLED WITH CO_2 ASSIMILATION PROTECTS PHOTOSYSTEM I FROM PHOTOINHIBITION UNDER MODERATE PEG-INDUCED OSMOTIC STRESS IN RICE

Photorespiration coupled with CO_2 assimilation is thought to be a defense system against abiotic stress. Wada et al. showed the importance of photorespiration for the protection of PSI under osmotic stress, using transgenic rice plants with altered Rubisco content. Rubisco is thought to be the rate-limiting factor for both photorespiration and CO_2 assimilation. Their results may contribute to improve abiotic stress tolerance.

PRIMARY METABOLITE RESPONSES TO OXIDATIVE STRESS IN EARLY-SENESCING AND PARAQUAT RESISTANT *Arabidopsis thaliana rcd1* (RADICAL-INDUCED CELL DEATH1)

The mutation of radical-induced cell death (RCD1) causes a resistant phenotype against methylviologen (MV), a herbicide generating ROS. *rcd1* mutant exerts tolerance to MV in an unknown way. Sipari et al. extensively analyzed metabolites by LC-MS and concluded that changes in primary metabolites cause the early senescing and MV-resistant *rcd1* phenotype. These findings will help to understand the ROS attenuation mechanism in plants, both in normal and stress conditions.

EFFICIENT PHOTOSYNTHETIC FUNCTIONING OF *Arabidopsis thaliana* THROUGH ELECTRON DISSIPATION IN CHLOROPLASTS AND ELECTRON EXPORT TO MITOCHONDRIA UNDER AMMONIUM NUTRITION

Long-term ammonium nutrition often disturbs growth and photosynthesis due to limited reductant utilization for ammonium assimilation. Podgórska et al. revealed that photosynthetic activity is supported by upregulation of cyclic electron flow around PSI, the plastid terminal oxidase, and the export of excess reductants from chloroplasts under long-term ammonium nutrition. Their results are important for understanding responses of photosynthetic regulation to environmental stresses.

A COMMONLY USED PHOTOSYNTHETIC INHIBITOR FAILS TO BLOCK ELECTRON FLOW TO PHOTOSYSTEM I IN INTACT SYSTEMS

Pharmacological approaches are commonly used to determine the sites of ROS generation by photosynthetic electron transport. Fitzpatrick et al. reported based on P700 absorption and MIMS measurements that the cytochrome b_6f complex inhibitor 2,4-dinitrophenylether of iodonitrothymol (DNP-INT) is unable to completely block photosynthetic electron transport. These results ask for independent confirmation since DNP-INT is used as an alternative to 2,5-dibromo-6-isopropyl-3-methyl-1,4-benzoquinone (DBMIB), especially in spin-trapping

assays used for ROS determination where DBMIB is known to interfere.

ATMOSPHERIC CO_2 CONCENTRATION AND N AVAILABILITY AFFECT THE BALANCE OF THE TWO PHOTOSYSTEMS IN MATURE LEAVES OF RICE PLANTS GROWN AT A FREE-AIR CO_2 ENRICHMENT SITE

Increasing atmospheric CO_2 concentration ($[CO_2]$) intensively affects photosynthesis and yield. The responses of photosynthesis to elevated $[CO_2]$ depends on nitrogen (N) availability. Ozaki et al. showed that elevated $[CO_2]$ and low N changed the balance of the two photosystems in leaves grown at a free-air CO_2 enrichment experimental facility. This change may induce cyclic electron flow, increasing non-photochemical quenching to avoid photoinhibition.

AUTHOR CONTRIBUTIONS

All authors contributed to the final manuscript.

Conflict of Interest: The authors declare that the research was conducted in the absence of any commercial or financial relationships that could be construed as a potential conflict of interest.

frontiers in Plant Science

MINI REVIEW
published: 22 November 2019
doi: 10.3389/fpls.2019.01534

New Light on Chloroplast Redox Regulation: Molecular Mechanism of Protein Thiol Oxidation

Keisuke Yoshida, Yuichi Yokochi and Toru Hisabori*

Laboratory for Chemistry and Life Science, Institute of Innovative Research, Tokyo Institute of Technology, Yokohama, Japan

Thiol-based redox regulation is a posttranslational protein modification that plays a key role in adjusting chloroplast functions in response to changing light conditions. Redox-sensitive target proteins are reduced upon illumination, which turns on (or off in a certain case) their enzyme activities. A redox cascade *via* ferredoxin, ferredoxin-thioredoxin reductase, and thioredoxin has been classically recognized as the key system for transmitting the light-induced reductive signal to target proteins. By contrast, the molecular mechanism underlying target protein oxidation, which is observed during light to dark transitions, remains undetermined over the past several decades. Recently, the factors and pathways for protein thiol oxidation in chloroplasts have been reported, finally shedding light on this long-standing issue. We identified thioredoxin-like2 as one of the protein-oxidation factors in chloroplasts. This protein is characterized by its higher redox potential than that of canonical thioredoxin, that is more favorable for target protein oxidation. Furthermore, 2-Cys peroxiredoxin and hydrogen peroxide are also involved in the overall protein-oxidation machinery. Here we summarize the newly uncovered "dark side" of chloroplast redox regulation, giving an insight into how plants rest their photosynthetic activity at night.

Keywords: chloroplast, 2-Cys peroxiredoxin, hydrogen peroxide, oxidation, redox regulation, thioredoxin, thioredoxin-like2

OPEN ACCESS

Edited by:
Kentaro Ifuku,
Kyoto University, Japan

Reviewed by:
Jean-Pierre Jacquot,
Université de Lorraine, France
Mirko Zaffagnini,
University of Bologna, Italy

****Correspondence:***
Keisuke Yoshida
yoshida.k.ao@m.titech.ac.jp

Specialty section:
This article was submitted to Plant Physiology, a section of the journal Frontiers in Plant Science

Received: *24 September 2019*
Accepted: *01 November 2019*
Published: *22 November 2019*

Citation:
Yoshida K, Yokochi Y and Hisabori T (2019) New Light on Chloroplast Redox Regulation: Molecular Mechanism of Protein Thiol Oxidation. Front. Plant Sci. 10:1534. doi: 10.3389/fpls.2019.01534

INTRODUCTION

Sunlight is the primary energy for photosynthesis, but is also the most variable environmental cue in plant habitats. It is thus critical for plant growth and maintenance to regulate photosynthesis in flexible and suitable ways. In fact, as the site for photosynthesis, chloroplasts have acquired multiple adaptive strategies to light. Accumulating research has expanded our understanding of how chloroplasts regulate their own physiology under continuously fluctuating light environments (Niyogi, 2000; Takahashi and Badger, 2011; Yamori, 2016), but further studies are needed for a better understanding.

Thiol-based redox regulation is one of the posttranslational protein modifications. The most well-known example is the dithiol/disulfide interconversion of a redox-active Cys pair. A key factor for the redox regulation is thioredoxin (Trx), a small soluble protein first discovered in *Escherichia coli* and now known to occur in all organisms (Laurent et al., 1964; Holmgren, 1985; Jacquot et al., 1997). Trx has a conserved amino acid sequence of WCGPC at its active site. Using a Cys pair in this motif, Trx mediates the dithiol/disulfide exchange reaction with its target proteins and thereby transmits reducing power to the targets. In addition to regulating the enzyme activity, Trx-derived reducing power can be used for the catalytic cycle itself by some proteins (*e.g.*, peroxiredoxin (Prx), Dietz, 2011).

As well as other organisms and subcellular compartments, plant chloroplasts commonly have a redox-regulatory system; however, its mode of action is critically different from that of others. Namely, chloroplast redox regulation is coupled with light. The electron transport chain (ETC) in the thylakoid membrane converts absorbed light energy into reducing power, a part of which drives the redox-regulatory system in chloroplasts. In this system, reducing power pooled by ferredoxin (Fd), a small [2Fe-2S] electron carrier protein (Arnon, 1988), is transferred to Trx *via* Fd-Trx reductase (FTR). FTR is a [4Fe-4S] cluster-containing heterodimeric protein that serves as the signaling hub to link the ETC to Trx (Dai et al., 2004). Trx in the reduced state, in turn, provides reducing power to the redox-sensitive target proteins in chloroplasts. As the example of redox-regulated proteins in chloroplasts, four Calvin-Benson cycle (CBC) enzymes (glyceraldehyde-3-phosphate dehydrogenase (GAPDH), fructose-1,6-bisphosphatase (FBPase), sedoheptulose-1,7-bisphosphatase (SBPase), and phosphoribulokinase (PRK)) are classically known (Michelet et al., 2013). Because these enzymes are activated upon reduction, a redox cascade composed by Fd, FTR, and Trx makes it possible to turn on CBC in a light-dependent manner (Buchanan, 1980; Buchanan et al., 2002). Our understanding of CBC redox regulation is even now growing. For example, its molecular details and evolutionary traits have been further elucidated by recent structural studies (FBPase and SBPase from *Physcomitrella patens*, Gütle et al., 2016; PRK from *Chlamydononas reinhardtii* and *Arabidopsis thaliana*, Gurrieri et al., 2019).

The Fd/FTR/Trx-based regulatory pathway was discovered by Buchanan and colleagues in 1970s (Buchanan et al., 1967; Buchanan et al., 1971; Buchanan and Wolosiuk, 1976; Schürmann et al., 1976; Wolosiuk and Buchanan, 1977). Since then, it has been firmly established as the hallmark of chloroplast redox regulation (Buchanan, 1980; Buchanan et al., 2002). Although this pathway was characterized mainly based on *in vitro* experiments, it became evident that chloroplast redox regulation works dynamically in living plants; we directly observed that several redox-regulated proteins are indeed shifted from the oxidized to reduced forms when plants are exposed to light (Konno et al., 2012; Yoshida et al., 2014). These studies also let us notice an important aspect with regard to the diurnal redox response. Once reduced proteins were gradually reoxidized along with the decrease in light intensity at dusk, and finally returned to the fully oxidized state at night. It is reasonable to consider that some oxidizing force must be present at this light to dark transition phase; however, its identity or nature remains elusive. Some candidate factors for protein thiol oxidation have been suggested, including molecular oxygen, reactive oxygen species, oxidized glutathione, or oxidized Trx (Wolosiuk and Buchanan, 1977; Leegood and Walker, 1980; Scheibe and Anderson, 1981), but there has been little consensus on this issue. It has been therefore a long-standing gap in our understanding of chloroplast redox regulation.

We have recently come to a major turning point in this issue. Recent biochemical and physiological studies have identified the factors and pathways supporting the protein-oxidation process in chloroplasts (Ojeda et al., 2018; Vaseghi et al., 2018; Yoshida et al., 2018). These findings provide novel mechanistic insights into the regulation of photosynthesis; that is, the dark deactivation of chloroplast enzymes (Jacquot, 2018). Here we briefly highlight this breakthrough in the redox field.

GENETIC AND FUNCTIONAL DIVERSITY OF REDOX-REGULATORY FACTOR PROTEINS IN CHLOROPLASTS

In addition to the light/dark response described above, the emergence of multiple Trx isoforms is considered as another key feature of the redox-regulatory system in plant chloroplasts. In the case of mammalian cells, the cytoplasm and mitochondria each contain only one Trx isoform (Spyrou et al., 1997). By contrast, plastidial Trx in a model plant *Arabidopsis thaliana* is encoded by as many as 10 nuclear genes, although some of these have limited expression in photosynthetic tissues (Belin et al., 2015; Okegawa and Motohashi, 2015; Yoshida et al., 2015). Furthermore, several proteins that have Trx-like amino acid sequence (CXXC) and can (potentially) mediate redox regulation are also found in chloroplasts. This multiplicity of redox-regulatory factor proteins is probably important for plants in flexibly regulating diverse chloroplast functions under changing light conditions.

Chloroplast Trx isoforms are phylogenically categorized into five subtypes (*f*-, *m*-, *x*-, *y*-, and *z*-type, **Figure 1**) (Lemaire et al., 2007; Serrato et al., 2013). They have different molecular characteristics including the redox potential and protein surface charge, which in turn confers different functions on each of Trx subtypes (Collin et al., 2003; Yoshida et al., 2015; Lemaire et al., 2018). Another well-studied example of redox-regulatory factors is the NADPH-Trx reductase C (NTRC), a unique NTR with a joint Trx domain (Cejudo et al., 2012). NTRC shows largely different redox-regulatory properties from those of Trx subtypes (Serrato et al., 2004; Pérez-Ruiz et al., 2006; Michalska et al., 2009; Yoshida and Hisabori, 2016). It was recently suggested that NTRC plays a pivotal role in keeping redox balance of 2-Cys Prx (2CP) in chloroplasts, which is critical for plant growth (Pérez-Ruiz et al., 2017; see below for details). The functional diversity of redox-regulatory factors, mainly the five Trx subtypes and NTRC, has been described in detail in recent reviews (Geigenberger et al., 2017; Cejudo et al., 2019; Nikkanen and Rintamäki, 2019; Yoshida and Hisabori, 2019; Zaffagnini et al., 2019). In the following section, we focus on the factor directly involved in protein thiol oxidation in chloroplasts.

IDENTIFICATION OF THIOREDOXIN-LIKE2 AS PROTEIN-OXIDATION FACTOR IN CHLOROPLASTS

Whereas multiple candidate proteins for the redox-regulatory factor have been identified from genomic and phylogenic studies (Meyer et al., 2006; Chibani et al., 2009), their molecular functions remain largely unclear. We biochemically characterized the function of one of such proteins, Trx-like2 (TrxL2) from *Arabidopsis*, allowing us to realize that this protein acts as a previously unidentified protein-oxidation factor in chloroplasts (**Figure 1**) (Yoshida et al., 2018). TrxL2 has an atypical Trx active site motif of WCRKC, and two isoforms (TrxL2.1 and TrxL2.2)

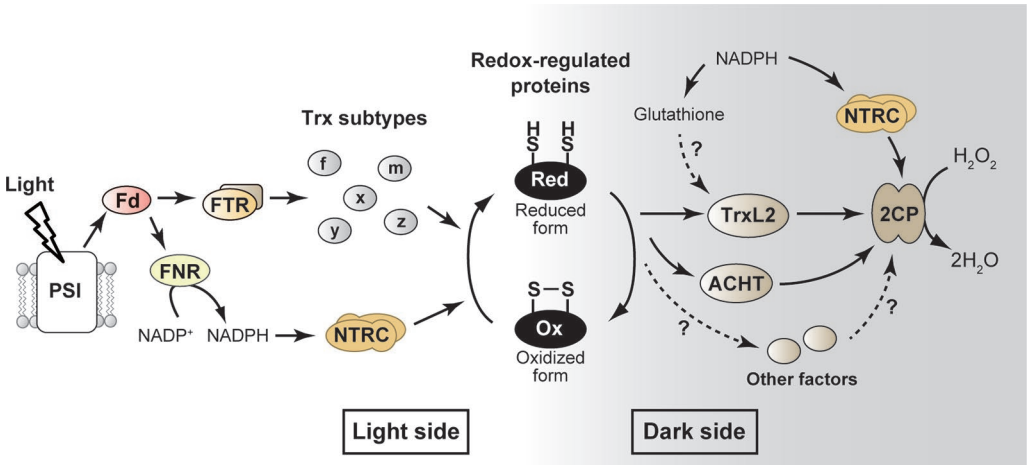

FIGURE 1 | Simplified model for the redox-regulatory system in chloroplasts. The well-studied "light side" and newly emerging "dark side" are shown. Arrows indicate the flow of reducing power. See text for details. ACHT, atypical Cys His-rich thioredoxin; 2CP, 2-Cys peroxiredoxin; Fd, ferredoxin; FNR, ferredoxin-$NADP^+$ reductase; FTR, ferredoxin-thioredoxin reductase; H_2O_2, hydrogen peroxide; NTRC, NADPH-thioredoxin reductase C; PSI, photosystem I; Trx, thioredoxin; TrxL2, thioredoxin-like2.

are present in *Arabidopsis* chloroplasts. Both TrxL2 isoforms had the ability to transmit reducing power, but their midpoint redox potentials were higher (less negative) than those of typical Trx subtypes (e.g., TrxL2.1, –258 mV; TrxL2.2, –245 mV; Trx-*f*1, –321 mV; Trx-*m*1, –335 mV at pH 7.5) (Yoshida et al., 2015; Yoshida and Hisabori, 2017; Yoshida et al., 2018). Possibly in connection with this fact, TrxL2 did efficiently oxidize several redox-regulated proteins in chloroplasts, including FBPase, SBPase, and Rubisco activase (RCA). By contrast, TrxL2 failed to reduce these proteins; it can be regarded, therefore, that TrxL2 is capable of mediating redox reactions in the opposite direction of typical Trx.

Just before our publication on *Arabidopsis* TrxL2 (Yoshida et al., 2018), the crystal structure of poplar TrxL2 was determined (Chibani et al., 2018). This achievement is helpful to understand the reaction mechanisms of TrxL2 at a molecular level. Overall conformation of TrxL2 is similar to that of the canonical Trx (Jeng et al., 1994; Weichsel et al., 1996; Capitani et al., 2000). In the oxidized state, TrxL2 forms a disulfide bond in the WCRKC motif, suggesting that its basic catalytic mode (i.e., catalysis *via* dithiol/disulfide conversion) is shared between Trx and TrxL2. One different point is that, due to the precluding action of Arg and Lys residues in the WCRKC motif, TrxL2 is unlikely to receive reducing power from FTR. In accordance with this structure-based implication, it was actually shown that TrxL2 cannot be reduced by FTR (Chibani et al., 2012; Yoshida et al., 2018). In combination with the high redox potential, these two positively-charged amino acid residues appear largely responsible for the functional specificity of TrxL2.

It is still ambiguous whether TrxL2 has a crosstalk with redox-related low molecular weight compounds. Chibani et al. (2012) suggested that glutathione serves as a reductant for poplar TrxL2. They also solved the structure of poplar TrxL2 in the glutathione-adducted form (Chibani et al., 2018). However, the glutathione-binding site was another Cys residue located outside the redox-active WCRKC motif. Such a Cys residue is not ubiquitously conserved in plant orthologs; therefore, there may be little generality of the TrxL2-glutathione interaction. We also observed glutathione-dependent reduction of *Arabidopsis* TrxL2, but its efficiency was limited (Yoshida et al., 2018). Furthermore, there is no evidence for the association of glutathione with TrxL2 *in vivo*. Thus, further studies are needed to clarify this possibility (**Figure 1**).

INVOLVEMENT OF 2-CYS PEROXIREDOXIN AND HYDROGEN PEROXIDE IN PROTEIN-OXIDATION PROCESS

Because *in vivo* protein levels of TrxL2 are not so high, TrxL2 must transfer reducing power to some molecule to keep an efficient protein-oxidation process (Yoshida et al., 2018). Screening for TrxL2-interacting partners allowed us to identify several chloroplast proteins that can physically bind to TrxL2. However, TrxL2 was unable to transfer reducing power to most of these proteins (but it could oxidize some of them). An exception was found in 2CP, which is the most abundant Prx in chloroplasts (Peltier et al., 2006) and serves to detoxify hydrogen peroxide (H_2O_2), a byproduct of photosynthesis (Asada, 1999). TrxL2 showed high activity for reducing 2CP, with an efficiency that greatly surpassed that of typical Trx (Yoshida et al., 2018; Yoshida et al., 2019). Given the high affinity of 2CP for H_2O_2 (Bernier-Villamor et al., 2004), it seems feasible that 2CP efficiently consumes the reducing power provided by TrxL2 through H_2O_2 detoxification. Using an *in vitro* reconstitution assay, we demonstrated that the TrxL2/2CP redox cascade acts as a novel system for oxidizing redox-regulated proteins and then draining reducing power to H_2O_2 (**Figure 1**). The *in vivo* function of this system was supported by the analyses of protein-oxidation dynamics in 2CP-deficient mutant plants in *Arabidopsis*; in these mutants, impaired oxidation of some chloroplast proteins (ATP synthase CF_1-γ subunit, FBPase, SBPase, and RCA) and

prolonged reduction of TrxL2 were evident during light to dark transitions (Yoshida et al., 2018).

Other research groups also suggested the involvement of 2CP and H_2O_2 in protein-oxidation process in chloroplasts (Ojeda et al., 2018; Vaseghi et al., 2018). Although different types of Prx reside in chloroplasts, a comprehensive study using several Prx-deficient mutants indicated that 2CP has a predominant role in protein-oxidation process (Ojeda et al., 2018). Notably, it was suggested that 2CP facilitates protein oxidation also in yeast (Veal et al., 2004) and human cells (Jarvis et al., 2012; Sobotta et al., 2015; Stöcker et al., 2018). However, their protein-oxidation pathways are clearly different from those in plant chloroplasts in terms that, in yeast and human cells, 2CP directly oxidizes target proteins.

It should be noted that NTRC may indirectly participate in the protein-oxidation process in chloroplasts by modulating the redox state of 2CP (**Figure 1**). Although several potential functions of NTRC have been suggested so far, its major role remains to be clarified. It has been demonstrated that NTRC exerts high 2CP-reducing activity *in vitro* (Pérez-Ruiz et al., 2006; Yoshida and Hisabori, 2016). In relation to this, Pérez-Ruiz et al. (2017) proposed the most convincing model for NTRC function *in vivo*. They found that the growth impairment phenotype of NTRC-deficient mutants is strikingly suppressed by a decrease in 2CP content. They concluded that NTRC controls the redox balance of 2CP, which is essential for optimal redox regulation in chloroplasts. It is therefore highly possible that the input of reducing power from NTRC and the upstream NADPH pool to 2CP affects protein-oxidation rate. The protein-oxidation response was partially impaired in NTRC-overexpressing plants, strongly supporting this idea (Ojeda et al., 2018).

DUAL ROLE OF TRXL2/2CP REDOX CASCADE

Most of redox-regulated proteins in chloroplasts (e.g., CBC enzymes) are deactivated upon oxidation. Therefore, the TrxL2/2CP redox cascade plays a role in switching such proteins off in the dark. However, the TrxL2/2CP pathway has a critically different function for a certain protein, the glucose-6-phosphate dehydrogenase (G6PDH). G6PDH catalyzes the first committed step of the oxidative pentose phosphate pathway (OPPP), a primary pathway for supplying NADPH under non-photosynthetic conditions (Kruger and von Schaewen, 2003). G6PDH is a unique type of redox-regulated protein that is activated by oxidation (Scheibe et al., 1989; Née et al., 2009). Our recent biochemical study revealed that the TrxL2/2CP pathway acts as an oxidative activator of G6PDH (Yoshida et al., 2019). This finding suggests that the TrxL2/2CP pathway shifts chloroplast metabolism to the night mode by playing a dual role of downregulating CBC and upregulating OPPP.

IMPLICATIONS OF PROTEIN-OXIDIZING NETWORK IN CHLOROPLASTS

In this mini review, we have mainly described the function of TrxL2 as a protein-oxidation factor based on our findings (Yoshida et al., 2018; Yoshida et al., 2019). It is highly plausible, however, that other chloroplast proteins with a Trx-like motif catalyze the protein thiol oxidation as well (**Figure 1**). In particular, the atypical Cys His-rich Trx (ACHT; alternative name, Trx-lilium) is a strong candidate for that process. Several ACHT isoforms from *Arabidopsis* have similar molecular features as TrxL2, as reflected by the high midpoint redox potential and the high efficiency of 2CP reduction (Dangoor et al., 2009; Yokochi et al., 2019). The protein-protein interaction of ACHT with 2CP was also shown by immunoprecipitation experiments (Dangoor et al., 2012; Cerveau et al., 2016). If ACHT serves as another protein-oxidation factor, the oxidizing targets and their difference from TrxL2 should be determined. In this regard, it is worth noting that one *Arabidopsis* isoform (ACHT4) may specifically oxidize the small subunit of ADP-glucose pyrophosphorylase, a redox-regulated protein involved in starch synthesis (Eliyahu et al., 2015). Interestingly, ACHT, unlike TrxL2 (exclusively localized to the stroma; Yoshida et al., 2018), is associated to the thylakoid membrane (Dangoor et al., 2012), implying the existence of functionally and spatially diverged protein-oxidizing networks in chloroplasts.

CONCLUDING REMARKS

Recent findings of protein-oxidation machinery have led to a breakthrough in understanding the redox-regulatory system in chloroplasts. At the same time, they have opened new avenues of research to unveil its overall regulatory network (Jacquot, 2018). As discussed in the above section, our knowledge of protein-oxidation factors is still fragmentary. Further identification of such factors, followed by elucidation of their functional diversity and coordination, may allow us to draw more complicated regulatory model than currently expected. As another key challenge, spatiotemporal H_2O_2 dynamics during the protein oxidation should be clarified, as H_2O_2 is an ultimate oxidizing force for the protein-oxidation system. Finally, it remains to be answered how protein thiol oxidation in chloroplasts is important for plants. It has been hypothesized to be helpful for avoiding wasteful energy consumption during the night, but its physiological impact on plants remains experimentally unclarified. Future research addressing this issue will advance our understanding of plant strategies to survive in the dynamic environments of the field.

AUTHOR CONTRIBUTIONS

KY wrote the manuscript. YY and TH commented on the manuscript. All authors approved the manuscript.

FUNDING

This work was supported by the Japan Society for the Promotion of Science (JSPS) KAKENHI Grant Number 16H06556 (to KY and TH) and 19H03241 (to KY), the Sumitomo Foundation (180881; to KY), and the Yoshinori Ohsumi Fund for Fundamental Research (to KY).

REFERENCES

Arnon, D. I. (1988). The discovery of ferredoxin: the photosynthetic path. *Trends Biochem. Sci.* 13 (1), 30–33. doi: 10.1016/0968-0004(88)90016-3

Asada, K. (1999). The water-water cycle in chloroplasts: scavenging of active oxygens and dissipation of excess photons. *Annu. Rev. Plant Physiol. Plant Mol. Biol.* 50, 601–639. doi: 10.1146/annurev.arplant.50.1.601

Belin, C., Bashandy, T., Cela, J., Delorme-Hinoux, V., Riondet, C., and Reichheld, J. P. (2015). A comprehensive study of thiol reduction gene expression under stress conditions in *Arabidopsis thaliana*. *Plant Cell Environ.* 38 (2), 299–314. doi: 10.1111/pce.12276

Bernier-Villamor, L., Navarro, E., Sevilla, F., and Lazaro, J. J. (2004). Cloning and characterization of a 2-Cys peroxiredoxin from *Pisum sativum*. *J. Exp. Bot.* 55 (406), 2191–2199. doi: 10.1093/jxb/erh238

Buchanan, B. B., and Wolosiuk, R. A. (1976). Photosynthetic regulatory protein found in animal and bacterial cells. *Nature* 264 (5587), 669–670. doi: 10.1038/264669a0

Buchanan, B. B., Kalberer, P. P., and Arnon, D. I. (1967). Ferredoxin-activated fructose diphosphatase in isolated chloroplasts. *Biochem. Biophys. Res. Commun.* 29 (1), 74–79. doi: 10.1016/0006-291x(67)90543-8

Buchanan, B. B., Schurmann, P., and Kalberer, P. P. (1971). Ferredoxin-activated fructose diphosphatase of spinach chloroplasts. Resolution of the system, properties of the alkaline fructose diphosphatase component, and physiological significance of the ferredoxin-linked activation. *J. Biol. Chem.* 246 (19), 5952–5959.

Buchanan, B. B., Schurmann, P., Wolosiuk, R. A., and Jacquot, J. P. (2002). The ferredoxin/thioredoxin system: from discovery to molecular structures and beyond. *Photosynth Res.* 73 (1-3), 215–222. doi: 10.1023/A:1020407432008

Buchanan, B. B. (1980). Role of light in the regulation of chloroplast enzymes. *Annu. Rev. Plant Physiol.* 31, 341–374. doi: 10.1146/annurev.pp.31.060180.002013

Capitani, G., Markovic-Housley, Z., DelVal, G., Morris, M., Jansonius, J. N., and Schurmann, P. (2000). Crystal structures of two functionally different thioredoxins in spinach chloroplasts. *J. Mol. Biol.* 302 (1), 135–154.

Cejudo, F. J., Ferrandez, J., Cano, B., Puerto-Galan, L., and Guinea, M. (2012). The function of the NADPH thioredoxin reductase C-2-Cys peroxiredoxin system in plastid redox regulation and signalling. *FEBS Lett.* 586 (18), 2974–2980. doi: 10.1016/j.febslet.2012.07.003

Cejudo, F. J., Ojeda, V., Delgado-Requerey, V., Gonzalez, M., and Perez-Ruiz, J. M. (2019). Chloroplast redox regulatory mechanisms in plant adaptation to light and darkness. *Front. Plant Sci.* 10, 380. doi: 10.3389/fpls.2019.00380

Cerveau, D., Kraut, A., Stotz, H. U., Mueller, M. J., Coute, Y., and Rey, P. (2016). Characterization of the *Arabidopsis thaliana* 2-Cys peroxiredoxin interactome. *Plant Sci.* 252, 30–41. doi: 10.1016/j.plantsci.2016.07.003

Chibani, K., Wingsle, G., Jacquot, J. P., Gelhaye, E., and Rouhier, N. (2009). Comparative genomic study of the thioredoxin family in photosynthetic organisms with emphasis on *Populus trichocarpa*. *Mol. Plant* 2 (2), 308–322. doi: 10.1093/mp/ssn076

Chibani, K., Tarrago, L., Gualberto, J. M., Wingsle, G., Rey, P., Jacquot, J. P., et al (2012). Atypical thioredoxins in poplar: the glutathione-dependent thioredoxin-like 2.1 supports the activity of target enzymes possessing a single redox active cysteine. *Plant Physiol.* 159 (2), 592–605. doi: 10.1104/pp.112.197723

Chibani, K., Saul, F., Didierjean, C., Rouhier, N., and Haouz, A. (2018). Structural snapshots along the reaction mechanism of the atypical poplar thioredoxin-like2.1. *FEBS Lett.* 592 (6), 1030–1041. doi: 10.1002/1873-3468.13009

Collin, V., Issakidis-Bourguet, E., Marchand, C., Hirasawa, M., Lancelin, J. M., Knaff, D. B., et al. (2003). The *Arabidopsis* plastidial thioredoxins: new functions and new insights into specificity. *J. Biol. Chem.* 278 (26), 23747–23752. doi: 10.1074/jbc.M302077200

Dai, S., Johansson, K., Miginiac-Maslow, M., Schurmann, P., and Eklund, H. (2004). Structural basis of redox signaling in photosynthesis: structure and function of ferredoxin:thioredoxin reductase and target enzymes. *Photosynth. Res.* 79 (3), 233–248. doi: 10.1023/B:PRES.0000017194.34167.6d

Dangoor, I., Peled-Zehavi, H., Levitan, A., Pasand, O., and Danon, A. (2009). A small family of chloroplast atypical thioredoxins. *Plant Physiol.* 149 (3), 1240–1250. doi: 10.1104/pp.108.128314

Dangoor, I., Peled-Zehavi, H., Wittenberg, G., and Danon, A. (2012). A chloroplast light-regulated oxidative sensor for moderate light intensity in *Arabidopsis*. *Plant Cell* 24 (5), 1894–1906. doi: 10.1105/tpc.112.097139

Dietz, K. J. (2011). Peroxiredoxins in plants and cyanobacteria. *Antioxid Redox Signal* 15 (4), 1129–1159. doi: 10.1089/ars.2010.3657

Eliyahu, E., Rog, I., Inbal, D., and Danon, A. (2015). ACHT4-driven oxidation of APS1 attenuates starch synthesis under low light intensity in *Arabidopsis* plants. *Proc. Natl. Acad. Sci. U. S. A.* 112 (41), 12876–12881. doi: 10.1073/pnas.1515513112

Geigenberger, P., Thormahlen, I., Daloso, D. M., and Fernie, A. R. (2017). The unprecedented versatility of the plant thioredoxin system. *Trends Plant Sci.* 22 (3), 249–262. doi: 10.1016/j.tplants.2016.12.008

Gurrieri, L., Del Giudice, A., Demitri, N., Falini, G., Pavel, N. V., Zaffagnini, M., et al. (2019). *Arabidopsis* and *Chlamydomonas* phosphoribulokinase crystal structures complete the redox structural proteome of the Calvin-Benson cycle. *Proc. Natl. Acad. Sci. U. S. A.* 116 (16), 8048–8053. doi: 10.1073/pnas.1820639116

Gutle, D. D., Roret, T., Muller, S. J., Couturier, J., Lemaire, S. D., Hecker, A., et al. (2016). Chloroplast FBPase and SBPase are thioredoxin-linked enzymes with similar architecture but different evolutionary histories. *Proc. Natl. Acad. Sci. U. S. A.* 113 (24), 6779–6784. doi: 10.1073/pnas.1606241113

Holmgren, A. (1985). Thioredoxin. *Annu. Rev. Biochem.* 54, 237–271. doi: 10.1146/annurev.bi.54.070185.001321

Jacquot, J. P., Lancelin, J. M., and Meyer, Y. (1997). Thioredoxins: structure and function in plant cells. *New Phytol.* 136, 543–570. doi: 10.1046/j.1469-8137.1997.00784.x

Jacquot, J. P. (2018). Dark deactivation of chloroplast enzymes finally comes to light. *Proc. Natl. Acad. Sci. U. S. A.* 115 (38), 9334–9335. doi: 10.1073/pnas.1814182115

Jarvis, R. M., Hughes, S. M., and Ledgerwood, E. C. (2012). Peroxiredoxin 1 functions as a signal peroxidase to receive, transduce, and transmit peroxide signals in mammalian cells. *Free Radic. Biol. Med.* 53 (7), 1522–1530. doi: 10.1016/j.freeradbiomed.2012.08.001

Jeng, M. F., Campbell, A. P., Begley, T., Holmgren, A., Case, D. A., Wright, P. E., et al (1994). High-resolution solution structures of oxidized and reduced *Escherichia coli* thioredoxin. *Structure* 2 (9), 853–868. doi: 10.1016/S0969-2126(94)00086-7

Konno, H., Nakane, T., Yoshida, M., Ueoka-Nakanishi, H., Hara, S., and Hisabori, T. (2012). Thiol modulation of the chloroplast ATP synthase is dependent on the energization of thylakoid membranes. *Plant Cell Physiol.* 53 (4), 626–634. doi: 10.1093/pcp/pcs018

Kruger, N. J., and von Schaewen, A. (2003). The oxidative pentose phosphate pathway: structure and organisation. *Curr. Opin. Plant Biol.* 6 (3), 236–246. doi: 10.1016/S1369-5266(03)00039-6

Laurent, T. C., Moore, E. C., and Reichard, P. (1964). Enzymatic synthesis of deoxyribonucleotides. IV. Isolation and characterization of thioredoxin, the hydrogen donor from *Escherichia coli B. J. Biol. Chem.* 239, 3436–3444.

Leegood, R. C., and Walker, D. A. (1980). Regulation of fructose-1,6-biphosphatase activity in intact chloroplasts. Studies of the mechanism of inactivation. *Biochim. Biophys. Acta* 593 (2), 362–370. doi: 10.1016/0005-2728(80)90073-0

Lemaire, S. D., Michelet, L., Zaffagnini, M., Massot, V., and Issakidis-Bourguet, E. (2007). Thioredoxins in chloroplasts. *Curr. Genet.* 51 (6), 343–365. doi: 10.1007/s00294-007-0128-z

Lemaire, S. D., Tedesco, D., Crozet, P., Michelet, L., Fermani, S., Zaffagnini, M., et al. (2018). Crystal structure of chloroplastic thioredoxin f2 from *Chlamydomonas reinhardtii* reveals distinct surface properties. *Antioxidants* 7 (12), 171. doi: 10.3390/antiox7120171

Meyer, Y., Riondet, C., Constans, L., Abdelgawwad, M. R., Reichheld, J. P., and Vignols, F. (2006). Evolution of redoxin genes in the green lineage. *Photosynth. Res.* 89 (2-3), 179–192. doi: 10.1007/s11120-006-9095-3

Michalska, J., Zauber, H., Buchanan, B. B., Cejudo, F. J., and Geigenberger, P. (2009). NTRC links built-in thioredoxin to light and sucrose in regulating starch synthesis in chloroplasts and amyloplasts. *Proc. Natl. Acad. Sci. U.S.A.* 106 (24), 9908–9913. doi: 10.1073/pnas.0903559106

Michelet, L., Zaffagnini, M., Morisse, S., Sparla, F., Perez-Perez, M. E., Francia, F., et al. (2013). Redox regulation of the Calvin-Benson cycle: something old, something new. *Front. Plant Sci.* 4, 470. doi: 10.3389/fpls.2013.00470

Nee, G., Zaffagnini, M., Trost, P., and Issakidis-Bourguet, E. (2009). Redox regulation of chloroplastic glucose-6-phosphate dehydrogenase: a new role for f-type thioredoxin. *FEBS Lett.* 583 (17), 2827–2832. doi: 10.1016/j.febslet.2009.07.035

Nikkanen, L., and Rintamaki, E. (2019). Chloroplast thioredoxin systems dynamically regulate photosynthesis in plants. *Biochem. J.* 476 (7), 1159–1172. doi: 10.1042/BCJ20180707

Niyogi, K. K. (2000). Safety valves for photosynthesis. *Curr. Opin. Plant Biol.* 3 (6), 455–460. doi: 10.1016/s1369-5266(00)00113-8

Ojeda, V., Perez-Ruiz, J. M., and Cejudo, F. J. (2018). 2-Cys peroxiredoxins participate in the oxidation of chloroplast enzymes in the dark. *Mol. Plant* 11 (11), 1377–1388. doi: 10.1016/j.molp.2018.09.005

Okegawa, Y., and Motohashi, K. (2015). Chloroplastic thioredoxin *m* functions as a major regulator of Calvin cycle enzymes during photosynthesis *in vivo*. *Plant J.* 84 (5), 900–913. doi: 10.1111/tpj.13049

Peltier, J. B., Cai, Y., Sun, Q., Zabrouskov, V., Giacomelli, L., Rudella, A., et al. (2006). The oligomeric stromal proteome of *Arabidopsis thaliana* chloroplasts. *Mol. Cell Proteomics* 5 (1), 114–133. doi: 10.1074/mcp.M500180-MCP200

Perez-Ruiz, J. M., Spinola, M. C., Kirchsteiger, K., Moreno, J., Sahrawy, M., and Cejudo, F. J. (2006). Rice NTRC is a high-efficiency redox system for chloroplast protection against oxidative damage. *Plant Cell* 18 (9), 2356–2368. doi: 10.1105/tpc.106.041541

Perez-Ruiz, J. M., Naranjo, B., Ojeda, V., Guinea, M., and Cejudo, F. J. (2017). NTRC-dependent redox balance of 2-Cys peroxiredoxins is needed for optimal function of the photosynthetic apparatus. *Proc. Natl. Acad. Sci. U. S. A.* 114 (45), 12069–12074. doi: 10.1073/pnas.1706003114

Scheibe, R., and Anderson, L. E. (1981). Dark modulation of NADP-dependent malate dehydrogenase and glucose-6-phosphate dehydrogenase in the chloroplast. *Biochim. Biophys. Acta* 636 (1), 58–64. doi: 10.1016/0005-2728(81)90075-X

Scheibe, R., Geissler, A., and Fickenscher, K. (1989). Chloroplast glucose-6-phosphate dehydrogenase: K_m shift upon light modulation and reduction. *Arch. Biochem. Biophys.* 274 (1), 290–297. doi: 10.1016/0003-9861(89)90441-4

Schurmann, P., Wolosiuk, R. A., Breazeale, V. D., and Buchanan, B. B. (1976). Two proteins function in regulation of photosynthetic CO_2 assimilation in chloroplasts. *Nature* 263 (5574), 257–258. doi: DOI 10.1038/263257a0

Serrato, A. J., Perez-Ruiz, J. M., Spinola, M. C., and Cejudo, F. J. (2004). A novel NADPH thioredoxin reductase, localized in the chloroplast, which deficiency causes hypersensitivity to abiotic stress in *Arabidopsis thaliana*. *J. Biol. Chem.* 279 (42), 43821–43827. doi: 10.1074/jbc.M404696200

Serrato, A. J., Fernandez-Trijueque, J., Barajas-Lopez, J. D., Chueca, A., and Sahrawy, M. (2013). Plastid thioredoxins: a "one-for-all" redox-signaling system in plants. *Front. Plant Sci.* 4, 463. doi: 10.3389/fpls.2013.00463

Sobotta, M. C., Liou, W., Stocker, S., Talwar, D., Oehler, M., Ruppert, T., et al. (2015). Peroxiredoxin-2 and STAT3 form a redox relay for H_2O_2 signaling. *Nat. Chem. Biol.* 11 (1), 64–70. doi: 10.1038/nchembio.1695

Spyrou, G., Enmark, E., Miranda-Vizuete, A., and Gustafsson, J. (1997). Cloning and expression of a novel mammalian thioredoxin. *J. Biol. Chem.* 272 (5), 2936–2941. doi: 10.1074/jbc.272.5.2936

Stocker, S., Maurer, M., Ruppert, T., and Dick, T. P. (2018). A role for 2-Cys peroxiredoxins in facilitating cytosolic protein thiol oxidation. *Nat. Chem. Biol.* 14 (2), 148–155. doi: 10.1038/nchembio.2536

Takahashi, S., and Badger, M. R. (2011). Photoprotection in plants: a new light on photosystem II damage. *Trends Plant Sci.* 16 (1), 53–60. doi: 10.1016/j.tplants.2010.10.001

Vaseghi, M. J., Chibani, K., Telman, W., Liebthal, M. F., Gerken, M., Schnitzer, H., et al. (2018). The chloroplast 2-cysteine peroxiredoxin functions as thioredoxin oxidase in redox regulation of chloroplast metabolism. *Elife* 7, e38194. doi: 10.7554/eLife.38194

Veal, E. A., Findlay, V. J., Day, A. M., Bozonet, S. M., Evans, J. M., Quinn, J., et al. (2004). A 2-Cys peroxiredoxin regulates peroxide-induced oxidation and activation of a stress-activated MAP kinase. *Mol. Cell* 15 (1), 129–139. doi: 10.1016/j.molcel.2004.06.021

Weichsel, A., Gasdaska, J. R., Powis, G., and Montfort, W. R. (1996). Crystal structures of reduced, oxidized, and mutated human thioredoxins: evidence for a regulatory homodimer. *Structure* 4 (6), 735–751. doi: 10.1016/s0969-2126(96)00079-2

Wolosiuk, R. A., and Buchanan, B. B. (1977). Thioredoxin and glutathione regulate photosynthesis in chloroplasts. *Nature* 266, 565–567. doi: 10.1038/266565a0

Yamori, W. (2016). Photosynthetic response to fluctuating environments and photoprotective strategies under abiotic stress. *J. Plant Res.* 129 (3), 379–395. doi: 10.1007/s10265-016-0816-1

Yokochi, Y., Sugiura, K., Takemura, K., Yoshida, K., Hara, S., Wakabayashi, K. I., et al. (2019). Impact of key residues within chloroplast thioredoxin-*f* on recognition for reduction and oxidation of target proteins. *J. Biol. Chem.* 294 (46), 17437–17450. doi: 10.1074/jbc.RA119.010401

Yoshida, K., and Hisabori, T. (2016). Two distinct redox cascades cooperatively regulate chloroplast functions and sustain plant viability. *Proc. Natl. Acad. Sci. U. S. A.* 113 (27), E3967–E3976. doi: 10.1073/pnas.1604101113

Yoshida, K., and Hisabori, T. (2017). Distinct electron transfer from ferredoxin-thioredoxin reductase to multiple thioredoxin isoforms in chloroplasts. *Biochem. J.* 474 (8), 1347–1360. doi: 10.1042/BCJ20161089

Yoshida, K., and Hisabori, T. (2019). Thiol-based redox regulation in plant chloroplasts in *Redox Homeostasis in Plants, Signaling and Communication in Plants*. Eds. Panda, S. K., and Yamamoto, Y. Y. (Switzerland: Springer), 1–17.

Yoshida, K., Matsuoka, Y., Hara, S., Konno, H., and Hisabori, T. (2014). Distinct redox behaviors of chloroplast thiol enzymes and their relationships with photosynthetic electron transport in *Arabidopsis thaliana*. *Plant Cell Physiol.* 55 (8), 1415–1425. doi: 10.1093/pcp/pcu066

Yoshida, K., Hara, S., and Hisabori, T. (2015). Thioredoxin selectivity for thiol-based redox regulation of target proteins in chloroplasts. *J. Biol. Chem.* 290 (23), 14278–14288. doi: 10.1074/jbc.M115.647545

Yoshida, K., Hara, A., Sugiura, K., Fukaya, Y., and Hisabori, T. (2018). Thioredoxin-like2/2-Cys peroxiredoxin redox cascade supports oxidative thiol modulation in chloroplasts. *Proc. Natl. Acad. Sci. U. S. A.* 115 (35), E8296–E8304. doi: 10.1073/pnas.1808284115

Yoshida, K., Uchikoshi, E., Hara, S., and Hisabori, T. (2019). Thioredoxin-like2/2-Cys peroxiredoxin redox cascade acts as oxidative activator of glucose-6-phosphate dehydrogenase in chloroplasts. *Biochem. J.* 476 (12), 1781–1790. doi: 10.1042/BCJ20190336

Zaffagnini, M., Fermani, S., Marchand, C. H., Costa, A., Sparla, F., Rouhier, N., et al. (2019). Redox homeostasis in photosynthetic organisms: novel and established thiol-based molecular mechanisms. *Antioxid Redox Signal* 31 (3), 155–210. doi: 10.1089/ars.2018.7617

Conflict of Interest: The authors declare that the research was conducted in the absence of any commercial of financial relationships that could be construed as a potential conflict of interest.

frontiers in Plant Science

MINI REVIEW
published: 08 January 2020
doi: 10.3389/fpls.2019.01640

Singlet Oxygen Metabolism: From Genesis to Signaling

*Vivek Dogra and Chanhong Kim**

Shanghai Center for Plant Stress Biology and Center of Excellence in Molecular Plant Sciences, Chinese Academy of Sciences, Shanghai, China

Singlet oxygen ($^1O_2$) is an excited state of molecular oxygen with an electron spin shift in the molecular orbitals, which is extremely unstable and highly reactive. In plants, $^1O_2$ is primarily generated as a byproduct of photosynthesis in the photosystem II reaction center (PSII RC) and the light-harvesting antenna complex (LHC) in the grana core (GC). This occurs upon the absorption of light energy when the excited chlorophyll molecules in the PSII transfer the excess energy to molecular oxygen, thereby generating $^1O_2$. As a potent oxidant, $^1O_2$ promotes oxidative damage. However, at sub-lethal levels, it initiates chloroplast-to-nucleus retrograde signaling to contribute to plant stress responses, including acclimation and cell death. The thylakoid membranes comprise two spatially separated $^1O_2$ sensors: β-carotene localized in the PSII RC in the GC and the nuclear-encoded chloroplast protein EXECUTER1 (EX1) residing in the non-appressed grana margin (GM). Finding EX1 in the GM suggests the existence of an additional source of $^1O_2$ in the GM and the presence of two distinct $^1O_2$-signaling pathways. In this review, we mainly discuss the genesis and impact of $^1O_2$ in plant physiology.

Keywords: singlet oxygen ($^1O_2$), grana core (GC), grana margin (GM), photoinhibition, retrograde signaling, β-carotene, EXECUTER1 (EX1)

OPEN ACCESS

Edited by:
Chikahiro Miyake,
Kobe University, Japan

Reviewed by:
Thomas Roach,
University of Innsbruck, Austria
Jean-David Rochaix,
Université de Genève, Switzerland

***Correspondence:**
Chanhong Kim
chanhongkim@sibs.ac.cn

Specialty section:
This article was submitted to Plant Physiology, a section of the journal Frontiers in Plant Science

Received: *24 September 2019*
Accepted: *21 November 2019*
Published: *08 January 2020*

Citation:
Dogra V and Kim C (2020) Singlet Oxygen Metabolism: From Genesis to Signaling. Front. Plant Sci. 10:1640. doi: 10.3389/fpls.2019.01640

SINGLET OXYGEN GENESIS IN PSII-LHC

Singlet oxygen ($^1O_2$) is a peculiar reactive oxygen species (ROS), generated *via* energy transfer from excited chlorophyll to molecular oxygen during photosynthesis mainly at the photosystem II light-harvesting antenna complex (PSII-LHC) located in the appressed region, namely the grana core (GC) of the thylakoid membrane (Foote, 1968; Gollnick, 1968; Krieger-Liszkay, 2005; Triantaphylidès and Havaux, 2009). Upon absorption of light energy, chlorophyll in LHC attains a high energy but short-lived (few ns, ~10^{-8} s) singlet excited state (^{1}Chl*). A part of this absorbed light energy in ^{1}Chl* is transferred to the reaction center chlorophyll P680 *via* resonance energy transfer to drive the photosynthetic electron transport chain (PETC). This process is referred to as photochemical quenching as it converts the harvested light energy into chemical energy (Demmig-Adams and Adams, 2000; Muller et al., 2001). However, chlorophyll molecules absorb the light energy that exceeds the capacity of photochemical quenching. To avoid unwanted consequences, this excess of non-utilized light energy from ^{1}Chl* is dissipated either as heat (called non-photochemical quenching, NPQ) or as fluorescence (Demmig-Adams and Adams, 2000; Muller et al., 2001). In addition, the energy from ^{1}Chl* also gets decayed *via* intersystem crossing (ISC, changing of spin in the molecular orbitals) which results in the formation of a lower energy triplet

excited state of chlorophyll (^{3}Chl*) with a comparatively longer half-life (~10^{-3} s) (Muller et al., 2001). The carotenoids present in the LHC, such as lutein and zeaxanthin, quench this ^{3}Chl* to prevent any unusual transfer of energy to other nearby molecules. However, if this ^{3}Chl* is not efficiently quenched, it reacts with molecular oxygen ($^3O_2$) released from the water-splitting reaction in the oxygen-evolving complex (OEC) and leads to the generation of $^1O_2$ (van Mieghem et al., 1995; Rinalducci et al., 2004; Santabarbara et al., 2007; Li et al., 2009) (**Figure 1**). This gain of energy results in an electron spin shift in the molecular orbitals, which makes $^1O_2$ very unstable and highly reactive.

In the PSII reaction center (RC), the P680 excites to a singlet state (^{1}P680*) once it absorbs light energy. ^{1}P680* then forms a radical pair with pheophytin (Pheo), $^1P680^+Pheo^-$, the first electron carrier intermediate, through a charge separation reaction (Vass et al., 1992; Adir et al., 2003; Hideg, 2004). This radical pair then transfers an electron to the primary electron acceptor quinone (Q_A), leading to the formation of the long-lived second radical pair $P680^+Q_A^-$ (Krieger-Liszkay, 2005). After donating its electron to Q_A, the oxidized $P680^+$ is re-reduced by extracting electrons from the water-splitting reaction in the OEC and returns to its ground state. However, if Q_A is reduced due to the blockage of downstream electron transport (also called the closed state of PSII RC), it cannot accept any further electrons (Durrant et al., 1990). Such a condition allows the recombination of the primary radical pair ($^3P680^+Pheo^-$) with P680 to a triplet state (Durrant et al., 1990; Krieger-Liszkay, 2005). The charge recombination reaction may also result in the formation of $^1P680^+Pheo^-$ which consequently decays into $^3P680^+Phe^-$ *via* ISC (Durrant et al., 1990; Krieger-Liszkay, 2005). The $^3P680^+Pheo^-$ subsequently dissociates into Pheo and ^{3}P680* (**Figure 1**). Although PSII RC carries two molecules of β-carotene, their proximity to P680 is more than the Van der Waal's distance of 3.6 Å, which is essential to quench ^{3}P680*. This allows ^{3}P680* to react with $^3O_2$ to generate $^1O_2$ (Durrant et al., 1990; van Mieghem et al., 1995; Hideg et al., 1998; Krieger-Liszkay, 2005; Santabarbara et al., 2007; Krieger-Liszkay et al., 2008) (**Figure 1**).

$^1O_2$ INCREASES UPON PHOTO INHIBITION

Under long-lasting or adverse light-stress conditions, the rate of $^1O_2$ generation exceeds the scavenging capacity of chloroplasts and results in the increased photodamage of PSII and

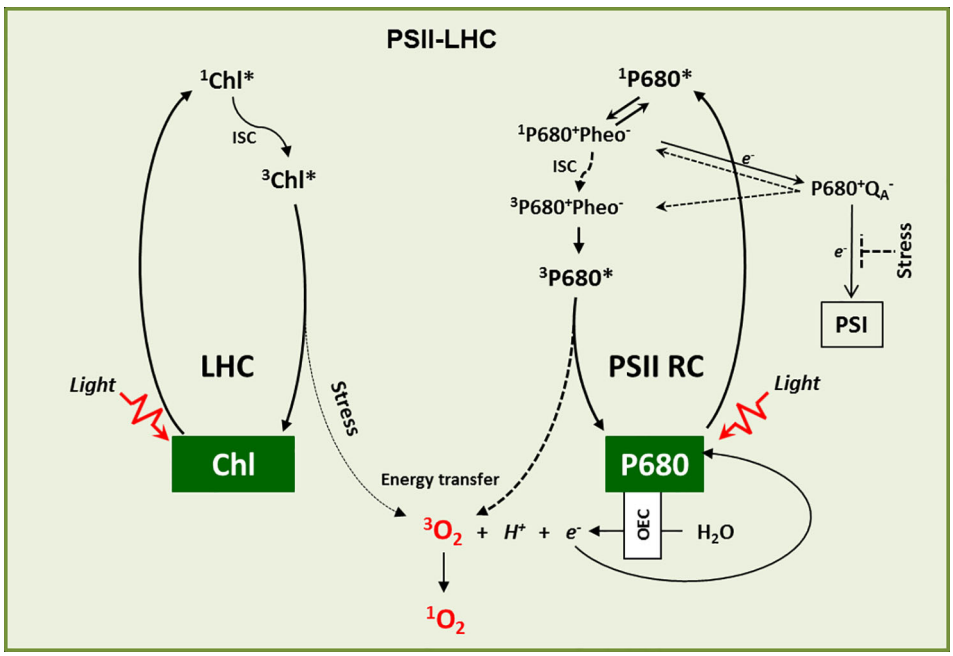

FIGURE 1 | $^1O_2$ genesis. $^1O_2$ is primarily generated in the LHC and PSII RC. In the LHC, upon absorption of light energy, Chl is excited from the ground state to its excited singlet state (^{1}Chl*), which by intersystem crossing (ISC) turns into a comparatively long-lived excited triplet state (^{3}Chl*). ^{3}Chl* is then quenched by carotenoids to come down to its ground state. However, under high light stress conditions it may react with ground state triplet oxygen ($^3O_2$), which leads to its excited singlet state ($^1O_2$). Similarly, P680 in the PSII RC attains excited singlet state (^{1}P680*) upon light absorption. The charge separation reaction between ^{1}P680* and Pheophytin (Pheo) results in the formation of the first radical pair $^1P680^+Pheo^-$, followed by electron transfer to quinone A (Q_A) and the formation of the second radical pair $^1P680^+Q_A^-$. After donating its electron to Q_A, the oxidized $P680^+$ is re-reduced through the water-splitting reactions of the oxygen-evolving complex (OEC). However, when the photosynthetic electron transport chain (PETC) is over-reduced, the radical pair $P680^+Q_A^-$ favors the charge recombination reactions to give rise either to $^3P680^+Pheo^-$ through spin reversal or to $^1P680^+Pheo^-$. The recombined radical pair $^1P680^+Pheo^-$ then decays into $^3P680^+Pheo^-$ *via* intersystem crossing. P680 dissociates from $^3P680^+Pheo^-$ and subsequently forms ^{3}P680*, which reacts with $^3O_2$ to form ground state P680 and $^1O_2$. Under stress conditions such as HL, cold, and drought, when the electron acceptor Q_A is highly reduced, charge recombination reactions stimulate the accumulation of ^{3}P680* and the production of $^1O_2$.

consequently decreased photosynthetic efficiency, a phenomenon called photoinhibition, (Hideg et al., 1998). Excess light enhances the rate of electron transfer in PSII, which can surpass the capacity of downstream electron acceptors in the photosynthetic electron transport chain, resulting in the over-reduction of Q_A (Vass et al., 1992). The reduced Q_A enhances the generation of $^1O_2$ *via* charge recombination reactions (Vass et al., 1992; Adir et al., 2003; Hideg, 2004) (**Figure 1**). Interestingly, not only the light-absorbing chlorophyll molecules in PSII but also the uncoupled or weakly coupled ones of the antenna complex generate $^1O_2$, thereby eventually inducing photoinhibition (Santabarbara et al., 2002). Besides, inactivation of the oxygen-evolving complex also leads to photoinhibition, referred to as donor-side photoinhibition (Keren et al., 1997). Plants grown under low light intensities can also exhibit photo-inactivation of PSII with an increased level of $^1O_2$, upon exposure to a flashlight (Szilard et al., 2005). In the presence of light, other stress factors (such as drought, cold, heat, salinity, and heavy metals) entail photoinhibition as a result of over-reduction of the photosynthetic electron transport chain (PETC) (Foyer and Noctor, 2005; Nishiyama et al., 2006; Takahashi and Murata, 2008; Li et al., 2009; Rochaix, 2011; Foyer et al., 2012; Nishiyama and Murata, 2014). The combination of HL with low temperature leads to photoinhibition as the low temperature slows down the PSII repair process (Baker, 1996). Treatments of plants with various herbicides also result in photoinhibition (Metz et al., 1986; Fufezan et al., 2002). The herbicide diuron (DCMU), e.g., blocks the electron transfer between Q_A and Q_B of PSII causing photoinhibition *via* $^1O_2$ (Metz et al., 1986).

PSII DAMAGE

Being a strong oxidant, $^1O_2$ induces irreversible photo-oxidative damage to the nearby biomolecules such as proteins, carotenoids, and lipids (Ravanat et al., 2000; Apel and Hirt, 2004; Davies, 2004; Watabe et al., 2007). Prime targets for $^1O_2$-driven chemical reactions are double bonds, e.g., in aromatic amino acids of proteins, polyunsaturated fatty acids (PUFA) in lipids and guanine bases in DNA, and thiol groups (Buettner, 1993). Besides, scavengers containing alternate double bonds or thiol groups, such as β-carotene, ascorbate, tocopherol, and glutathione, can also undergo oxidations upon a $^1O_2$ burst. Among these biomolecules, oxidation of lipids by $^1O_2$ primarily leads to a non-enzymatic peroxidation of PUFA, a hallmark of photo-oxidative damage (Mueller et al., 2006; Przybyla et al., 2008). Likewise, those amino acids containing side chains with alternate double bonds such as cysteine, histidine, methionine, tryptophan, tyrosine, and phenylalanine, all undergo oxidation by ROS (Michaeli and Feitelson, 1994). Tryptophan and its derivatives quench most of the $^1O_2$, followed by histidine, cysteine, methionine, tyrosine, and phenylalanine (Michaeli and Feitelson, 1994; Davies, 2004).

To alleviate photodamage, $^1O_2$ needs to be quenched by some molecular components in PSII either by energy transfer or through oxidative modifications (Foote and Denny, 1968; Gorman and Rodgers, 1992; Krieger-Liszkay and Trebst, 2006). Carotenoids, such as lutein and zeaxanthin residing in the close vicinity to Chl in LHC (less than the van der Waals distance of 3.6 Å), directly quench the excited $^3Chl^*$ and $^1O_2$ (Gorman and Rodgers, 1992; Telfer et al., 1994; Telfer, 2002; Krieger-Liszkay and Trebst, 2006). This physical quenching of $^3Chl^*/^1O_2$ excites the carotenoids to a higher energy triplet state ($^3Car^*$), which then undergoes a decay *via* ISC, triplet-triplet annihilation, or ground-state quenching (Edge and Truscott, 1999; Burke et al., 2000). In contrast to the carotenoids in LHC, the β-carotene molecules present in the PSII RC are situated far from $^3P680^*$ which prevents their direct quenching (Telfer et al., 1994). However, the distance between β-carotene and the $^1O_2$ generated in PSII RC is close enough for chemical quenching, leading to the oxidative modification of β-carotene (Foote and Denny, 1968; Krieger-Liszkay, 2005; Ramel et al., 2012a). Under light-stress conditions, a certain portion of $^1O_2$ evades the $^1O_2$ quenchers in PSII and diffuses into the thylakoid membrane, where it leads to lipid peroxidation. As a preventive measure, both tocopherol (Kruk et al., 2005) and PQ (Kruk and Trebst, 2008; Yadav et al., 2010), present in the thylakoid membranes, can detoxify $^1O_2$. In the stroma, ascorbate can also scavenge $^1O_2$ if it is released from the thylakoid membranes (Bisby et al., 1999).

Despite the efficient quenching by β-carotene, some amount of $^1O_2$ diffuses within the PSII RC leading to the irreversible modification of PSII RC proteins, especially D1 (Telfer, 2002; Vass and Cser, 2009). The irreversible modification hinders the electron transfer function of D1 and subsequently impairs the PSII activity (Aro et al., 1993) (**Figure 2**). The damaged PSII undergoes a repair process in the non-appressed grana called grana margin (GM) (Aro et al., 1993). The PSII repair involves the monomerization of the PSII dimer, followed by the migration of the PSII monomer from the GC to the GM, disassembly, degradation, and *de novo* synthesis of D1, insertion of the newly synthesized D1 protein into the thylakoid membrane concomitantly with the assembly of other components of PSII, migration of the PSII monomer to the grana core, and finally dimerization (Aro et al., 1993; Hakala et al., 2005). The GM-localized membrane-bound hexameric FtsH metalloprotease plays a crucial role in PSII proteostasis by degrading damaged D1 proteins (Kato et al., 2009; Malnoë et al., 2014). Since D1 binds chlorophyll in the PSII, chlorophyll molecules probably become unbound during disassembly allowing the efficient degradation of D1. Consistently, during the *de novo* synthesis of the D1 protein, the nascent polypeptide chain is directly inserted into the D1-depleted PSII along with recycled or newly synthesized chlorophyll molecules. Collectively, the $^1O_2$-driven oxidative modification of D1 seems to underline its turnover (Aro et al., 1993; Hakala et al., 2005; Kato et al., 2009; Malnoë et al., 2014). Besides D1, the D2 protein of the PSII RC also exhibits a decline upon a $^1O_2$ burst, indicating probable photodamage of D2 by $^1O_2$ (Koivuniemi et al., 1995; Jansen et al., 1999; Edelman and Mattoo, 2008). In accordance, recent studies have demonstrated that the oxidative modification is not limited to D1, but rather all PSII RC proteins including D2, CP43, and

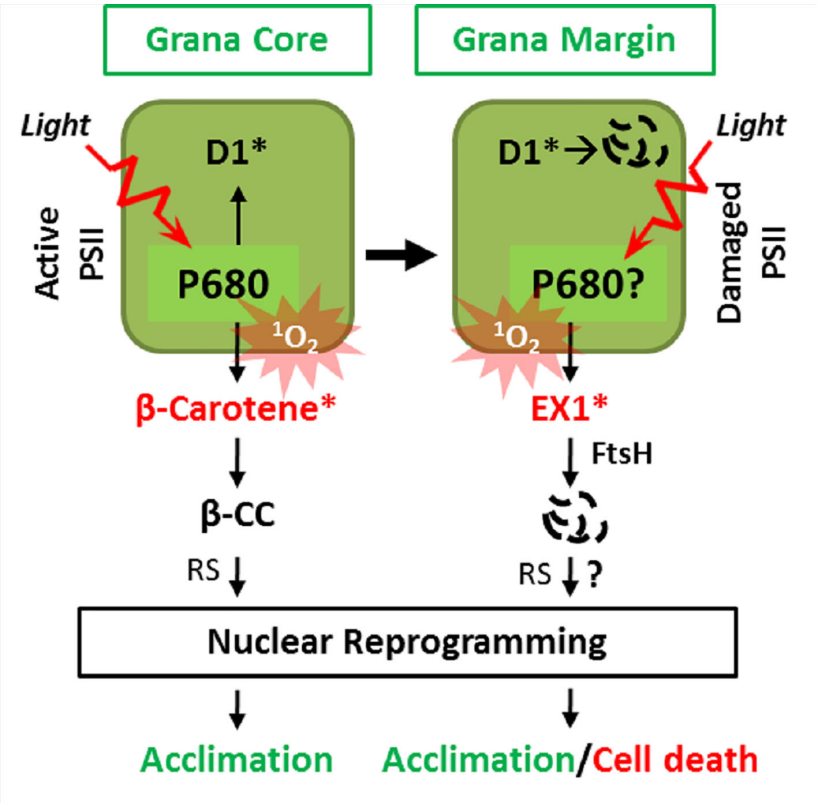

FIGURE 2 | Two spatially separated $^1O_2$ sensors and cognate retrograde signaling pathways. $^1O_2$ generated in the GC by the excited triplet state of P680 damages PSII RC, facilitating its repair in the GM. Under light stress conditions, the enhanced levels of $^1O_2$ result in the accumulation of β-cyclocitral (β-CC), a volatile oxidative product of β-carotene, which mediates retrograde signaling to activate genes involved in detoxification, photoprotection, and acclimation. In the GM, the unbound free chlorophyll molecules released during disassembly/reassembly of PSII or by *de novo* synthesis may generate $^1O_2$. The EX1 protein residing in the GM then senses the $^1O_2$ via its SOS domain and initiates $^1O_2$ signaling through the coordination of the FtsH protease. The EX1 proteolysis by FtsH appears to be essential for inducing changes in nuclear gene expression priming acclimation or cell death. The genuine signaling molecule(s) and the downstream signaling components involved in EX1-mediated signaling remain to be elucidated. *Denotes oxidized state.

CP47 get oxidized by $^1O_2$ (Dreaden Kasson et al., 2012; Dogra et al., 2019a; Dogra et al., 2019b; Duan et al., 2019). Though these oxidative modifications might be linked with the turnover, the precise relevance of these modifications in PSII proteins needs to be investigated.

β-CAROTENE ALSO ACT AS A $^1O_2$ SENSOR IN THE GC TO INITIATE RS

The primary function of ß-carotene residing in the PSII RC is to scavenge $^1O_2$ to prevent PSII damage (Foote and Denny, 1968; Ramel et al., 2012b). This scavenging, however, leads to its non-enzymatic oxidative modification into aldehydes and endo-peroxides (Foote and Denny, 1968; Ramel et al., 2012b). Under normal light conditions, the $^1O_2$-specific endo-peroxides of ß-carotene such as ß-cyclocitral (ß-CC), Dihydroactinidiolide (dhA), and β-ionone are only detectable at negligible levels. However, under high light (HL), these oxidation products accumulate to significant levels (Ramel et al., 2012b). These endo-peroxides accumulate in proportion to the extent of PSII photoinhibition, which supports the notion that the PSII RC is the primary site of $^1O_2$ generation under excess light conditions (Ramel et al., 2012a). Interestingly, these endo-peroxides of β-carotene are highly reactive, volatile, and electrophilic compounds, thus referred to as reactive electrophile species (RES) (Ramel et al., 2012b). Recent studies in Arabidopsis wild-type and *chlorina 1* (*ch1*) mutant plants revealed that ß-CC and to some extent dHA act as $^1O_2$-signaling molecules (Ramel et al., 2012b; Ramel et al., 2013; Shumbe et al., 2014). Exogenous application of these RES compounds activates a plant acclimation response which mitigates the HL-induced photo-oxidative damages including lipid peroxidation. Pretreatment with ß-CC induces the expression of genes involved in photo-protection to prevent lipid peroxidation, leaf bleaching, and to maintain the photochemical activity upon subsequent exposure to HL (Ramel et al., 2012b). ß-CC induces a specific subset of genes, referred to as $^1O_2$-responsive genes (SORGs), which are quite distinct from those induced by H_2O_2 (Ramel et al., 2012b) (**Figure 2**). As compared to ß-CC, dhA appears to induce a small subset of these SORGs (Shumbe et al., 2014), indicating that it is not a significant contributor in ß-carotene-mediated RS.

The β-CC, being volatile, probably reaches the cytosol and/or the nucleus where it induces SORGs *via* some signaling

components. An earlier genetic screen in the unicellular green alga *Chlamydomonas reinhardtii* has unveiled the small zinc finger protein Methylene Blue Sensitivity 1 (MBS1), localized both in the cytosol and the nucleus, as a probable downstream component of ß-CC-mediated $^1O_2$ signaling (Shao et al., 2013). Consistently, Arabidopsis *mbs1* mutant plants are not able to acclimate after pretreatment with β-CC to the lethal dose of HL stress (Shumbe et al., 2017). It was also shown that the MBS1 protein was required for the expression of a subset of β-CC-induced SORGs implicated in photo-acclimation (Shumbe et al., 2017). However, the precise mechanism of how MBS1 drives the gene expression remains unclear. A recent study reported that β-CC activates the TGAII/scarecrow like-14 (SCL14) transcription factors to induce detoxification-related genes required for the acclimation towards HL stress in Arabidopsis (D'Alessandro et al., 2018). Interestingly, the β-CC-mediated activation of TGAII/SCL14 TFs and downstream gene expression is independent of MBS1 (D'Alessandro et al., 2018), which suggests the existence of multiple components involved in this retrograde signaling operating in a spatio-temporal manner. Collectively, these observations conclude that the $^1O_2$ quencher β-carotene also act as a $^1O_2$ sensor in the PSII RC in the GC (**Figure 2**).

THE GRANA MARGIN-ASSOCIATED $^1O_2$ SENSOR EXECUTER1

Klaus Apel and his co-workers first demonstrated the signaling role of $^1O_2$ by utilizing the Arabidopsis *fluorescent* (*flu*) mutant (Meskauskiene et al., 2001). The *flu* mutant plants conditionally generate $^1O_2$ in chloroplasts upon a dark-to-light shift (Meskauskiene et al., 2001). In the dark, the FLU protein negatively regulates the accumulation of protochlorophyllide (Pchlide), a precursor of chlorophyll. Therefore, *flu* mutant plants initially grown under continuous light (permissive) conditions overaccumulate free Pchlide (non-protein-bound form) in the dark, which upon re-illumination acts as a potent photosensitizer (like ^{3}Chl*), leading to the $^1O_2$ generation (Meskauskiene et al., 2001). This intriguing characteristic of the *flu* mutant enabled the discovery that $^1O_2$ rapidly induces nuclear gene expression changes, which precede cell death in seedlings and growth inhibition in mature plants (Meskauskiene et al., 2001; op den Camp et al., 2003). Hence, the *flu* mutant is now used as a bio-tool for investigating the $^1O_2$-mediated signaling and the mechanisms of chloroplast-mediated stress responses including cell death and growth inhibition (Meskauskiene et al., 2001; op den Camp et al., 2003; Wagner et al., 2004; Lee et al., 2007). Using this biotool, the genetic basis of $^1O_2$-mediated signaling has been illustrated: the nuclear-encoded chloroplast protein EXECUTER 1 (EX1) mediates $^1O_2$-triggered nuclear gene expression changes, cell death, and growth inhibition (Wagner et al., 2004; Kim et al., 2012). Loss of EX1 significantly abolishes the $^1O_2$-induced stress responses in the *flu* mutant plants (Wagner et al., 2004; Lee et al., 2007). Also, EXECUTER2 (EX2), a close homolog of EX1, participates in the EX1-mediated $^1O_2$ signaling as a putative modulator (Lee et al., 2007). Loss of function of both EX1 and EX2 almost completely abrogates the $^1O_2$-triggered stress responses in the *flu* mutant upon a dark-to-light shift (Lee et al., 2007) as well as in wild-type plants exposed to moderate light stress (Kim et al., 2012). Besides activating cell death, EX1 and EX2 are also involved in local and systemic gene expression changes leading to acclimation toward HL stress (Carmody et al., 2016). Interestingly, the EX1-mediated signaling was found to be distinct and independent of the one mediated by ß-carotene (Ramel et al., 2013). This finding raises an important question regarding the reason for the existence of two independent $^1O_2$-signaling pathways.

Recent studies aiming to understand the mechanism of EX1-mediated $^1O_2$ signaling have provided the first hint for understanding these two signaling systems. It appears that EX1 mostly localizes in the GMs. This result indicates that EX1 resides away from the active PSII RC in the GC, the primary site of $^1O_2$ generation. In the GMs, EX1 associates with PSII RC proteins (undergoing repair) and the PSII repair machinery (**Figure 2**; Wang et al., 2016). The nearly exclusive localization of EX1 in the GM not only resolves the vagueness of the presence of two independent $^1O_2$-triggered retrograde signaling pathways but also suggests the presence of an additional site of $^1O_2$ generation (Wang et al., 2016; Dogra et al., 2018; Foyer, 2018) (**Figure 2**). The idea regarding the alternative site of $^1O_2$ generation (i.e., GM) is in line with an earlier study showing that $^1O_2$ may also compromise the *de novo* synthesis of D1, which takes place at the GM, by directly targeting the PSII repair machinery as observed for the chloroplast elongation factor G (CpEF-G) in *Synechocystis* sp. strain PCC6803 (Nishiyama et al., 2004). It is noteworthy that the oxidation of CpEF-G by $^1O_2$ in higher plants has not been reported to date.

Nevertheless, given the very short half-life (~200 ns) (Gorman and Rodgers, 1992) and imminent reactivity (Krieger-Liszkay, 2005), it is almost impossible that $^1O_2$ generated at PSII in the GC travels to the GM to oxidize the PSII repair machinery. Therefore, it is likely that the non-appressed thylakoid region may also generate $^1O_2$, perhaps during the PSII repair (Dogra et al., 2018). Another explanation might be that other reactive species with a more extended lifespan move from the GC to the GM to oxidize the PSII repair machinery. Although it remains to be elucidated, one may suppose that perturbations in the PSII repair may lead to the release of $^1O_2$ by tetrapyrrole molecules required for PSII reassembly. In fact, it was shown that EX1 also interacts with enzymes involved in chlorophyll biosynthesis (Wang et al., 2016).

OXIDATIVE MODIFICATION OF EXECUTER1 IS ESSENTIAL TO MEDIATE $^1O_2$ SIGNALING

Aiming to understand how EX1 mediates $^1O_2$ signaling, Wang et al. (2016) realized that EX1 undergoes degradation upon $^1O_2$ burst. This observation indicated that EX1 might undergo a post-

translational modification *via* $^1O_2$, and its associated protease may coordinate $^1O_2$ signaling. Accordingly, EX1 was found to associate with the FtsH protease in the GM (Wang et al., 2016). Given that the FtsH protease complex is involved in PSII repair (Kato and Sakamoto, 2009) and that EX1 is associated with PSII proteins in the GM, EX1 might also affect PSII repair. However, neither the presence nor absence of EX1 did modulate the PSII repair (Wang et al., 2016). Nonetheless, a resulting reverse genetic approach revealed that EX1 proteins undergo FtsH-dependent proteolysis, which turned out to be an essential step in initiating $^1O_2$ signaling (**Figure 2**). The loss of FtsH2, the major subunit of the FtsH protease, substantially compromises $^1O_2$ signaling in the *flu* mutant (Wang et al., 2016; Dogra et al., 2017; Dogra et al., 2019b) (**Figure 2**). Based on these observations, it was postulated that FtsH might recognize EX1 as a substrate probably upon its oxidation or conformational changes in response to $^1O_2$. Consistently, it was revealed that EX1 undergoes an oxidative post-translational modification (Oxi-PTM) at a specific tryptophan residue (Trp643) located in the domain of unknown function 3506 (DUF3506) upon exposure to $^1O_2$. This modification is indispensable for its degradation and the subsequent activation of RS. As Trp643 is present in the DUF3506 and this domain is vital for degradation, it is now dubbed as singlet oxygen senor (SOS) domain, and EX1 protein is designated as a $^1O_2$ sensor.

The EX1 proteolysis *via* the FtsH protease may release a yet unknown signaling molecule. A small EX1 proteolytic peptide per se may activate the $^1O_2$-triggered signaling cascade (**Figure 2**). Considering that EX2 also possess DUF3506, it is very likely that it might also undergo oxidative modification and the subsequent degradation. Further research addressing the possible release of a small peptide or signaling molecule correlated with EX1 degradation and the role of EX2 in EX1-mediated signaling would provide mechanistic insights into this retrograde signaling.

THYLAKOID LIPIDS CAN ALSO ACTIVATE $^1O_2$ SIGNALING *VIA* THEIR OXIDATIVE PRODUCTS

Besides proteins and carotenoids in PSII, $^1O_2$ also targets thylakoid lipids. Oxidation of the PUFAs in the lipids results in the accumulation of oxidized lipid products, also called oxylipins, in the thylakoid membrane. Many of these oxylipins are electrophilic due to their α,β-unsaturated carbonyl groups allowing them to react with electron-rich atoms in biological molecules. These lipid-derived RES include 12-oxo-phytodienoic acid (OPDA), phytoprostanes, aldehydes, and ketones (Imbusch and Mueller, 2000; Gobel et al., 2002; Mano, 2012). Some of these RES can alter the expression of nuclear genes to activate stress responses, including detoxification, defense, and cell death (Weber et al., 2004; Sattler et al., 2006; Mueller et al., 2008; Farmer and Mueller, 2013). The RES-driven nuclear gene expression changes overlap significantly with those induced by β-CC-mediated RS in Arabidopsis.

In green alga *Chlamydomonas reinhardtii*, pretreatment with a sub-lethal dose of $^1O_2$ induced rapid nuclear gene expression changes, conferring acclimation towards a subsequent challenge with a lethal dose of $^1O_2$ (Ledford et al., 2007). This pre-acclimation resulted in the significant upregulation of detoxification-related genes, such as *Glutathione Peroxidase* (*GPX5/GPXH*) and a *Glutathione-S-Transferase* (*GSTS1*), to sustain photo-oxidative stress (Ledford et al., 2007). The set of genes induced were similar to those induced by β-CC mediated signaling. However, the levels of β-CC were almost unchanged, whereas the lipid-derived α,β-unsaturated aldehydes, including 2-propenal (also called acrolein), hexenal, and malonaldehyde (MDA) were elevated in response to HL in Chlamydomonas (Roach et al., 2017), suggesting possible participation of these lipid-derived RES in this signaling. Notably, these lipid-derived RES tend to accumulate in response to $^1O_2$ stress not only in Chlamydomonas but also in plant leaves (Mano et al., 2010). Among these RES, acrolein comparatively shows higher accumulation. Although acrolein imposes toxicity to the plants by directly damaging photosynthetic apparatus (Mano et al., 2009), its exogenous treatment at comparatively lower levels can induce the expression of RES-responsive detoxification genes, including *GST1* (Roach et al., 2017; Roach et al., 2018). Recent findings show that carotene-derived RES β-CC activates SCL14/TGAII and NAC TFs to activate downstream detoxification system in Arabidopsis (D'Alessandro et al., 2018), on the other hand, lipid-derived RES activate *Singlet Oxygen Resistant 1* (*SOR1*), a bZIP10 transcription factor, to drive the expression of acclimation related genes in Chlamydomonas (Fischer et al., 2012). According to these recent findings, the role of the lipid-derived RES is apparent in $^1O_2$ signaling, though the precise mechanism of their perception and activation of downstream signaling remains to be elucidated. Because many RES molecules, both carotenoid- and lipid-derived, are generated simultaneously upon exposure to light stress, linking a RES to a particular RS pathway remains mostly unexplored.

CONCLUDING REMARK

The $^1O_2$ is generated as a byproduct of photosynthesis. In addition to its well-known damaging effect, at sub-lethal levels, $^1O_2$ seems to trigger distinct retrograde signaling pathways *via* oxidative modification of carotenoids, proteins, and lipids to activate multiple stress responses (Ledford et al., 2007; Kim et al., 2008; Triantaphylides and Havaux, 2009; Kim and Apel, 2013; Zhang et al., 2014; Zhu, 2016; Dogra et al., 2018). Recent studies have established that the thylakoid membranes are equipped with distinct $^1O_2$ sensors: β-carotene located in the GC and EX1 proteins localized in the GM, both of which undergo oxidative modifications to mediate independent $^1O_2$-signaling pathways (Ramel et al., 2012b; Dogra et al., 2019b). These studies also suggested that, besides the active PSII in the GC, the GM may also generate $^1O_2$,

perhaps during PSII repair (Wang et al., 2016; Dogra et al., 2018; Foyer, 2018). While the source of $^1O_2$ generation in the GC is well understood, it is unclear how the GM generates $^1O_2$. In these regards, further investigation on $^1O_2$ sensors would provide insights into the source of EX1 oxidation in the GM and the reason for the presence of two distinct $^1O_2$ signaling pathways. Although the role of thylakoids lipids is emerging as putative sensors of $^1O_2$, the precise mechanism by which the lipid peroxidation-mediated signaling activates the retrograde signaling need to be investigated.

AUTHOR CONTRIBUTIONS

VD and CK wrote the manuscript.

FUNDING

This work was supported by the Strategic Priority Research Program from the Chinese Academy of Sciences (Grant No. XDB27040102). VD acknowledge the President's International Fellowship Initiative (PIFI) postdoctoral fellowship from the Chinese Academy of Sciences (No. 2019PB0066).

ACKNOWLEDGMENTS

We sincerely acknowledge the contributions made by the scientists in the area of $^1O_2$ research, as mentioned in this manuscript. We apologize to the authors whose works could not be cited because of space constraints.

REFERENCES

Adir, N., Zer, H., Shochat, S., and Ohad, I. (2003). Photoinhibition - a historical perspective. *Photosynth. Res.* 76, 343–370. doi: 10.1023/A:1024969518145

Apel, K., and Hirt, H. (2004). Reactive oxygen species: metabolism, oxidative stress, and signal transduction. *Annu. Rev. Plant Biol.* 55, 373–399. doi: 10.1146/annurev.arplant.55.031903.141701

Aro, E. M., Virgin, I., and Andersson, B. (1993). Photoinhibition of photosystem II. inactivation, protein damage and turnover. *Biochim. Biophys. Acta* 1143, 113–134. doi: 10.1016/0005-2728(93)90134-2

Baker, N. R. (1996). "Photoinhibition of Photosynthesis," in *Light as an Energy Source and Information Carrier in Plant Physiology*. Eds. R. C. Jennings, G. Zucchelli, F. Ghetti and G. Colombetti (Boston, MA: Springer US), 89–97.

Bisby, R. H., Morgan, C. G., Hamblett, I., and Gorman, A. A. (1999). Quenching of singlet oxygen by trolox c, ascorbate, and amino acids: effects of ph and temperature. *J. Phys. Chem. A.* 103, 7454–7459. doi: 10.1021/jp990838c

Buettner, G. R. (1993). The pecking order of free radicals and antioxidants: lipid peroxidation, alpha-tocopherol, and ascorbate. *Arch. Biochem. Biophys.* 300 (2), 535–543. doi: 10.1006/abbi.1993.1074

Burke, M., Land, E. J., Mcgarvey, D. J., and Truscott, T. G. (2000). Carotenoid triplet state lifetimes. *J. Photochem. Photobiol. B.* 59, 132–138. doi: 10.1016/S1011-1344(00)00150-0

Carmody, M., Crisp, P. A., D'alessandro, S., Ganguly, D., Gordon, M., Havaux, M., et al. (2016). Uncoupling high light responses from singlet oxygen retrograde signaling and spatial-temporal systemic acquired acclimation. *Plant Physiol.* 171, 1734–1749. doi: 10.1104/pp.16.00404

D'alessandro, S., Ksas, B., and Havaux, M. (2018). Decoding beta-cyclocitral-mediated retrograde signaling reveals the role of a detoxification response in plant tolerance to photooxidative stress. *Plant Cell* 30, 2495–2511. doi: 10.1105/tpc.18.00578

Davies, M. J. (2004). Reactive species formed on proteins exposed to singlet oxygen. *Photochem. Photobiol. Sci.* 3, 17–25. doi: 10.1039/b307576c

Demmig-Adams, B., and Adams, W. W.3rd (2000). Harvesting sunlight safely. *Nature* 403, 371, 373–374. doi: 10.1038/35000315

Dogra, V., Duan, J., Lee, K. P., Lv, S., Liu, R., and Kim, C. (2017). FtsH2-dependent proteolysis of EXECUTER1 is essential in mediating singlet oxygen-triggered retrograde signaling in *Arabidopsis thaliana*. *Front. Plant Sci.* 8, 1145. doi: 10.3389/fpls.2017.01145

Dogra, V., Rochaix, J. D., and Kim, C. (2018). Singlet oxygen-triggered chloroplast-to-nucleus retrograde signalling pathways: an emerging perspective. *Plant Cell Environ.* 41, 1727–1738. doi: 10.1111/pce.13332

Dogra, V., Duan, J., Lee, K. P., and Kim, C. (2019a). Impaired PSII proteostasis triggers a UPR-like response in the var2 mutant of Arabidopsis. *J. Exp. Bot.* 70, 3075–3088. doi: 10.1093/jxb/erz151

Dogra, V., Li, M., Singh, S., Li, M., and Kim, C. (2019b). Oxidative post-translational modification of EXECUTER1 is required for singlet oxygen sensing in plastids. *Nat. Commun.* 10, 2834. doi: 10.1038/s41467-019-10760-6

Dreaden Kasson, T. M., Rexroth, S., and Barry, B. A. (2012). Light-induced oxidative stress, n-formylkynurenine, and oxygenic photosynthesis. *PloS One* 7, e42220. doi: 10.1371/journal.pone.0042220

Duan, J., Lee, K. P., Dogra, V., Zhang, S., Liu, K., Caceres-Moreno, C., et al. (2019). Impaired PSII proteostasis promotes retrograde signaling via salicylic acid. *Plant Physiol.* 180, 2182–2197. doi: 10.1104/pp.19.00483

Durrant, J. R., Giorgi, L. B., Barber, J., Klug, D. R., and Porter, G. (1990). Characterisation of triplet states in isolated photosystem II reaction centres: Oxygen quenching as a mechanism for photodamage. *Biochim. Biophys. Acta (BBA) - Bioenerg.* 1017, 167–175. doi: 10.1016/0005-2728(90)90148-W

Edelman, M., and Mattoo, A. K. (2008). D1-protein dynamics in photosystem II: the lingering enigma. *Photosynth. Res.* 98 (1–3), 609–620. doi: 10.1007/s11120-008-9342-x

Edge, R., and Truscott, T. G. (1999). "Carotenoid Radicals and the Interaction of Carotenoids with Active Oxygen Species," in *The Photochemistry of Carotenoids*. Eds. H. A. Frank, A. J. Young, G. Britton and R. J. Cogdell (Dordrecht: Springer Netherlands), 223–234. doi: 10.1007/0-306-48209-6_12

Farmer, E. E., and Mueller, M. J. (2013). ROS-mediated lipid peroxidation and RES-activated signaling. *Annu. Rev. Plant Biol.* 64, 429–450. doi: 10.1146/annurevarplant-050312-120132

Fischer, B. B., Ledford, H. K., Wakao, S., Huang, S. G., Casero, D., Pellegrini, M., et al. (2012). SINGLET OXYGEN RESISTANT 1 links reactive electrophile signaling to singlet oxygen acclimation in Chlamydomonas reinhardtii. *Proc. Natl. Acad. Sci. U.S.A.* 109, E1302–E1311. doi: 10.1073/pnas.1116843109

Foote, C. S. (1968). Mechanisms of photosensitized oxidation. There are several different types of photosensitized oxidation which may be important in biological systems. *Science* 162, 963–970. doi: 10.1126/science.162.3857.963

Foote, C. S., and Denny, R. W. (1968). Chemistry of singlet oxygen. VII. Quenching by beta.-carotene. *J. Am. Chem. Soc.* 90, 6233–6235. doi: 10.1016/S0040-4039(00)70787-8

Foyer, C. H., and Noctor, G. (2005). Redox homeostasis and antioxidant signaling: a metabolic interface between stress perception and physiological responses. *Plant Cell* 17, 1866–1875. doi: 10.1105/tpc.105.033589

Foyer, C. H., Neukermans, J., Queval, G., Noctor, G., and Harbinson, J. (2012). Photosynthetic control of electron transport and the regulation of gene expression. *J. Exp. Bot.* 63, 1637–1661. doi: 10.1093/jxb/ers013

Foyer, C. H. (2018). Reactive oxygen species, oxidative signaling and the regulation of photosynthesis. *Environ. Exp. Bot.* 154, 134–142. doi: 10.1016/j.envexpbot.2018.05.003

Fufezan, C., Rutherford, A. W., and Krieger-Liszkay, A. (2002). Singlet oxygen production in herbicide-treated photosystem II. *FEBS Lett.* 532, 407–410. doi: 10.1016/S0014-5793(02)03724-9

Gobel, C., Feussner, I., Hamberg, M., and Rosahl, S. (2002). Oxylipin profiling in pathogen-infected potato leaves. *Biochim. Biophys. Acta* 1584, 55–64. doi: 10.1016/S1388-1981(02)00268-8

Gollnick, K. (1968). "Type II Photosensitized Oxygenation Reactions," in *Oxidation of Organic Compounds*. (American Chemical Society) 78–101. doi: 10.1021/ba-1968-0077.ch067

Gorman, A. A., and Rodgers, M.a.J. (1992). Current perspectives of singlet oxygen detection in biological environments. *J. Photochem. Photobiol. B.* 14, 159–176. doi: 10.1016/1011-1344(92)85095-C

Hakala, M., Tuominen, I., Keranen, M., Tyystjarvi, T., and Tyystjarvi, E. (2005). Evidence for the role of the oxygen-evolving manganese complex in photoinhibition of Photosystem II. *Biochim. Biophys. Acta* 1706, 68–80. doi: 10.1016/j.bbabio.2004.09.001

Hideg, E., Kalai, T., Hideg, K., and Vass, I. (1998). Photoinhibition of photosynthesis *in vivo* results in singlet oxygen production detection via nitroxide-induced fluorescence quenching in broad bean leaves. *Biochemistry* 37, 11405–11411. doi: 10.1021/bi972890+

Hideg, E. (2004). Detection of free radicals and reactive oxygen species. *Methods Mol. Biol.* 274, 249–260. doi: 10.1385/1-59259-799-8:249

Imbusch, R., and Mueller, M. J. (2000). Formation of isoprostane F(2)-like compounds (phytoprostanes F(1)) from alpha-linolenic acid in plants. *Free Radic. Biol. Med.* 28, 720–726. doi: 10.1104/pp.109.146589

Jansen, M. A., Mattoo, A. K., and Edelman, M. (1999). D1-D2 protein degradation in the chloroplast. complex light saturation kinetics. *Eur. J. Biochem.* 260, 527–532. doi: 10.1046/j.1432-1327.1999.00196.x

Kato, Y., and Sakamoto, W. (2009). Protein quality control in chloroplasts: a current model of D1 protein degradation in the photosystem II repair cycle. *J. Biochem.* 146, 463–469. doi: 10.1093/jb/mvp073

Kato, Y., Miura, E., Ido, K., Ifuku, K., and Sakamoto, W. (2009). The variegated mutants lacking chloroplastic FtsHs are defective in D1 degradation and accumulate reactive oxygen species. *Plant Physiol.* 151, 1790–1801. doi: 10.1104/pp.109.146589

Keren, N., Berg, A., Van Kan, P. J., Levanon, H., and Ohad, I. (1997). Mechanism of photosystem II photoinactivation and D1 protein degradation at low light: the role of back electron flow. *Proc. Natl. Acad. Sci. U.S.A.* 94, 1579–1584. doi: 10.1073/pnas.94.4.1579

Kim, C., and Apel, K. (2013). Singlet oxygen-mediated signaling in plants: moving from flu to wild type reveals an increasing complexity. *Photosynth. Res.* 116, 455–464. doi: 10.1007/s11120-013-9876-4

Kim, C., Meskauskiene, R., Apel, K., and Laloi, C. (2008). No single way to understand singlet oxygen signalling in plants. *EMBO Rep.* 9, 435–439. doi: 10.1038/embor.2008.57

Kim, C., Meskauskiene, R., Zhang, S., Lee, K. P., Lakshmanan Ashok, M., Blajecka, K., et al. (2012). Chloroplasts of *Arabidopsis* are the source and a primary target of a plant-specific programmed cell death signaling pathway. *Plant Cell* 24, 3026–3039. doi: 10.1105/tpc.112.100479

Koivuniemi, A., Aro, E. M., and Andersson, B. (1995). Degradation of the D1- and D2-proteins of photosystem II in higher plants is regulated by reversible phosphorylation. *Biochemistry* 34, 16022–16029. doi: 10.1021/bi00049a016

Krieger-Liszkay, A. (2005). Singlet oxygen production in photosynthesis. *J. Exp. Bot.* 56, 337–346. doi: 10.1093/jxb/erh237

Krieger-Liszkay, A., and Trebst, A. (2006). Tocopherol is the scavenger of singlet oxygen produced by the triplet states of chlorophyll in the PSII reaction centre. *J. Exp. Bot.* 57, 1677–1684. doi: 10.1093/jxb/erl002

Krieger-Liszkay, A., Fufezan, C., and Trebst, A. (2008). Singlet oxygen production in photosystem II and related protection mechanism. *Photosynth. Res.* 98, 551–564. doi: 10.1007/s11120-008-9349-3

Kruk, J., and Trebst, A. (2008). Plastoquinol as a singlet oxygen scavenger in photosystem II. *Biochim. Biophys. Acta* 1777, 154–162. doi: 10.1016/j.bbabio.2007.10.008

Kruk, J., Hollander-Czytko, H., Oettmeier, W., and Trebst, A. (2005). Tocopherol as singlet oxygen scavenger in photosystem II. *J. Plant Physiol.* 162, 749–757. doi: 10.1016/j.jplph.2005.04.020

Ledford, H. K., Chin, B. L., and Niyogi, K. K. (2007). Acclimation to singlet oxygen stress in Chlamydomonas reinhardtii. *Eukaryot. Cell* 6, 919–930. doi: 10.1128/EC.00207-06

Lee, K. P., Kim, C., Landgraf, F., and Apel, K. (2007). EXECUTER1- and EXECUTER2-dependent transfer of stress-related signals from the plastid to the nucleus of Arabidopsis thaliana. *Proc. Natl. Acad. Sci. U.S.A.* 104, 10270–10275. doi: 10.1073/pnas.0702061104

Li, Z., Wakao, S., Fischer, B. B., and Niyogi, K. K. (2009). Sensing and responding to excess light. *Annu. Rev. Plant Biol.* 60, 239–260. doi: 10.1146/annurev.arplant.58.032806.103844

Malnoë, A., Wang, F., Girard-Bascou, J., Wollman, F.-A., and De Vitry, C. (2014). Thylakoid FtsH protease contributes to photosystem II and cytochrome b6f remodeling in chlamydomonas reinhardtii under stress conditions. *Plant Cell* 26, 373–390. doi: 10.1105/tpc.113.120113

Mano, J., Miyatake, F., Hiraoka, E., and Tamoi, M. (2009). Evaluation of the toxicity of stress-related aldehydes to photosynthesis in chloroplasts. *Planta* 230, 639–648. doi: 10.1007/s00425-009-0964-9

Mano, J. I., Tokushige, K., Mizoguchi, H., Fujii, H., and Khorobrykh, S. (2010). Accumulation of lipid peroxide-derived, toxic .ALPHA.,.BETA.-unsaturated aldehydes (E)-2-pentenal, acrolein and (E)-2-hexenal in leaves under photoinhibitory illumination. *Plant Biotechnol.* 27, 193–197. doi: 10.5511/plantbiotechnology.27.193

Mano, J. (2012). Reactive carbonyl species: their production from lipid peroxides, action in environmental stress, and the detoxification mechanism. *Plant Physiol. Biochem.* 59, 90–97. doi: 10.1016/j.plaphy.2012.03.010

Meskauskiene, R., Nater, M., Goslings, D., Kessler, F., Op Den Camp, R., and Apel, K. (2001). FLU: a negative regulator of chlorophyll biosynthesis in Arabidopsis thaliana. *Proc. Natl. Acad. Sci. U.S.A.* 98, 12826–12831. doi: 10.1073/pnas.221252798

Metz, J. G., Pakrasi, H. B., Seibert, M., and Arntzer, C. J. (1986). Evidence for a dual function of the herbicide-binding D1 protein in photosystem II. *FEBS Lett.* 205, 269–274. doi: 10.1016/0014-5793(86)80911-5

Michaeli, A., and Feitelson, J. (1994). Reactivity of singlet oxygen toward amino acids and peptides. *Photochem. Photobiol.* 59, 284–289. doi: 10.1111/j.1751-1097.1994.tb05035.x

Mueller, M. J., Mene-Saffrane, L., Grun, C., Karg, K., and Farmer, E. E. (2006). Oxylipin analysis methods. *Plant J.* 45, 472–489. doi: 10.1111/j.1365-313X.2005.02614.x

Mueller, S., Hilbert, B., Dueckershoff, K., Roitsch, T., Krischke, M., Mueller, M. J., et al. (2008). General detoxification and stress responses are mediated by oxidized lipids through TGA transcription factors in Arabidopsis. *Plant Cell* 20, 768–785. doi: 10.1105/tpc.107.054809

Muller, P., Li, X. P., and Niyogi, K. K. (2001). Non-photochemical quenching. A response to excess light energy. *Plant Physiol.* 125, 1558–1566. doi: 10.1104/pp.125.4.1558

Nishiyama, Y., and Murata, N. (2014). Revised scheme for the mechanism of photoinhibition and its application to enhance the abiotic stress tolerance of the photosynthetic machinery. *Appl. Microbiol. Biotechnol.* 98, 8777–8796. doi: 10.1007/s00253-014-6020-0

Nishiyama, Y., Allakhverdiev, S. I., Yamamoto, H., Hayashi, H., and Murata, N. (2004). Singlet oxygen inhibits the repair of photosystem II by suppressing the translation elongation of the D1 protein in Synechocystis sp. PCC 6803. *Biochemistry* 43, 11321–11330. doi: 10.1021/bi036178q

Nishiyama, Y., Allakhverdiev, S. I., and Murata, N. (2006). A new paradigm for the action of reactive oxygen species in the photoinhibition of photosystem II. *Biochim. Biophys. Acta* 1757, 742–749. doi: 10.1016/j.bbabio.2006.05.013

Op Den Camp, R. G., Przybyla, D., Ochsenbein, C., Laloi, C., Kim, C., Danon, A., et al. (2003). Rapid induction of distinct stress responses after the release of singlet oxygen in *Arabidopsis*. *Plant Cell* 15, 2320–2332. doi: 10.1105/tpc.014662

Przybyla, D., Gobel, C., Imboden, A., Hamberg, M., Feussner, I., and Apel, K. (2008). Enzymatic, but not non-enzymatic, 1O2-mediated peroxidation of polyunsaturated fatty acids forms part of the EXECUTER1-dependent stress response program in the flu mutant of *Arabidopsis thaliana*. *Plant J.* 54, 236–248. doi: 10.1111/j.1365-313X.2008.03409.x

Ramel, F., Birtic, S., Cuiné, S., Triantaphylidès, C., Ravanat, J.-L., and Havaux, M. (2012a). Chemical quenching of singlet oxygen by carotenoids in plants. *Plant Physiol.* 158, 1267–1278. doi: 10.1104/pp.111.182394

Ramel, F., Birtic, S., Ginies, C., Soubigou-Taconnat, L., Triantaphylides, C., and Havaux, M. (2012b). Carotenoid oxidation products are stress signals that mediate gene responses to singlet oxygen in plants. *Proc. Natl. Acad. Sci. U.S.A.* 109, 5535–5540. doi: 10.1073/pnas.1115982109

Ramel, F., Ksas, B., Akkari, E., Mialoundama, A. S., Monnet, F., Krieger-Liszkay, A., et al. (2013). Light-induced acclimation of the *Arabidopsis* chlorina1 mutant to singlet oxygen. *Plant Cell* 25, 1445–1462. doi: 10.1105/tpc.113.109827

Ravanat, J. L., Di Mascio, P., Martinez, G. R., Medeiros, M. H., and Cadet, J. (2000). Singlet oxygen induces oxidation of cellular DNA. *J. Biol. Chem.* 275, 40601–40604. doi: 10.1074/jbc.M006681200

Rinalducci, S., Pedersen, J. Z., and Zolla, L. (2004). Formation of radicals from singlet oxygen produced during photoinhibition of isolated light-harvesting

proteins of photosystem II. *Biochim. Biophys. Acta* 1608, 63–73. doi: 10.1016/j.bbabio.2003.10.009

Roach, T., Baur, T., Stoggl, W., and Krieger-Liszkay, A. (2017). Chlamydomonas reinhardtii responding to high light: a role for 2-propenal (acrolein). *Physiol. Plant* 161, 75–87. doi: 10.1111/ppl.12567

Roach, T., Stoggl, W., Baur, T., and Kranner, I. (2018). Distress and eustress of reactive electrophiles and relevance to light stress acclimation via stimulation of thiol/disulphide-based redox defences. *Free Radic. Biol. Med.* 122, 65–73. doi: 10.1016/j.freeradbiomed.2018.03.030

Rochaix, J. D. (2011). Regulation of photosynthetic electron transport. *Biochim. Biophys. Acta* 1807, 375–383. doi: 10.1016/j.bbabio.2010.11.010

Santabarbara, S., Cazzalini, I., Rivadossi, A., Garlaschi, F. M., Zucchelli, G., and Jennings, R. C. (2002). Photoinhibition *in vivo* and *in vitro* involves weakly coupled chlorophyll-protein complexes. *Photochem. Photobiol.* 75, 613–618. doi: 10.1562/0031-8655(2002)075<0613:PIVAIV>2.0.CO;2

Santabarbara, S., Agostini, G., Casazza, A. P., Syme, C. D., Heathcote, P., Böhles, F., et al. (2007). Chlorophyll triplet states associated with Photosystem I and Photosystem II in thylakoids of the green alga Chlamydomonas reinhardtii. *Biochim. Biophys. Acta (BBA) - Bioenerg.* 1767, 88–105. doi: 10.1016/j.bbabio.2006.10.007

Sattler, S. E., Mene-Saffrane, L., Farmer, E. E., Krischke, M., Mueller, M. J., and Dellapenna, D. (2006). Nonenzymatic lipid peroxidation reprograms gene expression and activates defense markers in Arabidopsis tocopherol-deficient mutants. *Plant Cell* 18, 3706–3720. doi: 10.1105/tpc.106.044065

Shao, N., Duan, G. Y., and Bock, R. (2013). A mediator of singlet oxygen responses in Chlamydomonas reinhardtii and *Arabidopsis* identified by a luciferase-based genetic screen in algal cells. *Plant Cell* 25, 4209–4226. doi: 10.1105/tpc.113.117390

Shumbe, L., Bott, R., and Havaux, M. (2014). Dihydroactinidiolide, a high light-induced beta-carotene derivative that can regulate gene expression and photoacclimation in Arabidopsis. *Mol. Plant* 7, 1248–1251. doi: 10.1093/mp/ssu028

Shumbe, L., D'alessandro, S., Shao, N., Chevalier, A., Ksas, B., Bock, R., et al. (2017). METHYLENE BLUE SENSITIVITY 1 (MBS1) is required for acclimation of Arabidopsis to singlet oxygen and acts downstream of beta-cyclocitral. *Plant Cell Environ.* 40, 216–226. doi: 10.1111/pce.12856

Szilard, A., Sass, L., Hideg, E., and Vass, I. (2005). Photoinactivation of photosystem II by flashing light. *Photosynth. Res.* 84, 15–20. doi: 10.1007/s11120-004-7161-2

Takahashi, S., and Murata, N. (2008). How do environmental stresses accelerate photoinhibition? *Trends Plant Sci.* 13, 178–182. doi: 10.1016/j.tplants.2008.01.005

Telfer, A., Dhami, S., Bishop, S. M., Phillips, D., and Barber, J. (1994). beta-Carotene quenches singlet oxygen formed by isolated photosystem II reaction centers. *Biochemistry* 33, 14469–14474. doi: 10.1021/bi00252a013

Telfer, A. (2002). What is beta-carotene doing in the photosystem II reaction centre? *Philos. Trans. R. Soc. Lond. B. Biol. Sci.* 357, 1431–1439; discussion 1439-1440, 1469-1470. doi: 10.1098/rstb.2002.1139

Triantaphylides, C., and Havaux, M. (2009). Singlet oxygen in plants: production, detoxification and signaling. *Trends Plant Sci.* 14, 219–228. doi: 10.1016/j.tplants.2009.01.008

Van Mieghem, F., Brettel, K., Hillman, B., Kamlowski, A., Rutherford, A. W., and Schlodder, E. (1995). Charge recombination reactions in photosystem ii. 1. yields, recombination pathways, and kinetics of the primary pair. *Biochemistry* 34, 4798–4813. doi: 10.1021/bi00014a038

Vass, I., and Cser, K. (2009). Janus-faced charge recombinations in photosystem II photoinhibition. *Trends Plant Sci.* 14, 200–205. doi: 10.1016/j.tplants.2009.01.009

Vass, I., Styring, S., Hundal, T., Koivuniemi, A., Aro, E., and Andersson, B. (1992). Reversible and irreversible intermediates during photoinhibition of photosystem II: stable reduced QA species promote chlorophyll triplet formation. *Proc. Natl. Acad. Sci. U.S.A.* 89, 1408–1412. doi: 10.1073/pnas.89.4.1408

Wagner, D., Przybyla, D., Op Den Camp, R., Kim, C., Landgraf, F., Lee, K. P., et al. (2004). The genetic basis of singlet oxygen-induced stress responses of Arabidopsis thaliana. *Science* 306, 1183–1185. doi: 10.1126/science.1103178

Wang, L., Kim, C., Xu, X., Piskurewicz, U., Dogra, V., Singh, S., et al. (2016). Singlet oxygen- and EXECUTER1-mediated signaling is initiated in grana margins and depends on the protease FtsH2. *Proc. Natl. Acad. Sci. U.S.A.* 113, E3792–E3800. doi: 10.1073/pnas.1603562113

Watabe, N., Ishida, Y., Ochiai, A., Tokuoka, Y., and Kawashima, N. (2007). Oxidation decomposition of unsaturated fatty acids by singlet oxygen in phospholipid bilayer membranes. *J. Oleo. Sci.* 56, 73–80. doi: 10.5650/jos.56.73

Weber, H., Chetelat, A., Reymond, P., and Farmer, E. E. (2004). Selective and powerful stress gene expression in *Arabidopsis* in response to malondialdehyde. *Plant J.* 37, 877–888. doi: 10.1111/j.1365-313x.2003.02013.x

Yadav, D. K., Kruk, J., Sinha, R. K., and Pospisil, P. (2010). Singlet oxygen scavenging activity of plastoquinol in photosystem II of higher plants: electron paramagnetic resonance spin-trapping study. *Biochim. Biophys. Acta* 1797, 1807–1811. doi: 10.1016/j.bbabio.2010.07.003

Zhang, S., Apel, K., and Kim, C. (2014). Singlet oxygen-mediated and EXECUTER-dependent signalling and acclimation of Arabidopsis thaliana exposed to light stress. *Philos. Trans. R. Soc. Lond. B. Biol. Sci.* 369, 20130227.

Zhu, J. K. (2016). Abiotic stress signaling and responses in plants. *Cell* 167, 313–324. doi: 10.1016/j.cell.2016.08.029

Conflict of Interest: The authors declare that the research was conducted in the absence of any commercial or financial relationships that could be construed as a potential conflict of interest.

frontiers in Plant Science

HYPOTHESIS AND THEORY
published: 30 January 2020
doi: 10.3389/fpls.2019.01778

Optimization of ATP Synthase c–Rings for Oxygenic Photosynthesis

Geoffry A. Davis[1] *and David M. Kramer*[1,2]*

[1] Department of Energy Plant Research Laboratory, Michigan State University, East Lansing, MI, United States, [2] Department of Biochemistry and Molecular Biology, Michigan State University, East Lansing, MI, United States

The conversion of sunlight into useable cellular energy occurs *via* the proton–coupled electron transfer reactions of photosynthesis. Light is absorbed by photosynthetic pigments and transferred to photochemical reaction centers to initiate electron and proton transfer reactions to store energy in a redox gradient and an electrochemical proton gradient (proton motive force, *pmf*), composed of a concentration gradient (ΔpH) and an electric field ($\Delta\psi$), which drives the synthesis of ATP through the thylakoid F_oF_1-ATP synthase. Although ATP synthase structure and function are conserved across biological kingdoms, the number of membrane–embedded ion–binding *c* subunits varies between organisms, ranging from 8 to 17, theoretically altering the H^+/ATP ratio for different ATP synthase complexes, with profound implications for the bioenergetic processes of cellular metabolism. Of the known *c*–ring stoichiometries, photosynthetic *c*–rings are among the largest identified stoichiometries, and it has been proposed that decreasing the c-stoichiometry could increase the energy conversion efficiency of photosynthesis. Indeed, there is strong evidence that the high H^+/ATP of the chloroplast ATP synthase results in a low ATP/nicotinamide adenine dinucleotide phosphate (NADPH) ratio produced by photosynthetic linear electron flow, requiring secondary processes such as cyclic electron flow to support downstream metabolism. We hypothesize that the larger *c* subunit stoichiometry observed in photosynthetic ATP synthases was selected for because it allows the thylakoid to maintain *pmf* in a range where ATP synthesis is supported, but avoids excess $\Delta\psi$ and ΔpH, both of which can lead to production of reactive oxygen species and subsequent photodamage. Numerical kinetic simulations of the energetics of chloroplast photosynthetic reactions with altered *c*–ring size predicts the energy storage of *pmf* and its effects on the photochemical reaction centers strongly support this hypothesis, suggesting that, despite the low efficiency and suboptimal ATP/NADPH ratio, a high H^+/ATP is favored to avoid photodamage. This has important implications for the evolution and regulation of photosynthesis as well as for synthetic biology efforts to alter photosynthetic efficiency by engineering the ATP synthase.

Keywords: photosynthesis, adenosine triphosphate synthase, proton motive force, singlet oxygen, electron transfer, bioenergetics

OPEN ACCESS

Edited by:
Cornelia Spetea, University of Gothenburg, Sweden

Reviewed by:
Mark Aurel Schöttler, Max Planck Institute of Molecular Plant Physiology, Germany
Mikko Tikkanen, University of Turku, Finland

***Correspondence:**
David M. Kramer
kramerd8@msu.edu

Specialty section:
This article was submitted to Plant Physiology, a section of the journal Frontiers in Plant Science

Received: *11 September 2019*
Accepted: *20 December 2019*
Published: *30 January 2020*

Citation:
Davis GA and Kramer DM (2020) Optimization of ATP Synthase c–Rings for Oxygenic Photosynthesis. Front. Plant Sci. 10:1778. doi: 10.3389/fpls.2019.01778

INTRODUCTION

Oxygenic photosynthetic membranes use light to excite electrons on special chlorophyll molecules to store energy in two forms. Redox energy is stored by light-driven extraction of electrons from water to reduce $NADP^+$ to nicotinamide adenine dinucleotide phosphate (NADPH). Phosphorylation potential is stored by a chemiosmotic mechanism (Mitchell, 1961; Mitchell, 1966), coupling the light driven electron transfer reactions to the generation of a proton electrochemical gradient (proton motive force, *pmf*), which in turn drives the synthesis of ATP from ADP + P_i through an F-type ATP synthase (reviewed in (Boyer, 1997; Junge and Nelson, 2015).

In green algae and higher plant chloroplasts, *pmf* is stored across the thylakoid membrane in both transmembrane electric field ($\Delta\psi$) and a proton concentration gradient (ΔpH) (Cruz et al., 2001), differing from mitochondrial respiratory membranes and most plama membranes, across which the *pmf* is primarily composed of $\Delta\psi$ (Kashket, 1981; Booth, 1985). Both components are thermodynamically interchangeable driving forces for the chloroplast ATP synthase (Hangarter and Good, 1982; Gräber et al., 1984) so that the total driving force for ATP synthesis can be described as:

$$pmf = \Delta\psi_{i-o} + \frac{2.3RT}{F}\Delta pH_{o-i} \quad (1)$$

where $\Delta\psi_{i\text{-}o}$ and $\Delta pH_{o\text{-}i}$ represent the electric field and proton gradient calculated as the difference in concentrations between the inside (lumen) and outside (stroma), R is the universal gas constant, and F is Faraday's constant.

During steady-state photosynthesis, *pmf* is generated by light-driven proton translocation and subsequently consumed by H^+ efflux from the lumen through the ATP synthase, which are regulated in interdependent ways. The formation of *pmf* is also governed by electron transfer rates, which in turn are controlled by "photosynthetic control," i.e., the slowing of plastoquinol (PQH_2) oxidation ten–fold from pH 7.5 to 5.5 at the cytochrome b_6f complex as lumen pH decreases below about 6.5 (Nishio and Whitmarsh, 1993; Hope et al., 1994; Takizawa et al., 2007). In effect, the formation of ΔpH and acidification of the lumen is self-controlled.

The consumption of *pmf* is regulated by control of ATP synthase activity (Kanazawa and Kramer, 2002; Cruz et al., 2005a; Takizawa et al., 2008), which at least in green algae and plants responds to decreases in the capacity of the cell to use photosynthetic energy by restricting the efflux of protons, resulting in buildup of *pmf* and subsequent acidification of the lumen, leading to increased photosynthetic control (reviewed in (Strand and Kramer, 2014) and activation of q_E, the rapidly reversible form of nonphotochemical quenching (NPQ) (Niyogi and Truong, 2013). As will be discussed below, the impact and mechanisms of *pmf* regulation may be different in other photosynthetic lineages, as in cyanobacteria in which some evidence suggests that pH may not regulate NPQ (Kirilovsky and Kerfeld, 2012).

The buildup of thylakoid ΔpH can have additional effects on the photosynthetic machinery. Strong lumen acidification has been shown, *in vitro*, to release Ca^{2+} from the photosystem II (PSII) oxygen evolving complex (OEC) (Krieger and Weis, 1993), as well as slowing the release of protons from the OEC during PSII turnover (Zaharieva et al., 2011). Based on surveys of experimental data on both pH–mediated regulation and damage to photosynthetic proteins, it was proposed that *pmf* is regulated so that the lumen pH remains above about 5.5 except under environmental stresses (Kramer et al., 1999). In this case, maintaining sufficient free energy in ATP (ΔG_{ATP}) requires the storage of at least part of *pmf* in the form of $\Delta\psi$ (Kramer et al., 2004; Cruz et al., 2005b; Zhang et al., 2009; Davis et al., 2016). This requirement has been validated by observations that the $\Delta\psi/\Delta$pH ratio is sensitive to environmental stresses (Avenson et al., 2004; Zhang et al., 2009; Davis et al., 2016) and is controlled by specific ion transporters (Checchetto et al., 2012; Armbruster et al., 2014; Kunz et al., 2014; Duan et al., 2016; Herdean et al., 2016a; Herdean et al., 2016b; Schneider et al., 2016; Hohner et al., 2019).

While $\Delta\psi$ can support ATP synthesis in thylakoids with only moderate or no lumen acidification (Hangarter and Good, 1982; Gräber et al., 1984), a large amplitude $\Delta\psi$ also has important secondary effects, most importantly in decreasing the free energy barrier for charge recombination in photosynthetic reaction centers (Crofts et al., 1971; Vos et al., 1991; Davis et al., 2016), thus enhancing the production of reactive oxygen species (ROS), particularly singlet oxygen ($^1O_2$) by PSII (Davis et al., 2016). Substantial rates of $^1O_2$ production can be observed even in wild-type plants during rapid fluctuations in actinic light, which generate large, transient amplitudes of $\Delta\psi$, which occur more rapidly than feedback regulation of the light reactions (Davis et al., 2017). We surmise that, because the core electron transfer protein complexes of photosynthesis (PSII, cytochrome b_6f, and PSI) are highly conserved across all oxygenic photosynthetic organisms (Hasan and Cramer, 2012; Cardona, 2015), the effects of *pmf* composition on these reactions are likely to represent a common (if not universal) constraint on photosynthetic energy storage, and that evolution will have selected for systems that can adequately balance the storage of *pmf* in $\Delta\psi$ and ΔpH to balance the needs for efficient ATP synthesis, homeostasis, and the avoidance of excess ROS production.

Natural Variation in the Stoichiometry of F_0 *c*-Subunits

ATP synthesis in F_0F_1 ATP synthases is thought to involve rotational movement of the membrane embedded F_0 portion driven by a single ion binding by each *c*–subunit, which is coupled to the catalytic turnover of the F_1 $\alpha_3\beta_3$ hexamer to release three ATP molecules per full turnover of the complex (reviewed in Junge and Nelson, 2015). In this mechanism, a full turnover of the F_1 enzyme is coupled to complete 360° rotation of the *c*–ring, generating three ATP per *c*-subunits, dictating that the number of protons required to generate three ATPs (n H^+/ATP) will be equal to the number of *c*-subunits (Watt et al., 2010). It should be noted that the actual H^+/ATP stoichiometries

have not yet been validated by direct experimentation, and some measurements, based on thermodynamics of *pmf* and ΔG_{ATP}, suggest H^+/ATP of about 4 for both spinach and *Escherichia coli*, independent of the *c* subunit stoichiometry (Turina et al., 2003; Steigmiller et al., 2008). On the other hand, the stoichiometries of bioenergetic processes are notoriously difficult to measure [see e.g., (Steigmiller et al., 2008; Ferguson, 2010)] and while we consider the actual stoichiometry as yet unresolved, the majority of evidence suggests that it should be predominantly controlled by the *c* subunit stoichiometry (Steigmiller et al., 2008). Despite differences in the number of *c* subunits in different organisms, the rotational catalysis mechanism appears to be conserved across biological kingdoms (von Ballmoos et al., 2009; Kuhlbrandt, 2019) and various bioenergetic membranes (Koumandou and Kossida, 2014). While the mechanisms of regulation and the absence/presence of certain peripheral subunits vary between species (Walker, 2013), the core subunits of both F_0 and F_1 portions are highly conserved, with the striking exception that the number of *c* subunits that compose the F_0 ring varies from 8 to 17 (**Figure 1**) (Pogoryelov et al., 2012; Kuhlbrandt, 2019), implying that different species evolved to have widely different H^+/ATP ratios.

The determinants of *c* subunit stoichiometry are not yet fully understood (Ferguson, 2000; Ferguson, 2010). Each *c* subunit forms two membrane–spanning α–helices embedded within the membrane connected by an F_1 facing loop (Vonck et al., 2002). Based on structural data from intact *c*–rings, amino acid differences near the N-terminal glycine motif may alter steric and chemical interactions between adjacent α–helices (Vonck et al., 2002), mediating how closely the *c* subunits can pack together (MacKenzie et al., 1997; Watt et al., 2010), with smaller amino acids providing closer packing and smaller *c*–ring stoichiometries (Pogoryelov et al., 2012). While the exact determinants for the *c*–ring stoichiometry is not yet evident, the size does appear to be genetically encoded, resulting from the *c* subunit primary sequence (Muller et al., 2001; Arechaga et al., 2002).

Expressing non–native *c* subunits, either from a different organism or by mutations, results in the assembly of functional chimeric ATP synthases (Laubinger et al., 1990; Suzuki et al., 2007; Liu et al., 2011; Pogoryelov et al., 2012). Supporting the role of *c* subunit primary sequence in determining ring size, replacing only the endogenous *c* subunit gene in *E. coli* ATP synthase with genes from other organisms resulted in *c*–ring stoichiometries matching the organism from which the exogenous *c* subunit was derived, rather than the host *E. coli* stoichiometry (Meier et al., 2005; Matthies et al., 2009). Importantly, the *c*–ring size appears to be determined solely by the sequence of the *c* subunits, and thus remains constant in a species, and does not vary with physiological state (Meyer Zu Tittingdorf et al., 2004; Ballhausen et al., 2009).

Adenosine Triphosphate Synthesis Energetics Are Impacted by *c*–Ring Stoichiometry

During catalytic turnover of the assembled ATP synthase, the overall rate limitation occurs in the F_1 portion (Feniouk et al., 2004) and has been attributed to nucleotide binding and exchange (Panke and Rumberg, 1996). However, in thylakoids, the rate of ATP synthase turnover is strongly dependent on the amplitude of *pmf* (Kramer and Crofts, 1989). The ATP synthase is inactive at low *pmf* (Kaplan et al., 1967; Smith et al., 1976), but above the threshold *pmf* required to activate the complex, essentially linear (ohmic) with *pmf* (Smith et al., 1976; Hangarter and Good, 1982; Kramer and Crofts, 1989; Junesch and Graber, 1991). This implies that the rate-limiting step *in vivo*

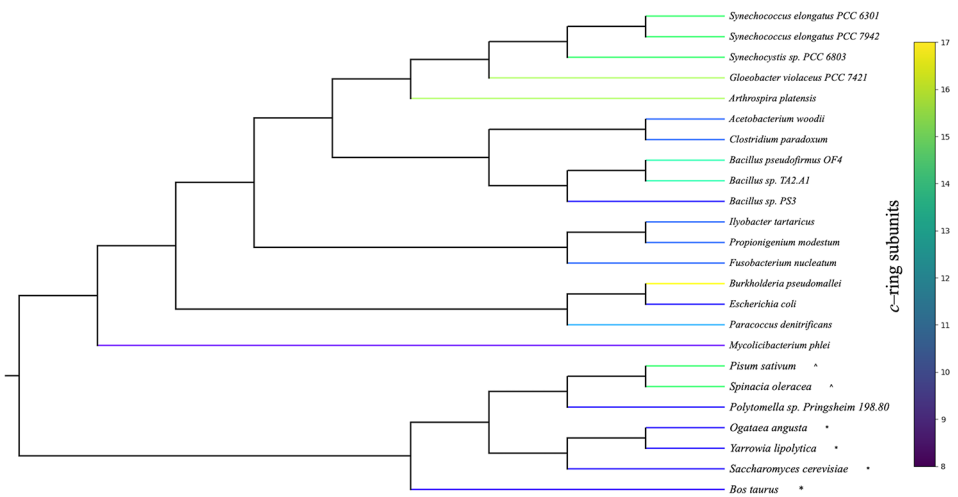

FIGURE 1 | Phylogenetic organization of organisms with known adenosine triphosphate (ATP) synthase *c–ring* stoichiometries. Rooted phylogeny of organisms with experimentally determined *c*–ring stoichiometries retrieved from the National Center for Biotechnology Information (NCBI) taxonomy database. Organism branches colored according to the number of *c* subunits found in the ATP synthase *c*–ring. Cyanobacterial stoichiometries were determined from photosynthetic membranes, and stoichiometries from mitochondria (*) and chloroplasts (^) are indicated for eukaryotic organisms.

requires *pmf*, and thus changing the *c* stoichiometry should alter not only the thermodynamics (von Ballmoos et al., 2009; Watt et al., 2010; Silverstein, 2014) but also the kineics of ATP synthesis. Indeed, ATP synthases with different *c*–ring stoichiometries have different *pmf* activation thresholds, with larger *c*–ring complexes becoming active (Kaim and Dimroth, 1999) and having higher turnover rates at lower *pmf* amplitudes (Pogoryelov et al., 2012). It has been postulated that the kinetic effects of larger rings are due to increased torque resulting from the smaller step-wise rotation imposed by each proton translocation (von Ballmoos et al., 2008; von Ballmoos et al., 2009), much as shifting to a lower gear on a bicycle allows a rider to mount a steeper hill but at the cost of more energy input per distance traveled.

It is intriguing that the number of *c* subunits in photosynthetic organisms are all on the high end (13–15 subunits) of the determined *c*–ring stoichiometries (Seelert et al., 2000; Pogoryelov et al., 2005; Pogoryelov et al., 2007), including *Gloeobacter violaceus* PCC 7421, a phylogenetically ancestral, low–light requiring cyanobacterium originally isolated from calcareous rocks (Rippka et al., 1974; Nakamura et al., 2003), which was found to contain a c_{15} ring (Pogoryelov et al., 2007).

The energy required to catalyze the synthesis of ATP (ΔG_{ATP}) is given by:

$$\Delta G_{ATP} = n * \Delta \mu_{H+} \quad (2)$$

where *n* is the H^+/ATP ratio required to generate each molecule of ATP dictated by the number of *c*–subunits. Assuming the same ΔG_{ATP} between organisms, larger *c*–rings should overcome the energetic barrier for ATP production with a smaller *pmf*, but with a higher overall energy (H^+) cost. The apparent high H^+/ATP ratio in chloroplasts (n=4.67) decreases the *pmf* required to overcome ΔG_{ATP}, allowing photosynthesis to produce ATP at a lower relative *pmf* (Kaim and Dimroth, 1999), reducing the requirement to maintain a large *pmf* (either ΔpH or $\Delta\psi$) during steady–state photosynthesis.

However, a higher H^+/ATP implies that the output of ATP/NADPH for linear electron flow (LEF) will be lower, and in the case of chloroplasts, should result in 2.57 ATP/2 NADPH, below that needed to support the assimilatory reactions of the Calvin-Benson-Bassham (CBB) cycle (Allen, 2003). The resulting energy imbalance requires that chloroplasts activate processes to make up the differences in response to photosynthetic output capacity (Kramer and Evans, 2011). These include cyclic electron flow (reviewed in Strand et al., 2016), the water-water-cycle (Asada, 1999), the malate valve (Scheibe, 2004), as well as balancing the adenylate and electron (either ferredoxin or NADPH) requirements of other metabolic processes (Noctor and Foyer, 2000; Walker et al., 2014; Morales et al., 2018) all of which consume (directly or indirectly) photosynthetic energy. Thus, the large *c* stoichiometries in chloroplasts decrease energy efficiency both at the ATP synthase itself and in imposing a need for additional ATP producing reactions that decrease overall quantum efficiency of photosynthesis.

The Role of the Adenosine Triphosphate Synthase in Feedback Regulation of Photosynthesis

Whereas mitochondria have been found to store *pmf* primarily in $\Delta\psi$, chloroplasts store a fraction of *pmf* as ΔpH; partly as a means of feedback regulation of the light reactions, chloroplasts have evolved mechanisms to alter the partitioning of *pmf* into ΔpH, probably to allow for lumen pH-induced regulation of light capture and electron flow to coordinate with downstream metabolic reactions and avoid over-reduction of PSI cofactors (Kanazawa et al., 2017), while maintaining sufficient $\Delta\psi$ to avoid over–acidification of the lumen (Kramer et al., 1999; Cruz et al., 2001). This has led some to hypothesize that the large *c*–ring stoichiometry in chloroplasts is required to accommodate a smaller $\Delta\psi$ (von Ballmoos et al., 2008). Using isolated ATP synthases incorporated into liposomes, the $\Delta\psi$ required to activate ATP synthesis activity was found to be inversely proportional to the *c*–ring size (Kaim and Dimroth, 1999), so that systems with larger stoichiometries should be able to produce ATP at lower *pmf* values. However, while this observation may explain a benefit of larger *c*–rings during induction, this fails to address why a large steady-state $\Delta\psi$ is not maintained by chloroplasts. Would the large *pmf* required for ATP synthesis with smaller *c* stoichiometries result in deleterious side reactions in the photosynthetic membrane, and if so, could this contribute to an apparent selection for larger *c*–rings?

Can *c*–Subunit Stoichiometry Be Tuned to Optimize the Thermodynamic Efficiency of Proton–Coupled Adenosine Triphosphate Synthesis?

Based on a flux model from available *pmf* and ATP substrate parameters, Silverstein (Silverstein, 2014) estimated that, with similar previous experimentally measured *pmf* and ΔG_{ATP} levels, the *E. coli* and bovine mitochondrial ATP synthases (c_{10} and c_8, respectively) should convert *pmf* to ΔG_{ATP} with about 25% higher efficiency compared to the chloroplast ATP synthase (c_{14}), and speculated that because photosynthetic organisms have access to readily available sunlight as an energy source, there may have been less evolutionary selection pressure to maximize the thermodynamic efficiency for ATP synthesis compared to organisms that rely on more scarce energy sources (fixed organic molecules). However, it is well known that photosynthetic organisms have adapted to grow in light-limiting conditions (Judd et al., 1964; Stomp et al., 2007; Scanlan et al., 2009), including low light requiring cyanobacteria which have been shown to also have large *c*-rings (Pogoryelov et al., 2007).

Here, we consider alternative reasons for why photosyntehtic organisms have evolved larger *c*-rings. As discussed elsewhere (Takizawa et al., 2007; Strand and Kramer, 2014), acidifying the thylakoid lumen can lead to pH–mediated downregulation of photosynthesis at least in plants and algae, or damage to photosynthetic components (Kramer et al., 1999), and robust

mechanisms for maintaining pH homeostasis have evolved to maintain *pmf* predominantly as $\Delta\psi$ across other bioenergetic membranes (Kashket, 1981; Booth, 1985; Moore et al., 1985). Our previous work, however, showed that high $\Delta\psi$ can have deleterious effects on photosynthetic machinery (Davis et al., 2016). We therefore propose that a high H^+/ATP stoichiometry was selected for because it allows photosynthesis to occur at high *pmf* while maintaining low $\Delta\psi$ and low ΔpH, thus preventing deleterious side reactions.

METHODS

Computational Kinetic Simulations of Photosynthetic Light Reactions with Altered *c*–Ring Sizes

To explore the impact of ATP synthase *c*–ring stoichiometry, the photosynthetic light reactions were modelled using a previously published model for the basic photosynthetic light reactions of C3 plants (Davis et al., 2017). Briefly, the model includes ordinary differential equations (ODE) with defined rate constants for electron and proton transfer reactions for the light reactions of photosynthesis, including those that generate and affect the thylakoid *pmf*, as well as the biophysical properties of the thylakoid membrane, and the impacts of *pmf* storage as $\Delta\psi$ and ΔpH on the rate of electron transfer *via* regulation of b_6f turnover, activation of the q_E component of NPQ, and the influence of $\Delta\psi$ on PSII electron recombination. The code allows simulations over time during different conditions. The underlying code and expanded descriptions for all ODE can be found online at Github (https://github.com/protonzilla/Delta_Psi_Py). As the *c*–ring stoichiometry does not appear to change within an organism (Ballhausen et al., 2009), the simulations treat the H^+/ATP ratio of the ATP synthase as constant for a given simulation, but can be changed between simulations. To investigate how the *c*–ring architecture impacts the light reactions, only the H^+/ATP ratio was altered as a constant throughout each simulation. The resulting simulations are available as **Supplementary Data Sheet 1**, as well as an interactive Jupyter notebook available online at Github in which the simulations can be recreated.

RESULTS AND DISCUSSION

Small *c*–Ring Architecture Limits Proton Motive Force Storage and Composition

Figure 2 shows outputs of our kinetic/thermodynamic simulations under conditions where the ATP synthase is active, but with no or very low net changes in proton flux, so that *pmf* approached equilibrium with ΔG_{ATP} over the course of the simulations. Physiologically this condition should occur at very low light, or when the chloroplast is placed in darkness but the ATP synthase regulatory thiols have not yet become fully oxidized. Thus, these estimates represent the minimum *pmf* needed to sustain ΔG_{ATP}.

Assuming a ΔG_{ATP} of 40 kJ/mol (Giersch et al., 1980), a decrease in the number of *c* subunits from 14 (chloroplast) (Seelert et al., 2000) to 8 (*Bos taurus* mitochondria) (Watt et al., 2010) results in an increase in the *pmf* required to maintain ΔG_{ATP} equilibrium in the dark from ~89 to ~155 mV (Eq. 2). If the fraction of *pmf* is equally partitioned between $\Delta\psi$ and ΔpH, this results in a ΔpH at ΔG_{ATP} of about 0.75 units with a c_{14} ring (Eq. 1). Assuming stromal pH of 7.8, the lumen pH should reach about 7, where the violaxanthin de-epoxidase (VDE) and the PsbS protein are inactive, and the b_6f complex is fully active (Takizawa et al., 2007), thus allowing for maximal photosynthetic efficiency at low light (**Figure 2**). By contrast, with a c_8 ATP synthase, ΔpH at ΔG_{ATP} should reach 1.3 units and a lumen pH of 6.5, which is sufficiently acidic to activate VDE and protonate PsbS, thus activating q_E, while slowing electron flow through the b_6f complex, even in the dark (**Figures 2B, C**). Small *c*-rings have even more severe lumen pH-related effects if *pmf* is stored predominantly in ΔpH, as previously discussed (Kramer et al., 1999; Kramer et al., 2003).

Similarly, the $\Delta\psi$ required just to maintain ΔG_{ATP} equilibrium in the dark increases by ~33 mV when going from c_{14} to c_8 if *pmf* was equally partitioned with ΔpH. During photosynthesis, *pmf* is held out of equilibrium from ΔG_{ATP} (see below) so that light-induced *pmf* generation should exacerbate these increases (**Figure 3**). Under this hypothetical smaller c_8 operating structure, photosynthetic *pmf* would either need to be limited to a lower total *pmf* than its current c_{14} state, or require a dramatic shift in *pmf* partitioning into $\Delta\psi$ to avoid near immediate over-acidification of the thylakoid lumen below ~5.5 (ΔpH 2.3 units assuming stromal pH 7.8 in the light) (Kramer et al., 1999), or the evolution of a less pH-sensitive oxygen evolving complex (Krieger and Weis, 1993). A shift in partitioning in favor of $\Delta\psi$ could occur *via* genetic regulation of counter-ion movement through ion transport expression (Davis et al., 2017), or an increase in the buffering capacity of the lumen, though this might require massive remodelling of thylakoids, or the use of high concentrations of mobile buffering groups such as polyamines (Ioannidis et al., 2012).

While the kinetic/thermodynamic model used to analyse changes in *c* stoichiometries was based upon higher plant light chloroplasts, it should be noted that in cyanobacteria, where photosynthetic and respiratory electron transport share the same membrane and quinone pool (Mullineaux, 2014), the *c* subunit stoichiometry and *pmf* partitioning will impact electron transfer within both processes due to the shared role of b_6f (Vermaas, 2001), though the *pmf*-dependencies of b_6f turnover, OEC stability, or PSII recombination reactions have not been well explored in these species. However, as discussed above, cyanobacterial thylakoid ATP synthase *c*–rings are similar in size to chloroplast *c*–rings rather than bacterial respiratory rings (e.g., *E. coli*), possibly indicating that a large *c*–ring, with its corresponding limitations and advantages, while not necessarily optimized for respiration is less unfavorable to respiratory electron transfer than a small *c*–ring is unfavourable to photosynthetic electron transfer.

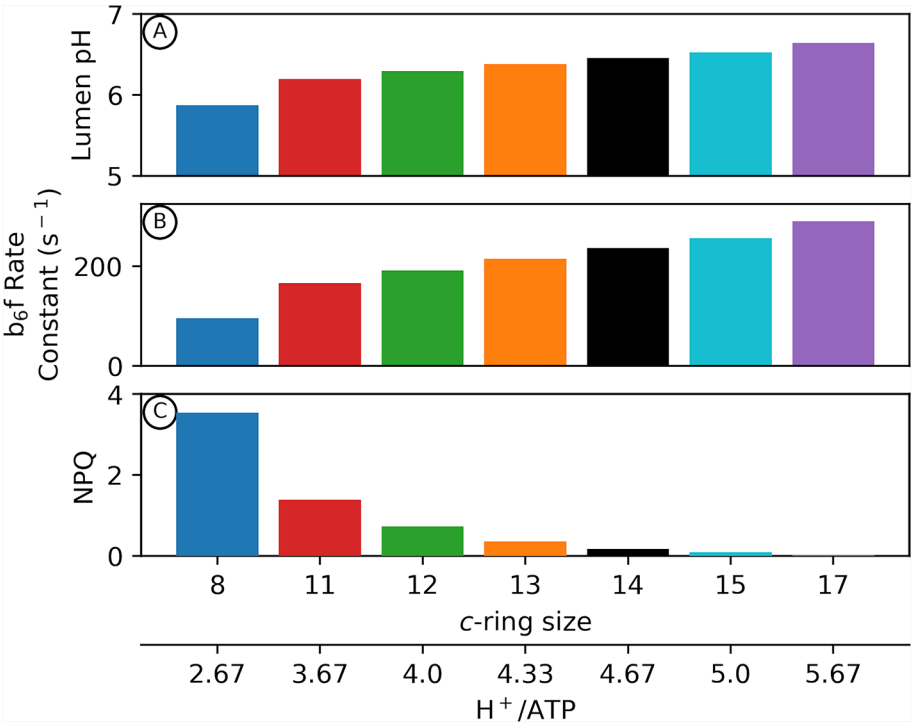

FIGURE 2 | Adenosine triphosphate (ATP) synthase *c*–ring size impacts photosynthetic physiology in the dark. Kinetic modelling of photosynthetic light reactions with altered ATP synthase *c* subunit stoichiometry. Simulated responses of the light reactions were performed as in Davis et al., 2017, with all standard conditions held constant except for the number of ATP synthase c subunits. The *pmf* required to maintain equilibrium with ΔG_{ATP} in the dark is variable depending upon the number of *c* subunits in the ATP synthase *c*–ring (Eq. 2). Changes in lumen pH in the dark due to alterations in *c*–ring size **(A)** can decrease cytochrome b_6f turnover rate **(B)** as well as activate pH–dependent nonphotochemical quenching (NPQ) in higher plants **(C)**.

We next considered the effects of light activation of electron flow (**Figure 3**). With sufficiently high ATP synthase activity, it should be possible to maintain near equilibrium between *pmf* and ΔG_{ATP} even during photosynthesis. *In vivo,* however, the chloroplast ATP synthase activity is not sufficient to allow equilibration to occur, even under ideal conditions, and further down-regulation of control of ATP synthase activity under adverse conditions results in substantial disequilibrium with ΔG_{ATP} (Buchanan, 1980; Kanazawa and Kramer, 2002). This disequilibrium may have evolved to control lumen pH to activate photosynthetic control and q_E (Kanazawa and Kramer, 2002; Avenson et al., 2004) while maintaining ATP homeostasis, or to maintain photosynthetic control by imposing rate limitations at the b_6f complex. It could also represent a fundamental limitation in the kinetic properties of the ATP synthase, though in this case, it is not clear why this limitation could be overcome by over-expressing the complex. In the current simulations, we set ATP synthase activity constant at the highest levels we have observed *in vivo* based on analyses of the decay of the electrochromic shift in the dark (Zaks et al., 2012; Davis et al., 2017).

While the dark, initial *pmf*, which is set be in equilibrium with ΔG_{ATP}, increases with smaller *c*–rings (**Figures 2** and **3**), the total light-induced *pmf* (**Figure 3** panel 2) is strongly limited to about the same extents regardless of the *c*–ring stoichiometry due to lumen pH–mediated photosynthetic control (**Figure 3** panel 5) and q_E. Therefore, the total light–induced *pmf* progressively decreases with smaller *c*–rings (**Figure 3** panels 2–4). Thus, the only way to increase total *pmf* storage in small *c*-rings is to store a higher fraction as $\Delta\psi$ (**Figure 3** panel 3). The light–induced *pmf* challenge is present at both low and high light intensities, with larger *c*–rings being preferential to photosynthetic electron transfer under all intensities. This is clearly seen in the rates of turnover of the b_6f complex (**Figure 3** panel 6). With larger *c*-rings, the lumen pH is above the pKa for PQH_2 oxidation at low light, so photosynthetic control is low, but at high light, lumen acidification increases ΔpH and the turnover rate of the b_6f complex decreases. In smaller *c*-rings, the lumen pH is initially sufficiently acidic that photosynthetic control is large even at low light, limiting electron flow and further acidification. Thus, *variable* photosynthetic control is lost with the smaller *c*-rings. Note that because PQH_2 oxidation is the rate-limiting step in linear electron flow, b_6f turnover can be estimated by the re-reduction kinetics of P_{700}^+. Given that ΔpH with smaller *c*-rings is saturated, we expect little effect of changing downstream reactions on photosynthetic control.

However, higher $\Delta\psi$ increases the rates of recombination reactions in PSII and $^1O_2$ production (**Figure 4**) (Davis et al., 2016). The PSII recombination rate depends on the concentration of

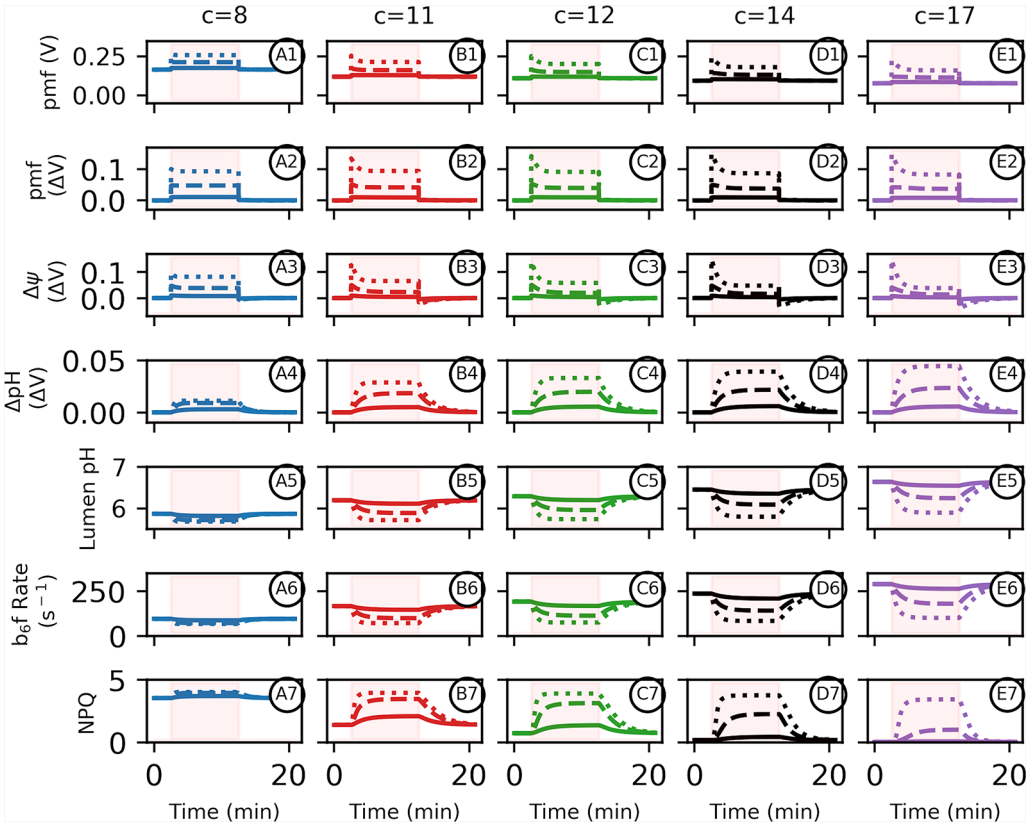

FIGURE 3 | Altered adenosine triphosphate (ATP) synthase *c*-subunit stoichiometry limits proton motive force (*pmf*) composition and pH–mediated regulatory processes during photosynthesis. Simulated responses of the light reactions were performed as in Davis et al., 2017, with all standard conditions held constant except for the number of ATP synthase *c*-subunits. Simulations were performed using 10 min of static light at either 20 (solid lines), 100 (dashed lines), or 1,000 (dotted lines) μmol photons $m^{-2}s^{-1}$. Intervals of light excitation are indicated by shaded regions. **(Panels 1–4)** The light–induced *pmf* **(1, 2A–D)** of ATP synthases with *c*–stoichiometries of 8 (blue, **column A**), 11 (red, **column B**), 12 (green, **column C**), 14 (black, **column D**), or 17 (purple, **column E**) are shown in units of volts, so that a ΔpH of one is equivalent to 0.06 V. The total *pmf* **(panel 2)**, Δψ **(panel 3)**, and ΔpH (**panel 4**) are shown as light–induced changes relative to the *pmf* dark values indicated as ΔV from dark values, to emphasize light–induced ATP synthase constraints. **(5)** Light–induced changes in lumen pH due to photosynthetic activity. Light intensities and *c*–ring composition as in **(1)**. **(6)** The relative rate constant for plastoquinol oxidation at the cytochrome b_6f complex and **(7)** the extent of nonphotochemical quenching q_E component for each *c*–ring size due to the light–induced changes in lumen pH.

charge–separated states capable of recombining as well as the energetics of electron sharing between redox intermediates, with the rate changing exponentially with Δψ. For the charge-separated state(s) forming $P^+Q_A^-$, where P^+ is the primary electron donor and Q_A the non-mobile PSII quinone, these changes correspond to:

$$v_{recombination} = [S_2Q_A^- + S_3Q_A^-] * k_r * 10^{\frac{\Delta E_{stab} - f * \Delta\psi}{0.06}} \quad (3)$$

where $[S_2Q_A^- + S_3Q_A^-]$ represents the fraction of PSII containing donor and acceptor side states capable of recombining from Q_A^-, k_r is the intrinsic rate of recombination from $S_2/S_3Q_A^-$ with no Δψ, ΔE_{stab} is the stabilization free energy of the charge-separated state $S_2/S_3Q_A^-$ expressed in eV, and *f* the distance between the charge-separated states normal to the membrane surface (Davis et al., 2016). As Δψ increases, the ΔE_{stab} of charge separated states decreases (de Grooth and van Gorkom, 1981; Vos et al., 1991), leading to an increase in the rate of recombination. Therefore, even with relatively small changes in the amount of energy stored as Δψ, the velocity of recombination will increase dramatically. This likely limits the amount of energy that can be stored safely across photosynthetic membranes as Δψ, as electron recombination through back–reactions can lead to generation of ROS (Rutherford et al., 2012; Davis et al., 2016).

As seen in **Figure 3**, relative to larger stoichiometries, the increased Δψ in smaller *c*–rings (**Figure 3** panel 3) is expected to increase the probability of PSII recombination reactions and $^1O_2$ generation. This small *c*–ring pitfall is exacerbated by the constitutive downregulation of electron transfer due to the lower lumen pH, limiting productive LEF and resulting in a more reduced quinone pool, which provides substrate for PSII recombination (**Supplementary Figures 1–8**). Dynamic light intensities (**Figure 4**), as would be expected in many natural environments, can induce large spikes in Δψ (Cruz et al., 2001; Davis et al., 2016) that can exacerbate PSII recombination-induced $^1O_2$ production, and our simulations suggest that this effect is worsened as *c* subunit stoichiometry decreases. Simulations of one

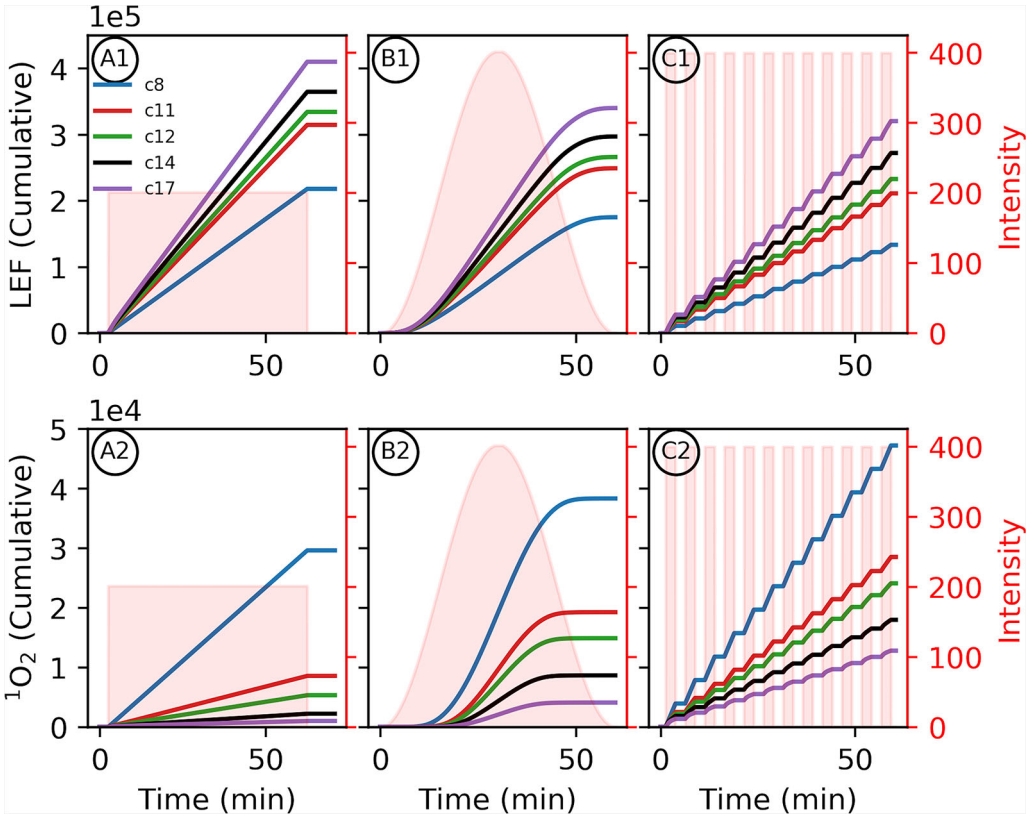

FIGURE 4 | Altered proton motive force (*pmf*) composition due to *c*-subunit stoichiometry limits photosynthetic productivity. Simulated responses of the light reactions were performed as in **Figure 3**. Variability in environment was simulated with 1-h light profiles of static light **(A1, 2)**, sinusoidal light **(B1, 2)**, or square wave fluctuating light **(C1, 2)** to provide the same total illumination during the simulation. **(1)** The total outputs for linear electron flow (LEF) over the course of the light simulations and **(2)** $^1O_2$ were integrated over the light treatment to give the cumulative totals. Shaded regions indicate the light profiles for each simulation.

hour of illumination at light intensities of various dynamics but equal total photon flux, recapitulate the increased production of $^1O_2$ with increasing intensity of light fluctuations (**Figure 4** panel 2). Smaller *c*–rings, as with static light, produce even more $^1O_2$ than the photosynthetic c_{14} with progressively more with more realistic, fluctuating light dynamics (**Figure 4C**). Coupled with the potential cellular damage from $^1O_2$, small *c*–rings, even with higher light intensities than static light, result in progressively less LEF over the course of illumination in dynamic conditions due to premature downregulation of quinol oxidation relative to large stoichiometries (**Figure 4** panel 1).

It therefore appears that a large *c*–ring stoichiometry, although arguably energetically inefficient in isolation (von Ballmoos et al., 2008; Silverstein, 2014), may in fact be far more physiologically efficient for photoautotrophic maintenance and organismal survival than a smaller stoichiometry. Additionally, the decrease in the chloroplast ATP synthase *pmf* activation threshold (Kaim and Dimroth, 1999) may have led to the additional advantage of photosynthetic ATP generation under even low light and low *pmf* conditions (Kramer and Crofts, 1989).

Are Large *c*-Rings an Evolutionary Adaptation to Utilize Large ΔpH and Synthesize Adenosine Triphosphate When Proton Motive Force Is Small?

Based on the arguments above for phototrophs, one might also expect to find higher *c*-stoichiometries in other organisms where *pmf* is constrained by similar needs to maintain physiologically permissive conditions. Interestingly, of the ATP synthase *c*-rings analyzed to date, the other group outside of oxygenic photoautotrophs that utilize larger (c_{13}) rings are alkaliphilic bacteria (Meier et al., 2007; Preiss et al., 2010). Due to their high pH growth conditions, these organisms are subjected to an "inverted" ΔpH, acidic inside the cell relative to outside, and must generate a high $\Delta\psi$ in order to allow H^+ driven ATP synthesis (Sturr et al., 1994; Olsson et al., 2003; Hicks et al., 2010). However, the inverted ΔpH works against total *pmf*, so that the operating *pmf* is lower than that in neutrophilic bacteria, possibly because there is a thermodynamic or structural limit to the amplitude of $\Delta\psi$ needed to counterbalance the negative ΔpH. Thus, a larger *c*-ring may be necessary to maintain sufficient *pmf* to overcome ΔG_{ATP}, which could explain the growth defects

found in the alkaliphilic *Bacillus pseudofirmus* OF4 with engineered smaller *c*-rings (Liu et al., 2011; Preiss et al., 2013).

More examples of *c*-ring architecture combined with *pmf* [or sodium motive force (*smf*)] measurements could resolve why some organisms have evolved to use larger, theoretically less efficient H^+/ATP ratios. The monophyly of oxygenic photosynthesis in a single group of bacteria (cyanobacteria) may have initiated *c*–ring constraints in chloroplasts. The *pmf* composition and dynamics in cyanobacteria has not yet been well studied, whereas an electrochromic shift of carotenoid pigments in the thylakoid membranes of eukaryotes (Bailleul et al., 2010), has allowed focused studies primarily in the green lineage (Bailleul et al., 2015). The recent report of a useable electrochromic shift in a cyanobacterium should make such studies possible (Viola et al., 2019).

While we emphasize the larger effects of changing *c* subunit stoichiometry by large amounts, but as expected, the effects of smaller changes on *pmf* are incremental, and thus we expect there to be subtler trade-offs. However, even small tradeoffs are expected to be important over evolutionary time scales. One additional, and interesting, tradeoff is that a c_{12} ring would be expected to balance the ATP/NADPH production by LEF with consumption by the CBB cycle, perhaps obviating the need for cyclic electron flow under some conditions. However, the overall ATP/NADPH demand is dynamic and should depend on which metabolic sinks are engaged (Heber, 1974; Krause and Heber, 1976; Edwards and Walker, 1983; Fernyhough et al., 1983; Kobayashi et al., 1995; Kramer and Evans, 2011), and thus energy balancing mechanisms should still be required. Making the rings are smaller than 12 subunits would introduce a different problem: an excess of ATP/NADPH production relative to consumption by the CBB cycle; interestingly, there are no established mechanisms to ameliorate this kind of imbalance (Kanazawa et al., 2020). This issue is more apparent (and acute) in cyanobacteria, which use dissipative oxygen reduction pathways to protect reactions centers from photodamage, but as a consequence introduce ATP/NADPH imbalances. Thus, a greater understanding of the *pmf* and ATP synthase architecture in cyanobacteria will enhance the understanding of bioenergetic interactions between photosynthetic electron transfer and ATP production. This understanding is crucial for any future synthetic biology approaches to alter photosynthetic ATP production either directly *via* the ATP synthase (Cardona et al., 2018), or indirectly *via* the H^+/e^- ratio of ATP/NADPH. These limitations and trade-offs, we predict, will likely hinder any gains in photosynthetic efficiency afforded by engineering smaller *c*–rings unless radical changes to the rest of photosynthesis are also made.

DATA AVAILABILITY STATEMENT

The datasets generated for this study can be found on github (https://github.com/protonzilla/Delta_Psi_Py) as a detailed Jupyter (www.jupyter.org) notebook.

AUTHOR CONTRIBUTIONS

GD and DK contributed to the design of simulations and interpretation of results. GD and DK contributed to the drafting and revising of the article.

FUNDING

Funding for GD and DK was supported by the US Department of Energy (DOE), Office of Basic Science, Basic Energy Sciences (BES) under award number DE-FG02-91ER20021.

SUPPLEMENTARY MATERIAL

The Supplementary Material for this article can be found online at: https://www.frontiersin.org/articles/10.3389/fpls.2019.01778/full#supplementary-material

SUPPLEMENTARY FIGURE 1 | Comparison of pmf composition and pH–mediated regulatory processes during photosynthesis in naturally occurring photosynthetic c-rings and c12 ring to balance ATP/NADPH with carbon assimilation. Simulated responses of the light reactions were performed as in Davis et al., 2017, with all standard conditions held constant except for the number of ATP synthase *c*-subunits. Simulations were performed using 10 minutes of static light at either 20 (solid lines), 100 (dashed lines), or 1000 (dotted lines) μmol photons $m^{-2}s^{-1}$ as in Figure 1. Intervals of light excitation are indicated by shaded regions. (Panels 1-4) The light–induced *pmf* (1, 2A-D) of ATP synthases with *c*–stoichiometries of 12 (green, column A), 13 (orange, column B), 14 (black, column C), or 15 (cyan, column D) are shown in units of volts, so that a ΔpH of one is equivalent to 0.06 V. The total *pmf* (panel 2), $\Delta\psi$ (panel 3), and ΔpH (panel 4) are shown as light–induced changes relative to the *pmf* dark values indicated as ΔV from dark values, to emphasize light–induced ATP synthase constraints. (5) Light–induced changes in lumen pH due to photosynthetic activity. Light intensities and *c*–ring composition as in (1). (6) The relative rate constant for plastoquinol oxidation at the cytochrome b_6f complex and (7) the extent of nonphotochemical quenching q_E component for each *c*–ring size due to the light–induced changes in lumen pH.

SUPPLEMENTARY FIGURE 2 | Altered ATP synthase c_8 stoichiometry impacts *pmf* composition and pH–mediated regulatory processes during photosynthesis under increasingly dynamic light environments. Simulated responses of the light reactions were performed as in Davis et al., 2017, with all standard conditions held constant except for the number of ATP synthase *c*-subunits. Simulations were performed using 1-hour of either static light (A), sinusoidal light (B), or square wave fluctuating light (C) with equal total photon flux over the total duration of each light treatment. Intervals of light excitation are indicated by shaded regions. (Panels 1-4) The light–induced *pmf* of ATP synthases with *c*–stoichiometries of 8 (blue) or 14 (black) are shown in units of volts, so that a ΔpH of one is equivalent to 0.06 V. The total *pmf* (panel 2), $\Delta\psi$ (panel 3), and ΔpH (panel 4) are shown as light–induced changes relative to the *pmf* dark values indicated as ΔV from dark values, to emphasize light–induced ATP synthase constraints. (5) Light–induced changes in lumen pH due to photosynthetic activity. Light intensities and *c*–ring composition as in (1). (6) The relative rate constant for plastoquinol oxidation at the cytochrome b_6f complex and (7) the extent of nonphotochemical quenching q_E component for each *c*–ring size due to the light–induced changes in lumen pH.

SUPPLEMENTARY FIGURE 3 | Altered ATP synthase c_{11} stoichiometry impacts *pmf* composition and pH–mediated regulatory processes during photosynthesis under increasingly dynamic light environments. Simulated responses of the light reactions were performed as in Davis et al., 2017, with all standard conditions held constant except for the number of ATP synthase *c*-subunits. Simulations were performed using 1-hour of either static light (A), sinusoidal light (B), or square wave fluctuating light (C) with equal total photon flux over the total duration of each light treatment. Intervals of

light excitation are indicated by shaded regions. (Panels 1-4) The light–induced *pmf* of ATP synthases with c–stoichiometries of 11 (red) or 14 (black) are shown in units of volts, so that a ΔpH of one is equivalent to 0.06 V. The total *pmf* (panel 2), $\Delta\psi$ (panel 3), and ΔpH (panel 4) are shown as light–induced changes relative to the *pmf* dark values indicated as ΔV from dark values, to emphasize light–induced ATP synthase constraints. (5) Light–induced changes in lumen pH due to photosynthetic activity. Light intensities and *c*–ring composition as in (1). (6) The relative rate constant for plastoquinol oxidation at the cytochrome b6f complex and (7) the extent of nonphotochemical quenching q_E component for each *c*–ring size due to the light–induced changes in lumen pH.

SUPPLEMENTARY FIGURE 4 | Altered ATP synthase c_{12} stoichiometry impacts *pmf* composition and pH–mediated regulatory processes during photosynthesis under increasingly dynamic light environments. Simulated responses of the light reactions were performed as in Davis et al., 2017, with all standard conditions held constant except for the number of ATP synthase *c*-subunits. Simulations were performed using 1-hour of either static light (A), sinusoidal light (B), or square wave fluctuating light (C) with equal total photon flux over the total duration of each light treatment. Intervals of light excitation are indicated by shaded regions. (Panels 1-4) The light–induced *pmf* of ATP synthases with *c*–stoichiometries of 12 (green) or 14 (black) are shown in units of volts, so that a ΔpH of one is equivalent to 0.06 V. The total *pmf* (panel 2), $\Delta\psi$ (panel 3), and ΔpH (panel 4) are shown as light–induced changes relative to the *pmf* dark values indicated as ΔV from dark values, to emphasize light–induced ATP synthase constraints. (5) Light–induced changes in lumen pH due to photosynthetic activity. Light intensities and *c*–ring composition as in (1). (6) The relative rate constant for plastoquinol oxidation at the cytochrome b6f complex and (7) the extent of nonphotochemical quenching q_E component for each *c*–ring size due to the light–induced changes in lumen pH.

SUPPLEMENTARY FIGURE 5 | Altered ATP synthase c_{13} stoichiometry impacts *pmf* composition and pH–mediated regulatory processes during photosynthesis under increasingly dynamic light environments. Simulated responses of the light reactions were performed as in Davis et al., 2017, with all standard conditions held constant except for the number of ATP synthase *c*-subunits. Simulations were performed using 1-hour of either static light (A), sinusoidal light (B), or square wave fluctuating light (C) with equal total photon flux over the total duration of each light treatment. Intervals of light excitation are indicated by shaded regions. (Panels 1-4) The light–induced pmf of ATP synthases with *c*–stoichiometries of 13 (orange) or 14 (black) are shown in units of volts, so that a ΔpH of one is equivalent to 0.06 V. The total *pmf* (panel 2), $\Delta\psi$ (panel 3), and ΔpH (panel 4) are shown as light–induced changes relative to the *pmf* dark values indicated as ΔV from dark values, to emphasize light–induced ATP synthase constraints. (5) Light–induced changes in lumen pH due to photosynthetic activity. Light intensities and *c*–ring composition as in (1). (6) The relative rate constant for plastoquinol oxidation at the cytochrome b6f complex and (7) the extent of nonphotochemical quenching q_E component for each *c*–ring size due to the light–induced changes in lumen pH.

SUPPLEMENTARY FIGURE 6 | Altered ATP synthase c_{15} stoichiometry impacts *pmf* composition and pH–mediated regulatory processes during photosynthesis under increasingly dynamic light environments. Simulated responses of the light reactions were performed as in Davis et al., 2017, with all standard conditions held constant except for the number of ATP synthase *c*-subunits. Simulations were performed using 1-hour of either static light (A), sinusoidal light (B), or square wave fluctuating light (C) with equal total photon flux over the total duration of each light treatment. Intervals of light excitation are indicated by shaded regions. (Panels 1-4) The light–induced pmf of ATP synthases with c–stoichiometries of 15 (cyan) or 14 (black) are shown in units of volts, so that a ΔpH of one is equivalent to 0.06 V. The total *pmf* (panel 2), $\Delta\psi$ (panel 3), and ΔpH (panel 4) are shown as light–induced changes relative to the *pmf* dark values indicated as ΔV from dark values, to emphasize light–induced ATP synthase constraints. (5) Light–induced changes in lumen pH due to photosynthetic activity. Light intensities and c–ring composition as in (1). (6) The relative rate constant for plastoquinol oxidation at the cytochrome b_6f complex and (7) the extent of nonphotochemical quenching q_E component for each *c*–ring size due to the light–induced changes in lumen pH.

SUPPLEMENTARY FIGURE 7 | Altered ATP synthase c_{17} stoichiometry impacts *pmf* composition and pH–mediated regulatory processes during photosynthesis under increasingly dynamic light environments. Simulated responses of the light reactions were performed as in Davis et al., 2017, with all standard conditions held constant except for the number of ATP synthase *c*-subunits. Simulations were performed using 1-hour of either static light (A), sinusoidal light (B), or square wave fluctuating light (C) with equal total photon flux over the total duration of each light treatment. Intervals of light excitation are indicated by shaded regions. (Panels 1-4) The light–induced *pmf* of ATP synthases with *c*–stoichiometries of 17 (purple) or 14 (black) are shown in units of volts, so that a ΔpH of one is equivalent to 0.06 V. The total pmf (panel 2), $\Delta\psi$ (panel 3), and ΔpH (panel 4) are shown as light–induced changes relative to the *pmf* dark values indicated as ΔV from dark values, to emphasize light–induced ATP synthase constraints. (5) Light–induced changes in lumen pH due to photosynthetic activity. Light intensities and *c*–ring composition as in (1). (6) The relative rate constant for plastoquinol oxidation at the cytochrome b_6f complex and (7) the extent of nonphotochemical quenching q_E component for each *c*–ring size due to the light–induced changes in lumen pH.

SUPPLEMENTARY FIGURE 8 | Altered *pmf* composition due to *c*-subunit stoichiometry limits photosynthetic productivity. Simulated responses of the light reactions were performed as in figures 3 and 4. Variability in environment was simulated with 1-hour light profiles of static light (A1, 2), sinusoidal light (B1, 2), or square wave fluctuating light (C1, 2) to provide the same total illumination during the simulation. (1) The total outputs for linear electron flow (LEF) over the course of the light simulations and (2) 1O2 were integrated over the light treatment to give the cumulative totals. Shaded regions indicate the light profiles for each simulation.

REFERENCES

Allen, J. F. (2003). Cyclic, pseudocyclic and noncyclic photophosphorylation: new links in the chain. *Trends Plant Sci.* 8, 15–19. doi: 10.1016/s1360-1385(02)00006-7

Arechaga, I., Butler, P. J. G., and Walker, J. E. (2002). Self-assembly of ATP synthase subunit c rings. *FEBS Lett.* 515, 189–193. doi: 10.1016/S0014-5793(02)02447-X

Armbruster, U., Carrillo, L. R., Venema, K., Pavlovic, L., Schmidtmann, E., Kornfeld, A., et al. (2014). Ion antiport accelerates photosynthetic acclimation in fluctuating light environments. *Nat. Commun.* 5, 5439. doi: 10.1038/ncomms6439

Asada, K. (1999). THE water-water cycle in chloroplasts: scavenging of active oxygens and dissipation of excess photons. *Annu. Rev. Plant Physiol. Plant Mol. Biol.* 50, 601–639. doi: 10.1146/annurev.arplant.50.1.601

Avenson, T. J., Cruz, J. A., and Kramer, D. M. (2004). Modulation of energy-dependent quenching of excitons in antennae of higher plants. *Proc. Natl. Acad. Sci. U.S.A.* 101, 5530–5535. doi: 10.1073/pnas.0401269101

Bailleul, B., Cardol, P., Breyton, C., and Finazzi, G. (2010). Electrochromism: a useful probe to study algal photosynthesis. *Photosynth. Res.* 106, 179–189. doi: 10.1007/s11120-010-9579-z

Bailleul, B., Berne, N., Murik, O., Petroutsos, D., Prihoda, J., Tanaka, A., et al. (2015). Energetic coupling between plastids and mitochondria drives CO2 assimilation in diatoms. *Nature* 524, 366–369. doi: 10.1038/nature14599

Ballhausen, B., Altendorf, K., and Deckers-Hebestreit, G. (2009). Constant c10 ring stoichiometry in the Escherichia coli ATP synthase analyzed by cross-linking. *J. Bacteriol.* 191, 2400–2404. doi: 10.1128/JB.01390-08

Booth, I. R. (1985). Regulation of cytoplasmic pH in bacteria. *Microbiol. Rev.* 49, 359–378.

Boyer, P. D. (1997). The ATP synthase–a splendid molecular machine. *Annu. Rev. Biochem.* 66, 717–749. doi: 10.1146/annurev.biochem.66.1.717

Buchanan, B. B. (1980). Role of light in the regulation of chloroplast enzymes. *Annu. Rev. Plant Physiol. Plant Mol. Biol.* 31, 341–374. doi: 10.1146/annurev.pp.31.060180.002013

Cardona, T., Shao, S., and Nixon, P. J. (2018). Enhancing photosynthesis in plants: the light reactions. *Essays Biochem.* 62, 85–94. doi: 10.1042/EBC20170015

Cardona, T. (2015). A fresh look at the evolution and diversification of photochemical reaction centers. *Photosynth. Res.* 126, 111–134. doi: 10.1007/s11120-014-0065-x

Checchetto, V., Segalla, A., Allorent, G., La Rocca, N., Leanza, L., Giacometti, G. M., et al. (2012). Thylakoid potassium channel is required for efficient photosynthesis in cyanobacteria. *Proc. Natl. Acad. Sci. U. S. A.* 109, 11043–11048. doi: 10.1073/pnas.1205960109

Crofts, A. R., Wraight, C. A., and Fleischmann, D. E. (1971). Energy conservation in photochemical reactions of photosynthesis and its relation to delayed fluorescence. *FEBS Lett.* 15, 89–100. doi: 10.1016/0014-5793(71)80031-5

Cruz, J. A., Sacksteder, C. A., Kanazawa, A., and Kramer, D. M. (2001). Contribution of electric field ($\Delta\psi$) to steady-state transthylakoid proton motive force (pmf) in vitro and in vivo. Control of pmf parsing into $\Delta\psi$ and ΔpH by ionic strength. *Biochemistry* 40, 1226–1237. doi: 10.1021/bi0018741

Cruz, J. A., Avenson, T. J., Kanazawa, A., Takizawa, K., Edwards, G. E., and Kramer, D. M. (2005a). Plasticity in light reactions of photosynthesis for energy production and photoprotection. *J. Exp. Bot.* 56, 395–406. doi: 10.1093/jxb/eri022

Cruz, J. A., Kanazawa, A., Treff, N., and Kramer, D. M. (2005b). Storage of light-driven transthylakoid proton motive force as an electric field ($\Delta\psi$) under steady-state conditions in intact cells of Chlamydomonas reinhardtii. *Photosynth. Res.* 85, 221–233. doi: 10.1007/s11120-005-4731-x

Davis, G. A., Kanazawa, A., Schottler, M. A., Kohzuma, K., Froehlich, J. E., Rutherford, A. W., et al. (2016). Limitations to photosynthesis by proton motive force-induced photosystem II photodamage. *Elife* 5. doi: 10.7554/eLife.16921

Davis, G. A., Rutherford, A. W., and Kramer, D. M. (2017). Hacking the thylakoid proton motive force for improved photosynthesis: modulating ion flux rates that control proton motive force partitioning into $\Delta\psi$ and ΔpH. *Philos. Trans. R. Soc. L. B. Biol. Sci.* 372. doi: 10.1098/rstb.2016.0381

de Grooth, B. G., and van Gorkom, H. J. (1981). External electric field effects on prompt and delayed fluorescence in chloroplasts. *Biochim. Biophys. Acta* 635, 445–456. doi: 10.1016/0005-2728(81)90104-3

Duan, Z., Kong, F., Zhang, L., Li, W., Zhang, J., and Peng, L. (2016). A bestrophin-like protein modulates the proton motive force across the thylakoid membrane in Arabidopsis. *J. Integr. Plant Biol.* 58, 848–858. doi: 10.1111/jipb.12475

Edwards, G., and Walker, D. A. (1983). *C3, C4: Mechanisms, and cellular and environmental regulation, of photosynthesis* (Oxford, UK: Blackwell Scientific Publications).

Feniouk, B. A., Kozlova, M. A., Knorre, D. A., Cherepanov, D. A., Mulkidjanian, A. Y., and Junge, W. (2004). The proton-driven rotor of ATP synthase: ohmic conductance (10 fS), and absence of voltage gating. *Biophys. J.* 86, 4094–4109. doi: 10.1529/biophysj.103.036962

Ferguson, S. J. (2000). ATP synthase: what dictates the size of a ring? *Curr. Biol.* 10, R804–R808. doi: 10.1016/S0960-9822(00)00765-X

Ferguson, S. J. (2010). ATP synthase: from sequence to ring size to the P/O ratio. *Proc. Natl. Acad. Sci. U.S.A.* 107, 16755–16756. doi: 10.1073/pnas.1012260107

Fernyhough, P., Foyer, C., and Horton, P. (1983). The influence of metabolic state on the level of phosphorylation of the light-harvesting chlorophyll-protein complex in chloroplasts isolated from maize mesophyll. *Biochim. Biophys. Acta* 725, 155–161. doi: 10.1016/0005-2728(83)90235-9

Giersch, C., Heber, U., Kobayashi, Y., Inoue, Y., Shibata, K., and Heldt, H. W. (1980). Energy charge, phosphorylation potential and proton motive force in chloroplasts. *Biochim. Biophys. Acta* 590, 59–73. doi: 10.1016/0005-2728(80)90146-2

Gräber, P., Junesch, U., and Schatz, G. H. (1984). Kinetics of proton-transport-coupled ATP-synthesis in chloroplasts. Activation of the ATPase by an artificially generated ΔpH and $\Delta\psi$. *Berichte Der. Bunsen-Gesellschaft-Physical Chem. Chem. Phys.* 88, 599–608. doi: 10.1002/bbpc.19840880706

Hangarter, R. P., and Good, N. E. (1982). Energy thresholds for ATP synthesis in chloroplasts. *Biochim. Biophys. Acta* 681, 397–404. doi: 10.1016/0005-2728(82)90181-5

Hasan, S. S., and Cramer, W. A. (2012). On rate limitations of electron transfer in the photosynthetic cytochrome b6f complex. *Phys. Chem. Chem. Phys.* 14, 13853–13860. doi: 10.1039/c2cp41386h

Heber, U. (1974). Metabolite exchange between chloroplasts and cytoplasm. *Annu. Rev. Plant Physiol. Plant Mol. Biol.* 25, 393–421. doi: 10.1146/annurev.pp.25.060174.002141

Herdean, A., Nziengui, H., Zsiros, O., Solymosi, K., Garab, G., Lundin, B., et al. (2016a). The Arabidopsis thylakoid chloride channel AtCLCe functions in chloride homeostasis and regulation of photosynthetic electron transport. *Front. Plant Sci.* 7, 115. doi: 10.3389/fpls.2016.00115

Herdean, A., Teardo, E., Nilsson, A. K., Pfeil, B. E., Johansson, O. N., Unnep, R., et al. (2016b). A voltage-dependent chloride channel fine-tunes photosynthesis in plants. *Nat. Commun.* 7, 11654. doi: 10.1038/ncomms11654

Hicks, D. B., Liu, J., Fujisawa, M., and Krulwich, T. A. (2010). F1F0-ATP synthases of alkaliphilic bacteria: lessons from their adaptations. *Biochim. Biophys. Acta* 1797, 1362–1377. doi: 10.1016/j.bbabio.2010.02.028

Hohner, R., Correa Galvis, V., Strand, D. D., Voelkner, C., Kraemer, M., Messer, M., et al. (2019). Photosynthesis in Arabidopsis thaliana is unaffected by the function of the vacuolar K+ channel TPK3. *Plant Physiol.* doi: 10.1104/pp.19.00255

Hope, A. B., Valente, P., and Matthews, D. B. (1994). Effects of pH on the kinetics of redox reactions in and around the cytochrome bf complex in an isolated system. *Photosynth. Res.* 42, 111–120. doi: 10.1007/bf02187122

Ioannidis, N. E., Cruz, J. A., Kotzabasis, K., and Kramer, D. M. (2012). Evidence that putrescine modulates the higher plant photosynthetic proton circuit. *PLoS One* 7, e29864. doi: 10.1371/journal.pone.0029864

Judd, D. B., Macadam, D. L., and Wyszecki, G. (1964). Spectral distribution of typical daylight as a function of correlated color temperature. *J. Opt. Soc. Am.* 54, 1031. doi: 10.1364/josa.54.001031

Junesch, U., and Graber, P. (1991). The rate of ATP-synthesis as a function of delta pH and delta psi catalyzed by the active, reduced H(+)-ATPase from chloroplasts. *FEBS Lett.* 294, 275–278. doi: 10.1016/0014-5793(91)81447-G

Junge, W., and Nelson, N. (2015). ATP synthase. *Annu. Rev. Biochem.* 84, 631–657. doi: 10.1146/annurev-biochem-060614-034124

Kaim, G., and Dimroth, P. (1999). ATP synthesis by F-type ATP synthase is obligatorily dependent on the transmembrane voltage. *EMBO J.* 18, 4118–4127. doi: 10.1093/emboj/18.15.4118

Kanazawa, A., and Kramer, D. M. (2002). In vivo modulation of nonphotochemical exciton quenching (NPQ) by regulation of the chloroplast ATP synthase. *Proc. Natl. Acad. Sci. U.S.A.* 99, 12789–12794. doi: 10.1073/pnas.182427499

Kanazawa, A., Ostendorf, E., Kohzuma, K., Hoh, D., Strand, D. D., Sato-Cruz, M., et al. (2017). Chloroplast ATP synthase modulation of the thylakoid proton motive force: implications for photosystem i and photosystem ii photoprotection. *Front. Plant Sci.* 8, 719. doi: 10.3389/fpls.2017.00719

Kanazawa, A., Davis, G. A., Fisher, N., Neofotis, P., and Kramer, D. M. (2020). "Diversity in photoprotection and energy balancing in terrestrial and aquatic phototrophs," in *Photosynthesis in Algae*. Eds. A. W. Larkum, A. R. Grossman and J. A Raven. (Dordrecht: Springer).

Kaplan, J. H., Uribe, E., and Jagendorf, A. T. (1967). ATP hydrolysis caused by acid-base transition of spinach chloroplasts. *Arch. Biochem. Biophys.* 120, 365–370. doi: 10.1016/0003-9861(67)90252-4

Kashket, E. R. (1981). Proton motive force in growing Streptococcus lactis and Staphylococcus aureus cells under aerobic and anaerobic conditions. *J. Bacteriol.* 146, 369–376. doi: 10.1128/JB.146.1.369-376.1981

Kirilovsky, D., and Kerfeld, C. A. (2012). The orange carotenoid protein in photoprotection of photosystem II in cyanobacteria. *Biochim. Biophys. Acta* 1817, 158–166. doi: 10.1016/j.bbabio.2011.04.013

Kobayashi, Y., Kaiser, W., and Heber, U. (1995). Bioenergetics of carbon assimilation in intact chloroplasts: Coupling of proton to electron transport at the ratio H+/e=3 is incompatible with H+/ATP=3 in ATP synthesis. *Plant Cell Physiol.* 36, 1629–1637. doi: 10.1093/oxfordjournals.pcp.a078930

Koumandou, V. L., and Kossida, S. (2014). Evolution of the F0F1 ATP synthase complex in light of the patchy distribution of different bioenergetic pathways across prokaryotes. *PLoS Comput. Biol.* 10, e1003821. doi: 10.1371/journal.pcbi.1003821

Kramer, D. M., and Crofts, A. R. (1989). Activation of the chloroplast ATPase measured by the electrochromic change in leaves of intact plants. *Biochim. Biophys. Acta* 976, 28–41. doi: 10.1016/s0005-2728(89)80186-0

Kramer, D. M., and Evans, J. R. (2011). The importance of energy balance in improving photosynthetic productivity. *Plant Physiol.* 155, 70–78. doi: 10.1104/pp.110.166652

Kramer, D. M., Sacksteder, C. A., and Cruz, J. A. (1999). How acidic is the lumen? *Photosynth. Res.* 60, 151–163. doi: 10.1023/a:1006212014787

Kramer, D. M., Cruz, J. A., and Kanazawa, A. (2003). Balancing the central roles of the thylakoid proton gradient. *Trends Plant Sci.* 8, 27–32. doi: 10.1016/S1360-1385(02)00010-9

Kramer, D. M., Avenson, T. J., and Edwards, G. E. (2004). Dynamic flexibility in the light reactions of photosynthesis governed by both electron and proton transfer reactions. *Trends Plant Sci.* 9, 349–357. doi: 10.1016/j.tplants.2004.05.001

Krause, G. H., and Heber, U. (1976). "Energetics of intact chloroplasts," in *Topics in photosynthesis - Volume 1. The intact chloroplast*. Ed. J. Barber (Amsterdam, Netherlands: Elsevier/North-Holland Biomedical Press, The Netherlands), 171–214.

Krieger, A., and Weis, E. (1993). The role of calcium in the pH-dependent control of photosystem II. *Photosynth. Res.* 37, 117–130. doi: 10.1007/bf02187470

Kuhlbrandt, W. (2019). Structure and Mechanisms of F-Type ATP Synthases. *Annu. Rev. Biochem.* doi: 10.1146/annurev-biochem-013118-110903

Kunz, H. H., Gierth, M., Herdean, A., Satoh-Cruz, M., Kramer, D. M., Spetea, C., et al. (2014). Plastidial transporters KEA1, -2, and -3 are essential for chloroplast osmoregulation, integrity, and pH regulation in Arabidopsis. *Proc. Natl. Acad. Sci. U.S.A.* 111, 7480–7485. doi: 10.1073/pnas.1323899111

Laubinger, W., Deckers-Hebestreit, G., Altendorf, K., and Dimroth, P. (1990). A hybrid adenosinetriphosphatase composed of F1 of Escherichia coli and F0 of Propionigenium modestum is a functional sodium ion pump. *Biochemistry* 29, 5458–5463. doi: 10.1021/bi00475a008

Liu, J., Fackelmayer, O. J., Hicks, D. B., Preiss, L., Meier, T., Sobie, E. A., et al. (2011). Mutations in a helix-1 motif of the ATP synthase c-subunit of Bacillus pseudofirmus OF4 cause functional deficits and changes in the c-ring stability and mobility on sodium dodecyl sulfate-polyacrylamide gel electrophoresis. *Biochemistry* 50, 5497–5506. doi: 10.1021/bi2005009

MacKenzie, K. R., Prestegard, J. H., and Engelman, D. M. (1997). A transmembrane helix dimer: structure and implications. *Science* 276 (5309), 131–133. doi: 10.1126/science.276.5309.131

Matthies, D., Preiss, L., Klyszejko, A. L., Muller, D. J., Cook, G. M., Vonck, J., et al. (2009). The c13 ring from a thermoalkaliphilic ATP synthase reveals an extended diameter due to a special structural region. *J. Mol. Biol.* 388, 611–618. doi: 10.1016/j.jmb.2009.03.052

Meier, T., Yu, J., Raschle, T., Henzen, F., Dimroth, P., and Muller, D. J. (2005). Structural evidence for a constant c11 ring stoichiometry in the sodium F-ATP synthase. *FEBS J.* 272, 5474–5483. doi: 10.1111/j.1742-4658.2005.04940.x

Meier, T., Morgner, N., Matthies, D., Pogoryelov, D., Keis, S., Cook, G. M., et al. (2007). A tridecameric c ring of the adenosine triphosphate (ATP) synthase from the thermoalkaliphilic Bacillus sp. strain TA2.A1 facilitates ATP synthesis at low electrochemical proton potential. *Mol. Microbiol.* 65, 1181–1192. doi: 10.1111/j.1365-2958.2007.05857.x

Meyer Zu Tittingdorf, J. M. W., Rexroth, S., Schafer, E., Schlichting, R., Giersch, C., Dencher, N. A., et al. (2004). The stoichiometry of the chloroplast ATP synthase oligomer III in Chlamydomonas reinhardtii is not affected by the metabolic state. *Biochim. Biophys. Acta* 1659, 92–99. doi: 10.1016/j.bbabio.2004.08.008

Mitchell, P. (1961). Coupling of phosphorylation to electron and hydrogen transfer by a chemi-osmotic type of mechanism. *Nature* 191, 144–148. doi: 10.1038/191144a0

Mitchell, P. (1966). Chemiosmotic coupling in oxidative and photosynthetic phosphorylation. *Biol. Rev. Camb. Philos. Soc.* 41, 445–502. doi: 10.1111/j.1469-185X.1966.tb01501

Moore, A. L., Rich, P. R., Douce, R., and Day, R. A. (1985). "Organization of the Respiratory Chain and Oxidative Phosphorylation," in *Higher Plant Cell Respiration*. Eds. R. Douce and D. A. Day (Berlin: Springer), 134–172.

Morales, A., Yin, X., Harbinson, J., Driever, S. M., Molenaar, J., Kramer, D. M., et al. (2018). In silico analysis of the regulation of the photosynthetic electron transport Chain in C3 Plants. *Plant Physiol.* 176, 1247–1261. doi: 10.1104/pp.17.00779

Muller, D. J., Dencher, N. A., Meier, T., Dimroth, P., Suda, K., Stahlberg, H., et al. (2001). ATP synthase: constrained stoichiometry of the transmembrane rotor. *FEBS Lett.* 504, 219–222. doi: 10.1016/S0014-5793(01)02708-9

Mullineaux, C. W. (2014). Co-existence of photosynthetic and respiratory activities in cyanobacterial thylakoid membranes. *Biochim. Biophys. Acta* 1837, 503–511. doi: 10.1016/j.bbabio.2013.11.017

Nakamura, Y., Kaneko, T., Sato, S., Mimuro, M., Miyashita, H., Tsuchiya, T., et al. (2003). Complete genome structure of Gloeobacter violaceus PCC 7421, a cyanobacterium that lacks thylakoids. *DNA Res.* 10, 137–145. doi: 10.1093/dnares/10.4.137

Nishio, J. N., and Whitmarsh, J. (1993). Dissipation of the proton electrochemical potential in intact chloroplasts (II. The pH gradient monitored by cytochrome f reduction kinetics). *Plant Physiol.* 101, 89–96. doi: 10.1104/pp.101.1.89

Niyogi, K. K., and Truong, T. B. (2013). Evolution of flexible non-photochemical quenching mechanisms that regulate light harvesting in oxygenic photosynthesis. *Curr. Opin. Plant Biol.* 16, 307–314. doi: 10.1016/j.pbi.2013.03.011

Noctor, G., and Foyer, C. H. (2000). Homeostasis of adenylate status during photosynthesis in a fluctuating environment. *J. Exp. Bot.* 51 Spec No, 347–356. doi: 10.1093/jexbot/51.suppl_1.347

Olsson, K., Keis, S., Morgan, H. W., Dimroth, P., and Cook, G. M. (2003). Bioenergetic properties of the thermoalkaliphilic Bacillus sp. strain TA2.A1. *J. Bacteriol.* 185, 461–465. doi: 10.1128/JB.185.2.461-465.2003

Panke, O., and Rumberg, B. (1996). Kinetic modelling of the proton translocating CF0CF1-ATP synthase from spinach. *FEBS Lett.* 383, 196–200. doi: 10.1016/0014-5793(96)00246-3

Pogoryelov, D., Yu, J., Meier, T., Vonck, J., Dimroth, P., and Muller, D. J. (2005). The c15 ring of the Spirulina platensis F-ATP synthase: F1/F0 symmetry mismatch is not obligatory. *EMBO Rep.* 6, 1040–1044. doi: 10.1038/sj.embor.7400517

Pogoryelov, D., Reichen, C., Klyszejko, A. L., Brunisholz, R., Muller, D. J., Dimroth, P., et al. (2007). The oligomeric state of c rings from cyanobacterial F-ATP synthases varies from 13 to 15. *J. Bacteriol.* 189, 5895–5902. doi: 10.1128/jb.00581-07

Pogoryelov, D., Klyszejko, A. L., Krasnoselska, G. O., Heller, E. M., Leone, V., Langer, J. D., et al. (2012). Engineering rotor ring stoichiometries in the ATP synthase. *Proc. Natl. Acad. Sci. U.S.A.* 109, E1599–E1608. doi: 10.1073/pnas.1120027109

Preiss, L., Yildiz, O., Hicks, D. B., Krulwich, T. A., and Meier, T. (2010). A new type of proton coordination in an F(1)F(o)-ATP synthase rotor ring. *PLoS Biol.* 8, e1000443. doi: 10.1371/journal.pbio.1000443

Preiss, L., Klyszejko, A. L., Hicks, D. B., Liu, J., Fackelmayer, O. J., Yildiz, O., et al. (2013). The c-ring stoichiometry of ATP synthase is adapted to cell physiological requirements of alkaliphilic Bacillus pseudofirmus OF4. *Proc. Natl. Acad. Sci. U.S.A.* 110, 7874–7879. doi: 10.1073/pnas.1303333110

Rippka, R., Waterbury, J., and Cohenbazire, G. (1974). A cyanobacterium which lacks Thylakoids. *Arch. Microbiol.* 100, 419–436. doi: 10.1007/bf00446333

Rutherford, A. W., Osyczka, A., and Rappaport, F. (2012). Back-reactions, short-circuits, leaks and other energy wasteful reactions in biological electron transfer: redox tuning to survive life in O(2). *FEBS Lett.* 586, 603–616. doi: 10.1016/j.febslet.2011.12.039

Scanlan, D. J., Ostrowski, M., Mazard, S., Dufresne, A., Garczarek, L., Hess, W. R., et al. (2009). Ecological genomics of marine picocyanobacteria. *Microbiol. Mol. Biol. Rev.* 73, 249–24+. doi: 10.1128/mmbr.00035-08

Scheibe, R. (2004). Malate valves to balance cellular energy supply. *Physiol. Plant.* 120, 21–26. doi: 10.1111/j.0031-9317.2004.0222.x

Schneider, A., Steinberger, I., Herdean, A., Gandini, C., Eisenhut, M., Kurz, S., et al. (2016). The evolutionarily conserved protein PHOTOSYNTHESIS AFFECTED MUTANT71 is required for efficient manganese uptake at the thylakoid membrane in Arabidopsis. *Plant Cell* 28, 892–910. doi: 10.1105/tpc.15.00812

Seelert, H., Poetsch, A., Dencher, N. A., Engel, A., Stahlberg, H., and Muller, D. J. (2000). Structural biology. Proton-powered turbine of a plant motor. *Nature* 405, 418–419. doi: 10.1038/35013148

Silverstein, T. P. (2014). An exploration of how the thermodynamic efficiency of bioenergetic membrane systems varies with c-subunit stoichiometry of F1F0 ATP synthases. *J. Bioenerg. Biomembr.* 46, 229–241. doi: 10.1007/s10863-014-9547-y

Smith, D. J., Stokes, B. O., and Boyer, P. D. (1976). Probes of initial phosphorylation events in ATP synthesis by chloroplasts. *J. Biol. Chem.* 251, 4165–4171.

Steigmiller, S., Turina, P., and Graber, P. (2008). The thermodynamic H+/ATP ratios of the H+-ATPsynthases from chloroplasts and Escherichia coli. *Proc. Natl. Acad. Sci. U. S. A.* 105, 3745–3750. doi: 10.1073/pnas.0708356105

Stomp, M., Huisman, J., Stal, L. J., and Matthijs, H. C. (2007). Colorful niches of phototrophic microorganisms shaped by vibrations of the water molecule. *ISME J.* 1, 271–282. doi: 10.1038/ismej.2007.59

Strand, D. D., and Kramer, D. M. (2014). "Control of Non-Photochemical Exciton Quenching by the Proton Circuit of Photosynthesis," in *Non-Photochemical Quenching and Energy Dissipation in Plants, Algae and Cyanobacteria*. Eds. B. DemmigAdams, G. Garab, W. Adams and Govindjee, (Dordrecht: Springer), 387–408. doi: 10.1007/978-94-017-9032-1_18

Strand, D. D., Fisher, N., and Kramer, D. M. (2016). *Distinct Energetics and Regulatory Functions of the Two Major Cyclic Electron Flow Pathways in Chloroplasts*. Ed. H. Kirchhoff Wymondham (Norfolk, United Kingdom: Caister Academic Press).

Sturr, M. G., Guffanti, A. A., and Krulwich, T. A. (1994). Growth and bioenergetics of alkaliphilic Bacillus firmus OF4 in continuous culture at high pH. *J. Bacteriol.* 176, 3111–3116. doi: 10.1128/jb.176.11.3111-3116.1994

Suzuki, T., Ozaki, Y., Sone, N., Feniouk, B. A., and Yoshida, M. (2007). The product of uncI gene in F1Fo-ATP synthase operon plays a chaperone-like role to assist c-ring assembly. *Proc. Natl. Acad. Sci. U. S. A.* 104, 20776–20781. doi: 10.1073/pnas.0708075105

Takizawa, K., Cruz, J. A., Kanazawa, A., and Kramer, D. M. (2007). The thylakoid proton motive force in vivo. Quantitative, non-invasive probes, energetics, and regulatory consequences of light-induced pmf. *Biochim. Biophys. Acta* 1767, 1233–1244. doi: 10.1016/j.bbabio.2007.07.006

Takizawa, K., Kanazawa, A., and Kramer, D. M. (2008). Depletion of stromal P(i) induces high "energy-dependent" antenna exciton quenching (qE) by decreasing proton conductivity at CF(O)-CF(1) ATP synthase. *Plant Cell Env.* 31, 235–243. doi: 10.1111/j.1365-3040.2007.01753.x

Turina, P., Samoray, D., and Graber, P. (2003). H+/ATP ratio of proton transport-coupled ATP synthesis and hydrolysis catalysed by CF0F1-liposomes. *EMBO J.* 22, 418–426. doi: 10.1093/emboj/cdg073

Vermaas, W. F. J. (2001). "Photosynthesis and Respiration in Cyanobacteria," in *eLS* (American Cancer Society). doi: 10.1038/npg.els.0001670

Viola, S., Bailleul, B., Yu, J., Nixon, P., Selles, J., Joliot, P., et al. (2019). Probing the electric field across thylakoid membranes in cyanobacteria. *Proc. Natl. Acad. Sci. U. S. A.* 116, 21900–21906. doi: 10.1073/pnas.1913099116

von Ballmoos, C., Cook, G. M., and Dimroth, P. (2008). Unique rotary ATP synthase and its biological diversity. *Annu. Rev. Biophys.* 37, 43–64. doi: 10.1146/annurev.biophys.37.032807.130018

von Ballmoos, C., Wiedenmann, A., and Dimroth, P. (2009). Essentials for ATP synthesis by F1F0 ATP synthases. *Annu. Rev. Biochem.* 78, 649–672. doi: 10.1146/annurev.biochem.78.081307.104803

Vonck, J., von Nidda, T. K., Meier, T., Matthey, U., Mills, D. J., Kuhlbrandt, W., et al. (2002). Molecular architecture of the undecameric rotor of a bacterial Na +-ATP synthase. *J. Mol. Biol.* 321, 307–316. doi: 10.1016/S0022-2836(02)00597-1

Vos, M. H., van Gorkom, H. J., and van Leeuwen, P. J. (1991). An electroluminescence study of stabilization reactions in the oxygen-evolving complex of Photosystem II. *Biochim. Biophys. Acta* 1056, 27–39. doi: 10.1016/s0005-2728(05)80069-6

Walker, B. J., Strand, D. D., Kramer, D. M., and Cousins, A. B. (2014). The response of cyclic electron flow around photosystem I to changes in photorespiration and nitrate assimilation. *Plant Physiol.* 165, 453–462. doi: 10.1104/pp.114.238238

Walker, J. E. (2013). The ATP synthase: the understood, the uncertain and the unknown. *Biochem. Soc. Trans.* 41, 1–16. doi: 10.1042/bst20110773

Watt, I. N., Montgomery, M. G., Runswick, M. J., Leslie, A. G., and Walker, J. E. (2010). Bioenergetic cost of making an adenosine triphosphate molecule in animal mitochondria. *Proc. Natl. Acad. Sci. U.S.A.* 107, 16823–16827. doi: 10.1073/pnas.1011099107

Zaharieva, I., Wichmann, J. M., and Dau, H. (2011). Thermodynamic limitations of photosynthetic water oxidation at high proton concentrations. *J. Biol. Chem.* 286, 18222–18228. doi: 10.1074/jbc.M111.237941

Zaks, J., Amarnath, K., Kramer, D. M., Niyogi, K. K., and Fleming, G. R. (2012). A kinetic model of rapidly reversible nonphotochemical quenching. *Proc. Natl. Acad. Sci. U.S.A.* 109, 15757–15762. doi: 10.1073/pnas.1211017109

Zhang, R., Cruz, J. A., Kramer, D. M., Magallanes-Lundback, M. E., Dellapenna, D., and Sharkey, T. D. (2009). Moderate heat stress reduces the pH component of the transthylakoid proton motive force in light-adapted, intact tobacco leaves. *Plant. Cell Environ.* 32, 1538–1547. doi: 10.1111/j.1365-3040.2009.02018.x

Conflict of Interest: The authors declare that the research was conducted in the absence of any commercial or financial relationships that could be construed as a potential conflict of interest.

frontiers in Plant Science

ORIGINAL RESEARCH
published: 26 February 2020
doi: 10.3389/fpls.2020.00103

Efficient Photosynthetic Functioning of *Arabidopsis thaliana* Through Electron Dissipation in Chloroplasts and Electron Export to Mitochondria Under Ammonium Nutrition

Anna Podgórska[1], Radosław Mazur[2], Monika Ostaszewska-Bugajska[1], Katsiaryna Kryzheuskaya[1], Kacper Dziewit[1], Klaudia Borysiuk[1], Agata Wdowiak[1], Maria Burian[1], Allan G. Rasmusson[3] and Bożena Szal[1]*

[1] Institute of Experimental Plant Biology and Biotechnology, Faculty of Biology, University of Warsaw, Warsaw, Poland, [2] Institute of Biochemistry, Faculty of Biology, University of Warsaw, Warsaw, Poland, [3] Department of Biology, Lund University, Lund, Sweden

OPEN ACCESS

Edited by:
Ko Noguchi,
Tokyo University of Pharmacy and Life Sciences, Japan

Reviewed by:
Dinakar Challabathula,
Central University of Tamil Nadu, India
Toru Hisabori,
Tokyo Institute of Technology, Japan

***Correspondence:**
Anna Podgórska
apodgorski@biol.uw.edu.pl

Specialty section:
This article was submitted to Plant Physiology, a section of the journal Frontiers in Plant Science

Received: 30 October 2019
Accepted: 23 January 2020
Published: 26 February 2020

Citation:
Podgórska A, Mazur R, Ostaszewska-Bugajska M, Kryzheuskaya K, Dziewit K, Borysiuk K, Wdowiak A, Burian M, Rasmusson AG and Szal B (2020) Efficient Photosynthetic Functioning of Arabidopsis thaliana Through Electron Dissipation in Chloroplasts and Electron Export to Mitochondria Under Ammonium Nutrition. Front. Plant Sci. 11:103. doi: 10.3389/fpls.2020.00103

An improvement in photosynthetic rate promotes the growth of crop plants. The sink-regulation of photosynthesis is crucial in optimizing nitrogen fixation and integrating it with carbon balance. Studies on these processes are essential in understanding growth inhibition in plants with ammonium (NH_4^+) syndrome. Hence, we sought to investigate the effects of using nitrogen sources with different states of reduction (during assimilation of NO_3^- versus NH_4^+) on the photosynthetic performance of *Arabidopsis thaliana*. Our results demonstrated that photosynthetic functioning during long-term NH_4^+ nutrition was not disturbed and that no indication of photoinhibition of PSII was detected, revealing the robustness of the photosynthetic apparatus during stressful conditions. Based on our findings, we propose multiple strategies to sustain photosynthetic activity during limited reductant utilization for NH_4^+ assimilation. One mechanism to prevent chloroplast electron transport chain overreduction during NH_4^+ nutrition is for cyclic electron flow together with plastid terminal oxidase activity. Moreover, redox state in chloroplasts was optimized by a dedicated type II NAD(P)H dehydrogenase. In order to reduce the amount of energy that reaches the photosynthetic reaction centers and to facilitate photosynthetic protection during NH_4^+ nutrition, non-photochemical quenching (NPQ) and ample xanthophyll cycle pigments efficiently dissipate excess excitation. Additionally, high redox load may be dissipated in other metabolic reactions outside of chloroplasts due to the direct export of nucleotides through the malate/oxaloacetate valve. Mitochondrial alternative pathways can downstream support the overreduction of chloroplasts. This mechanism correlated with the improved growth of *A. thaliana* with the overexpression of the alternative oxidase 1a (AOX1a) during NH_4^+ nutrition. Most remarkably, our findings

demonstrated the capacity of chloroplasts to tolerate NH_4^+ syndrome instead of providing redox poise to the cells.

Keywords: nitrogen assimilation, ammonium toxicity syndrome, photosynthetic efficiency, redox dissipation, alternative oxidase, oxidative damage, non-photochemical quenching, redox export

INTRODUCTION

Photosynthesis enables several anabolic reactions and provides energy for the metabolism and growth of plants. Unfavorable changes in the environment are quickly perceived by plants to minimize disturbances in electron transport flows. Different stress factors, such as changes in light intensity or nutrient availability, affect the intracellular metabolism of plants, and consequently, fluctuations in energy or redox state develop in cells. One natural factor, which directly affects chloroplast redox state, is the use of different nitrogen sources. Electrons (é) from the photosynthetic electron transport chain (chlETC) can be used for nitrogen assimilation into amino acids. The bioenergetically expensive version involves the nourishment of plants with nitrate (NO_3^-), which initially undergoes a two-step reduction. In this case, NO_3^- reduction is expected to consume up to 20% of the total reductants produced by photosynthetic light reactions (Noctor and Foyer, 1998) because of the activity of nitrite reductase (NiR) accepting 6é and of 2-oxoglutarate aminotransferase (GOGAT) accepting 2é. The efficiency of their function is dependent on the transfer of electrons directly from reduced ferredoxin (Fd), and consequently they compete with ferredoxin $NADP^+$ oxidoreductase (FNR), thereby decreasing the nicotinamide adenine dinucleotide phosphate (NADPH) formation. The alternative to NO_3^- assimilation is the instant growth of plants on ammonium (NH_4^+), which does not need to be reduced, thereby saving much of the cell's reducing power. Surprisingly, when plants are nourished with NH_4^+ as the sole source of nitrogen, developmental disorders arise (Britto and Kronzucker, 2002; Bittsánszky et al., 2015; Esteban et al., 2016). Most crop plants show strong growth inhibition and other toxicity symptoms (Podgórska and Szal, 2015; Liu and von Wirén, 2017) in response to NH_4^+ nutrition, making this condition largely considered to be a severe one. However, the cause of this syndrome is yet to be elucidated. It was previously hypothesized that NH_4^+ could primarily act as a photophosphorylation uncoupler and could consequently disrupt photosynthesis, but this was negated, considering that free NH_4^+ could not accumulate to dangerously high concentrations in plant tissues (Gerendás et al., 1997; Zhu et al., 2000). After NH_4^+ ions are taken up, they are quickly incorporated into amino acids through continuous GOGAT activity to prevent poise of the cell. It was further hypothesized that during stress conditions, that are causing the overreduction of chloroplasts, including NH_4^+ nutrition, this could consequently lead to photoinhibition (Zhu et al., 2000; Guo et al., 2005). Moreover, when NADPH is accumulating and not enough terminal acceptor sides ($NADP^+$) are available for the chlETC electron flow, the receiving molecule would be molecular oxygen (O_2) in the Mehler reaction that results in the formation of reactive oxygen species (ROS). In our previous study, we have demonstrated that in contrast to whole tissues or plant mitochondria, in chloroplasts neither overreduction nor signs of oxidative stress were detected during the long-term growth of *Arabidopsis thaliana* with NH_4^+ (Podgórska et al., 2013). Yet how chloroplasts can deal with the rigorous changes in redox homeostasis during NH_4^+ nutrition has remained unknown.

The safe function of photosynthetic light reactions is based on the synchronized activity of photosystem I (PSI) and photosystem II (PSII) in the linear photosynthetic electron transfer (LET) chain. Hence, efficient electron sinks for PSI are highly desired to minimize the risk of photoinhibitory conditions and ROS generation when NH_4^+ is supplied. The Mehler reaction can also be considered as electron drainage, considering that one electron is reconstituted for superoxide anion radical ($O_2^{\cdot-}$) generation. In order to promptly minimize the damage, superoxide dismutase (SOD) reduces $O_2^{\cdot-}$ to hydrogen peroxide (H_2O_2), which is scavenged in an ascorbate-dependent reaction. Hence, potent antioxidant systems are necessary to reduce ROS accumulation in chloroplasts. Plants also have other mechanisms to prevent photodamage, and they accomplish so by utilizing excess reductants when the photon flux density exceeds the energy requirement of CO_2 fixation, nitrogen assimilation, and other anabolic reactions. One of the mechanisms that balance reductants and energy demand is cyclic electron transport (CET), which functions in the chlETC without the accumulation of NADPH (Munekage et al., 2002). This cycle is branched into two independent pathways, including the NADH dehydrogenase-like (NDH) complex constitutively associating with PSI and the route mediated by proton gradient regulation 5 (PGR5) and PGR5-like photosynthetic phenotype 1 (PGRL1) proteins (Suorsa et al., 2016). Furthermore, the plastid terminal oxidase (PTOX), can receive electrons from the plastoquinol (PQH_2) pool. Another way to prevent redox input at PSI is to limit the electron flow from PSII. Also damage to PSII is a valid risk. Excess light energy absorbed by the antenna proteins of PSII can be dissipated as heat through the non-photochemical quenching (NPQ) process, which consists of four components. The major component of NPQ is qE, which involves the dissipation of excess light energy in the antenna light-harvesting complex II (LHCII) to heat before it reaches the reaction center. Another component is the state transition (qT), which occurs when light adsorption is balanced between the photosystems through the relocation of LHCII proteins in proximity to PSI. Another important component of NPQ is the temporary photoinhibition of PSII (qI), an effect that can be induced by the damage of D1 protein in PSII. Another component is the zeaxanthin dependent quenching (qZ), in which xanthophyll cycle carotenoids trigger NPQ after the

conversion of violaxanthin to zeaxanthin in the process of de-epoxidation.

The main metabolic pathway influencing the redox and energy state of chloroplasts is the Calvin-Benson-Bassham (CBB) cycle, which starts with the carboxylation activity of ribulose-1,5-bisphosphate-carboxylase/oxygenase (RUBISCO). The regulation of the redox status of the chloroplasts is also accomplished through photorespiration, a process initiated by the oxygenase activity of RUBISCO. In the photorespiratory metabolic pathway, the reactions localized in the chloroplasts, peroxisomes, and mitochondria are engaged. Moreover, a direct way to regulate the chloroplastic redox homeostasis is the redox-shuttling activity of the oxaloacetate/malate (OAA/Mal) valve (Selinski and Scheibe, 2014). The reduction of oxaloacetate to malate by the $NADP^+$-dependent malate dehydrogenase ($NADP^+$-MDH) gives rise to malate export from chloroplast. Subsequently, malate is then transported from the cytosol to the mitochondrial matrix. Both the processes of photorespiration and the OAA/Mal valve can be seen as the transfer of reducing power from chloroplasts to mitochondria. In these processes, mitochondrial NADH is produced by the activity of glycine carboxylase complex (GDC) or mitochondrial NAD^+-MDH respectively.

Mitochondria are essential as downstream electron acceptors during NH_4^+ nutrition (Guo et al., 2005). External or internal type II dehydrogenases can directly accept electrons, alternatively to complex I (NADH dehydrogenase), in the mitochondrial electron transport chain (mtETC), but this process cannot be completed without the alternative oxidase (AOX), which has the unique function of transporting electrons from reduced ubiquinone to molecular oxygen (Vanlerberghe, 2013). Clearly, these alternative pathways are important in preventing overreduction in chloroplasts and in balancing whole-cell redox state (Vishwakarma et al., 2015). In transgenic plants, there is strong evidence that the major role of AOX is to prevent ROS production in the mtETC (Cvetkovska and Vanlerberghe, 2012). The most abundant AOX gene in *Arabidopsis* is *AOX1a,* and it responds to several stresses (Clifton et al., 2006).

Although it has been widely accepted that nitrogen assimilation is closely linked with photosynthetic performance, their primary effects on plant functioning are yet to be characterized. Moreover, the effects of different nitrogen growth regimes, differing in their reduction state whether NO_3^- or NH_4^+ is used as a nutrient, can affect these processes. In this study, we aimed to determine the major protecting machinery of the photosynthetic apparatus of plants challenged with NH_4^+ nutrition. This knowledge is vital in understanding the fine-tuning of photosynthesis and the resistance of plants to environmental stresses.

MATERIALS AND METHODS

Plant Samples and Growth Conditions

Experiments were performed on *A. thaliana* ecotype Columbia-0 wild type (WT) and on derived transgenic plants, which were transformed with *AOX1a* under the control of the CaMV 35S promoter selected by Umbach et al. (2005). The incorporation of sense-constructs gave rise to the overexpressor (XX-2) mutants, while the insertion of the antisense-construct created the suppressor (AS-12) line. After their seed germination in 1% agar in ½ x Murashige & Skoog for one week, the plants were supplemented with nutrient medium (Lasa et al., 2002). The hydroponics cultures in an Araponics growth system (Liege, Belgium) were established for 8 weeks, while the liquid medium was renewed twice a week. The plants were differentiated into receiving either of the two exclusive sources of nitrogen: 5 mM NO_3^- or 5 mM NH_4^+, as previously done by Podgórska et al. (2013). The culture was maintained for 8 h in 150 µmol m^{-2} s^{-1} photosynthetically active radiation (PAR; daylight and warm white 1:1, LF-40W, Piła, Poland) at 21 °C and for 18 h at dark at 18 °C, during the day/night cycle. The WT plants nourished with NO_3^- were considered as the control. All the assays were carried out on leaf samples or organelles isolated at 12:00, after 3 h of illumination.

To analyze their phenotypic distinction, several rosettes were randomly harvested from independent plant cultures grown with either NO_3^- or NH_4^+. Subsequently, their respective fresh weight (FW) was determined.

Parameters of Photosynthetic Performance

In vivo gas exchange parameters on well-developed leaves were determined using an infrared gas analyzer (LI-6800; LI-COR, Lincoln, NE, USA). The photosynthetic rate of each leaf was measured at atmospheric CO_2 concentration of 400 µmol CO_2 mol^{-1} air at 22 °C and under the light intensity of 150 µmol photons m^{-2} s^{-1} at 90% red light with 70% humidity. The net assimilation rate (A_{net}) of CO_2 was calculated per leaf area.

Chlorophyll (chl) *a* fluorescence images were recorded using the Maxi version of Imaging-PAM chlorophyll fluorescence system (Heinz Walz, Germany). Before they were measured, the *A. thaliana* rosettes were dark-adapted for at least 30 min. The fluorescence images were recorded with a resolution of 640 × 480 pixels and with the camera parameters set to avoid saturation of the charge-coupled device (CCD) wells. Minimal (F_0) fluorescence was determined using weak blue modulating light of 0.5 µmol photons m^{-2} s^{-1}, whereas maximal (F_M) fluorescence was measured through 0.84 s of saturation blue light pulse with 2,700 µmol photons m^{-2} s^{-1}. After 60 s of dark relaxation the blue actinic light of 391 µmol photons m^{-2} s^{-1} was employed, and saturation pulses at 20-s time intervals were applied. After 200 s, actinic light was switched off, and additional saturation pulses for approximately 15 min of dark relaxation were applied. At all saturation pulses, the maximum (F_M') fluorescence values were measured, and the minimum (F_0') fluorescence was calculated as $F_0' = F_0(F_V/F_M + F_0/F_M')$. The recorded data were analyzed using ImagingWinGigE software. The photosynthetic parameters: F_V/F_M, Y(II), NPQ, and qL were calculated according to the formulae previously specified by Mazur et al. (2016). The qE and qI components of NPQ ware calculated according to Müller et al. (2001).

Isolation of Chloroplasts and Thylakoids

Intact chloroplasts were isolated, according to the method of Romanowska and Albertsson (1994) with minor modifications. Each fresh leaf tissue weighing 2 g was homogenized using a knife blender in 40-mL cool preparation medium composed of 4-(2-hydroxyethyl)-1-piperazineethanesulfonic acid HEPES-KOH with pH 7.4, 330 mM mannitol, 1 mM $MgCl_2$, 5 mM NaCl, 1 mM ethylenediaminetetraacetic acid (EDTA), and 10 mM NaF. After its filtration through an 80-µm nylon mesh, each homogenate was centrifuged at 3,600 × g for 6 min. The pellet was resuspended in suspension buffer containing 20 mM HEPES-KOH with pH 7.4, 330 mM sorbitol, 1 mM $MgCl_2$, 5 mM NaCl, and 10 mM NaF and was washed twice using the same washing buffer. The isolated chloroplasts were ground in potter homogenizer.

Thylakoid membranes were isolated according to Garstka et al. (2005) as modified in Garstka et al. (2007). Each fresh leaf tissue weighing 2 g was homogenized using a knife blender in 40-ml cool preparation medium composed of 20 mM Tricine-NaOH with pH 7.5, 330 mM sorbitol, 40 mM L-ascorbic acid, 15 mM NaCl, 4 mM $MgCl_2$, and 10 mM NaF. After its filtration through an 80-µm nylon mesh, the homogenate was centrifuged for 4 min at 2,000 × g. The pellet was agitated in a buffered medium (20 mM Tricine–NaOH with pH 7.0, 15 mM NaCl, and 4 mM $MgCl_2$) and subsequent centrifugation at 6,000 × g for 10 min was performed. The obtained thylakoid membranes were washed twice in suspension buffer.

Evaluation of Photochemical Efficiency

The electron flow between both photosystems was assayed as light dependent oxygen evolution in the Clark electrode (Hansatech). The maximum photochemical capacity of PSII and PSI was measured in isolated chloroplasts using 0.1 mM methylviologen (MV) as an electron acceptor and with 5 mM sodium azide.

The corresponding maximal capacities of PSI and PSII were spectrophotometrically measured, as described by Vernon and Cardon (1982). The total activity of PSI in light was determined as the oxidation of 0.2 mM N,N,N′,N′-tetramethyl-*p*-phenylenediamine (TMPD) with 0.5 mM MV as the electron acceptor, whereas the total activity of PSII was measured in isolated chloroplasts as the direct reduction of 0.1 mM 2,6-dichlorophenolindophenol (DCPIP).

Blue-Native PAGE and Two-Dimensional SDS PAGE Assays

For the native separation of protein complexes, blue native polyacrylamide gel electrophoresis (BN-PAGE) was performed, according to the methods of Rogowski et al. (2019) with modifications by Mazur et al. (2019). First thylakoid membranes were suspended in 1x native PAGE buffer from the sample preparation kit (Invitrogen, Carlsbad, California, USA) and were solubilized with 1% n-dodecyl β-D-maltoside (DDM). After centrifugation at 18,000 x g for 15 min, 1% Coomassie brilliant blue G-250 was added to the supernatant. Samples containing 8.3 µg of chlorophyll were separated on 4%–16%-gradient acrylamide gel (Invitrogen) in 1x anode and 1x cathode dark blue buffer (Invitrogen). During electrophoresis, the cathode buffer was changed to light blue version. Finally, the destaining of gels was performed with 0.5 M 6-aminocaproic acid in 25 mM imidazole-HCl with pH 7.0, and the gels were immediately scanned. The protein complexes were identified, and the abundance of PSI-NDH was quantified based on the densitometry of bands using Image-Lab 5.2 software (Bio-Rad), after the correction for background.

The detached protein lanes from BN-PAGE were utilized for the separation in second dimension, as described by Mazur et al. (2019). After the denaturation of the protein complexes in 125 mM Tris-HCl with pH 6.8, 5 M urea, 10% glycerol, 5% sodium dodecyl sulfate (SDS), and 5% β-mercaptoethanol for 30 min at 65°C, the gel stripes were separated in 12% acrylamide gel containing 6 M urea and 0.1% SDS. The gels were washed, and the gel staining was conducted in 0.1% silver nitrate (Shevchenko et al., 1996). The gels were scanned, and the visual analysis of the composition and arrangement of the chlorophyll protein complexes was performed.

Analysis of Protein Levels

In order to determine their protein abundance, the extracts were subjected to SDS-PAGE, as previously described in Podgórska et al. (2018). Briefly, the leaf tissues were homogenized with 3x extraction buffer. To keep the AOX and NDC proteins reduced, the samples were supplemented with 100 mM 1,4-dithiothreitol (DTT). For the measurement of protein abundance, these extracts were correspondingly used to estimate the levels of AOX1/2 (15 µl), PTOX (5 µl), ascorbate peroxidase (APX, 15 µl), glycine decarboxylase complex H subunit (GDC-H) (5 µl), serine hydroxymethyltransferase (SHMT, 2.5 µl), and hydroxypyruvate reductase (HPR, 5 µl) as well as RUBISCO (2 µl of 10x diluted extracts). Furthermore, 9 µg chl of the isolated chloroplast extracts was used to measure the abundance of NDC1, and another 9 µg chl of the isolated thylakoid extracts was utilized to evaluate the concentration of ATPase α-subunit. The Western blotting of the primary antibodies: anti-AOX diluted at 1:1000, anti-PTOX diluted at 1:4000, anti-APX diluted at 1:2000, anti-GDC-H diluted at 1:5000, anti-SHMT diluted at 1:5000, anti-HPR diluted at 1:200, anti-RUBISCO diluted at 1:5000, anti-NDC1 diluted at 1:5000, and antiATPase α-subunit diluted at 1:5000 (all from Agrisera, Vännäs, Sweden except HPR) was conducted overnight at 4°C. Then it was followed by the incubation of the anti-rabbit secondary antibody conjugated to horseradish peroxidase (HRP) (diluted at 1:25000; Bio-Rad) for 1 h at room temperature (RT). After their chemiluminescence identification, the corresponding stained polypeptides were identified based on their molecular masses. The protein levels were quantified based on the densitometry of bands using Image-Lab 5.2 software (Bio-Rad), after the correction for background.

The levels of carbonylated protein derivatives in the isolated chloroplasts were quantified, according to the methods of Juszczuk et al. (2008) with minor modifications. After derivatization using 10 mM 2,4-dinitrophenylhydrazine (DNPH) in 10% trifluoracetic acid, the extracts containing 0.55 µg of chlorophyll were separated in 10% SDS-PAGE. Antibodies to the dinitrophenyl group (diluted at 1:1000;

Sigma) were used as the primary antibodies, after which the anti-rabbit secondary antibodies (diluted 1:25000; Bio-Rad) were utilized. The amounts of oxidized proteins were visualized through chemiluminescence, and the staining intensity of the entire blot lane was quantified through densitometry using Image-Lab 5.2 software (Bio-Rad), after the correction for background.

Measurement of Enzyme Activity and Protein Content

The SOD isoforms in the isolated chloroplasts were identified in 12% native acrylamide gel, as described by Sehmer et al. (1998). The exposure of bright areas was based on the inhibition of nitroblue tetrazolium (NBT) reduction by SOD activity and was quantified through the densitometry of bands using Image-Lab 5.2 software (Bio-Rad), after the correction for background.

The activity of NAD^+-MDH was detected after the separation of foliar protein extracts in 8% native acrylamide gel, as described by Beeler et al. (2014). The enzyme activity was developed with 1 mM malate, 0.5 mM NAD^+, 0.4 mM NBT, 27 μM phenazine methosulfate, and 15 mM $MgCl_2$ in 100 mM Tris-HCl with pH 8.0. The exposure of purple formazan bands was quantified through the densitometry of bands using Image-Lab 5.2 software (Bio-Rad), after the correction for background. The activity of $NADP^+$-MDH was spectrophotometrically assayed as the NADPH-dependent reduction of OAA (Keryer et al., 2004). The maximal enzyme activity was measured after the reductive activation of extracts with 10 mM DTT for 30 min at RT.

Protein concentration was measured according to the methods of Bradford (1976) using bovine serum albumin as the standard.

Detection of Oxidative Stress-Related Metabolites

The H_2O_2 content of the leaf tissues was quantified based on the peroxidase-coupled assay, as described by Veljovic-Jovanovic et al. (2001). The accuracy of each reaction was controlled through internal standard determination, respectively applying 5 mM H_2O_2 to the same reaction mixture.

The low-mass antioxidants of leaf tissues were also measured. Ascorbic acid concentration was determined through the colorimetric bi-pirydyl method described by Okamura (1980). The levels of the reduced form of ascorbate (AsA) and dehydroascorbate (DHA) were calculated in the presence and absence of DTT.

The extent of lipid peroxidation in membranes was estimated by tracing malondialdehyde (MDA) concentration (Hodges et al., 1999). The content of MDA was corrected for interfering compounds in samples, where the specific substrate thiobarbituric acid was not added to the reaction mixture.

Quantitative Real Time Polymerase Chain Reactions

RNA isolation, complementary DNA generation, and RNAse digestion were conducted, as described by Podgórska et al. (2018). Quantitative real-time polymerase chain reactions (RT-qPCR) were performed at an annealing temperature of 60 °C for all genes. Transcript abundance was normalized to the transcript level of the reference gene protein phosphatase 2A (*PP2A*), as described by Czechowski et al. (2005), and the results were expressed in relation to the WT plants grown on NO_3^- (value of 1), according to the method of Pfaffl (2001). New primer pairs were designed for *NADP-MDH* (5'–AGGGAGATGGAGATTATGAACTTG–3' and 5'–CAGTTCCGCTTCCGACTTG–3'), *PGR5* (5'–CCATTGCCTTACACTCTCAGGT–3' and 5'–AAGCCCTTGTCTCTGTTTTGC–3'), and NAD(P)H: plastoquinone oxidoreductase subunit L (*NDHL*) (5'–CCCAACGACACTCTTCTTCATAAT–3' and 5'–TGCTAAGGCTGGATGGTCAAT–3'). The *Arabidopsis* Genome Initiative locus identifiers for the genes investigated in this study were AT5G58330 (*NADP-MDH*), AT2G05620 (*PGR5*), AT1G70760 (*NDHL*), and AT1G13320 (protein phosphatase 2A, *PP2A*).

Identification of Pigments

Chlorophyll was extracted in 80% acetone, and the concentration was calculated based on the extinction coefficients reported by Porra et al. (1989).

For the carotenoid analysis, pigments were extracted as described earlier (Szalonek et al., 2015). The extracted pigments were separated, according to the methods of Cuttriss et al. (2007) with some modifications, using Prominence HPLC system (Shimadzu). The 5-μl samples were injected into an Atlantis™ dC18 (3 μm, 100 Å, 3.0 x 150 mm) with Supelguard™ Ascentis™ C18 guard column (5 μm, 4.0 x 20 mm) and were eluted at 30°C with a constant flow rate of 1 ml min^{-1} using ethyl acetate gradient in acetonitrile, water, and triethylamine at 9:1:0.01 (v/v/v). The gradient was distributed with the following conditions: 0%–67% ethyl acetate in 1–31 min, 67%–100% ethyl acetate in 31–32 min, and 100% ethyl acetate with additional hold time of 1 min. In the next 2 min, the concentration of ethyl acetate was decreased to 0%, and the hold time was lengthened for 2 min more before the next injection. The separation of samples was monitored by the SPD-M20A prominence diode array detector (Shimadzu) at a range of 200–800 nm (1.2 nm resolution). The carotenoids were identified based on retention times and absorption spectra. For the quantification, the chromatogram at 436 nm was integrated using LCsolution v1.21 software (Shimadzu). The de-epoxidation state (DEPS) was calculated as (Z + 0.5A)/(Z + A + V), where Z, A, and V are zeaxanthin, antheraxanthin, and violaxanthin, respectively.

Statistical Analysis

All data were expressed as the mean values ± standard deviations (SD) of 3–15 measurements taken from 3–5 independent plant cultures. The experimental data from different genotypes of the plants, which were nourished with either NO_3^- or NH_4^+, were statistically analyzed through one-way analysis of variance (ANOVA) with Tukey's post-hoc test using Statistica 13.1 software (StatSoft, Inc., Tulsa, OK, USA). The results with p-value ≤ 0.05 were considered statistically significant.

RESULTS

Oxidative Stress and Antioxidant Defense in Chloroplasts

We aimed to verify if NH_4^+ nutrition is a stress factor to chloroplasts in *A. thaliana* grown with either NO_3^- or NH_4^+ as the sole source of nitrogen. As the first step, the scavenging capacity of chloroplast antioxidants was determined. The major ROS produced in the chlETC might be $O_2^{\cdot -}$, and accordingly, the activity of SOD was higher in the plants nourished with NH_4^+ (**Figure 1A**). The subsequent product of SOD activity should be H_2O_2, which would need to be further utilized. The protein levels of the thylakoid and stromal APX were higher in plants in the presence of NH_4^+ (**Figure 1B**). If ROS production could not be balanced by the antioxidant systems, it could lead to tissue damage. The peroxidation levels of the membrane lipids were lower in the chloroplasts exposed to NH_4^+ nutrition (**Figure 1C**). Similarly to the results of Podgórska et al. (2013), the carbonylation levels in the chloroplast proteins were generally lower upon NH_4^+ nutrition (**Figure 1D**).

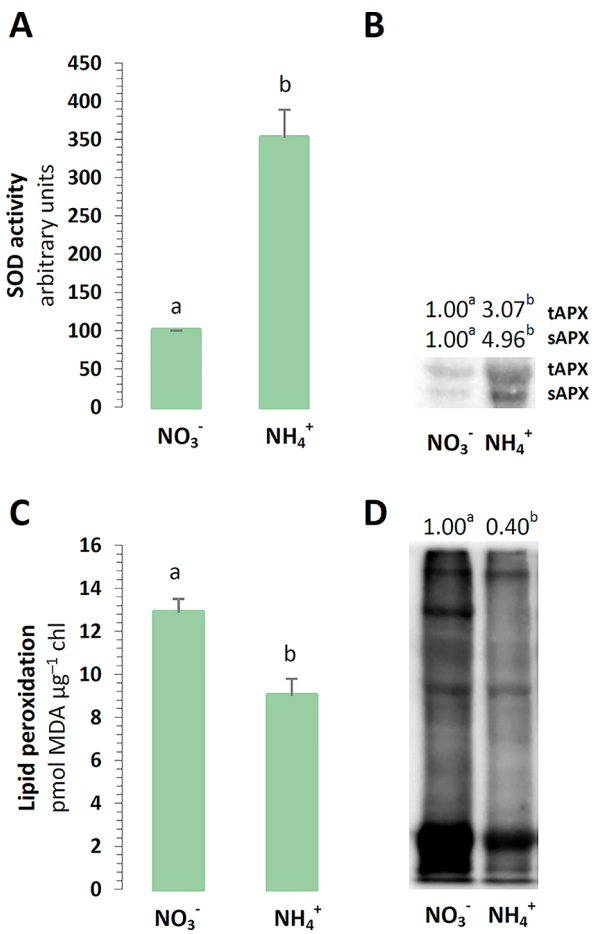

FIGURE 1 | Defense towards reactive oxygen species (ROS) and oxidative stress markers in *Arabidopsis thaliana* nourished with 5 mM NH_4^+ or 5 mM NO_3^- (control) as the only source of nitrogen. **(A)** Total activity of superoxide dismutase (SOD) in chloroplasts. **(B)** Protein abundance of thylakoid and stromal ascorbate peroxidase (tAPX, 38 kDa; sAPX, 33 kDa). **(C)** Lipid peroxidation in isolated chloroplasts. **(D)** Content of protein-bound carbonyls in chloroplasts. Representative immunoblots are shown out of n = 3–4 independent replicates. Bars or bands with different letters indicate significant difference ($p \leq 0.05$).

Photosynthetic Pigment Levels

To carry on the identification of changes in chloroplast defense, the light absorbing antennae systems of the plants were analyzed. The chl *a* and chl *b* contents of the major pigments in the leaves were not affected by the nitrogen source (**Figure 2A**). Moreover, aside from absorbing and transferring light energy, carotenoids could also serve as photoprotective agents. A cycle of three carotenoids: violaxanthin, antheraxanthin, and zeaxanthin could additionally quench overexcitation energy in the chlETC. The content of all xanthophylls was induced in the plants nourished with NH_4^+ (**Figure 2B**). Essentially, the de-epoxidation of violaxanthin to zeaxanthin could affect the efficiency of the xanthophyll cycle in photoprotection. Despite the higher total xanthophyll content, the de-epoxidation state (DEPS) was lower during NH_4^+ nutrition (**Figure 2C**). Lutein, the major xanthophyll, which could act as a protective shield, was greater in plants nourished with NH_4^+ (**Figure 2D**).

Organization of the Photosynthetic Apparatus and Antenna Complexes

Photosynthetic light reactions take place in thylakoid membranes, and their efficiency could depend on the organization of multi-subunit protein complexes and light-harvesting complexes. The BN-PAGE gels containing equal amounts of chlorophyll per lane revealed that the distribution of the major bands was intensified during NH_4^+ nutrition (**Figure 3A**). The band corresponding to megacomplexes showed significantly greater abundance of PSI-NDH in the thylakoids of the plants nourished with NH_4^+ (**Figure 3A**). To a similar extent all bands that represent supercomplexes (PSII-LHCII) were of higher abundance in thylakoids of NH4+ grown plants (**Figure 3A**). The abundance of the megacomplexes and supercomplexes were very low in the control. The only band that was identified to be less pronounced in the thylakoids of the plants under NH_4^+ nutrition was that of the ATPase complex (**Figure 3A**). To further characterize their abundances, the constituent subunit pattern of the thylakoid membrane protein complexes was analyzed after separation in the second dimension. The image of the 2D-SDS-PAGE proteins of the WT thylakoids showed a typical pattern observed in *A. thaliana* plants (**Figure 3B**). The thylakoid membranes were isolated after 3 h of light, so a PSII monomer without CP43 subunit was visible, indicating the activation of the PSII repair cycle. This band was more intensive in the thylakoids isolated from the plants under NH_4^+ nutrition. Based on the 2D-PAGE, D1 and D2 proteins (around 30 kDa), and CP47 and CP43 proteins (around 47 and 43 kDa), were more abundant in PSII dimer fractions in the plants nourished with NO_3^- (**Figure 3B**, arrowheads), while in response to NH_4^+ nutrition these proteins had higher abundance

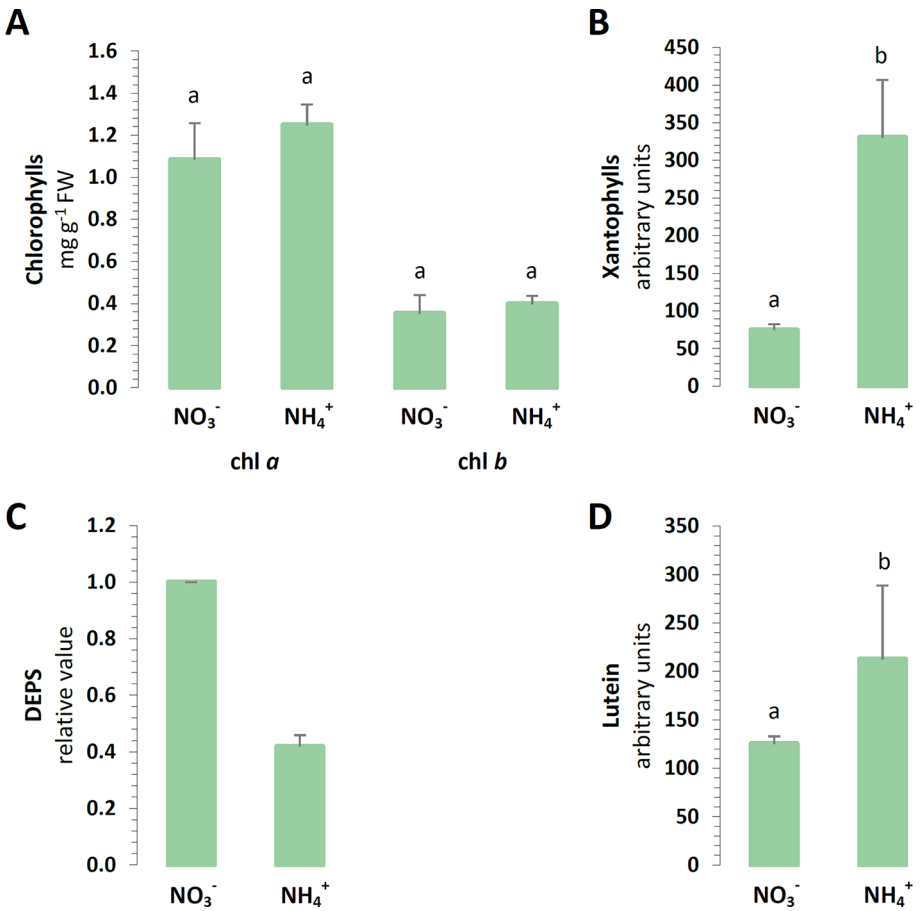

FIGURE 2 | Foliar pigment levels in *A. thaliana* nourished with 5 mM NH_4^+ or 5 mM NO_3^- (control) as the only source of nitrogen. **(A)** Levels of chlorophyll (chl) *a* and chl *b*. **(B)** Content of xanthophyll cycle pigments. **(C)** De-epoxidation state (DEPS) of xanthophylls. **(D)** Content of lutein. Bars with different letters indicate significant difference ($p \leq 0.05$).

in PSII monomer and PSII monomer without CP43 fractions (**Figure 3B**, asterisks). Moreover, considerably higher amount of CP43 was also present in CP monomer fraction (**Figure 3B**, circle) in NH_4^+ than in NO_3^- nourished plants. Taken together, these observations show that PSII repair cycle is more active under NH_4^+ nutrition.

Photosynthetic Capacity

In order to estimate the functional state of the photosynthetic apparatus of the plants, the capacity of its components was measured *in vitro*. The efficiency of the chlETC was higher during NH_4^+ nutrition (**Figure 4A**), and the activity of PSI and PSII in the presence of artificial electron acceptors was respectively induced under NH_4^+ nutrition (**Figure 4B**).

To further examine the photosynthetic efficiency of the plants under NH_4^+ nutrition, their photosynthetic yield was analyzed. During the final step of the photosynthetic light reactions, a chloroplast ATP-synthase could use the proton motive force generated by the chlETC to produce ATP. The protein level of the α-ATPase subunit was slightly lower in the plants treated with NH_4^+, but this difference was not statistically significant (**Figure 5A**). The energy gained during photosynthetic light driven reactions could be used in the CBB cycle for carbon reactions. The photosynthetic CO_2 assimilation rate was even 10 times lower in the plants nourished with NH_4^+ (**Figure 5B**). The carboxylation reaction of photosynthesis could involve RUBISCO to facilitate CO_2 fixation. A decrease in RUBISCO protein abundance was observed in the plants under NH_4^+ nutrition (**Figure 5A**).

Electron Routes in the chlETC

For their optimal energy production, the chloroplasts could branch their electron routes to recycle electrons without the accumulation of reductive power. The engagement of cyclic electron transport around PSI was initially focused on, considering that energy is produced in these reactions without NADPH accumulation. The expression of *PGR5* was induced in relation to NH_4^+ nutrition (**Figure 6A**), and also the expression of *NDHL* was upregulated in the plants treated with NH_4^+ (**Figure 6A**). Furthermore, a type II NAD(P)H-dependent

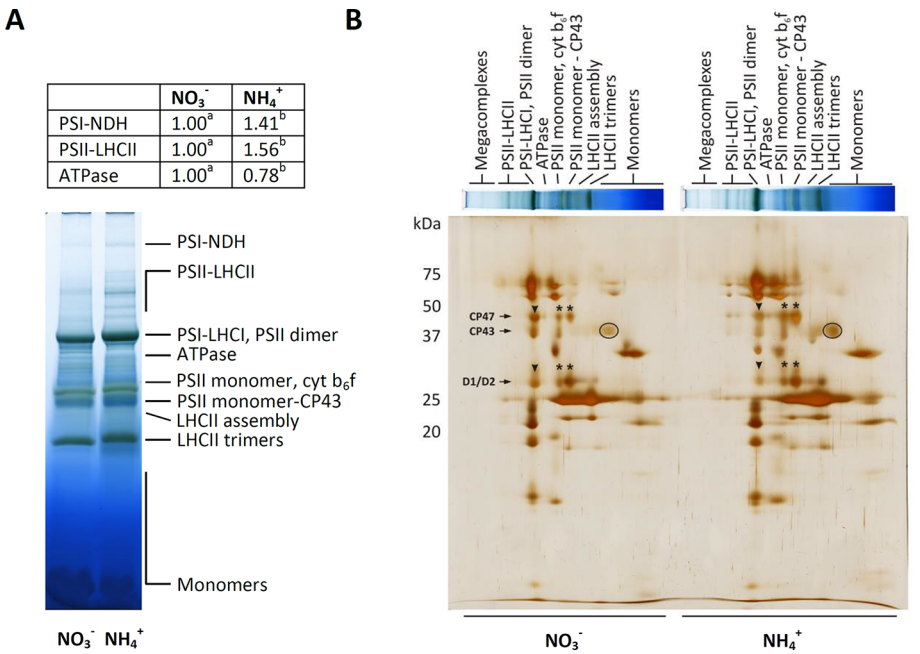

	NO_3^-	NH_4^+
PSI-NDH	1.00[a]	1.41[b]
PSII-LHCII	1.00[a]	1.56[b]
ATPase	1.00[a]	0.78[b]

FIGURE 3 | Composition of the photosynthetic protein complexes in *A. thaliana* nourished with 5 mM NH_4^+ or 5 mM NO_3^- (control) as the only source of nitrogen. **(A)** Identification of thylakoid protein complexes in Blue Native (BN)-polyacrylamide gel electrophoresis (PAGE)-gel. Thylakoid membranes were solubilized in 1% dodecyl maltoside (DDM), and the protein extracts containing 8.3 µg of chlorophyll were separated by electrophoresis. Bands with different letters quantified by densitometry indicate significant difference ($p \leq 0.05$). **(B)** Patterns of thylakoid protein complexes in second dimension by 2D-PAGE. BN-PAGE strips were denatured and separated on sodium dodecyl sulfate (SDS)-Urea-PAGE and were silver-stained. Representative gels are shown out of n = 3–6 independent replicates.

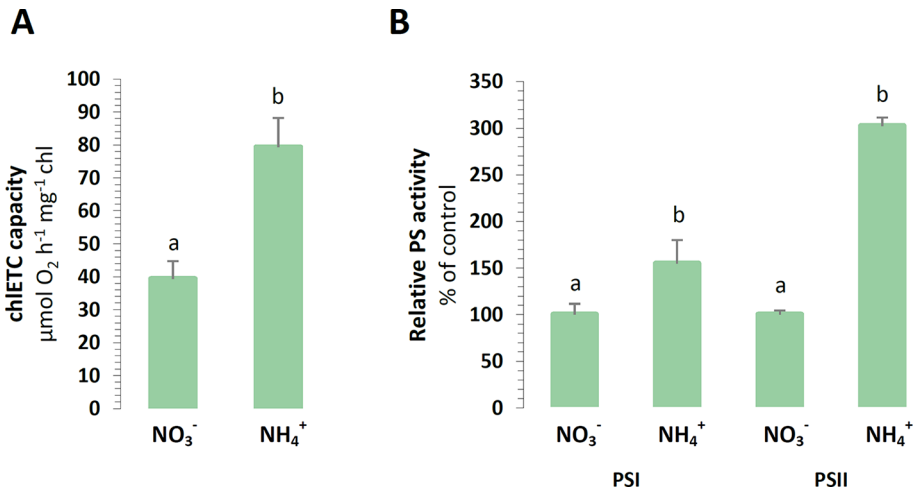

FIGURE 4 | Capacity of chloroplast electron transport chain in *A. thaliana* nourished with 5 mM NH_4^+ or 5 mM NO_3^- (control) as the only source of nitrogen. **(A)** Total electron transport chain capacity. **(B)** Capacity of Photosystem I (PSI) and Photosystem II (PSII). Bars with different letters indicate significant difference ($p \leq 0.05$).

quinone oxidoreductase that is associate with plastoglobules could reduce the PQ pool in chloroplasts. The protein abundance of the chloroplast NDC1 was higher in the plants under NH_4^+ nutrition (**Figure 6B**). Another protective function associated with PTOX could be accepting electrons from PQ, thereby competing with the chlETC. PTOX could reduce the number of electrons available for the photosynthetic electron flow, and therefore, this chlororespiratory activity would be

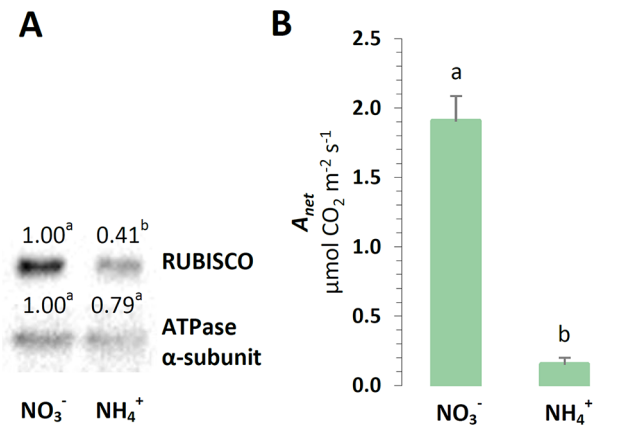

FIGURE 5 | Photosynthetic performance in *A. thaliana* nourished with 5 mM NH_4^+ or 5 mM NO_3^- (control) as the only source of nitrogen. **(A)** Protein abundance of Ribulose-1,5-bisphosphate-carboxylase/oxygenase (RUBISCO, 50 kDa) and ATPase α-subunit (α-ATPase, 55 kDa). Representative immunoblots are shown out of n = 3–4 independent replicates. **(B)** Photosynthesis net rate (A_{net}). Bars or bands with different letters indicate significant difference ($p \leq 0.05$).

required upon the fluctuation of the reduction status of the chloroplast. The protein levels of PTOX incrementally increased in the plants nourished with NH_4^+ (**Figure 6B**).

Pathways Engaged in the Export of Reductants Out of Chloroplasts

It has been postulated that the photorespiratory cycle not only recovers carbon, but it also mediates the partitioning of metabolites between chloroplast peroxisomes and mitochondria and facilitates the net oxidation of NADPH in the process. Nevertheless, the analyzed enzymes related to photorespiration were unaffected in the plants grown on different nitrogen sources. No changes in the protein levels of mitochondrial GDC-H, SHMT, or peroxisomal HPR were detected during NH_4^+ nutrition (**Figure 7A**).

Another enzyme responsible for the direct export of reductive power out of chloroplasts could be NADP-MDH, so it was investigated whether the electron flow through the OAA/Mal valve would lead to reductant dissipation in the mitochondria. The maximal enzyme activity and expression of chloroplast *NADP-MDH* was strongly upregulated in all the plants nourished with NH_4^+ (**Figures 7B, C**). Hence, the activity of the other forms of NAD-MDH was vital to the drainage of electrons into the mitochondria, as it was induced in the plants during NH_4^+ nutrition (**Supplementary Figure 8B**).

Efficiency of Photosynthesis and NPQ

The photochemistry of PSII was measured *in vivo* in the dark-adapted leaves of all the plants. The maximal quantum yield of PSII (F_V/F_M) was marginally increased in the WT plants nourished with NH_4^+, compared to those under NO_3^- nutrition (**Figure 8A**). To further explore the role of AOX1a in chloroplast functioning under NH_4^+ nutrition, the photosynthetic performance of the transgenic plants was analyzed. In the AS-12 and XX-2 mutants, the F_V/F_M values were minimally increased in the plants nourished with NH_4^+, compared to those under NO_3^- nutrition (**Figure 8A**). In the dark-adapted WT plants nourished with NO_3^- and illuminated with actinic light of high intensity, the effective quantum yield of PSII-Y(II) gradually increased, whereas in those under steady-state light conditions at the end of illumination, the quantum yield reached approximately 0.3, which was higher than 0.23 in the plants nourished with NH_4^+ (**Figure 8B**). After the dark recovery phase of WT plants, the Y(II) parameter reaches a higher value under

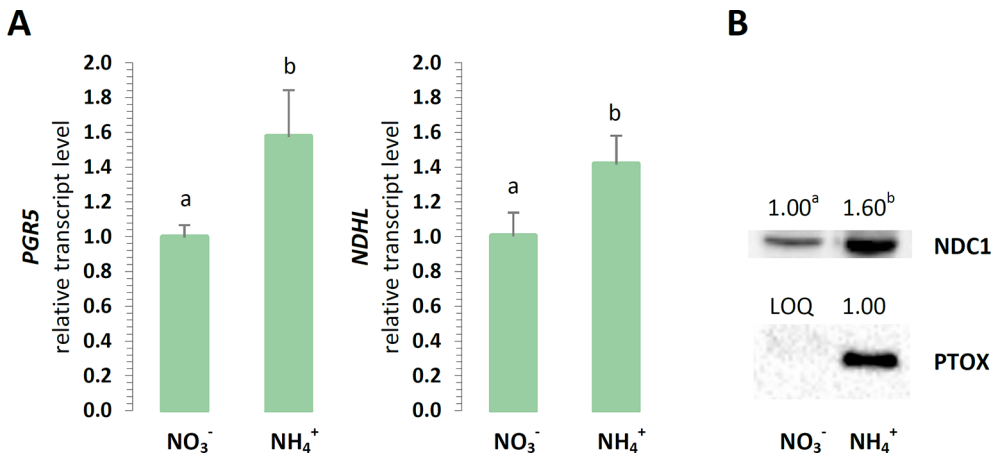

FIGURE 6 | Electron dissipation from the chloroplast electron transport chain in *A. thaliana* nourished with 5 mM NH_4^+ or 5 mM NO_3^- (control) as the only source of nitrogen. **(A)** Transcript levels of NAD(P)H:plastoquinone oxidoreductase subunit L (*NDHL*) and proton gradient regulation 5 (*PGR5*). The relative expression was set to 1 in WT plants grown with NO_3^- (control) for reference. **(B)** Protein abundance of NAD(P)H dehydrogenase C1 (NDC1, 51 kDa) and plastid terminal oxidase (PTOX, 37 kDa; LOQ, under limit of quantification). Representative immunoblots are shown out of n = 3–4 independent replicates. Bars or bands with different letters indicate significant difference ($p \leq 0.05$).

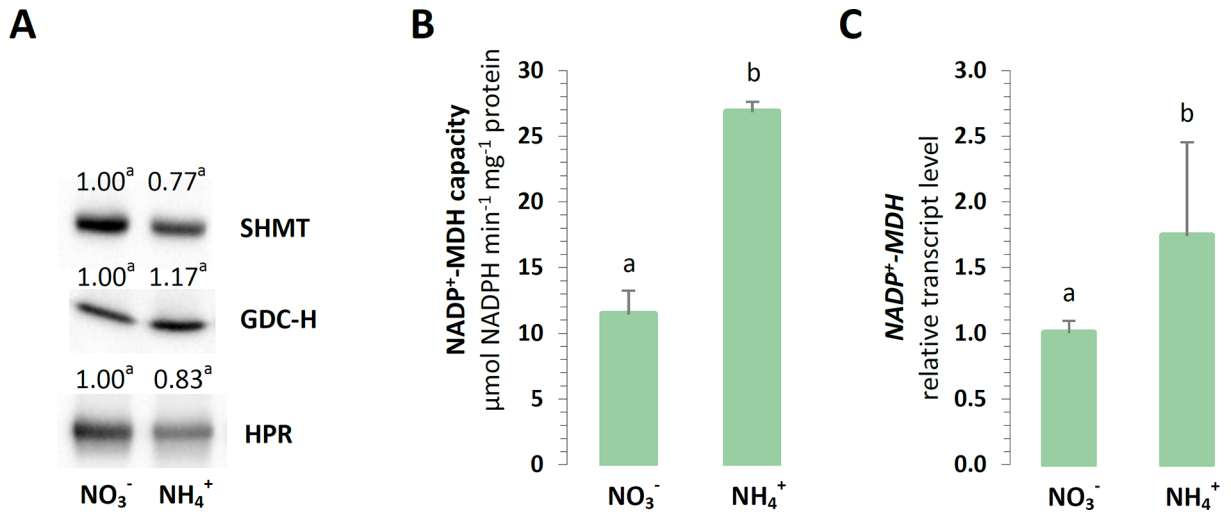

FIGURE 7 | Export of reductants out of chloroplasts in *A. thaliana* nourished with 5 mM NH_4^+ or 5 mM NO_3^- (control) as the only source of nitrogen. **(A)** Protein abundance of mitochondrial serine hydroxymethyltransferase (SHMT, 53 kDa); mitochondrial glycine decarboxylase complex H subunit (GDC-H, 16 kDa); and peroxisome hydroxypyruvate reductase (HPR, 43 kDa). Representative immunoblots are shown out of n = 3–4 independent replicates. **(B)** Capacity of NADP-malate dehydrogenase (NADP-MDH). **(C)** Transcript level of chloroplast *NADP-MDH*. The relative expression is set to 1 in WT plants grown with NO_3^- (control) for reference. Bars or bands with different letters indicate significant difference ($p \leq 0.05$).

NH_4^+ nutrition (**Figures 8B, C**), which corresponds to higher F_V/F_M values, than in the control (**Figure 8A**). In the AS-12 mutant, there was no significant difference in the time course of Y(II) during illumination in both treatments, but the values of the steady-state Y(II) reached around 0.2 (**Figure 8B**). The response of the XX-2 mutant in both the NO_3^- or NH_4^+ conditions was similar to those of the WT plants, but the Y(II) values in the XX-2 mutant were lower than those in the WT plants (**Figure 8B**).

Given that chlorophyll fluorescence could reflect the photoprotection-related effects in chloroplasts, the NPQ of the excess light energy that was absorbed could discriminate between AOX1a antisense and an overexpressor mutants grown on different nitrogen sources. The NPQ value in the WT plants nourished with NO_3^- rapidly increased to its maximum and remained stable towards the end of illumination (**Figure 8B**). In contrast, in the plants nourished with NH_4^+, the rise in NPQ was more gradual, compared to those under NO_3^- nutrition, but the increase lasted throughout the illumination. Moreover, in the steady-state conditions, the NPQ values of the plants under NH_4^+ nutrition were 50% higher than those of the plants during NO_3^- nutrition (**Figure 8B**). After the dark recovery phase, the NPQ values were still the same, indicating that the photoinhibition of PSII was similar in both treatments. In contrast to the corresponding results in the WT plants, there was no difference in the initial phase of the NPQ increase in the AS-12 mutant in both treatments. Furthermore, the NPQ values under steady-state conditions were similar to those observed in the WT plants (**Figure 8B**). The NPQ changes in the XX-2 mutant were similar to those in the WT plants in both treatments (**Figure 8B**). The photochemical quenching parameter (qL) in the WT plants nourished with NO_3^- was higher than in those with NH_4^+ nutrition, and after the dark recovery phase, the qL value was fully restored (**Figure 8B**). There was no difference in the qL of the AS-12 mutant in both treatments, whereas the qL values of the XX-2 mutant were similar to those of the WT plants (**Figure 8B**).

Phenotype and Oxidative Stress Markers During the Overexpression or Suppression of AOX1a

Considering that AOX is crucial to the redox regulation of photosynthetic organisms (Noguchi and Yoshida, 2007; Rasmusson et al., 2008), the occurrence of NH_4^+ nutrition-related oxidative stress was analyzed in the plant tissues modified for the protein abundance of AOX1a (**Supplementary Figure 1**). The growth of WT plants was generally reduced when NH_4^+ was used as the sole nitrogen source, compared to when NO_3^- was utilized. The rosette size and FW of the antisense AOX1a mutants were unchanged in the WT plants in both conditions, while the overexpression of AOX1a resulted in improved growth parameters (**Figure 9A**). The FW of XX-2 mutants was approximately 15% higher when they were nourished with NO_3^- and even 50% higher under NH_4^+ nutrition, compared to the FW of the WT plants.

To assess the impact of AOX1a on the occurrence of stress in the plants in response to NH_4^+ nutrition, their ROS and antioxidant levels were determined. NH_4^+ nutrition augmented the H_2O_2 content of the leaf tissues in all genotypes (**Figure 9B**). The major low-mass antioxidant is ascorbate, and the total ascorbate pool was substantially enlarged in the AS-12 mutant

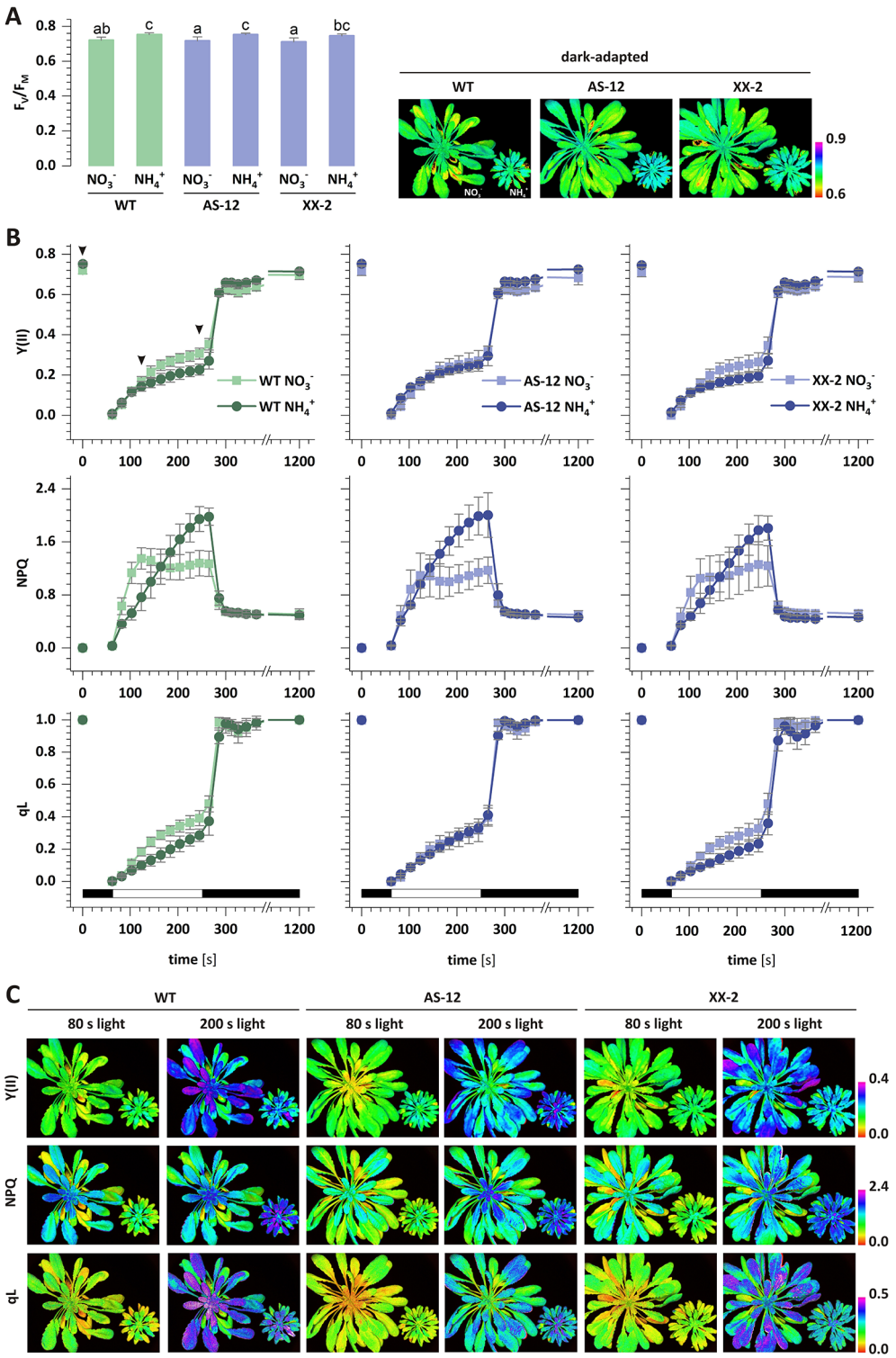

FIGURE 8 | The efficiency of photosynthetic light reactions in transgenic *AOX1a* (antisense, AS-12 or overexpression, XX-2) or WT plants nourished with 5 mM NH_4^+ or 5 mM NO_3^- (control) as the only source of nitrogen. Photosynthetic parameters: **(A)** F_V/F_M; and **(B)** Y(II), non-photochemical quenching (NPQ) and qL were measured during actinic light illumination of dark-adapted plants, followed by a dark recovery phase. **(C)** Images represent the distribution of the respective parameter values in *A. thaliana* rosettes in two time points: 80 s and 200 s of actinic illumination and in dark-adapted state (only for F_V/F_M). Selected time points are indicated by arrowhead in panel B plot. Black and white bars on plots represent dark and illumination phases of the measurement, respectively. Data are mean values ± SD from at least eight leaves. Results with different letters indicate significant difference ($p \leq 0.05$).

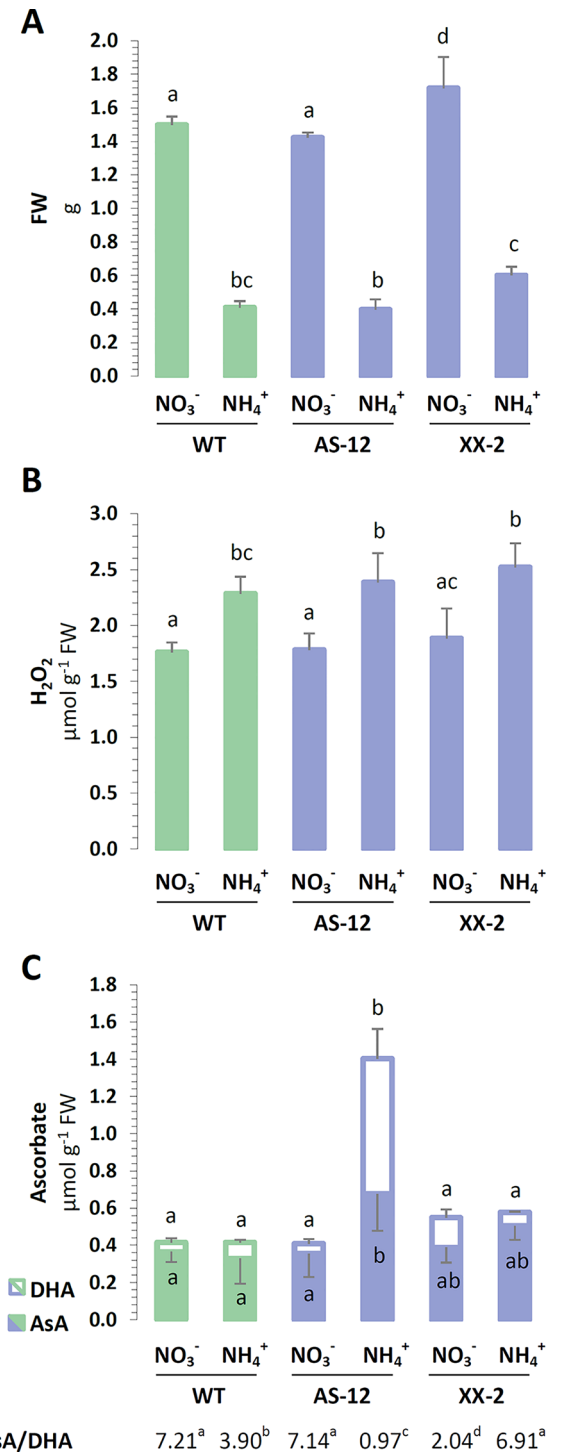

FIGURE 9 | Characterization of *A. thaliana* after 8 weeks of hydroponics culture with 5 mM NO_3^- or 5 mM NH_4^+ as the sole nitrogen source. AOX1a suppressing line (AS-12) and overexpressing line (XX-2) were derived from the presented wild type (WT, Col-0) plants. **(A)** Fresh weight (FW) of rosettes on respective nitrogen sources. **(B)** Hydrogen peroxide (H_2O_2) content of leaves. **(C)** Concentration of reduced ascorbate (AsA) and dehydroascorbate (DHA) as well as the derived AsA/DHA ratio. Bars with different letters indicate significant difference ($p \leq 0.05$).

plants nourished with NH_4^+ (**Figure 9C**). The increase in ascorbate was mainly due to higher DHA content, consequently the ratio of AsA to DHA was lower in the WT plants and was even more reduced in the AS-12 mutant plants when they were nourished with NH_4^+ (**Figure 9C**). Compared to the WT plants, the XX-2 mutant had an oxidized ascorbate redox state when growing on NO_{3-}. These findings suggest that the ascorbate pool is oxidized when plants are challenged with the dysfunction of AOX1a and under NH_4^+ nutrition, whereas the overexpression of AOX1a improves the resistance of the plants to NH_4^+ nutrition. The metabolic differences between AOX1a mutants and WT plants were not pronounced; the full results of the photosynthetic dependent parameters are shown in the **Supplementary Materials**.

DISCUSSION

Ammonium Nutrition Leads to Perturbation of the Oxidation-Reduction Status of Chloroplasts But Does Not Result in the Oxidative Damage of the Biomolecules in These Organelles

Considering that NH_4^+ as the nitrogen source was expected to cause the overreduction of the chlETC. In our previous study, prolonged NH_4^+ nutrition increased the redox state of *Arabidopsis* leaf tissue (Podgórska et al., 2013) and consequently increased the ROS level in leaves (Podgórska et al., 2013; Podgórska et al., 2015). Nevertheless, the oxidative damage of biomolecules occurred in the mitochondria (Podgórska et al., 2013) but not in the chloroplasts under long-term NH_4^+ nutrition. In the present study the chloroplasts were characterized by lower abundance of oxidized proteins or by lesser lipid peroxidation (**Figures 1C, D**), hence, oxidative stress did not occur in the chloroplasts in response to NH_4^+ nutrition. It can be achieved by limiting the chloroplast ROS production or by enhancing the antioxidant system capacity or by both. Moreover, the $O_2^{\cdot -}$ derived from the Mehler reaction is eventually converted into water due to the activity of the chloroplast-associated SOD and APX, closing the water-to-water cycle, which is also named as pseudo-cyclic electron transport chain (Shikanai and Yamamoto, 2017). There is no clear data concerning chloroplastic ROS production under NH_4^+ nutrition, but Zhu et al. (2000) and Gerendás et al. (1997) substantiated the stimulation of the Mehler reaction in plants nourished with NH_4^+. In our current study, the activity of SOD was stimulated in the chloroplasts of the plants under NH_4^+ nutrition (**Figures 1A, B**). SOD has to cooperate with other enzymatic H_2O_2 scavengers to totally reduce ROS in Mehler-peroxidase reactions (Foyer and Harbinson, 1994), the protein levels of thylakoid and stromal APX were also augmented in the chloroplasts of the plants nourished with NH_4^+ (**Figure 1B**). Nonetheless, we previously demonstrated that long-term growth of *A. thaliana* did not affect the activity of the chloroplast-localized ascorbate recycling enzymes dehydroascorbate reductase (DHAR) and monodehydroascorbate reductase

(MDHAR) (Podgórska et al., 2013). Another H_2O_2-responsive antioxidant in chloroplasts could be peroxiredoxin Q (PRXQ) whose protein level was found to be higher in *A. thaliana* under NH_4^+ nutrition (Podgórska et al., 2018). Unfortunately, we were not able to measure ascorbate directly in isolated chloroplasts, which is one of the most important antioxidants. Ascorbate is not only needed in the Mehler-peroxidase reactions, but it is also a substrate for violaxanthin de-epoxidase (VDE) in xanthophyll cycle. The concentration of other water-soluble antioxidants such as glutathione was increased in the chloroplasts under NH_4^+ nutrition (Podgórska et al., 2013). Considering that plants need to immediately detect the changes in their redox status to prevent further damage in their chloroplasts, thioredoxins had been proposed as redox sensors and transmitters. The up-regulation of chloroplast NADPH-dependent thioredoxin reductase C (NTRC), and the Fd-dependent thioredoxins TRXx or TRXy2 in the NH_4^+-nourished *A. thaliana* (Podgórska et al., 2018) could suggest them to be important mediators in redox signaling.

An Increase in Energy-Dependent NPQ and the Upregulation of the Cyclic chlETC Ensure the chlETC Functioning Under NH_4^+ Nutrition

Plants have developed a network of adaptive and protective mechanisms through the regulation of electron transport in the chlETC and dissipation of energy absorbed by photosynthetic pigments. Higher chlETC capacity (**Figure 4A**) and enhanced activity of PSI and PSII *in vitro* (**Figure 4B**) were observed during the exclusive nutrition of the plants with NH_4^+, suggesting that no damage of the photosystems was induced by NH_4^+ stress. However, this observation did not necessarily reflect the functioning of the photosystems *in vivo* when all the protective and adaptive mechanisms were activated. The BN-PAGE analysis of the thylakoid-localized complexes revealed that the abundance of the PSII-LHCII complexes was greater in the plants nourished with NH_4^+ (**Figure 3A**). Moreover, the subtle differences in the migration of bands corresponding to PSI, PSII dimer (**Figure 3A**) and the variations in the abundance of spots corresponding to specific proteins (**Figure 3B**) signify that NH_4^+ nutrition induces structural modification in photosynthetic apparatus. Nevertheless, further analysis on this is needed. PSII is considered as the photosystem primarily exposed to photodamage (Baker, 2008), so an analysis of chl *a* fluorescence kinetics can display the functional state of PSII *in vivo*. Our results showed that the marginally higher value of the maximal quantum yield of PSII in the NH_4^+-nourished plants (**Figure 8B**) corresponded to the upregulated activity of PSII *in vitro*, but the curves illustrating the parameters related to the usage of absorbed energy for photochemical reactions indicated that the processes were significantly downregulated in the NH_4^+-nourished plants during light period (**Figures 8B, C**). The NPQ values were initially high in the plants nourished with NO_3^-, but they became eventually higher in the plants responding to NH_4^+ nutrition (**Figure 8B**). Whereas the value for qI is unchanged during NH_4^+ nutrition (**Supplementary Figure 9A**), suggesting that PSII photoinhibitory quenching is not induced. Findings on *Phaseolus vulgaris* grown with NH_4^+ refute the occurrence of photoinhibition (Zhu et al., 2000). The photoinhibition of PSII only occurs if the rate of damage exceeds the rate of repair. Alencar et al. (2019) demonstrated that in rice supplied with NH_4^+, the abundance of protein D1 was unchanged. Based on BN-PAGE profiles (**Figure 3B**), the activity of D1 repair cycle may be increased in NH_4^+-nourished plants. Moreover, the PSII monomer without CP43 subunit in the plants under NH_4^+ nutrition (**Figure 3B**) was more abundant, validating the possibly higher activity of PSII repair cycle.

NH_4^+ nutrition extensively increased the qE quenching parameter in *A. thaliana*, indicating that excitation energy was lost as heat (**Supplementary Figure 9B**). Apart from LET, the specific role of CET and pseudocyclic electron transport in the generation of ΔpH needed for the induction of qE has been strongly postulated. In our current study, NH_4^+ nutrition induced both CET branches as it was affirmed by the increased expression of *PGR5* (**Figure 6A**), by the significantly greater abundance of NDH-PSI supercomplex (**Figure 3A**), and by *NDHL* expression (**Figure 6A**), all together creating an safety valve for PSI (**Figure 10**). Besides being induced by the rise of ΔpH across the thylakoid membrane *via* the protonation of the PSII subunit S protein (PsbS), qE is also dependent on the metabolism of xanthophyll pigments (Ware et al., 2014 and references therein). The formation of photoprotective states in higher plants possibly requires a structural reorganization of the photosynthetic membranes involving the dissociation of LHCII from PSII promoted by de-epoxidation of violaxanthin to zeaxanthin (Johnson et al., 2011). In addition, the formation of qZ is strictly dependent on zeaxanthin but independent of PsbS (Liu et al., 2019). The relaxation of qZ depends on zeaxanthin epoxidation, and it is linked to the kinetics of the zeaxanthin pool. Pools of carotenoids involved in the xanthophyll cycle were extensively augmented under NH_4^+ nutrition (**Figure 2B**), so the changes in qZ were also possibly induced. In contrast to this, zeaxanthin production was reduced in *P. vulgaris* grown in the presence of NH_4^+ (Bendixen et al., 2001). The role and mechanism of the carotenoid-dependent component of NPQ have to be further studied, considering that NH_4^+ nutrition resulted in higher zeaxanthin level but lower de-epoxidation states (DEPS) of the xanthophyll cycle pigments (**Figure 2C**). Furthermore, the high lutein levels during NH_4^+ nutrition substantiated the importance of carotenoids in *Arabidopsis* under NH_4^+ nutrition (**Figure 2D**).

The Upregulated CET/NDC1—PTOX Pathways Under NH_4^+ Nutrition May Function as an Efficient Membrane-Localized Reductant Sink in Chloroplasts

In higher plants, PTOX is responsible for the carotenoid biosynthesis during the developmental processes in chloroplasts (Krieger-Liszkay and Feilke, 2016). Nevertheless, its presence in mature tissues suggests that PTOX may also be involved in other processes: chlororespiration and light-independent oxygen consumption in the chloroplasts,

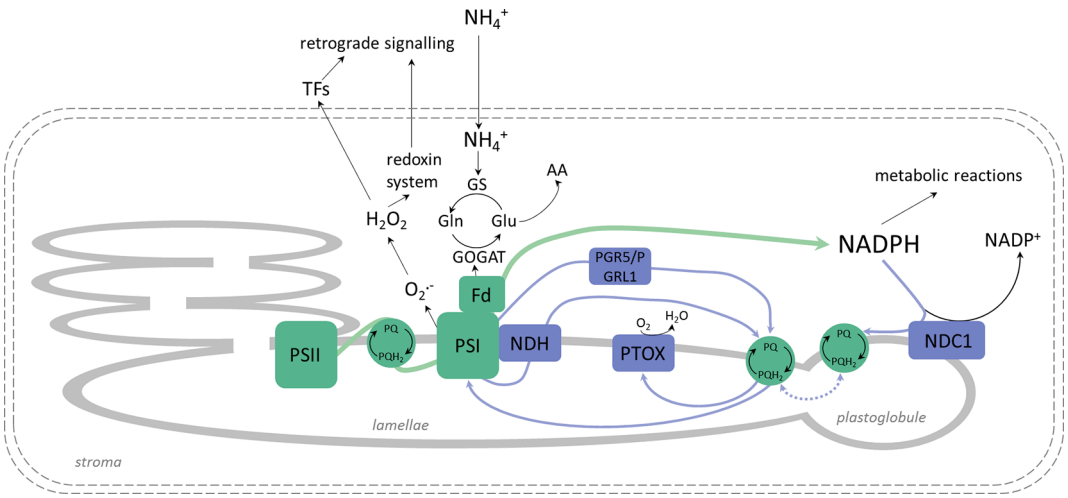

FIGURE 10 | Changes in chlETC functioning, linear electron transport (LET; green arrows) route and alternative electron pathways (blue arrows) under NH_4^+ nutrition. The inevitable activity of the glutamine synthetase - glutamine:2-oxoglutarate aminotransferase (GS-GOGAT) cycle consumes electrons from ferredoxin (Fd) for NH_4^+ assimilation into amino acids (AA). Higher NAD(P)H dehydrogenase C1 (NDC1) protein abundance in plastoglobules transfers electrons from NADPH to plastoquinone (PQ), balancing the stromal redox pool. Consequently, less free PQ are available for cyclic electron transport (CET), and the PQ pool is more reduced in grana lamellae. Electrons from photosystem I (PSI) enter pseudocyclic electron transport (water-to-water cycle), which may lead to reactive oxygen species (ROS) production in chloroplasts. H_2O_2 may be engaged in signaling, and plastid terminal oxidase (PTOX) may act as the positive regulator of chloroplast to nucleolus retrograde signaling or communication with the alternative oxidase (AOX).

permitting plastoquinol oxidation during the dark period (Nawrocki et al., 2019); regulation of the CET pathway (Joët et al., 2002); and/or protection from oxidative stress (Stepien and Johnson, 2009). During NH_4^+ nutrition PQH_2-associated with CET activity may be a natural substrate for PTOX activity. Such hypothesis was confirmed by the enormous increase in the PTOX protein levels (**Figure 6B**) and CET elements (**Figure 6A**) under NH_4^+ nutrition in our current study. Moreover, NDC1 activity also influences the redox state of the plastoglobule-localized PQ pool (van Wijk and Kessler, 2017), and considering that plastoglobules are integral with the edges of the stroma lamellae (Fatihi et al., 2015), it can be assumed that both the plastoglobule and stroma lamellae PQ subpools mix together. Therefore, we suggest that non-photochemical PQ reduction due to NDC1 activity is a pathway that is naturally parallel to other light-dependent PQ-reducing processes in thylakoids and that NDC1 activity can be recognized as an alternative sink pathway that balances the excess chloroplastic NADPH under NH_4^+ nutrition. The possible alternative electron route consistent of NDC1 together with PTOX can function as electron dissipation when plants are nourished with NH_4^+ (**Figure 10**). Such hypothesis is corroborated by the markedly upregulated protein levels of NDC1 in the plants under NH_4^+ nutrition (**Figure 6B**). Remarkably, PTOX is considered an important component of redox sensing in higher plants in relation to the redoxin system (Kambakam et al., 2016; Feilke et al., 2017; and references therein), which regulates several chloroplast-localized processes including PSI assembly (Zhu et al., 2016) and improves the tolerance of plants to stress (Johnson and Stepien, 2016).

Redox Equivalents Not Used in the CBB Cycle May Be Effectively Exported From Chloroplasts Under NH_4^+ Nutrition

The photosynthetic electron transport chain is not tightly linked to the CBB cycle because many different chloroplast-localized metabolic pathways, including nitrogen assimilation, sulfur assimilation, chloroplast redoxin functioning, etc., with different requirements for ATP and reductants, compete with one another. NH_4^+ nutrition is one of the events, which are suspected to influence chloroplast redox and energy status. In fact in our previous study, we have shown that the status of adenylates in the chloroplasts was affected, and the plants were characterized by lower ATP/ADP ratio under NH_4^+ nutrition (Podgórska et al., 2013). The observed ATP deficit in the NH_4^+-nourished plants correlates with the lower ATP synthase complex abundance and the α-subunit of ATP synthase protein level (**Figures 3A** and **5A**), suggesting that less chloroplastic ATP may be produced during NH_4^+ nutrition. Nonetheless, the elevated CET in the NH_4^+-nourished plants could still contribute to a possibly increased ATP production. Certainly, our findings imply that lower ATP availability during NH_4^+ nutrition affects the CO_2 assimilation in CBB cycle (**Figure 5B**). A reduced CO_2 assimilation rate was observed in NH_4^+-grown rice (Alencar et al., 2019) and *Arabidopsis* seedlings (Hoffmann et al., 2007). Moreover, through their Northern blotting analysis, a slightly lower RUBISCO expression in *Arabidopsis* seedlings supplied with NH_4^+ was further documented (Hoffmann et al., 2007). In our current study, NH_4^+ nutrition lowered the abundance of RUBISCO in the plants (**Figure 5A**). It can be expected that, although the CBB cycle was

restricted under NH_4^+ nutrition (**Figures 5A, B**), the other energy and redox-consuming reactions were activated during NH_4^+ nutrition. As previously anticipated by Podgórska et al. (2013), the higher activity of the GS-GOGAT cycle could alleviate the reductive stress in chloroplasts during NH_4^+ nutrition.

Photorespiration is integral to stress response in green tissues (Voss et al., 2013). Adjustments in the photorespiratory cycle flow signify the need to export the excess reducing equivalents from chloroplasts, considering that the NADH obtained from the decarboxylation of Gly can be further oxidized in the mtETC. Therefore, photorespiratory reactions are deemed essential under NH_4^+ nutrition (Guo et al., 2007). Contrary to that assumption and based on the protein abundance of photorespiratory enzymes GDC-H, SHMT and HPR (**Figure 7A**), we do not expect this process to be strongly activated in *Arabidopsis* during long-term NH_4^+ nutrition. This subject still warrants further investigation, considering that elevated rates of photorespiration under NH_4^+ nutrition were documented in *P. vulgaris* (Zhu et al., 2000) and in rice (Alencar et al., 2019). Another way for the efficient redox equivalent export from chloroplasts can be mediated by $NADP^+$-MDH activity in the OAA/Mal shuttle (Scheibe, 2004). During NO_3^- nutrition, the lack of $NADP^+$-MDH can be favorable to keep more reductants for reduction reactions (Selinski and Scheibe, 2014). However, our current findings imply that under certain circumstances such as NH_4^+ nutrition and when excess reductants are available in the chloroplasts, a greater expression of *$NADP^+$-MDH* (**Figure 7B**) together with the higher maximal activity of $NADP^+$-MDH (**Figure 7C**) may facilitate reductant outflow towards the cytosol. In addition, an upregulated activity of NAD^+-MDH isoforms under NH_4^+ nutrition (**Supplementary Figure 8B**) may indicate that reductants are efficiently transferred between cellular compartments and are possibly oxidized in mitochondria, which are considered as cellular redox-balancing organelles.

Reduced Expression of Mitochondrial AOX1a Modifies Photosynthetic Parameters Under NO_3- Nutrition, But NH_4^+ Does Not Increase Observed Changes

The major role of mitochondria is to regulate cellular redox balance (Noctor et al., 2007), considering the presence of alternative pathways in the mtETC (Noguchi and Yoshida, 2007; Rasmusson et al., 2008). Under intensive light conditions, AOX contributes more to prevent chloroplast/cellular redox poise (Yoshida et al., 2007). Similarly, our current findings indicate that the activity of AOX is crucial in plants nourished with NH_4^+ when excess reductants need to be dissipated. In fact, we observed differences in the overexpressor plant growth rate under NH_4^+ nutrition; the growth of XX-2 plants was less restricted (**Figure 9A**). Moreover, as a marker of oxidative damage to chloroplasts, the extent of lipid peroxidation of chloroplastic membranes was not induced in XX-2 when nourished with NH_4^+ (**Supplementary Figure 3B**). Surprisingly, the modification of *AOX1a* expression did not drastically change the cellular metabolism of the plants under NH_4^+ nutrition (Supplementary materials). Neither the overexpression nor suppression of *AOX1a* affected the H_2O_2 content of whole tissues in response to NH_4^+ nutrition (**Figure 9B**). However, among the evaluated cellular ROS scavengers, which were not disturbed in the transformants (**Supplementary Figure 2**), only ascorbate was significantly affected. The antisense plants seemingly had to raise their total ascorbate content (**Figure 9C**) to achieve redox homeostasis. At the same time, the overexpressor mutants showed a more reduced ascorbate status when nourished with NH4+ (**Figure 9C**). Previous studies have shown that during optimal growth conditions, AOX1a-defective plants do not manifest alterations in their photosynthetic performance, or NPQ (Umbach et al., 2005; Giraud et al., 2008; Gandin et al., 2012; Vishwakarma et al., 2015), but the changes in the mtETC functioning of the AOX1a-suppressor plants may be a burden for them as they keep their photosynthetic rates efficient under stress. In the presence of stress factors such as intensive light and chilling or drought photoinhibition may intensify and ROS production may increase in AOX1a antisense plants (Watanabe et al., 2008; Giraud et al., 2008; Florez-Sarasa et al., 2011). Under NH_4^+ nutrition, there were no parameters indicating photoinhibition of PSII because the F_V/F_M values were similar among all the genotypes (**Figure 8A**). We have also not observed any influence of the overexpression of AOX1a on the photosynthetic parameters *in vivo* during light period (**Figure 8B**). Given that AOX is highly induced by NH_4^+ nutrition (Escobar et al., 2006; Podgórska et al., 2018), we suppose that additional, genetically-forced increase in the quantity of AOX protein may have no cumulative effect on metabolic improvement, at least in the level of photosynthetic parameters. However, the dysfunction of AOX resulted in significant changes in the parameters characterizing photochemical quenching and the initial phase of NPQ (**Figure 8B**). Under the control NO_3^- conditions, the lower levels of AOX1a reduced the effective utilization of light-derived energy in photochemical reactions, but this effect was not modulated by nourishing the plants with reduced form of nitrogen. Contrary to the findings on the WT plants nourished with NH_4^+, AS-12 plants did not show faster induction of NPQ in the first phase of light conditions. NH_4^+ nutrition does not further alter photosynthetic performance in *AOX1a* knockout mutants (Hachiya et al., 2010; Gandin et al., 2014), similar to the findings in our current study.

DATA AVAILABILITY STATEMENT

All datasets generated and analyzed for this study are included in the article/**Supplementary Material**.

AUTHOR CONTRIBUTIONS

AP and BS designed the experiments. AP, MO-B, KB, and KK measured enzyme activity and performed Licor analysis, whereas AP and BS evaluated the metabolite levels. AP, KK, and KD conducted the RTq-PCR analysis. AP and RM performed the BN-PAGE. RM carried out the pigment analysis and PAM-

imaging. BS, MO-B, AT, and MB worked on the immunoblots. AT did the statistical analysis, and MO-B prepared the figures. AP and BS wrote the manuscript, which was later revised by RM and AR.

FUNDING

The publication process was co-financed from the resources of the University of Warsaw. Analysis of MDH was supported by the intramural grant 501/86/0112600-35 (DSM) provided to KB by the Ministry of Science and Higher Education through the Faculty of Biology, University of Warsaw.

ACKNOWLEDGMENTS

We thank Dr. Izabela Juszczuk of the Faculty of Biology, University of Warsaw for the technical support. We are grateful to Prof. Leszek Kleczkowski of the Umeå Plant Science Centre for providing the HPR antibodies.

SUPPLEMENTARY MATERIAL

The Supplementary Material for this article can be found online at: https://www.frontiersin.org/articles/10.3389/fpls.2020.00103/full#supplementary-material

REFERENCES

Alencar, V. T. C. B., Lobo, A. K. M., Carvalho, F. E. L., and Silveira, J. A. G. (2019). High ammonium supply impairs photosynthetic efficiency in rice exposed to excess light. *Photosynth. Res.* 140, 321–335. doi: 10.1007/s11120-019-00614-z

Baker, N. R. (2008). Chlorophyll fluorescence: a probe of photosynthesis *in vivo*. *Annu. Rev. Plant Biol.* 59, 89–113. doi: 10.1146/annurev.arplant.59.032607.092759

Beeler, S., Liu, H. C., Stadler, M., Schreier, T., Eicke, S., Lue, W. L., et al. (2014). Plastidial NAD-dependent malate dehydrogenase is critical for embryo development and heterotrophic metabolism in *Arabidopsis*. *Plant Physiol.* 164, 1175–1190. doi: 10.1104/pp.113.233866

Bendixen, R., Gerendás, J., Schinner, K., Sattelmacher, B., and Hansen, U. P. (2001). Difference in zeaxanthin formation in nitrate-and ammonium-grown *Phaseolus vulgaris*. *Physiol. Plant* 111, 255–261. doi: 10.1034/j.1399-3054.2001.1110218.x

Bittsánszky, A., Pilinszky, K., Gyulai, G., and Komives, T. (2015). Overcoming ammonium toxicity. *Plant Sci.* 231, 184–190. doi: 10.1016/j.plantsci.2014.12.005

Bradford, M. M. (1976). A rapid and sensitive method for quantification of microgram quantities of protein utilizing the principle of protein-dye binding. *Anal. Biochem.* 72, 248–254. doi: 10.1006/abio.1976.9999

Britto, D. T., and Kronzucker, H. J. (2002). NH_4^+ toxicity in higher plants: a critical review. *J. Plant Physiol.* 159, 567–584. doi: 10.1078/0176-1617-0774

Clifton, R., Millar, A. H., and Whelan, J. (2006). Alternative oxidases in Arabidopsis: a comparative analysis of differential expression in the gene family provides new insights into function of non-phosphorylating bypasses. *Biochim. Biophys. Acta* 1757, 730–741. doi: 10.1016/j.bbabio.2006.03.009

Cuttriss, A. J., Chubb, A., Alawady, A., Grimm, B., and Pogson, B. (2007). Regulation of lutein biosynthesis and prolamellar body formation in *Arabidopsis*. *Funct. Plant Biol.* 34, 663–672. doi: 10.1071/FP07034

Cvetkovska, M., and Vanlerberghe, G. C. (2012). Alternative oxidase modulates leaf mitochondrial concentrations of superoxide and nitric oxide. *New Phytol.* 195, 32–39. doi: 10.1111/j.1469-8137.2012.04166.x

Czechowski, T., Stitt, M., Altmann, T., Udvardi, M. K., and Scheible, W. R. (2005). Genome-wide identification and testing of superior reference genes for transcript normalization in *Arabidopsis*. *Plant Physiol.* 139, 5–17. doi: 10.1104/pp.105.063743

Escobar, M. A., Geisler, D. A., and Rasmusson, A. G. (2006). Reorganization of the alternative pathways of the *Arabidopsis* respiratory chain by nitrogen supply: opposing effects of ammonium and nitrate. *Plant J.* 45, 775–788. doi: 10.1111/j.1365-313X.2005.02640.x

Esteban, R., Ariz, I., Cruz, C., and Moran, J. F. (2016). Review: mechanisms of ammonium toxicity and the quest for tolerance. *Plant Sci.* 248, 92–101. doi: 10.1016/j.plantsci.2016.04.008

Fatihi, A., Latimer, S., Schmollinger, S., Block, A., Dussault, P. H., Vermaas, W. F., et al. (2015). A dedicated type II NADPH dehydrogenase performs the penultimate step in the biosynthesis of vitamin K1 in *Synechocystis* and *Arabidopsis*. *Plant Cell.* 27, 1730–1741. doi: 10.1105/tpc.15.00103

Feilke, K., Ajlani, G., and Krieger-Liszkay, A. (2017). Overexpression of plastid terminal oxidase in Synechocystis sp. PCC 6803 alters cellular redox state. *Philos. Trans. R. Soc. Lond. B Biol. Sci.* 372, 20160379. doi: 10.1098/rstb.2016.0379

Florez-Sarasa, I., Flexas, J., Rasmusson, A. G., Umbach, A. L., Siedow, J. N., and Ribas-Carbo, M. (2011). *In vivo* cytochrome and alternative pathway respiration in leaves of Arabidopsis thaliana plants with altered alternative oxidase under different light conditions. *Plant Cell Environ.* 34, 1373–1383. doi: 10.1111/j.1365-3040.2011.02337.x

Foyer, C. H., and Harbinson, J. (1994). "Oxygen metabolism and the regulation of photosynthetic electron transport," in *Causes of photooxidative stress and amelioration of defense systems in plants*. Eds. C. H. Foyer and P. M. Mullineaux (Boca Raton: CRC Press), 1–42.

Gandin, A., Duffes, C., Day, D. A., and Cousins, A. B. (2012). The absence of alternative oxidase AOX1a results in altered response of photosynthetic carbon assimilation to increasing CO_2 in *Arabidopsis thaliana*. *Plant Cell Physiol.* 53, 1627–1637. doi: 10.1093/pcp/pcs107

Gandin, A., Denysyuk, M., and Cousins, A. B. (2014). Disruption of the mitochondrial alternative oxidase (AOX) and uncoupling protein (UCP) alters rates of foliar nitrate and carbon assimilation in *Arabidopsis thaliana*. *J. Exp. Bot.* 65, 3133–3142. doi: 10.1093/jxb/eru158

Garstka, M., Drozak, A., Rosiak, M., Venema, J. H., Kierdaszuk, B., Simeonova, E., et al. (2005). Light-dependent reversal of dark-chilling induced changes in chloroplast structure and arrangement of chlorophyll-protein complexes in bean thylakoid membranes. *Biochim. Biophys. Acta* 1710, 13–23. doi: 10.1016/j.bbabio.2005.08.006

Garstka, M., Venema, J. H., Rumak, I., Gieczewska, K., Rosiak, M., Koziol-Lipinska, J., et al. (2007). Contrasting effect of dark-chilling on chloroplast structure and arrangement of chlorophyll - protein complexes in pea and tomato: plants with a different susceptibility to non-freezing temperature. *Planta* 226, 1165–1181. doi: 10.1007/s00425-007-0562-7

Gerendás, J., Zhu, Z., Bendixen, R., Ratcliffe, R. G., and Sattelmacher, B. (1997). Physiological and biochemical processes related to ammonium toxicity in higher plants. *J. Plant Nutr. Soil Sci.* 160, 239–251. doi: 10.1002/jpln.19971600218

Giraud, E., Ho, L. H., Clifton, R., Carroll, A., Estavillo, G., Tan, Y. F., et al. (2008). The absence of alternative oxidase 1a in *Arabidopsis* results in acute sensitivity to combined light and drought stress. *Plant Physiol.* 147, 595–610. doi: 10.1104/pp.107.115121

Guo, S., Schinner, K., Sattelmacher, B., and Hansen, U. P. (2005). Different apparent CO_2 compensation points in nitrate-and ammonium-grown *Phaseolus vulgaris* and the relationship to non-photorespiratory CO_2 evolution. *Physiol. Plant* 123, 288–301. doi: 10.1111/j.1399-3054.2005.00467.x

Guo, S., Zhou, Y., Gao, Y., Li, Y., and Shen, Q. R. (2007). New insights into the nitrogen form effect on photosynthesis and photorespiration. *Pedosphere* 17, 601–610. doi: 10.1016/S1002-0160(07)60071-X

Hachiya, T., Watanabe, C. K., Boom, C., Tholen, D., Takahara, K., Kawai-Yamada, M., et al. (2010). Ammonium-dependent respiratory increase is dependent on the cytochrome pathway in *Arabidopsis thaliana* shoots. *Plant Cell Environ.* 33, 1888–1897. doi: 10.1111/j.1365-3040.2010.02189.x

Hodges, D., DeLong, J., Forney, C. F., and Prange, R. K. (1999). Improving the thiobarbituric acid-reactive-substances assay for estimating lipid peroxidation in plant tissues containing anthocyanin and other interfering compounds. *Planta* 207, 604–611. doi: 10.1007/s004250050524

Hoffmann, A., Milde, S., Desel, C., Hümpel, A., Kaiser, H., Hammes, E., et al. (2007). N form–dependent growth retardation of *Arabidopsis thaliana* seedlings as revealed from physiological and microarray studies. *J. Plant Nutr. Soil Sci.* 170, 87–97. doi: 10.1002/jpln.200625032

Joët, T., Genty, B., Josse, E. M., Kuntz, M., Cournac, L., and Peltier, G. (2002). Involvement of a plastid terminal oxidase in plastoquinone oxidation as evidenced by expression of the *Arabidopsis thaliana* enzyme in tobacco. *J. Biol. Chem.* 277, 31623–31630. doi: 10.1074/jbc.M203538200

Johnson, G. N., and Stepien, P. (2016). Plastid terminal oxidase as a route to improving plant stress tolerance: known knowns and known unknowns. *Plant Cell Physiol.* 57, 1387–1396. doi: 10.1093/pcp/pcw042

Johnson, M. P., Goral, T. K., Duffy, C. D., Brain, A. P., Mullineaux, C. W., and Ruban, A. V. (2011). Photoprotective energy dissipation involves the reorganization of photosystem II light-harvesting complexes in the grana membranes of spinach chloroplasts. *Plant Cell. 23*, 1468–1479. doi: 10.1105/tpc.110.081646

Juszczuk, I. M., Tybura, A., and Rychter, A. M. (2008). Protein oxidation in the leaves and roots of cucumber plants (*Cucumis sativus* L.), mutant MSC16 and wild type. *J. Plant Physiol.* 165, 355–365. doi: 10.1016/j.jplph.2007.06.021

Kambakam, S., Bhattacharjee, U., Petrich, J., and Rodermel, S. (2016). PTOX mediates novel pathways of electron transport in etioplasts of *Arabidopsis*. *Mol. Plant* 9, 1240–1259. doi: 10.1016/j.molp.2016.06.008

Keryer, E., Collin, V., Lavergne, D., Lemaire, S., and Issakidis-Bourguet, E. (2004). Characterization of Arabidopsis mutants for the variable subunit of ferredoxin: thioredoxin reductase. *Photosynth. Res.* 79, 265–274. doi: 10.1023/B:PRES.0000017173.46185.3e

Krieger-Liszkay, A., and Feilke, K. (2016). The dual role of the plastid terminal oxidase PTOX: between a protective and a pro-oxidant function. *Front. Plant Sci.* 6, 1147. doi: 10.3389/fpls.2015.01147

Lasa, B., Frechilla, S., Apricio-Tejo, P. M., and Lamsfus, C. (2002). Alternative pathway respiration is associated with ammonium ion sensitivity in spinach and pea plants. *Plant Growth Regul.* 37, 49–55. doi: 10.1023/A:1020312806239

Liu, Y., and von Wirén, N. (2017). Ammonium as a signal for physiological and morphological responses in plants. *J. Exp. Bot.* 68, 2581–2592. doi: 10.1093/jxb/erx086

Liu, J., Lu, Y., Hua, W., and Last, R. L. (2019). A new light on photosystem II maintenance in oxygenic photosynthesis. *Front. Plant Sci.* 10, 975. doi: 10.3389/fpls.2019.00975

Müller, P., Li, X. P., and Niyogi, K. K. (2001). Non-photochemical quenching. A response to excess light energy. *Plant Physiol.* 125, 1558–1566. doi: 10.1104/pp.125.4.1558

Mazur, R., Sadowska, M., Kowalewska, Ł., Abratowska, A., Kalaji, H. M., Mostowska, A., et al. (2016). Overlapping toxic effect of long term thallium exposure on white mustard (*Sinapis alba* L.) photosynthetic activity. *BMC Plant Biol.* 16, 191. doi: 10.1186/s12870-016-0883-4

Mazur, R., Mostowska, A., Szach, J., Gieczewska, K., Wójtowicz, J., Bednarska, K., et al. (2019). Galactolipid deficiency disturbs spatial arrangement of the thylakoid network in *Arabidopsis thaliana* plants. *J. Exp. Bot.* 70, 4689–4704. doi: 10.1093/jxb/erz219

Munekage, Y., Hojo, M., Meurer, J., Endo, T., Tasaka, M., and Shikanai, T. (2002). PGR5 is involved in cyclic electron flow around photosystem I and is essential for photoprotection in *Arabidopsis*. *Cell* 110, 361–371. doi: 10.1016/S0092-8674(02)00867-X

Nawrocki, W. J., Buchert, F., Joliot, P., Rappaport, F., Bailleul, B., and Wollman, F. A. (2019). Chlororespiration controls growth under intermittent light. *Plant Physiol.* 179, 630–639. doi: 10.1104/pp.18.01213

Noctor, G., and Foyer, C. H. (1998). A re-evaluation of the ATP: NADPH budget during C_3 photosynthesis: a contribution from nitrate assimilation and its associated respiratory activity? *J. Exp. Bot.* 49, 1895–1908. doi: 10.1093/jxb/49.329.1895

Noctor, G., De Paepe, R., and Foyer, C. H. (2007). Mitochondrial redox biology and homeostasis in plants. *Trends Plant Sci.* 12, 125–134. doi: 10.1016/j.tplants.2007.01.005

Noguchi, K., and Yoshida, K. (2007). Interaction between photosynthesis and respiration in illuminated leaves. *Mitochondrion* 8, 87–99. doi: 10.1016/j.mito.2007.09.003

Okamura, M. (1980). An improved method for determination of L-ascorbic acid and L-dehydroascorbic acid in blood plasma. *Clin. Chem. Acta* 103, 259–268. doi: 10.1016/0009-8981(80)90144-8

Pfaffl, M. W. (2001). A new mathematical model for relative quantification in real-time RT-PCR. *Nucleic Acids Res.* 29, e45. doi: 10.1093/nar/29.9.e45

Podgórska, A., and Szal, B. (2015). "The role of reactive oxygen species under ammonium nutrition," in *Reactive oxygen and nitrogen species signaling and communication in clants*. Eds. K. J. Gupta and A. U. Igamberdiev (Switzerland: Springer, International Publishing), 133–153. doi: 10.1007/978-3-319-10079-1_7

Podgórska, A., Gieczewska, K., Łukawska-Kuźma, K., Rasmusson, A. G., Gardeström, P., and Szal, B. (2013). Long-term ammonium nutrition of *Arabidopsis* increases the extrachloroplastic NAD(P)H/$NAD(P)^+$ ratio and mitochondrial reactive oxygen species level in leaves but does not impair photosynthetic capacity. *Plant Cell Environ.* 36, 2034–2045. doi: 10.1111/pce.12113

Podgórska, A., Ostaszewska, M., Gardeström, P., Rasmusson, A. G., and Szal, B. (2015). In comparison with nitrate nutrition, ammonium nutrition increases growth of the *frostbite1 Arabidopsis* mutant. *Plant Cell Environ.* 38, 224–237. doi: 10.1111/pce.12404

Podgórska, A., Ostaszewska-Bugajska, M., Borysiuk, K., Tarnowska, A., Jakubiak, M., Burian, M., et al. (2018). Suppression of external NADPH dehydrogenase—NDB1 in *Arabidopsis thaliana* confers improved tolerance to ammonium toxicity *via* efficient glutathione/redox metabolism. *Int. J. Mol. Sci.* 19, 1412. doi: 10.3390/ijms19051412

Porra, R. J., Thompson, W. A., and Kriedemann, P. E. (1989). Determination of accurate extinction coefficients and simultaneous equations for assaying chlorophylls a and b extracted with four different solvents: verification of the concentration of chlorophyll standards by atomic absorption spectroscopy. *Biochim. Biophys. Acta Bioenerg.* 975, 384–394. doi: 10.1016/S0005-2728(89)80347-0

Rasmusson, A. G., Geisler, D. A., and Møller, I. M. (2008). The multiplicity of dehydrogenases in the electron transport chain of plant mitochondria. *Mitochondrion* 8, 47–60. doi: 10.1016/j.mito.2007.10.004

Rogowski, P., Wasilewska-Dębowska, W., Krupnik, T., Drożak, A., Zienkiewicz, M., Krysiak, M., et al. (2019). Photosynthesis and organization of maize mesophyll and bundle sheath thylakoids of plants grown in various light intensities. *Environ. Exp. Bot.* 162, 72–86. doi: 10.1016/j.envexpbot.2019.02.006

Romanowska, E., and Albertsson, P. A. (1994). Isolation and characterization of the cytochrome *bf* complex from whole thylakoids, grana and stroma lamellae vesicles from spinach chloroplasts. *Plant Cell Physiol.* 35, 557–568. doi: 10.1093/oxfordjournals.pcp.a078630

Scheibe, R. (2004). Malate valves to balance cellular energy supply. *Physiol. Plant* 120, 21–26. doi: 10.1111/j.0031-9317.2004.0222.x

Sehmer, L., Fontaine, V., Antoni, F., and Dizengremel, P. (1998). Effects of ozone and elevated atmospheric carbon dioxide on carbohydrate metabolism of spruce needles. Catabolic and detoxification pathways. *Physiol. Plant* 102, 605–611. doi: 10.1034/j.1399-3054.1998.1020416.x

Selinski, J., and Scheibe, R. (2014). Lack of malate valve capacities lead to improved N-assimilation and growth in transgenic A. thaliana plants. *Plant Signal Behav.* 9, e29057. doi: 10.4161/psb.29057

Shevchenko, A., Wilm, M., Vorm, O., and Mann, M. (1996). Mass spectrometric sequencing of proteins from silver-stained polyacrylamide gels. *Anal. Chem.* 68, 850–858. doi: 10.1021/ac950914h

Shikanai, T., and Yamamoto, H. (2017). Contribution of cyclic and pseudo-cyclic electron transport to the formation of proton motive force in chloroplasts. *Mol. Plant* 10, 20–29. doi: 10.1016/j.molp.2016.08.004

Stepien, P., and Johnson, G. N. (2009). Contrasting responses of photosynthesis to salt stress in the glycophyte *Arabidopsis* and the halophyte *Thellungiella*: role of the plastid terminal oxidase as an alternative electron sink. *Plant Physiol.* 149, 1154–1165. doi: 10.1104/pp.108.132407

Suorsa, M., Rossi, F., Tadini, L., Labs, M., Colombo, M., Jahns, P., et al. (2016). PGR5-PGRL1-dependent cyclic electron transport modulates linear electron transport rate in *Arabidopsis thaliana*. *Mol. Plant* 9, 271–288. doi: 10.1016/j.molp.2015.12.001

Szalonek, M., Sierpien, B., Rymaszewski, W., Gieczewska, K., Garstka, M., Lichocka, M., et al. (2015). Potato annexin STANN1 promotes drought tolerance and mitigates light stress in transgenic *Solanum tuberosum* L. plants. *PloS One* 10, e0132683. doi: 10.1371/journal.pone.0132683

Umbach, A. L., Fiorani, F., and Siedow, J. N. (2005). Characterization of transformed *Arabidopsis* with altered oxidase levels and analysis of effect on reactive oxygen species in tissue. *Plant Physiol.* 139, 1806–1820. doi: 10.1104/pp.105.070763

van Wijk, K. J., and Kessler, F. (2017). Plastoglobuli: plastid microcompartments with integrated functions in metabolism, plastid developmental transitions, and environmental adaptation. *Annu. Rev. Plant Biol.* 68, 253–289. doi: 10.1146/annurev-arplant-043015-111737

Vanlerberghe, G. C. (2013). Alternative oxidase: a mitochondrial respiratory pathway to maintain metabolic and signaling homeostasis during abiotic and biotic stress in plants. *Int. J. Mol. Sci.* 14, 6805–6847. doi: 10.3390/ijms14046805

Veljovic-Jovanovic, S. D., Pignocchi, C., Noctor, G., and Foyer, C. H. (2001). Low ascorbic acid in the *vtc-1* mutant of *Arabidopsis is* associated with decreased growth and intracellular redistribution of the antioxidant system. *Plant Physiol.* 127, 426–435. doi: 10.1104/pp.010141

Vernon, L. P., and Cardon, S. (1982). Direct spectrophotometric measurement of photosystem I and photosystem II activities of photosynthetic membrane preparations from *Cyanophora paradoxa*, *Phormidium laminosum*, and spinach. *Plant Physiol.* 70, 442–445. doi: 10.1104/pp.70.2.442

Vishwakarma, A., Tetali, S. D., Selinski, J., Scheibe, R., and Padmasree, K. (2015). Importance of the alternative oxidase (AOX) pathway in regulating cellular redox and ROS homeostasis to optimize photosynthesis during restriction of the cytochrome oxidase pathway in *Arabidopsis thaliana*. *Ann. Bot.* 116, 555–569. doi: 10.1093/aob/mcv122

Voss, I., Sunil, B., Scheibe, R., and Raghavendra, A. S. (2013). Emerging concept for the role of photorespiration as an important part of abiotic stress response. *Plant Biol.* 15, 713–722. doi: 10.1111/j.1438-8677.2012.00710.x

Ware, M. A., Belgio, E., and Ruban, A. V. (2014). Comparison of the protective effectiveness of NPQ in *Arabidopsis* plants deficient in PsbS protein and zeaxanthin. *J. Exp. Bot.* 66, 1259–1270. doi: 10.1093/jxb/eru477

Watanabe, C. K., Hachiya, T., Terashima, I., and Noguchi, K. (2008). The lack of alternative oxidase at low temperature leads to a disruption of the balance in carbon and nitrogen metabolism, and to an up-regulation of antioxidant defence systems in *Arabidopsis thaliana* leaves. *Plant Cell Environ.* 31, 1190–1202. doi: 10.1111/j.1365-3040.2008.01834.x

Yoshida, K., Terashima, I., and Noguchi, K. (2007). Up-regulation of mitochondrial alternative oxidase concomitant with chloroplast over-reduction by excess light. *Plant Cell Physiol.* 48, 606–614. doi: 10.1093/pcp/pcm033

Zhu, Z., Gerendás, J., Bendixen, R., Schinner, K., Tabrizi, H., Sattelmacher, B., et al. (2000). Different tolerance to light stress in NO_3^- and NH_4^+-grown *Phaseolus vulgaris* L. *Plant Biol.* 2, 558–570. doi: 10.1055/s-2000-7498

Zhu, Y., Liberton, M., and Pakrasi, H. B. (2016). A novel redoxin in the thylakoid membrane regulates the titer of photosystem I. *J. Biol. Chem.* 291, 18689–18699. doi: 10.1074/jbc.M116.721175

Conflict of Interest: The authors declare that the research was conducted in the absence of any commercial or financial relationships that could be construed as a potential conflict of interest.

frontiers in Plant Science

ORIGINAL RESEARCH
published: 28 February 2020
doi: 10.3389/fpls.2020.00194

Primary Metabolite Responses to Oxidative Stress in Early-Senescing and Paraquat Resistant *Arabidopsis thaliana rcd1 (Radical-Induced Cell Death1)*

Nina Sipari[1,2]*, *Jenna Lihavainen*[1,3], *Alexey Shapiguzov*[4,5], *Jaakko Kangasjärvi*[4] *and Markku Keinänen*[2]

[1] Viikki Metabolomics Unit, Faculty of Biological and Environmental Sciences, University of Helsinki, Helsinki, Finland, [2] Department of Environmental and Biological Sciences, University of Eastern Finland, Joensuu, Finland, [3] Department of Plant Physiology, Umeå University, Umeå, Sweden, [4] Organismal and Evolutionary Biology Research Programme, Faculty of Biological and Environmental Sciences, University of Helsinki, Helsinki, Finland, [5] Institute of Plant Physiology, Russian Academy of Sciences, Moscow, Russia

OPEN ACCESS

Edited by:
Kentaro Ifuku,
Kyoto University, Japan

Reviewed by:
Kjell Sergeant,
Luxembourg Institute of Science and Technology, Luxembourg
Md Sanaullah Biswas,
Bangabandhu Sheikh Mujibur Rahman Agricultural University, Bangladesh

***Correspondence:**
Nina Sipari
nina.sipari@helsinki.fi

Specialty section:
This article was submitted to Plant Physiology, a section of the journal Frontiers in Plant Science

Received: 30 October 2019
Accepted: 10 February 2020
Published: 28 February 2020

Citation:
Sipari N, Lihavainen J, Shapiguzov A, Kangasjärvi J and Keinänen M (2020) Primary Metabolite Responses to Oxidative Stress in Early-Senescing and Paraquat Resistant Arabidopsis thaliana rcd1 (Radical-Induced Cell Death1). Front. Plant Sci. 11:194. doi: 10.3389/fpls.2020.00194

Rcd1 (*radical-induced cell death1*) is an *Arabidopsis thaliana* mutant, which exhibits high tolerance to paraquat [methyl viologen (MV)], herbicide that interrupts photosynthetic electron transport chain causing the formation of superoxide and inhibiting NADPH production in the chloroplast. To understand the biochemical mechanisms of MV-resistance and the role of RCD1 in oxidative stress responses, we performed metabolite profiling of wild type (Col-0) and *rcd1* plants in light, after MV exposure and after prolonged darkness. The function of RCD1 has been extensively studied at transcriptomic and biochemical level, but comprehensive metabolite profiling of *rcd1* mutant has not been conducted until now. The mutant plants exhibited very different metabolic features from the wild type under light conditions implying enhanced glycolytic activity, altered nitrogen and nucleotide metabolism. In light conditions, superoxide production was elevated in *rcd1*, but no metabolic markers of oxidative stress were detected. Elevated senescence-associated metabolite marker levels in *rcd1* at early developmental stage were in line with its early-senescing phenotype and possible mitochondrial dysfunction. After MV exposure, a marked decline in the levels of glycolytic and TCA cycle intermediates in Col-0 suggested severe plastidic oxidative stress and inhibition of photosynthesis and respiration, whereas in *rcd1* the results indicated sustained photosynthesis and respiration and induction of energy salvaging pathways. The accumulation of oxidative stress markers in both plant lines indicated that MV-resistance in *rcd1* derived from the altered regulation of cellular metabolism and not from the restricted delivery of MV into the cells or chloroplasts. Considering the evidence from metabolomic, transcriptomic and biochemical studies, we propose that RCD1 has a negative effect on reductive metabolism and rerouting of the energy production pathways. Thus, the altered, highly active reductive metabolism, energy salvaging pathways and

redox transfer between cellular compartments in *rcd1* could be sufficient to avoid the negative effects of MV-induced toxicity.

Keywords: *Arabidopsis thaliana*, RCD1, paraquat, methyl viologen, metabolite profiling, oxidative stress, senescence, glycolysis

INTRODUCTION

Reactive oxygen species (ROS) such as superoxide ($O_2^{\bullet-}$) and hydrogen peroxide (H_2O_2) are important signaling molecules inevitably formed in aerobic energy metabolism. Although basal levels of ROS are required for normal plant performance and development, in excess they cause oxidative stress that could damage cells and trigger physiological and programmed metabolic pathways, which can induce cell death (Noctor et al., 2015; Mittler, 2017; Waszczak et al., 2018). Plants have developed antioxidant systems and complex signaling networks to maintain redox homeostasis and energy metabolism, and to integrate ROS signals with other cellular signals. Despite the high capacity and redundancy of the ROS scavenging systems, alterations in ROS levels have potentially wide-ranging consequences for metabolic processes, including rearrangements in central metabolic pathways and energy metabolism (Baxter et al., 2007; Scarpeci and Valle, 2008; Lehmann et al., 2009; Noctor et al., 2015; Mittler, 2017).

Typically, exposure to excessive levels of ROS causes the down-regulation of anabolic metabolism (e.g. Calvin cycle) while favoring catabolic metabolism, such as oxidative pentose phosphate pathway (OPPP) and lipid, protein and starch degradation, to provide substrates for the production of ATP and reducing power in the form of NAD(P)H. In *Arabidopsis,* changes in gene expression and sugar levels indicated altered metabolism in response to treatment with ROS-generating herbicide, methyl viologen (MV), and the responses resembled transcriptomic changes in plants adapted to darkness (Scarpeci and Valle, 2008).

Soluble sugars play a central role in energy metabolism and signaling, but also a multifaceted role in respect to ROS (Couée et al., 2006). Soluble sugars can be directed to OPPP for NADPH production, which can contribute to ROS scavenging, or they can be involved in ROS-producing metabolic pathways. NADPH has also a dual role in ROS homeostasis, because it serves as a donor of reducing power for ROS processing and facilitates apoplastic ROS generation by the plasma membrane NADPH oxidases. Furthermore, NADP(H), as well as NAD(H), essentially link metabolism to redox signaling, and alterations in their concentrations and redox states strongly affect metabolic pathways involved in ROS responses (Munné-Bosch et al., 2013; Noctor and Mhamdi, 2017).

Paraquat (MV) is widely used for weed control and as a tool in plant science as an electron acceptor of Photosystem I (PSI) and inducer of ROS generation. In chloroplast, MV inhibits photosynthesis by attracting electrons from PSI, which in turn inhibits the reduction of ferredoxin and the production of NADPH (Calderbank, 1968; Farrington et al., 1973). At the same time, superoxide ($O_2^{\bullet-}$) is formed from O_2 in the MV redox cycle while NADPH is consumed (Cochemé and Murphy, 2009). Chloroplastic superoxide dismutase (SOD) converts superoxide to H_2O_2, which is further scavenged by antioxidant system or translocated to other cell compartments (Asada, 1994; Foyer et al., 1994). Without photosynthetic activity, as in plants in darkness or in yeast or animal cells, MV induces the production of ROS in mitochondria (Lambert and Bondy, 1989; Bowler et al., 1991; Taylor et al., 2002; Cui et al., 2019). In yeast and animal cells, MV attracts electrons from various mitochondrial enzymes (e.g. NADPH dehydrogenases) and complexes I and III (Lambert and Bondy, 1989; Cochemé and Murphy, 2008), but the mitochondrial targets of MV in plant cells have not been characterized.

Several mechanisms have been proposed to account for MV-resistance in higher plants, including sequestration of MV, detoxification of ROS by enzymatic antioxidants (Fuerst and Vaughn, 1990; Hart and Di Tomaso, 1994; Tsugane et al., 1999; Chen et al., 2009; Xi et al., 2012; Li et al., 2013), reduced poly (ADP-ribose)polymerase (PARP) activity and/or increased NADH levels (De Block et al., 2005; Ishikawa et al., 2009; Ogawa et al., 2009). Polyamines and their transporters have been proposed to have a role in MV-resistance due to the structural similarities of the herbicide and polyamines and the non-specific transport of MV into vacuoles (Benavides et al., 2000; Fujita et al., 2012; Li et al., 2013; Fujita and Shinozaki, 2014).

Arabidopsis thaliana rcd1 (radical-induced cell death1) shows high resistance to MV-induced chloroplastic ROS but is sensitive to ozone and apoplastic superoxide (Ahlfors et al., 2004; Fujibe et al., 2004; Katiyar-Agarwal et al., 2006). RCD1 is a PARP-like protein, belonging to the SRO-gene family (Similar-to-RCD1), yet it has no direct PARP-activity (Jaspers et al., 2009). However, RCD1 has been suggested to be a candidate target for PARP-inhibitors, as SRO-proteins possess a PARP-like domain and are involved in stress responses similarly to PARP-proteins (Rissel et al., 2017). RCD1 has been implicated in redox signaling from both chloroplasts (Fujibe et al., 2004; Hiltscher et al., 2014; Cui et al., 2019; Shapiguzov et al., 2019) and mitochondria (Brosché et al., 2014; Cui et al., 2019; Shapiguzov et al., 2019). RCD1 interacts with several transcription factors that are involved in developmental processes or plant stress responses (Jaspers et al., 2009). RCD1 negatively regulates ANAC013 and ANAC017, which positively regulates mitochondrial dysfunction stimulon genes (Shapiguzov et al., 2019). The MV tolerance in *rcd1* has been previously associated with altered redox status, the high expression of plastidic SOD and ascorbate peroxidase (APX) (Fujibe et al., 2004) and the higher expression of *AOX* genes

(Brosché et al., 2014). Nevertheless, no unambiguous cause for MV tolerance in *rcd1* has been found.

The alterations in redox status and metabolite exchange between organelles (e.g. redox valves, redox-regulated transporters) coordinate cellular functions during stress and developmental stages. There are two main redox valves in photosynthetic plant cells, the chloroplastic malate valve driven by photosynthetically produced NADPH that increases subcellular (in mitochondria, peroxisomes, cytosol, and plastids) NADH/NAD^+ ratios (Krömer and Scheibe, 1996; Selinski and Scheibe, 2019), and the mitochondrial citrate valve, driven by increased reduction level in mitochondria, that reduces subcellular NADP pools (Igamberdiev and Gardeström, 2003). In addition, the mitochondrial malate-aspartate shuttle transfers reducing equivalents from cytoplasm to mitochondria while coupling the TCA cycle to nitrogen assimilation by interconversion and shuttling of oxaloacetate (OAA), aspartate (Asp), glutamate (Glu), α-ketoglutarate (α-KG) and malate. In plants, the TCA cycle is also tightly connected to the GABA shunt, which is the main producer of succinate and which can bypass two steps of the TCA cycle. The catabolism of GABA in mitochondria is also linked to the interconversion of pyruvate (Pyr) and α-KG to alanine (Ala) and Glu (Studart-Guimarães et al., 2007; Fait et al., 2008).

Various TCA cycle organic acids (di- and tricarboxylic acids) and dicarboxylic amino acids (Asp, Glu) are also transported between organelles by di/tricarboxylate transporters *via* a counter-exchange mechanism (Linka and Weber, 2010; Facchinelli and Weber, 2011) α-KG is transported to the chloroplasts *via* 2-OG/malate transporter for ammonium assimilation in the GS/GOGAT cycle, but its enzymatic origin may vary. α-KG is most likely provided by cytosolic and mitochondrial isocitrate dehydrogenases (ICDH's) and aspartate aminotransferases (AAT's). NAD-dependent ICDH are only found in mitochondria, but NADP-dependent isoforms of ICDH are localized in cytosol, mitochondria, peroxisomes or chloroplasts (Hodges, 2002; Foyer et al., 2011). The conversion of isocitrate to α-KG by NADP-ICDH not only produces NADPH, but also functions as a crossroads of shuttling carbon (and reducing power) between organelles, cross-linking metabolic processes (TCA, amino acid biosynthesis, nitrogen assimilation, fatty acid synthesis and energy production). Although ICDH is also found in the plastids, the site of the GS/GOGAT pathway, the cytosolic ICDH is reported to play a major role (90%) in α-KG production for amino acid synthesis and to be predominant isoform in plants in control growth conditions (Mhamdi et al., 2010; review by Foyer et al., 2011). This is in line with previous studies of TCA cycle to function only partially in light while mitochondrial citrate (precursor for α-KG) is exported to cytosol (and/or other organelles) for amino acid assimilation. However, the loss of cytosolic NADP-ICDH activity did not have a large impact on leaf compounds associated to C and N metabolism, indicating fine-tuned redundancies between the isoforms localized in other cell organelles (Foyer et al., 2011; Mhamdi and Noctor, 2015). The activation of citrate efflux from mitochondria to cytosol decreases the carbon flow to the rest of the TCA cycle leading to reduced levels of mainly malate and fumarate due to redox and thioredoxin regulation (Daloso et al., 2015).

To study the function of RCD1 in plant energy metabolism, untargeted metabolite profiling was performed to assess the metabolic features of *rcd1* mutant in light, in response to MV exposure and after extended darkness. The primary metabolite responses of MV-resistant (*rcd1*) and MV-sensitive (Col-0) plant lines were compared to elucidate the tolerance mechanisms in the mutant plants. The possible functions of RCD1 in the regulation of cellular redox status, and central carbon and nitrogen metabolism are discussed.

MATERIALS AND METHODS

Plant Material

A. thaliana wild type (Col-0) and *rcd1-4* (GK-229D11, Col-0 background) seedlings were grown on 1× MS with 0.5% Phytagel without sucrose on plates (metabolomics) or on multi-well plates (histochemical staining). Plants were grown under 12-h photoperiod in 150 μmol m^{-2} s^{-1} light for 14 days. Prior to the dark period (12 h night), 5 ml (plates) or 0.5 ml (wells) of MQ water (control) or MV (50 μM) was added. The seedlings were kept in the growth room conditions either for 16 h in darkness (for the dark treatment), or exposed to 12 h of darkness overnight followed by 4 h of growth light in the morning (for light and MV treatments). Seedlings for metabolite analysis were harvested, and pooled plant samples (approx. 100 mg) were snap-frozen in liquid nitrogen and stored at -80°C. Seedlings were pooled due to small size and to ensure detectability of low concentration metabolites. Experiment was performed once with 2-h light exposure time and twice with 4-h light exposure, in presence of MV, or extended darkness. The results from all three experiments were consistent, even though plants showed more intensive responses with 4-h exposures and data from one 4-h experiment is shown.

Metabolite Extraction and Derivatization

Primary metabolites were analyzed with gas chromatography–mass spectrometry (GC-MS) according to Roessner et al. (2000) and starch was analyzed from the plant residue after extraction of soluble metabolites with the method described in Smith and Zeeman (2006). GC-MS analysis was executed for 6–8 pooled plant samples. Plant material was homogenized with a ball mill (TissueLyser II, Qiagen, Germany) with 1–1.5 mm glass beads. Powdered plant material was extracted twice, first with 1 ml of 100% methanol (Merck) and then with 80% (v/v) aqueous methanol. Internal standards (benzoic-d_5 acid, glycerol-d_8, 4-methylumbelliferone) were added to each sample during the first extraction step. During both extraction steps, samples were vortexed for 30 min and centrifuged for 5 min at 13,000 rpm (13,500×g) at 4°C. The supernatants were combined and an aliquot of 100 μl was transferred to a vial and dried in a vacuum (MiVac Duo concentrator, GeneVac Ltd, Ipswich, UK). Quality control

samples were prepared by combining aliquots of samples from each plant line and each treatment. The vials were treated with nitrogen gas and stored at -80°C prior to derivatization and GC-MS analysis. The samples were redissolved in 40 µl of methoxyamine hydrochloride (MAHC, Sigma) (20 mg ml^{-1}) in pyridine (VWR) and incubated for 90 min at 30°C at 150 rpm. The samples were then silylated with 80µl N-methyl-N-(trimethylsilyl) trifluoroacetamide with 1% trimethylchlorosilane (MSTFA with 1% TMCS, Thermo Scientific) for 90 min at 37°C at 150 rpm, and 100 µl of hexane (Sigma) containing alkane series (C10–C40, Supelco) was added to each sample.

Metabolite Analysis by Gas Chromatography–Mass Spectrometry

The GC-MS system consisted of Agilent 7890A chromatograph system with Agilent 7000 Triple quadrupole mass spectrometer and GC PAL autosampler and injector (CTC Analytics). Sample (1 µl) was injected in splitless mode in a single tapered liner with glass wool (Topaz 4 mm ID Restek). Inlet temperature was set to 260°C. Helium flow in the column (Agilent HP-5MS Ultra Inert, length 30 m, 0.25 mm ID, 0.25 µm film thickness combined with Agilent Ultimate Plus deactivated fused silica, length 5 m, 0.25 mm ID) was 1.2 ml min^{-1} and purge flow was 46 ml min^{-1}. MSD interface temperature was 180°C, MS source 230°C and quadrupole 150°C. The oven temperature program was as follows: 2 min at 50°C, followed by a 7°C min^{-1} ramp to 260°C, 15°C min^{-1} to 325°C, 4 min at 325°C and post-run at 50°C for 4.5 min. Mass spectra were collected with a scan range of 55-550 *m*/z. Deconvolution, component detection and quantification were conducted with Metabolite Detector (2.06 beta) (Hiller et al., 2009), and co-eluting components were confirmed with AMDIS (version 2.66, NIST). To confirm the identification of two detected metabolites, commercial standards of 3-hydroxy-3-methyl-glutarate (3-HMG), and 2-hydroxy-glutarate (2-HG) were analyzed. Metabolites were annotated based on standards or retention index and mass spectrum matched to databases and spectral libraries (Golm GMD database, Human Metabolome Database (HMDB), Fiehn GC/MS Metabolomics RTL library A.01.00, NIST, Wiley Registry MS-7^{th} edition). The relative contents of the metabolites were calculated by normalizing the peak areas by the peak area of the internal standard (ISTD, glycerol-d_8) and the fresh weight (g) of the sample. The list of metabolites detected by GC-MS is in **Supplementary Table S1**. The redox status indicator ratios were calculated as in Kolbe et al. (2006) for isocitrate dehydrogenase (ICDH) or malate dehydrogenase (MDH). According to Kolbe et al. (2006) the NAD(P)-reduction state can be calculated with product/substrate ratio of NAD(P)-linked reactions like ICDH or MDH. The list of other NAD(P)H-producing dehydrogenases, with products and substrates were taken from Schertl and Braun (2014), and the ratios (product/substrate ratio) were calculated if both product and substrate were detected (**Supplementary Figure S1**).

Histochemical Determination of Reactive Oxygen Species

The seedlings for histochemical detection were grown and exposed to MV identically to the seedlings for metabolite analysis as described in *Plant material*. Hydrogen peroxide and superoxide production were detected by staining plants with 3,3′-diaminobenzidine (DAB) as in Daudi et al. (2012) or with nitrotetrazolium blue (NBT) as in Jabs et al. (1996). After 16-h dark period (dark samples) or 12-h darkness overnight followed by 4.5 h of growth light, MQ water or MV solution was removed, and 1 ml of DAB or NBT solution was added to each well and infiltrated in a vacuum under dim light (<10 µmol m^{-2} s^{-1}). Plants were then exposed to growth light (150 µmol m^{-2} s^{-1}) for 30 min to stimulate ROS production, and/or kept in dark for 60 min, and then destained in 15 ml tubes.

Statistical Analysis

Significant main effects of plant line, treatment and line × treatment interactions on individual metabolite levels and metabolite ratios were tested by two-way ANOVA with false discovery rate correction for multiple analysis, p-value < 0.05 considered significant (MassProfilerPro, Agilent). Significant effects on the metabolite levels were then visualized in Venn diagram. Principal component analysis (PCA) was performed to visualize general variation in the GC-MS data (MassProfilerPro). ANOVA-simultaneous component analysis was performed with 100 permutations to test the effects of plant line, treatment and their interaction (line × treatment) on the overall variation in the metabolite data [MetaboAnalyst, (Xia and Wishart, 2016)]. Orthogonal projections to latent structures discriminant analysis (OPLS-DA) was performed to study the differences of metabolite levels between the plant lines in control light conditions (Simca P+ version 15, Umetrics). In addition, OPLS-DA models were produced separately for *rcd1* and Col-0 comparing light to dark or to MV samples (see model diagnostics in **Supplementary Table S2**). S-plots were combined to produce shared and unique structures (SUS) plots to compare metabolite responses of *rcd1* and Col-0 to extended darkness or to MV treatment. PCA, OPLS-DA, and two-way ANOVA were performed without missing value imputation with log10-transformed data scaled by unit variance. Pathway analysis was performed to identify relevant metabolic pathways that differed between *rcd1* and Col-0 in control light conditions, after extended darkness and after MV treatment (MetaboAnalyst). Metabolic pathway enrichment analysis was based on 150 annotated metabolites in KEGG pathways. Data were log_{10}-transformed, scaled by unit variance and missing values were imputed with k-nearest-neighbour (KNN) method. Pathway topology analysis was based on relative-betweenness centrality measurement and the significance of pathway enrichment analysis was tested with a global test algorithm. P-values derived from pathway enrichment analysis were natural base (e)-transformed.

RESULTS AND DISCUSSION

Metabolite Profiles of *rcd1* and Col-0 Differ From Each Other and in Response to Methyl Viologen Treatment

Multivariate statistics were used to investigate the metabolite profiles of *rcd1* and wild type Col-0 plants in light (L), after MV exposure (MV) in light and after extended darkness (D) (**Figure 1**). The visual phenotypes of the two-week-old seedlings of *rcd1* mutant and Col-0 plants did not differ at the time of sampling (**Supplementary Figure S2**). However, based on their metabolite profiles, the plant lines were separated in PCA by the first principal component explaining 21.2% of the total variation (**Figure 1A**). Out of the 488 metabolites detected by GC-MS (plus starch), the levels of 320 metabolites were significantly different between the plant lines (**Figure 1B**, **Supplementary Table S3**). Samples from light conditions (L) and from extended darkness (D) were separated by the second principal component explaining 12.2% of the variation (**Figure 1A**). Since the responses to extended darkness were mainly similar in both plant lines (**Figures 1A** and **2A**), the large number of metabolites displaying significant line × treatment interaction (217 metabolites, **Figure 1B**) described primarily the different responses of *rcd1* and Col-0 to MV treatment (**Figure 2B**). In Col-0, MV samples were separated by the second principal component from the light samples and grouped close to the dark samples in PCA (**Figure 1A**). In marked contrast, MV samples of *rcd1* grouped close to the light samples (**Figure 1A**), which is in line with the MV-resistance of *rcd1*. The effects of line ($p < 0.01$), treatment ($p < 0.01$), and interaction term ($p = 0.05$) were significant in ANOVA-simultaneous component analysis (**Supplementary Figure S3**). Thus, the metabolite results were interpreted in the context of all three experimental conditions.

In pathway enrichment analysis, the metabolic pathways which were consistently enriched in *rcd1* irrespective of treatment, were connected to carbon fixation; aromatic amino acid and BCAA (+Lys) biosynthesis; purine, pyrimidine, nucleotide and ubiquinone metabolism; photorespiration and Thr metabolism; Arg and Pro metabolism; isoquinoline alkaloid as well as phenylpropanoid biosynthesis (**Figure 3**, **Supplementary Table S4**). In control conditions, several metabolite ratios describing photorespiration (Gly/Ser), nitrogen assimilation (Glu/Asp, Asn/Asp, Gln/Glu, Pro/Glu) and/or redox status [e.g. Cit/α-KG, 2-HG/α-KG, (Mal × Glu)/(Asp × α-KG)] were similar in both lines except xanthine/urate ratio, which was significantly higher in *rcd1* (**Figures 4** and **5**, **Supplementary Tables S1** and **S3**). The metabolite ratios had a similar response in both lines to extended darkness, except for Pro/Glu ratio, which showed no change in Col-0, while the ratio was 1.5-fold higher in *rcd1* in darkness than in light. The most significant differences between Col-0 and *rcd1* were detected in response to MV exposure (**Figures 4** and **5**). The two plant lines had an opposite response in amino acid and redox status indicator ratios, except Gly/Ser and xanthine/urate ratios (**Figure 5**). Both Gly/Ser and xanthine/urate ratios had similar response in both plant lines, but the response in *rcd1* was

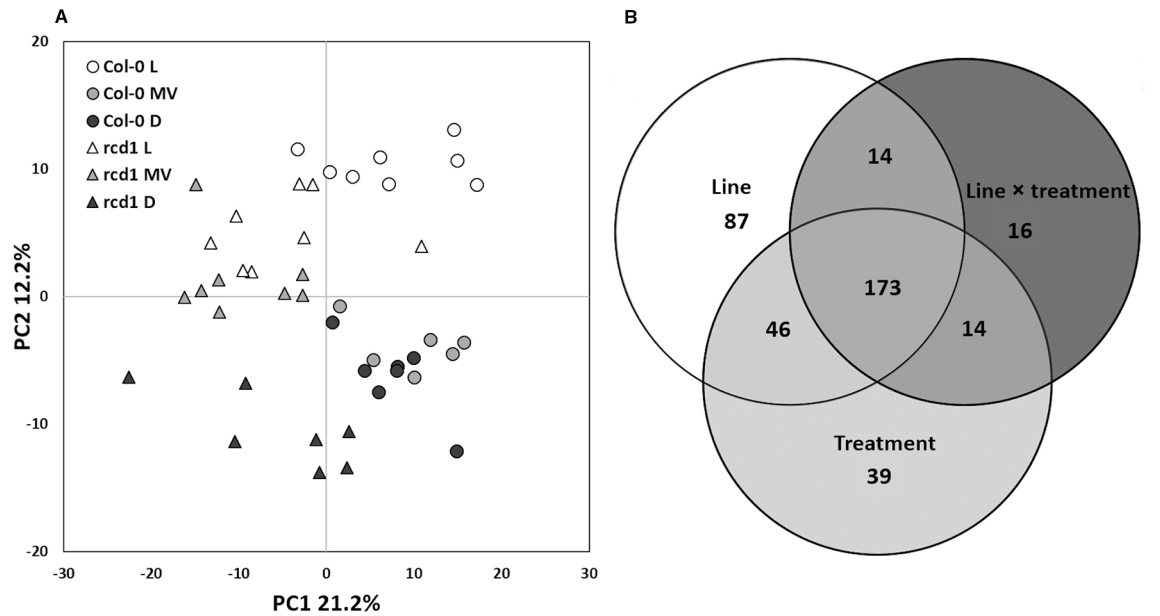

FIGURE 1 | (A) Statistical analysis of GC-MS metabolite data of Col-0 and *rcd1* plants. Scores plot of principal component analysis of 489 metabolites. The first principal component separates the two plant lines and treatments are separated based on the second principal component, n = 6–8. Symbols and colors indicate different plant lines and conditions: circle and triangle indicate Col-0 and *rcd1*, and white, light gray and black indicate light/control (L), paraquat exposure (MV) and dark (D) conditions, respectively. **(B)** Venn diagram shows statistically significant effects of plant line (white), treatment (light gray) and line×treatment (dark gray) interaction on metabolite levels, two-way ANOVA, $p < 0.05$). The details of statistical results and the list of metabolites are in **Supplementary Tables S1** and **S3**.

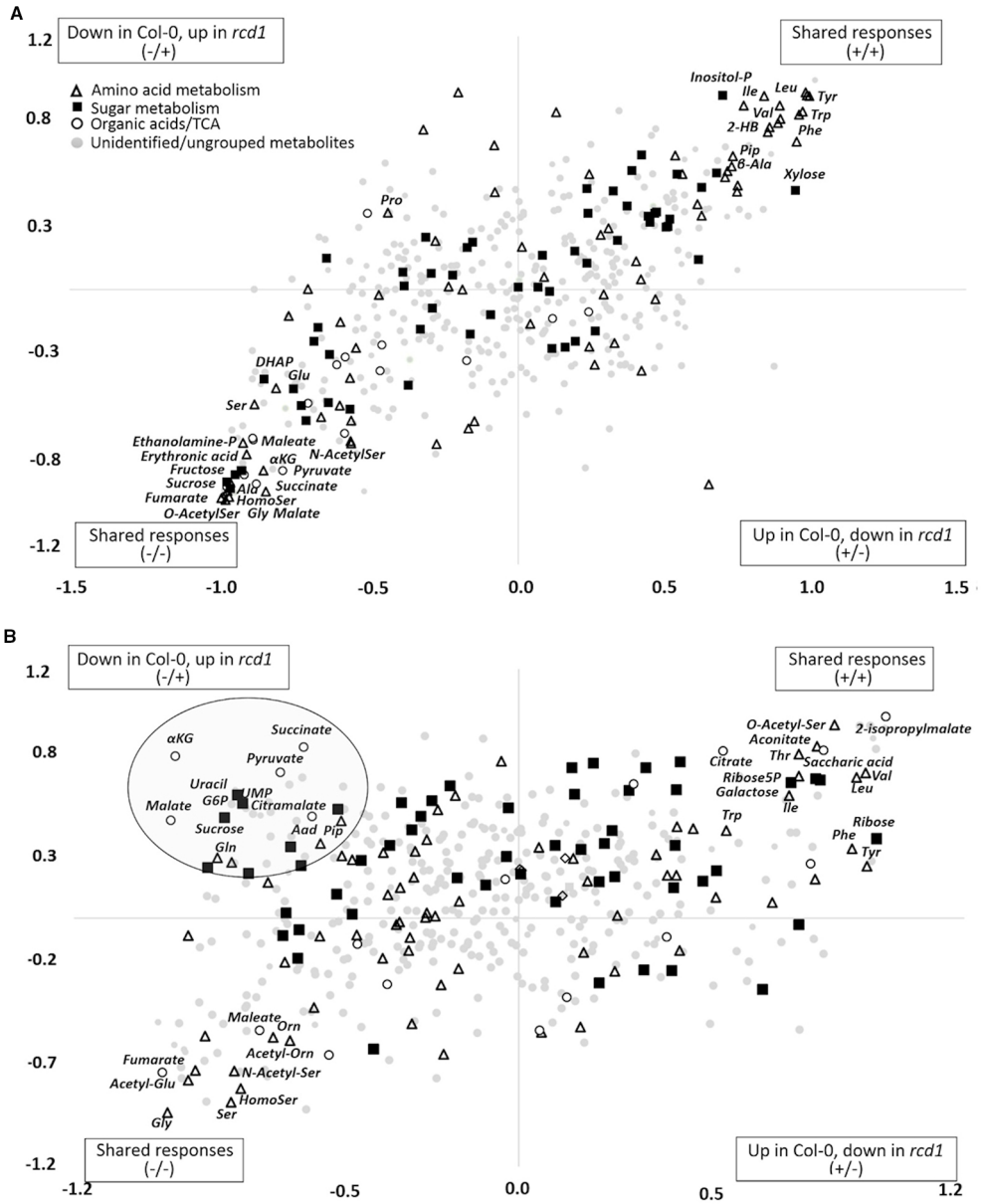

FIGURE 2 | (A) Shared and unique structures (SUS)-plot of discriminant analysis (OPLS-DA) comparing metabolite responses of *rcd1* and Col-0 to extended darkness and to **(B)** MV treatment. Metabolites displaying similar responses in both plant lines are in upper right or lower left corner. Metabolites located along the axes display line-specific responses and metabolites located in the upper left or lower right corner display opposite responses in the plant lines. p(corr) is the OPLS-DA loading scaled as correlation coefficient. Dot shapes and colors indicate different metabolite groups. White triangle: amino acid metabolism, black square: sugar metabolism, white circle: organic acids/TCA cycle, light gray circle: unidentified/ungrouped metabolites (n = 6-8). The list of metabolite correlation coefficient values are in **Supplementary Table S6**.

significantly weaker (Gly/Ser) and/or the ratio remained significantly higher (xanthine/urate).

Altered Reactive Oxygen Species Production in *rcd1*

Seedlings were stained with DAB (3,3′-diaminobenzidine) and with NBT (nitro blue tetrazolium) to detect hydrogen peroxide (H_2O_2) and superoxide ($O_2^{\bullet-}$) production, respectively (**Supplementary Figure S4**). NBT-staining revealed higher superoxide production in *rcd1* than in Col-0 in light conditions, yet no difference in superoxide production was observed in either of the plant lines in dark (**Supplementary Figure S4**). Induction of ROS production after 30 min exposure of light during staining, can already be seen in *rcd1* seedlings (**Supplementary Figures S4B, D**), indicating that superoxide production in *rcd1,* and the function of RCD1 are related to

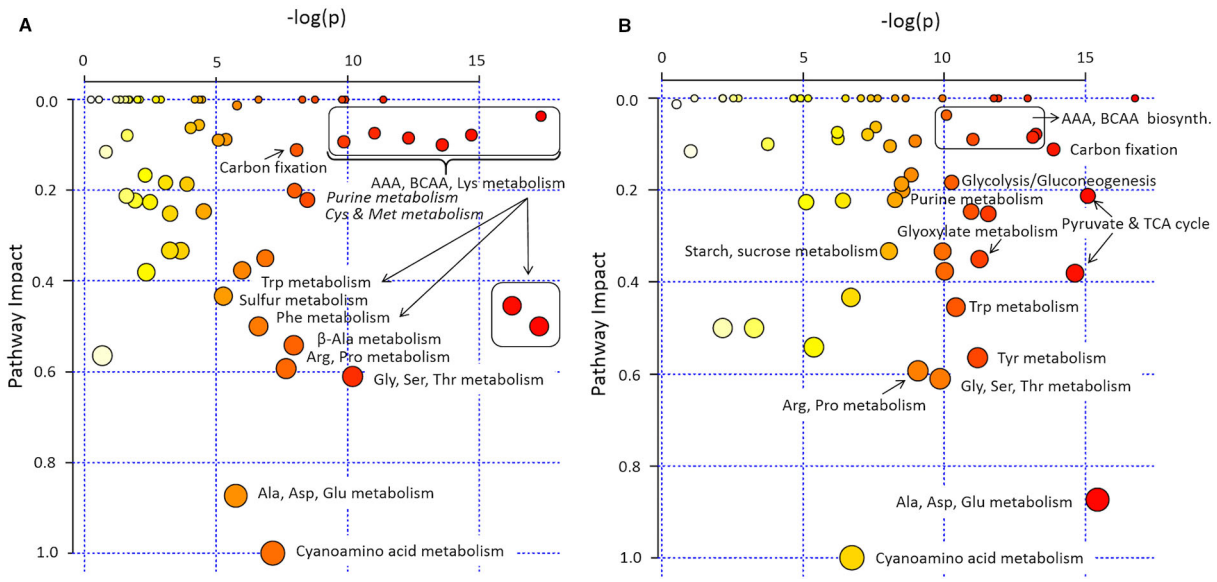

FIGURE 3 | Pathway enrichment analysis of *rcd1* primary metabolite profile. **(A)** Light/control condition, **(B)** after 4h paraquat (MV) exposure in light (4 h light + 12 h in dark). Size of the node represents the intensity of the impact of plant line on the KEGG pathway based on the impact of each metabolite in a given pathway. Colour scale represents the significance of the pathway impact [-log(p); natural, e-base-log-transformation]. The list of pathways with their impact and -log(p) values are in **Supplementary Table S4**.

light-dependent processes. Increased superoxide production in *rcd1* has been published previously with older plants (Zhu et al., 2013; Shapiguzov et al., 2019), but not with young, 2-week old seedlings. However, no increase in H_2O_2 production was detected in *rcd1*, irrespective of age (**Supplementary Figure S4**) (Zhu et al., 2013; Shapiguzov et al., 2019). MV exposure caused a substantial increase of H_2O_2 in Col-0, but not in *rcd1* (**Supplementary Figure S4A**). By contrast, superoxide production slightly decreased in *rcd1* after MV exposure (**Supplementary Figures S4B, D**).

Metabolic Features of *rcd1*

In control light conditions, pathway enrichment analysis showed that carbon fixation, amino acid metabolism and nucleotide metabolism were the most significantly changed in *rcd1* (**Figure 3A**). The levels of several glycolytic intermediates (sugars and sugar phosphates), amino acids [Aromatic; Phe, Tyr, Trp; BCAA's; Ile, Leu, Val; Lys; β-Ala; Met; His; Thr; Arg; GABA; N-acetyl-Glu (NAG); N-acetyl-Orn (NAO) and ornithine], and polyamines (spermidine, putrescine, agmatine) were higher in *rcd1* than in Col-0 (**Figure 4A**, **Supplementary Figure S5**, and **Tables S1**, **S3**, and **S5**). Starch content was slightly, but consistently, higher in *rcd1* than in Col-0 in all conditions (**Figure 4B**). In light, the glutamine/glutamate (Gln/Glu) ratio, an indicator of nitrogen assimilation, was higher in *rcd1* than in Col-0 (**Figure 5**), corresponding to the enhanced production of many nitrogen containing metabolites in *rcd1*. Low levels of asparagine (Asn) with its precursor, 3-cyano-alanine (**Figure 4A**) brought further evidence of altered N metabolism in *rcd1*. Mutant plants showed also higher levels of metabolites related to catabolism of Lys [pipecolate, 2-amino adipate, 2-HG, 2-hydroxy-butyrate (2-HB)] and Leu (3-HMG) (**Figure 4A**). The decreased metabolites in *rcd1* included citramalate and TCA cycle intermediates; fumarate and malate (**Figure 4C**), as well as metabolites of shikimate pathway: shikimate, *cis*- and *trans*-sinapates and -sinapoyl malates. Both the accumulation of AAA and BCAA metabolites and reduction of Asp, Asn, 3-cyano-Ala, fumarate, malate, citramalate and shikimate, sinapates and sinapoylmalates levels (**Figure 4**) have been associated with plant senescence in *Arabidopsis* (Watanabe et al., 2013). In addition, the free amino acid profile in *rcd1* resembled the changes in free amino acids that occur also during the induction of systemic acquired resistance in *Arabidopsis* (Návarová et al., 2012). Pathway enrichment analysis supported the results from individual metabolite data, and in addition to primary metabolism, also secondary metabolism such as phenylpropanoid biosynthesis was altered in *rcd1* (**Supplementary Table S4**). Nucleotide metabolism was significantly altered in *rcd1*, as the levels of most purines and pyrimidines analyzed, as well as metabolites related to nucleotide catabolism, were consistently higher in *rcd1* than in Col-0 regardless of the treatment (**Figure 4E**). The levels of xanthine, allantoin, inosine, nicotinic acid, 5-hydroxy-Trp, β-Ala, 3-aminoisobutyrate, thymine, guanine, adenosine and AMP were all higher in *rcd1* than in Col-0 (**Figure 4**, **Supplementary Tables S1** and **S3**). Only the levels of orotic and uric acid were lower in *rcd1* than in Col-0 (**Figure 4E**, **Supplementary Tables S1** and **S3**). Xanthine and uric acid levels are connected to redox regulated xanthine oxidase/dehydrogenase enzyme in cytosol (Ma et al., 2016), and the xanthine/urate ratio was significantly

FIGURE 4 | Continued

FIGURE 4 | Metabolite levels in Col-0 and *rcd1* in control light conditions (white), after MV exposure (light gray) and after extended darkness (dark gray). **(A)** Amino acid and polyamine metabolism, **(B)** carbohydrate metabolism **(C)** TCA cycle, **(D)** ROS indicators and **(E)** nucleotide metabolism. Statistically significant main effects of plant line (L), treatment (T) and line × treatment interaction (L × T) on metabolite levels were tested with two-way ANOVA ($p < 0.05^*$, $p < 0.01^{**}$). Data are mean ± SE, n = 3–8, in arbitrary units (AU) mg^{-1} (FW).

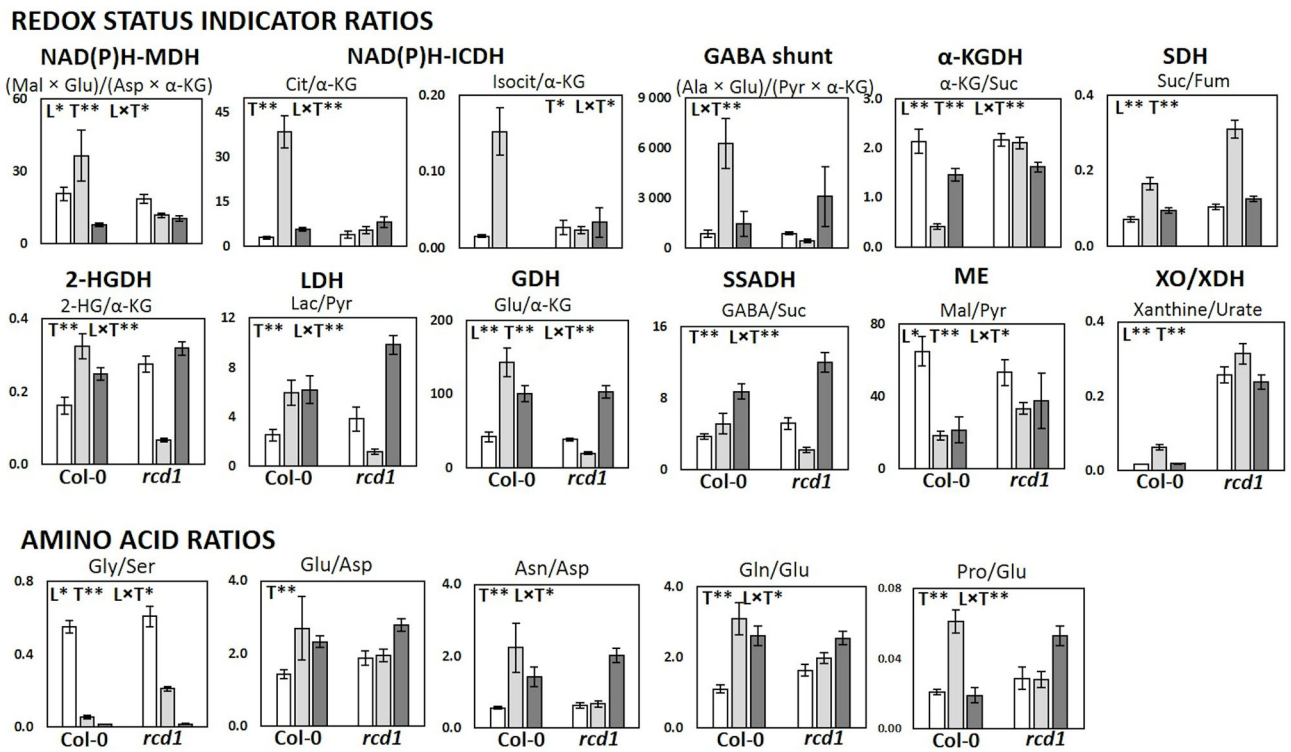

FIGURE 5 | Metabolic and redox status indicator ratios in Col-0 and *rcd1* in control light conditions (white), after MV exposure (light gray) and after extended darkness (dark gray). Statistically significant effects of plant lines (L), treatment (T) and line × treatment interaction (L × T) on metabolite ratios were tested with two-way ANOVA ($p < 0.05^*$, $p < 0.01^{**}$). Data are mean ± SE, n = 3–8.

higher in *rcd1* than in Col-0 irrespective of the treatment (**Figures 4E** and **5**).

Metabolite Responses to Extended Darkness

The *rcd1* mutant responded to extended darkness similarly with Col-0, with the levels of various metabolites remaining consistently higher as in light conditions (**Figures 2A** and **4**). Typical effects of extended darkness were seen in both plant lines in the levels of metabolites linked to glycolysis (sucrose, fructose, glucose, pyruvate, and sorbose), sucrose biosynthesis, photorespiration (glycine, serine, glycolate, and glycerate), TCA cycle (succinate, malate, fumarate, α-ketoglutarate, aconitate, and citrate) and protein catabolism (**Figures 2A** and **4**). Accumulation of AAAs and BCAAs and Lys, and decrease in Ala, Gly, Ser and Asp levels in both *rcd1* and Col-0 after prolonged night is a typical plant response to darkness (Araújo et al., 2010). Amino acids and their precursors accumulate due to inhibited protein synthesis, induced protein degradation, and because of delayed activation of mitochondrial degradation enzymes (BCAA's, AAA's and Lys) after illumination has ended (Araújo et al., 2010). The Gly/Ser ratio decreased in extended darkness, as photorespiration was inhibited (**Figure 5**). As Calvin cycle and CO_2 assimilation are inhibited in darkness due to depletion of photosynthetic NADPH and ATP, the levels of precursors and intermediates from glycolytic pathway decreased, while the levels of hexose phosphates and glucose remained the same due to activation of light-regulated chloroplastic OPPP and starch degradation (**Figure 4B**). The levels of pyruvate and TCA cycle intermediates declined (**Figure 4C**), indicating not only the depletion in carbon supply to the TCA cycle, but also NADPH shortage from chloroplastic (light regulated) NADP-dependent malate-OAA-shuttle, which transfers reducing power to oxidative phosphorylation (COX). Also reduced DHAP levels can be seen in both lines as chloroplastic transport to cytosol *via* triose phosphate transporter (TPT) is inhibited in the dark (Dietz and Heber, 1984; Flügge, 1999), due to repressed conversion of GAP to DHAP as NADPH is needed as a substrate (**Figure 4B**). The most prominent differences between the dark responses in *rcd1*

and Col-0 were seen in the levels of proline (Pro) and asparagine (Asn). Proline accumulated in *rcd1* plants, whereas in Col-0 the levels decreased in response to extended darkness (**Figures 2A** and **4A**). Asn accumulated in *rcd1*, but there were no significant changes in Col-0 (**Figures 2A** and **4A**). Enriched pathways after extended darkness in *rcd1* were related to AAAs, BCAAs (+ Lys), photorespiration and carbon fixation, as well as nucleotide, starch and sucrose metabolism, which were also enriched in the mutant in light conditions (**Figure 3A**, **Supplementary Table S4**). As the plant lines responded similarly to extended darkness, the function of RCD1 in the regulation of central carbon and nitrogen metabolism is mainly linked to light-dependent processes.

The Possible Role of RCD1 in Central Carbon Metabolism

The consistently high levels of several glycolytic intermediates (**Figure 4B**, **Supplementary Figure S5**). indicated enhanced glycolytic activity in *rcd1* mutant that is supported by the previous data on transcriptomics (Brosché et al., 2014) and carbohydrate fluxes (Shapiguzov et al., 2019) The expression of three genes that encode glycolysis-related enzymes, 2,3-bisphosphoglycerate-independent phosphoglycerate mutase, cytosolic pyruvate kinase and fructose-bisphosphate aldolase (aldolase, FBA6) were up-regulated in *rcd1* (Brosché et al., 2014). Aldolase is shared between glycolysis and gluconeogenesis, while pyruvate kinase catalyzes the final step in glycolysis, dephosphorylating phosphoenolpyruvate (PEP) to pyruvate while generating ATP. As the glycolytic metabolite levels were high in *rcd1*, but pyruvate and TCA cycle intermediate levels did not correlate with the increase of glycolytic precursors in control conditions (L), we assume that the additional carbon flux is mainly redirected to cytosolic OPPP, and to starch and sucrose biosynthesis instead of mitochondria. This is consistent with the elevated levels of OPPP-derived metabolites (AAAs, His, sugars, and nucleic acids), starch and sucrose in *rcd1* mutant (**Figure 4** and **Supplementary Figure S5**). Additional evidence of changed carbohydrate metabolism comes from [U-^{14}C] glucose feeding study that revealed enhanced carbon flux to starch and sucrose in *rcd1* (Shapiguzov et al., 2019). In addition to increased glycolytic activity, the elevated levels of OPPP-derived metabolites and sugars in *rcd1* under light conditions suggest increased OPPP activity that can lead to more reductive conditions in the cytosol through the production of NAD(P)H. Cytosolic and chloroplastic OPPPs contribute to redox homeostasis and ROS scavenging through NADPH production, but are regulated in a different manner (Hauschild and von Schaewen, 2003; Couée et al., 2006; Bolouri-Moghaddam et al., 2010; Esposito, 2016). The cytosolic OPPP activity stays rather constant in light or dark conditions, but can be induced by various stresses, continuous light, or in darkness, if metabolizable sugars are available (Hauschild and von Schaewen, 2003; Esposito, 2016). By contrast, the activity of the chloroplastic OPPP is normally inhibited in light, but in darkness the inhibition is removed by redox regulation (Esposito, 2016), and in response to MV treatment, the activity of plastidic OPPP was elevated, but the activity of cytosolic OPPP did not change (Hauschild and von Schaewen, 2003).

Directing carbon flow between glycolysis and cytosolic OPPP may involve also redox control through the key regulators of glycolysis and energy metabolism. In the plant cytosol, the NADPH for carbon reduction is mainly provided by three enzymes, NADP-dependent isocitrate dehydrogenase (IDH), glucose-6-phosphate dehydrogenase (G6PDH, OPPP), and NADP-glyceraldehyde-3-phosphate dehydrogenase (GAPN) (Noctor, 2006). The NAD-dependent GAPDH (GAPDH), is highly sensitive to ROS (Schneider et al., 2018) and the H_2O_2-induced oxidative stress has been reported to increase mitochondrial association of cytosolic AtGAPDHs as well as their transport to the nucleus (Sweetlove et al., 2002; Zaffagnini et al., 2013). As there is another non-phosphorylating, NADP-dependent glyceraldehyde dehydrogenase (GAPN), which is less sensitive to ROS, the continuous, but diminished carbon flux to TCA cycle during oxidative stress can continue. Increased activity of cytosolic, NADPH-producing GAPN has been observed in maize and in wheat after MV exposure (Bustos et al., 2008). Also cytosolic thioredoxins maintain GAPDHs in active, reduced state and thioredoxin expression (trx-h5) is induced by ROS generation, such as in Arabidopsis Col-0 plants exposed to MV (Scarpeci and Valle, 2008). However, cytosolic thioredoxin-h5 (trx-h5) expression was down-regulated in *rcd1* (Brosché et al., 2014) that may impair the regulation of cytosolic redox status in addition to increased ROS production and glycolytic metabolites (and redirected carbon flow to OPPP). Also slightly decreased/similar levels of TCA cycle intermediates in *rcd1* could be explained by these "moonlighting" properties of glycolytic enzymes.

RCD1 Is Involved in Nitrogen Metabolism

The most consistent and significant differences in pathway enrichment analysis in *rcd1* when compared to Col-0 were connected to nitrogen metabolism, mainly to metabolism of AAAs, BCAAs and Lys, Gly, Ser and Thr as well as nucleoside (purine, pyrimidine) metabolism in all three treatments (L, D, MV) (**Figure 3**, **Supplementary Table S4**). α-Ketoglutarate (α-KG) is not only an intermediate of the TCA cycle, but also a key carbon backbone donor (precursor of Glu) for several amino acids integrating carbon and nitrogen metabolism. On the other hand, Glu functions also as an amino-group donor for amino acids. While sugar and sugar-P levels (C metabolism) were consistently increased in *rcd1* (**Figure 4B**), there were no distinct accumulation of α-KG, adjacent TCA cycle intermediates, or Glu and Gln in control conditions. However, majority of amino acid levels were increased in *rcd1*, suggesting that the excess C (and N) are directed to amino acid and nucleoside biosynthesis, instead of TCA cycle. *Rcd1* mutant displayed low levels of only three amino acids; cyano-alanine, Asp and Asn, while downstream metabolites Lys, Met, Ile, and Thr levels were high (**Supplementary Figure S5**). This suggests inhibited conversion of Asp to Asn, and enhanced carbon flow to Lys and other downstream metabolites. On the other hand, in extended darkness, *rcd1* displayed high Asn levels. Altered Asp

and Asn levels in *rcd1* can be explained by the high expression of cytosolic aspartate amino transferase (AAT2, Brosché et al., 2014) that has been shown to coordinate the biosynthesis of Asp in light and its conversion to Asn in the dark (Schultz et al., 1998). AAT2 catalyzes also the reversible transamination reaction of Glu and oxaloacetate (OAA) to Asp and α-ketoglutarate, connecting nitrogen metabolism to pivotal carbon flux (TCA cycle), and to shuttling of reducing equivalents between mitochondria and cytosol (malate-Asp shuttle) (Wilkie and Warren, 1998). In a similar manner, the excess glycolytic carbon flux (and N assimilation *via* Gln) could be directed to amino acid biosynthesis *via* C3 metabolites (PEP, pyruvate, 3-PGA) instead of TCA cycle.

The significant accumulation of AAAs is a typical plant response to dark-induced senescence, to systemic acquired resistance, defense priming and to abiotic stress (Araújo et al., 2010; Návarová et al., 2012; Watanabe et al., 2013) due to activated biosynthesis (chloroplast) as well as inhibited catabolism (mitochondria). Shikimate route enzymes can also be activated by the loss of RCD1/STO-inhibition of COP1/HY5 pathway (Jiang et al., 2009). The accumulation of BCAAs followed the same pattern as AAA's in *rcd1*. The biosynthesis of both BCAAs and AAAs requires carbon backbone precursors that are derived from OPPP and glycolysis, NADPH as a substrate and Glu as an amino donor. Thus, surplus of chloroplastic NADPH and excess of cytosolic OPPP derived precursors likely contribute to the constantly high levels of AAAs and BCAAs in *rcd1*.

RCD1 Plays a Role in Regulating Nucleotide Metabolism and Cellular Redox Homeostasis

In addition to the elevation of glycolytic intermediate and OPPP-derived metabolite levels, altered xanthine/urate ratio supports the hypothesis that cytosolic environment is more reduced in *rcd1* than in Col-0 (**Figure 5**). Xanthine oxidase/dehydrogenase (XO/XDH) is an enigmatic enzyme, which has both oxidase (XO) and dehydrogenase (XDH) activities (Vorbach et al., 2003). In plants, the opposing roles have been reported to be regulated by spatially distinct substrate availability (Ma et al., 2016). In presence of NAD^+, XDH is activated and enzyme acts as a dehydrogenase taking part in purine catabolism by converting xanthine to urate in the cytosol. Urate is transported to peroxisomes for degradation through allantoin, which is further catabolized in endoplastic reticulum to glyoxylate, ammonia and carbon dioxide. In the presence of NADH, XO is activated and enzyme acts as an oxidase, producing ROS ($O_2^{\bullet-}$) from O_2 but with no or inhibited conversion of xanthine to urate (Ma et al., 2016). The levels of xanthine, urate, and glycolytic metabolites suggest that cytosolic NAD(P)H levels could be higher in *rcd1* than in Col-0, and that in *rcd1* the XO/XDH acts predominantly as an oxidase. The ability of XO to be rapidly converted to XDH under various forms of stress and damage makes it an ideal component for fast innate immune and oxidative stress responses. *Atxdh1* mutant displays xanthine accumulation, premature senescence and extensive cell death (Brychkova et al., 2008) mirroring the phenotypes of *rcd1*.

Elevated superoxide production in *rcd1* was detected only under light indicating that ROS have to derive from light-related processes (**Supplementary Figure S4**). Shapiguzov et al. (2019) proposed that RCD1 is involved as a co-regulator in acclimation and adjustment-related processes that affect chloroplastic redox status *via* mitochondrial processes. Highly reduced state of 2-cysteine peroxiredoxin (2-CysPrx) and activated NADPH-dependent malate dehydrogenase (NADPH-MDH) in *rcd1* seedlings suggested reduced availability of electron acceptors and activation of transfer of reductive power out of chloroplasts and altered ferredoxin/thioredoxin (Fd/TRX) regulation. Several chloroplastic OPPP and Calvin cycle enzymes are also redox regulated by Fd/TRX system (Entus et al., 2002). Interestingly, MV exposure reduced superoxide production in *rcd1,* but with no adjoining accumulation of H_2O_2 from superoxide scavenging as seen in Col-0. This may suggest that over-reduced environment in *rcd1* could account for the observed higher rate of $O_2^{\bullet-}$ generation, and the introduction of highly effective redox cycler (paraquat, MV), which limits the pool of intracellular reductant (NAD(P)H) levels (Cochemé and Murphy, 2009), limits also following $O_2^{\bullet-}$ production in *rcd1*.

In contrast to MV exposure, the levels of metabolite markers of chloroplastic or mitochondrial oxidative stress were not elevated in *rcd1* in control light conditions. This implies that higher cytosolic NAD(P)H levels may enhance extracellular ROS production in *rcd1 via* NADPH-oxidase family enzymes in the plasma membrane (Respiratory Burst Oxidase Homologs, RBOH) or in other cellular compartments (vacuole, endoplasmic reticulum (ER) or nuclei), and contribute to the elevated superoxide levels (Torres and Dangl, 2005). Reductive environment in the cytosol and the concurrent production of extracellular ROS *via* NADPH oxidases could also explain the hypersensitivity of *rcd1* to ozone and apoplastic superoxide (Overmyer et al., 2000).

The metabolite features of *rcd1* mutant suggested changed anabolic and catabolic processes connected to purine and pyrimidine metabolism. The levels of UMP and uridine were high in *rcd1* after MV treatment indicating activation of pyrimidine (uridine) salvage pathway. Uridine nucleotides can be formed by energy-consuming *de novo* synthesis or by the energy-saving recycling of nucleobases resulting from nucleotide catabolism (Mainguet et al., 2009). Activation of uridine salvage pathway in *rcd1* is supported by the high transcript levels of UKL2 in *rcd1* (Brosché et al., 2014). Uridine kinase (UKL2) is involved not only in uridine salvage pathway, but also in starch, sucrose (via UDP-glucose) and lignin biosynthesis (Chen and Thelen, 2011).

In *Arabidopsis*, NAD is synthetized from Asp, and besides redox reactions NAD can act as a substrate for generation of ADP-ribose, poly(ADP-ribos)ylation and deacetylation of proteins (Hashida et al., 2009). During those processes, NAD is degraded and must be recycled in NAD salvage pathway, which is known to play a key role in e.g. plant abiotic stress tolerance (Li et al., 2015). Several metabolites connected to NAD biosynthesis and salvage pathway (e.g. nicotinic acid, AMP, Rib-5-P) were higher in *rcd1*, except precursor Asp, which was

significantly decreased in *rcd1*, which suggests that the pathway is influenced by RCD1. Two UDP-glucosyl transferase family protein transcripts (UGT74F2, UGT76B1/SGAT1) are down-regulated in *rcd1* (Brosché et al., 2014). The enzymes transfer glucose from UDP-glucose to nicotinic acid in a NAD salvage pathway and accordingly *ugt74f2* mutant accumulates free nicotinic acid (Li et al., 2015). Further evidence of altered nucleotide metabolism in *rcd1* stems from transcriptomic study that showed altered expression of genes that are connected to NAD metabolism (NUDX6; NUDX10) and PARP activity (PARP2) (Brosché et al., 2014). NUDIX hydrolases have also been associated with the prevention of excessive accumulation of NADH and inhibition of oxidative stress. AtNUDX enzymes cleave either NADH or ADP-ribose (Ogawa et al., 2005), and both NUDX6 (down-regulated in *rcd1*) and NUDX10 (up-regulated in *rcd1*) show activity as ADP-ribose pyrophosphatase. Only NUDX6 shows substantial activity to NADH and the intracellular NADH levels are high in the *nudx6* knock-out mutant (Ogawa et al., 2016). In addition, NUDX6 has a link to the regulation of cytosolic redox status as it induces the expression of TRX-h5. Accordingly, the transcript levels of both NUDX6 and TRX-h5 were low and the levels of PARP2 transcripts were elevated in *rcd1* (Brosché et al., 2014). Taken together, these findings suggest that RCD1 is involved in nucleotide metabolism, NAD metabolism and cellular NADH levels.

Accumulation of Senescence Markers in *rcd1*

Senescence-associated metabolites (**Figure 4**, **Supplementary Figure S5**) accumulated in *rcd1* already at an early developmental stage while senescence-related gene expression was mainly down-regulated in *rcd1* (Brosché et al., 2014). This indicates that the early senescence observed in *rcd1* mutants is an atypical phenomenon. The *rcd1* mutant accumulated hydroxy acids (e.g. 3-HMG, 2-HG, 2-HB) that arise from mitochondrial degradation of Lys and BCAAs. HMG-CoA (3-hydroxy-3-methyl-glutaryl-CoA) is an intermediate in both mitochondrial Leu catabolism and cytosolic mevalonate (MEV) pathway, whereas 3-HMG is a degradation product of HMG-CoA with unknown function and regulation in plants. The altered metabolism of BCAAs and AAAs can be seen also in significantly elevated levels of 3-HMG (6-fold) in *rcd1*. In plants, the accumulation (10-fold) of 3-HMG have been detected in senescing leaves (Watanabe et al., 2013), but its function has remained unclear. In mammals, a defect in HMG lyase in mitochondria has been reported to cause breakdown of HMG-CoA to toxic 3-HMG, instead of conversion of HMG-CoA to acetoacetate and acetyl-CoA (Faull et al., 1976; Puisac et al., 2010). The defect in HMG lyase and the accumulation of 3-HMG enhance ROS formation, lipid peroxidation and xanthine oxidase activity and inhibit mitochondrial respiratory chain (COX) by inactivation of Cyt c (Struecker da Rosa et al., 2016). 2-Hydroxy acids play an integral role in plant metabolism and are involved in several fundamental pathways, including photorespiration, TCA cycle, glyoxylate cycle, methylglyoxal pathway and lysine catabolism. 2-Hydroxyglutaric acid (2-HG) is an end product of mitochondrial Lys catabolism (Araújo et al., 2010; Engqvist et al., 2011; Engqvist et al., 2014) and like 3-HMG, it is also reported to be a metabolic marker for mitochondrial dysfunction, to induce oxidative stress and to perturb energy homeostasis in mammals (Gelman et al., 2018; Ye et al., 2018). 2-HG belongs to a group of known senescence markers in plants together with AAAs, BCAAs, pipecolic acid and α-amino adipic acid (Engqvist et al., 2011; Watanabe et al., 2016), all of which showed elevated levels in *rcd1*. 2-HG accumulation causes dose-dependent inhibition of cytochrome c oxidase activity (complex IV), yet in plants, no specific phenotype or toxic effects have been related to high levels of 2-HG (Hüdig et al., 2015). The accumulation of senescence markers and impaired catabolism of amino acids in mitochondria could be related to the function of RCD1 in coordinating genes in mitochondrial dysfunction stimulon through ANAC013 and ANAC017 interaction, or possibly caused indirectly by other factors, such as increased ROS production or redox imbalance.

Metabolite Responses to Methyl Viologen and Possible Resistance Mechanisms

Differing Metabolite Responses to the Methyl Viologen—Col-0 vs *rcd1*

The metabolite responses to the MV exposure differed greatly between *rcd1* and Col-0 plants (**Figures 2** and **5**). In *rcd1*, pathways related to TCA cycle and pyruvate metabolism, carbon fixation, glycolysis, starch and sucrose, inositol phosphate, amino acid and nucleotide metabolism were most significantly enriched after MV exposure (**Figure 3B**). Accordingly, the levels of many sugars and sugar phosphates (sucrose, glucose-6-P, fructose-6-P, PEP, DHAP, inositol, inositol-P, and trehalose) showed different responses to MV treatment in *rcd1* and Col-0 (**Figures 2B** and **4B**). However, the most prominent differences between Col-0 and *rcd1*, when comparing the control conditions to MV-exposure in the pathway enrichment analysis, were the pyruvate and TCA cycle metabolism, and glycolysis/gluconeogenesis (**Figures 3A, B**).

In Col-0 after MV exposure, citrate and aconitate levels were higher and the levels of metabolites downstream in TCA cycle were lower than in control conditions (**Figures 2B** and **4C**). Although the principal site of action of MV in plants is in chloroplasts (PSI), clear indications of increased ROS production was observed in both chloroplastic and mitochondrial oxidative stress marker levels (**Figures 4C, D**). The accumulation of citrate and aconitate, as well as the decline in the levels of downstream metabolites of TCA cycle indicated inhibition of mitochondrial aconitase and respiration in Col-0, as aconitase is known to be highly sensitive to ROS, particularly to H_2O_2 and superoxide (Verniquet et al., 1991). By contrast, in *rcd1*, the levels of all detected TCA cycle intermediates, except fumarate, as well as Ala, pyruvate and citramalate increased or remained high after MV exposure (**Figures 2B** and **4B, C**). Citramalate is not an actual intermediate of TCA cycle, but after it was detected in *Arabidopsis* by Fiehn et al. (2000), it has been suggested that

there might be a similar kind of TCA cycle bypass also in *Arabidopsis* as there is in bacteria (Grant and Smith, 2000). The levels and responses of citramalate correlated with malate, succinate, pyruvate, α-KG levels and even Ala (originates from pyruvate) in both plant lines, suggesting a tight connection between citramalate and TCA cycle. In addition, the levels of Asp and Glu, which are linked to mitochondrial malate-aspartate shuttle, followed the same response patterns as the TCA cycle intermediates (**Figures 4A, C**).

The metabolite ratios, which have been previously used as redox status indicators in Kolbe et al. (2006) or describing the function of NAD(P)H producing mitochondrial enzymes (Schertl and Braun, 2014) differed between Col-0 and *rcd1* during MV exposure. The metabolite ratios indicating activities of malate dehydrogenase (NAD(P)H-MDH), isocitrate dehydrogenase (NAD(P)H-ICDH), glutamate dehydrogenase (GDH), 2-hydroxyglutarate dehydrogenase (2-HGDH), and lactate dehydrogenase (LDH) as well as amino acid Pro/Glu ratio were elevated in Col-0 during MV-induced oxidative stress, while the ratios declined or had no significant change in *rcd1* (**Figure 5**, **Supplementary Tables S1** and **S3**). The product(s)/substrate(s) ratios related to GABA shunt and Ala aminotransferase (ALAT) had also a similar response to MV as NAD(P)-MDH, NAD(P)H-ICDH, GDH, D-2HGDH, and LDH. The metabolite ratio for α-KG dehydrogenase (α-KGDH) behaved in an opposite manner, decreasing in Col-0 and increasing in *rcd1* during the MV exposure (**Figure 5**, **Supplementary Tables S1** and **S3**). The differing responses to MV in both individual TCA cycle metabolite levels as well as the redox status ratios indicate sustained respiration flux and increased glycolytic activity to produce pyruvate to feed the TCA cycle in *rcd1* during MV exposure.

In addition to altered TCA cycle metabolite levels, the decline of sucrose, fructose, glucose-6P and mannose-6P levels is in line with reduced photosynthetic activity, glycolysis, and sucrose biosynthesis in MV-sensitive Col-0 after MV exposure (**Figure 4B**) as well as with MV- (Scarpeci and Valle, 2008) and menadione-induced oxidative stress responses (Baxter et al., 2007; Lehmann et al., 2009). In addition, the majority of pyrimidine nucleotide, nucleobase and their catabolite levels were reduced during MV exposure in Col-0 (**Figure 4E**). However, the levels of sucrose, glucose-6P, UMP and uracil levels increased in *rcd1* during MV exposure mirroring the responses of TCA cycle metabolites, while the majority of detected sugar levels in *rcd1* remained high (**Figure 4B**). AMP, ribose and adenosine levels were elevated in Col-0 after MV exposure, which could be due to ROS-induced increased PARG (Poly-(ADP-Ribose) Glycohydrolase) or NUDIX (nucleoside diphosphate-linked moiety X hydrolase) activity, producing AMP and ribose from polyADP ribose (Formentini et al., 2009). The high content of soluble carbohydrates and starch in *rcd1* indicated that carbon fixation was not hindered in the mutant plants after MV exposure. Thus, we can assume that there is no severe NADPH depletion in *rcd1* chloroplasts due to the MV-redox cycle, and the Calvin cycle continues to assimilate CO_2 generating sugars. Unlike in Col-0, chloroplastic OPPP is not activated, however cytosolic OPPP continues to function, as it is not as sensitive to redox regulation as its corresponding plastidic pathway (Scarpeci and Valle, 2008; Esposito, 2016). The activity of cytosolic OPPP is presumably increased in *rcd1* due to enhanced glycolytic activity and elevated hexose levels (Hauschild and von Schaewen, 2003). Both glycolysis and OPPP generate reductive power (NAD(P)H) that can feed the antioxidant system and ROS processing under MV-induced ROS generation in the cytosol and other cellular locations as a result of efficient transfer of reducing equivalents between organelles.

The Gly/Ser ratio, a classic indicator of photorespiratory activity (Wingler et al., 1999; Wingler et al., 2000), decreased in both plant lines after MV exposure: a 10-fold decrease in MV-treated Col-0 plants, but only 3-fold decrease in *rcd1* plants (**Figure 5**). In Col-0, the strong decline in Gly/Ser ratio during MV exposure relates to the decrease in photosynthetic activity, reduced NADPH/NADP ratio and mitochondrial damage (glycine decarboxylase inhibition) (Taylor et al., 2002; Noguchi and Yoshida, 2008), whereas in *rcd1*, the levels of glycolytic intermediates (and sucrose) stayed elevated and photosynthetic activity was reported to continue during MV exposure (Shapiguzov et al., 2019). As well as the enhanced glycolysis and TCA cycle metabolite results in *rcd1* during MV exposure, the decline in Gly/Ser ratio could be related to the increase in mitochondrial NADH/NAD^+ ratio that inhibits glycine decarboxylase complex (Noguchi and Yoshida, 2008; Watanabe et al., 2016).

Increase in Common Stress Markers Indicate Oxidative Stress in Both Plant Lines

Apart from significantly different metabolite responses to MV between *rcd1* and Col-0, the two plant lines exhibited also common responses to MV (**Figure 2B**, **Supplementary Table S6**). Common responses to MV included a decrease in the levels of ornithine precursors, N-acetyl-glutamate (NAG) and N-acetyl-ornithine (NAO) (**Figure 4A**) and an accumulation of oxidative stress markers 2-isopropylmalate and O-acetyl serine (OAS), and of OPPP intermediates ribose-5P and sedoheptulose-7P, and saccharic acid, an oxidized form of glucose (**Figures 2B** and **4D**). Similarly to aconitase, its chloroplastic homolog, isopropylmalate isomerase (IPMI), is highly sensitive to ROS (Ellerström et al., 1992). IPMI is involved in Leu biosynthesis and it catalyzes the isomerization of 2-isopropylmalate to 3-isopropylmalate. Inhibition of IPMI and the subsequent accumulation of 2-isopropylmalate were evident in both plant lines after MV exposure (**Figure 4D**). This indicated that MV reached its primary site of action and triggered the overproduction of ROS in the chloroplasts in both plant lines. Another indicator of oxidative stress was the accumulation of a known oxidative stress marker, O-acetyl serine (OAS), which is related to sulfur and cysteine biosynthesis distributed across cytosol, mitochondria and

chloroplast (Saito, 2004; Kawashima et al., 2005; Lehmann et al., 2009) (**Figure 4D**). The cyclic ornithine pathway in planta is localized in the chloroplast and consumes both ATP and NADPH (Chen et al., 2006). As the N-acetylglutamate kinase (NAGK) uses ATP and N-acetylglutamyl-5-P reductase (NAGPR) uses NADPH as a substrate, depletion of both ATP and NADPH during extended darkness and MV-induced oxidative stress in chloroplasts inhibits the cyclic pathway, and the levels of ornithine precursors, N-acetylglutamate (NAG) and N-acetyl-ornithine (NAO) decrease (Slocum, 2005), which can be seen in both plant lines (**Figure 4A**). The accumulation of ribose-5P (R5P), sedoheptulose-7P (Sedo-7P) and metabolites derived from E4P and R5P, suggest OPPP activation (Baxter et al., 2007; Lehmann et al., 2009) in both lines. Also the clear accumulation of saccharic acid (**Figure 4D**), an oxidized form of glucose, was detected in both lines. These metabolite responses are characteristic under enhanced generation of ROS (Baxter et al., 2007; Lehmann et al., 2009; Noctor et al., 2015), which suggests that the MV-resistance in *rcd1* is a result of altered cellular metabolism and not related to diminished delivery of MV into the cells or chloroplasts.

Role of TCA Cycle and Mitochondrial Processes to Methyl Viologen Tolerance

Previous studies have shown that the flux through mETC (mitochondrial Electron Transport Chain) is altered in *rcd1*, as respiration through alternative oxidases (AOX) is strongly enhanced (Brosché et al., 2014; Shapiguzov et al., 2019). Moreover, potassium cyanide (KCN), an inhibitor of complex IV, decreased oxygen consumption in Col-0 significantly, but did not affect oxygen consumption in *rcd1* (Shapiguzov et al., 2019). Respiration through AOX is less efficient in ATP production due to inhibited proton pumping in complexes III and IV (COX) causing decreased proton gradient across the membranes. Thus, enhanced respiration flux through AOXs in *rcd1* could lead to the induction of alternative ATP producing pathways such as glycolysis and energy-saving salvage pathways, which can be seen in the metabolomic profile of *rcd1*. Apart from transcriptional control of their expression, AOX isoforms in *Arabidopsis* are redox regulated and their activity and transcription is induced by high pyruvate and/or isoform-specific keto acids (Selinski et al., 2018), of which pyruvate and α-KG were elevated in *rcd1* in MV treatment. Also, high non-phosphorylating respiration flux through AOX is a consequence of increased NADH levels and the elevated expression of alternative NAD(P)H dehydrogenases on the mitochondrial inner membrane (Clifton et al., 2006; Elhafez et al., 2006). Elevated expression of external alternative NAD(P)H-ubiquinone oxidoreductase B3 (NDB3) in *rcd1* (Brosché et al., 2014) is further evidence of altered redox state of *rcd1* mitochondria, and which correlates with metabolomic results and significantly different redox status indicator ratios in this study.

As discussed previously, the most significant differences between Col-0 and *rcd1* in all treatments (L, MV, D) were connected to BCAA and AAA metabolism (**Figures 2** and **3**). In addition, during MV treatment (but not in L or D) the most enhanced pathways between Col-0 and *rcd1* are the TCA cycle and pyruvate metabolism, as well as carbon fixation and sugar metabolism (glycolysis/gluconeogenesis). The differences in carbon fixation (e.g. Calvin cycle) and sugar metabolism is in line with previous results as the photosynthesis is inhibited in Col-0 during MV treatment, but continues in *rcd1* (Shapiguzov et al., 2019). The elevated levels of TCA cycle intermediates (except fumarate) after MV exposure could result from over-active citrate valve, which transports accumulated reducing power out of mitochondria (**Figure 4C**). In plants, depending on the metabolic requirements, redox status and signaling, the fluxes through the mitochondrial TCA cycle can vary (Oliver and McIntosh, 1995; Igamberdiev and Gardeström, 2003; Daloso et al., 2015; Igamberdiev and Bykova, 2018). The increased mitochondrial NAD(P)H levels activate the citrate valve, and excess reducing power is transferred to cytosol or to the other organelles. Partial TCA cycle is reported to be activated in illuminated plants due to the increased mitochondrial redox level, especially in photorespiratory conditions (Igamberdiev and Gardeström, 2003; Igamberdiev and Bykova, 2018), while the normal; full TCA cycle is active during the night. NADH inhibits not only the activity of TCA cycle enzymes isocitrate dehydrogenase (NAD-IDH) and α-ketoglutarate dehydrogenase (α-KGDH), but also (TCA cycle precursor) pyruvate dehydrogenase (PDH) (Oliver and McIntosh, 1995). NAD-IDH is also noncompetitively inhibited by NADPH (McIntosh and Oliver, 1992). The responses of the redox status indicator ratios (**Figure 5**) support the hypothesis of altered redox status in *rcd1* and had a significantly different response to MV exposure in Col-0 and *rcd1*. Citrate/α-KG and isocitrate/α-KG ratios, which describe the status of NAD-IDH, increased significantly in Col-0, but remained in the same level in *rcd1* as in control conditions (light, partial TCA cycle). The α-KG/succinate ratio, which describes the α-KGDH status, decreased in Col-0, but again remained in the same level as in light conditions in *rcd1*. These results indicate that MV exposure does not have the same effect to the mitochondrial redox status in *rcd1* as in wild-type Col-0, even though (organellar specific) increased oxidative stress marker levels indicate ROS production in all cell compartments in both lines during MV exposure (**Figures 4C, D**).

CONCLUSION

In addition to photosynthetic metabolism, glycolysis, OPPP and mitochondrial TCA cycle are central nodes of primary metabolism which provide carbon backbones for basal and secondary metabolism, are involved in energy production (ATP) and connect the oxidation of carbon with the reduction of NAD(P) to NAD(P)H. The primary metabolite profile in *rcd1*

indicates altered and compartmentalized redox regulation and reorganized energy production. The increased levels of glycolytic and OPPP-derived metabolites as well as altered xanthine/urate ratio indicate altered metabolic regulation and redox imbalance in *rcd1*. We propose that overactive reductive metabolism, activation of energy salvaging pathways and efficient redox transfer between organelles is sufficient to overcome the negative effects of MV-induced chloroplastic oxidative stress in the mutant plants. Accumulation of carbohydrates, BCAAs and AAAs, hydroxy acids and other amino acid catabolites in *rcd1* as well as elevated production of superoxide in *rcd1* in control/light conditions, indicate increased superoxide generation to be connected to altered carbon and nitrogen metabolism and light-dependent reactions in *rcd1*, yet no induction of any of the plastidic oxidative stress markers were detected. The localization of increased superoxide generation as well as organ specific enzyme activities of both redox regulated and enzymes connected to ROS production in the mutant plants needs further studies. Based on previous findings (Shapiguzov et al., 2019) and metabolite features of *rcd1* in our study, we suggest that RCD1 coordinates energy metabolism by negatively regulating reductive metabolism.

DATA AVAILABILITY STATEMENT

All datasets generated for this study are included in the article/ **Supplementary Material**.

AUTHOR CONTRIBUTIONS

AS provided all the plant material for starch and metabolite analysis, and performed all the ROS production measurements and stainings. NS and JL performed all of the metabolite and statistical analyses. NS, JL, AS, and MK designed the experiments together. NS, JL, and MK interpreted the results and wrote the manuscript. All authors (NS, JL, AS, MK, JK) were involved in conceptualization and commented the manuscript.

SUPPLEMENTARY MATERIAL

The Supplementary Material for this article can be found online at: https://www.frontiersin.org/articles/10.3389/fpls.2020.00194/full#supplementary-material

REFERENCES

Ahlfors, R., Lång, S., Overmyer, K., Jaspers, P., Brosché, M., Tauriainen, A., et al. (2004). *Arabidopsis* RADICAL INDUCED CELL DEATH1 belongs to the WWE protein-protein interaction domain protein family and modulates abscisic acid, ethylene, and methyl jasmonate responses. *Plant Cell* 16, 1925–1937. doi: 10.1105/tpc.021832

Araújo, W. L., Ishizaki, K., Nunes-Nesi, A., Larson, T. R., Tohge, T., Krahnert, I., et al. (2010). Identification of the 2-Hydroxyglutarate and Isovaleryl-CoA Dehydrogenases as alternative electron donors linking lysine catabolism to the electron transport chain of *Arabidopsis* mitochondria. *Plant Cell* 22, 1549–1563. doi: 10.1105/tpc.110.075630

Asada, K. (1994). "Production and action of active oxygen species in photosynthetic tissues," in *Photo-oxidative stresses in plants: causes and amelioration*. Ed. C. Foyer and P. Mullineaux (BocaRaton: CRC Press Inc.), 77–104.

Baxter, C. J., Redestig, H., Schauer, N., Repsilber, D., Patil, K. R., Nielsen, J., et al. (2007). The metabolic response of heterotrophic arabidopsis cells to oxidative stress. *Plant Physiol.* 143 (1), 312–325. doi: 10.1104/pp.106.090431

Benavides, M. P., Gallego, S. M., Comba, M. E., and Tomaro, M. L. (2000). Relationship between polyamines and paraquat toxicity in sunflower leaf discs. *Plant Growth Regul.* 31, 215–224. doi: 10.1023/A:100631692600

Bolouri-Moghaddam, M. R., Le Roy, K., Xiang, L., Rolland, F., and Van den Ende, W. (2010). Sugar signalling and antioxidant network connections in plant cells. *FEBS J.* 277, 2022–2037. doi: 10.1111/j.1742-4658.2010.07633.x

Bowler, M., Slooten, L., Vandenbranden, S., De Rycke, R., Botterman, J., Sybesma, C., et al. (1991). Manganese superoxide dismutase can reduce cellular damage mediated by oxygen radicals in transgenic plants. *EMBO J.* 10, 1723–1732. doi: 10.1002/j.1460-2075.1991.tb07696.x

Brosché, M., Blomster, T., Salojärvi, J., Cui, F., Sipari, N., Leppälä, J., et al. (2014). Transcriptomics and functional genomics of ROS-induced cell death regulation by RADICAL-INDUCED CELL DEATH1. *PloS Genet.* 10 (2), 1–16. doi: 10.1371/journal.pgen.1004112

Brychkova, G., Alikulov, Z., Fluhr, R., and Sagi, M. (2008). A critical role for ureides in dark and senescence-induced purine remobilization is unmasked in the *Atxdh1* Arabidopsis mutant. *Plant J.* 54, 496–509. doi: 10.1111/j.1365-313X.2008.03440.x

Bustos, D., Lascano, R., Villasuso, A. L., Machado, E., Racagni, G., Senn, M. E., et al. (2008). Reductions in maize root tip elongation by salt and osmotic stress do not correlate with apoplastic O2•− levels. *Ann. Bot.* 102, 551–559. doi: 10.1093/aob/mcn141

Calderbank, A. (1968). The bipyrydinium herbicides. *Adv. Pest Cont. Res.* 8, 127–235.

Chen, M., and Thelen, J. J. (2011). Plastid uridine salvage activity is required for photoassimilate allocation and partitioning in *Arabidopsis*. *Plant Cell* 23, 2991–3006. doi: 10.1105/tpc.111.085829

Chen, Y. M., Ferrar, T. S., Lohmeir-Vogel, E., Morrice, N., Mizuno, Y., Berenger, B., et al. (2006). The PII signal transduction protein of *Arabidopsis thaliana* forms an arginine-regulated complex with plastid N-acetyl glutamate kinase. *J. Biol. Chem.* 281, 5726–5733. doi: 10.1074/jbc.M510945200

Chen, R., Sun, S., Wang, C., Li, Y., Liang, Y., An, F., et al. (2009). The Arabidopsis PARAQUAT RESISTANT2 gene encodes an S-nitrosoglutathione reductase that is a key regulator of cell death. *Cell Res.* 19, 1377–1387. doi: 10.1038/cr.2009.117

Clifton, R., Millar, A. H., and Whelan, J. (2006). Alternative oxidases in Arabidopsis: A comparative analysis of differential expression in the gene family provides new insights into function of non-phospho-rylating bypasses. *Biochim. Biophys. Acta* 1757, 730–741. doi: 10.1016/j.bbabio.2006.03.009

Cochemé, H. M., and Murphy, M. P. (2008). Complex I is the major site of mitochondrial superoxide production by paraquat. *J. Biol. Chem.* 283 (4), 1786–1798. doi: 10.1074/jbc.M708597200

Cochemé, H. M., and Murphy, M. P. (2009). Chapter 22 the uptake and interactions of the redox cycler paraquat with mitochondria. *Methods Enzymol.* 456, 395–417. doi: 10.1016/S0076-6879(08)04422-4

Couée, I., Sulmon, C., Gouesbet, G., and Amrani, A. E. (2006). Involvement of soluble sugars in reactive oxygen species balance and responses to oxidative stress in plants. *J. Exp. Bot.* 57, 449–459. doi: 10.1093/jxb/erj027

Cui, F., Brosché, M., Shapiguzov, A., He, X.-Q., Vainonen, J. P., Leppälä, J., et al. (2019). Interaction of methyl viologen-induced chloroplast and mitochondrial signalling in. *Arabidopsis Free Radical Biol. Med.* 134, 555–566. doi: 10.1016/j.freeradbiomed.2019.02.006

Daloso, D. M., Müller, K., Obata, T., Florian, A., Tohge, T., Bottcher, A., et al. (2015). Thioredoxin, a master regulator of the tricarboxylic acid cycle in plant mitochondria. *Proc. Natl. Acad. Sci. U. S. A.* 112, E1392–E1400. doi: 10.1073/pnas.1424840112

Daudi, A., Cheng, Z., O'Brien, J. A., Mammarella, N., Khan, S., Ausubel, F. M., et al. (2012). *The* apoplastic oxidative burst peroxidase in Arabidopsis is a major component of pattern-triggered immunity. *Plant Cell* 24 (1), 275–287. doi: 10.1105/tpc.111.093039

De Block, M., Verduyn, C., De Brouwer, D., and Cornelissen, M. (2005). Poly (ADP-ribose) polymerase in plants affects energy homeostasis, cell death and stress tolerance. *Plant J.* 41 (1), 95–10. doi: 10.1111/j.1365-313X.2004.02277.x

Dietz, K. J., and Heber, U. (1984). Rate limiting factors in leaf photosynthesis.1. Carbon fluxes in the Calvin cycle. *Biochim. Biophys. Acta* 767, 432–443. doi: 10.1016/0005-2728(84)90041-0

Elhafez, D., Murcha, M. W., Clifton, R., Soole, K. L., Day, D. A., and Whelan, J. (2006). Characterization of mitochondrial alternative NAD (P) H dehydrogenases in Arabidopsis: intraorganelle location and expression. *Plant Cell Physiol.* 47 (1), 43–54. doi: 10.1093/pcp/pci221

Ellerström, M., Josefsson, L. G., Rask, L., and Ronne, H. (1992). Cloning of a cDNA for rape chloroplast 3-isopropylmalate dehydrogenase by genetic complementation in yeast. *Plant Mol. Biol.* 18 (3), 557–566. doi: 10.1007/BF00040671

Engqvist, M. K. M., Kuhn, A., Wienstroer, J., Weber, K., Jansen, E. E. W., Jakobs, C., et al. (2011). Plant D-2-Hydroxyglutarate dehydrogenase participates in the catabolism of lysine especially during senescence. *J. Biol. Chem.* 286pp (13), 11382–11390. doi: 10.1074/jbc.M110.194175

Engqvist, M. K., Esser, C., Maier, A., Lercher, M. J., and Maurino, V. G. (2014). Mitochondrial 2-hydroxyglutarate metabolism. *Mitochondrion* 19, 275–281. doi: 10.1016/j.mito.2014.02.009

Entus, R., Poling, M., and Herrmann, K. M. (2002). Redox regulation of Arabidopsis 3-Deoxy-d-*arabino*-Heptulosonate7-phosphate synthase. *Plant Physiol.* 129 (4), 1866–1871. doi: 10.1104/pp.002626

Esposito, S. (2016). Nitrogen assimilation, abiotic stress and Glucose 6-Phosphate Dehydrogenase: the full circle of reductants. *Plants* 5 (2), 24. doi: 10.3390/plants5020024

Facchinelli, F., and Weber, A. P. M. (2011). The metabolite transporters of the plastid envelope: an update. *Front. Plant Sci.* 2 (50). doi: 10.3389/fpls.2011.00050

Fait, A., Fromm, H., Walter, D., Galili, G., and Fernie, A. R. (2008). Highway or byway: the metabolic role of the GABA shunt in plants. *Trends Plant Sci.* 13, 14–19. doi: 10.1016/j.tplants.2007.10.005

Farrington, J. A., Ebert, M., Land, E. J., and Fletcher, K. (1973). Bipyrillidium quaternary salts and related compounds. V. Pulse radiolysis studies of the reaction of paraquat radical with oxygen. Implications for the mode of action of bipyridyl herbicides. *Biochim. Biophys. Acta* 314, 372–381. doi: 10.1016/0005-2728(73)90121-7

Faull, K. F., Bolton, P. D., Halpern, B., Hammond, J., and Danks, D. M. (1976). The urinary organic acid profile associated with 3-hydroxy-3-methylglutaric aciduria. *Clin. Chim. Acta* 73, 553–559. doi: 10.1016/0009-8981(76)90160-1

Fiehn, O., Kopka, J., Dörmann, P., Altmann, T., Trethewey, R. N., and Willmitzer, L. (2000). Metabolite profiling for plant functional genomics. *Nat. Biotechnol.* 18, 1157–1161. doi: 10.1038/81137

Flügge, U. I. (1999). Phosphate translocators in plastids. *Annu. Rev. Plant Physiol. Plant Mol. Biol.* 50, 27–45. doi: 10.1146/annurev.arplant.50.1.27

Formentini, L., Macchiarulo, A., Cipriani, G., Camaioni, E., Rapizzi, E., Pellicciari, R., et al. (2009). Poly(ADP-ribose) catabolism triggers AMP-dependent mitochondrial energy failure. *J. Biol. Chem.* 284 (26), 17668–17676. doi: 10.1074/jbc.M109.002931

Foyer, C. H., Descourvieres, P., and Kunert, K. J. (1994). Protection against oxygen radicals: important defense mechanism studied in transgenic plants. *Plant Cell Environ.* 17, 507–523. doi: 10.1111/j.1365-3040.1994.tb00146.x

Foyer, C. H., Noctor, G., and Hodges, M. (2011). Respiration and nitrogen assimilation: targeting mitochondria-associated metabolism as a means to enhance nitrogen use efficiency. *J. Exp. Bot.* 62 (4), 1467–1482. doi: 10.1093/jxb/erq453

Fuerst, E. P., and Vaughn, K. C. (1990). Mechanisms of paraquat resistance. *Weed Technol.* 4, 150–156. doi: 10.1017/S0890037X0002515X

Fujibe, T., Saji, H., Arakawa, K., Yabe, N., Takeuchi, Y., and Yamamoto, K. T. (2004). A methyl viologen-resistant mutant of *Arabidopsis*, which is allelic to ozone-sensitive *rcd1*, is tolerant to supplemental ultraviolet-B irradiation. *Plant Physiol.* 134, 275–285. doi: 10.1104/pp.103.033480

Fujita, M., and Shinozaki, K. (2014). Identification of polyamine transporters in plants: paraquat transport provides crucial clues. *Plant Cell Physiol.* 55 (5), 855–861. doi: 10.1093/pcp/pcu032

Fujita, M., Fujita, Y., Iuchi, S., Yamada, K., Kobayashi, Y., Urano, K., et al. (2012). Natural variation in a polyamine transporter determines paraquat tolerance in Arabidopsis. *Proc. Natl. Acad. Sci. U. S. A.* 109, 6343–6347. doi: 10.1073/pnas.1121406109

Gelman, S. J., Naser, F., Mahieu, N. G., McKenzie, L. D., Dunn, G. P., Chheda, M. G., et al. (2018). Consumption of NADPH for 2-HG synthesis increases pentose phosphate pathway flux and sensitizes cells to oxidative stress. *Cell Rep.* 22 (2), 512–522. doi: 10.1016/j.celrep.2017.12.050

Grant, M., and Smith, S. (2000). Meeting report*; communal weeding*. *Genome Biol. I: Rep.* 4024.1–404024. doi: 10.1186/gb-2000-1-6-reports4024

Hüdig, M., Maier, A., Scherrers, I., Seidel, L., Jansen, E. E. W., Mettle-Altmann, T., et al. (2015). Plants possess a cyclic mitochondrial metabolic pathway similar to the mammalian metabolic repair mechanism involving Malate Dehydrogenase and L-2-Hydroxyglutarate Dehydrogenase. *Plant Cell Physiol.* 56 (9), 1820–1830. doi: 10.1093/pcp/pcv108

Hart, J. J., and Di Tomaso, J. M. (1994). Sequestration and oxygen radical detoxification as mechanisms of paraquat resistance. *Weed Sci.* 42 (2), 277–284. doi: 10.1017/S0043174500080395

Hashida, S., Takahashi, H., and Uchimiya, H. (2009). The role of NAD biosynthesis in plant development and stress responses. *Ann. Bot.* 103 (6), 819–824. doi: 10.1093/aob/mcp019

Hauschild, R., and von Schaewen, A. (2003). Differential regulation of Glucose-6-phosphate dehydrogenase isoenzyme activities in potato. *Plant Physiol.* 133, 47–62. doi: 10.1104/pp.103.025676

Hiller, K., Hangebrauk, J., Jäger, C., Spura, J., Schreiber, K., and Schomburg, D. (2009). MetaboliteDetector: comprehensive analysis tool for targeted and nontargeted GC/MS based metabolome analysis. *Anal. Chem.* 81 (9), 3429. doi: 10.1021/ac802689c

Hiltscher, H., Rudnik, R., Shaikhali, J., Heiber, I., Mellenthin, M., Meirelles Duarte, I., et al. (2014). The *radical induced cell death* protein 1 (RCD1) supports transcriptional activation of genes for chloroplast antioxidant enzymes. *Front. Plant Sci.* 4755, 1–14. doi: 10.3389/fpls.2014.00475

Hodges, M. (2002). Enzyme redundancy and the importance of 2-oxoglutarate in plant ammonium assimilation. *J. Exp. Bot.* 53, 905–916. doi: 10.1093/jexbot/53.370.905

Igamberdiev, A. U., and Bykova, N. V. (2018). Role of organic acids in the integration of cellular redox metabolism and mediation of redox signalling in photosynthetic tissues of higher plants. *Free Radic. Biol. Med.* 122, 74–85 doi: 10.1016/j.freeradbiomed.2018.01.016

Igamberdiev, A. U., and Gardeström, P. (2003). Regulation of NAD- and NADP-dependent isocitrate dehydrogenases by reduction levels of pyridine nucleotides in mitochondria and cytosol of pea leaves. *Biochim. Biophys. Acta* 1606, 117–125. doi: 10.1016/S0005-2728(03)00106-3

Ishikawa, K., Ogawa, T., Hirosue, E., Nakayama, Y., Harada, K., Fukusaki, E., et al. (2009). Modulation of the Poly(ADP-ribosyl)ation reaction *via the* Arabidopsis ADP-Ribose/NADH Pyrophosphohydrolase, AtNUDX7, is involved in the response to oxidative stress. *Plant Physiol.* 151, 741–754. doi: 10.1104/pp.109.140442

Jabs, T., Dietrich, R. A., and Dangl, J. L. (1996). Initiation of runaway cell death in an *Arabidopsis* mutant by extracellular superoxide. *Science* 273, 1853–1856. doi: 10.1126/science.273.5283.1853

Jaspers, P., Blomster, T., Brosché, M., Salojärvi, J., Ahlfors, R., Vainonen, J. P., et al. (2009). Unequally redundant RCD1 and SRO1 mediate stress and developmental responses and interact with transcription factors. *Plant J.* 60, 268–279. doi: 10.1111/j.1365-313X.2009.03951.x

Jiang, L., Wang, Y., Björn, L. O., and Li, S. (2009). Arabidopsis RADICAL-INDUCED CELL DEATH1 is involved in UV-B signaling. *Photochem. Photobiol. Sci.* 8, 838–846. doi: 10.1039/b901187k

Katiyar-Agarwal, S., Zhu, J., Kim, K., Agarwal, M., Fu, X., and Huang, A. (2006). The plasma membrane Na+/H+ antiporter SOS1 interacts with RCD1 and functions in oxidative stress tolerance in *Arabidopsis*. *Proc. Natl. Acad. Sci. U.S.A.* 103, 18816–18821. doi: 10.1073/pnas.0604711103

Kawashima, C. G., Berkowitz, O., Hell, R., Noji, M., and Saito, K. (2005). Characterization and expression analysis of a serine acetyltransferase gene family involved in a key step. *Plant Physiol.* 137, 220–230. doi: 10.1104/pp.104.045377

Kolbe, A., Oliver, S. N., Fernie, A. R., Stitt, M., van Dongen, J. T., and Geigenberger, P. (2006). Combined transcript and metabolite profiling of Arabidopsis leaves reveals fundamental effects of the Thiol-Disulfide status on plant metabolism. *Plant Phys.* 141, 412–422. doi: 10.1104/pp.106.08120

Krömer, S., and Scheibe, R. (1996). Function of the chloroplastic malate valve for respiration during photosynthesis. *Biochem. Soc. Trans.* 24 (3), 761–766. doi: 10.1042/bst0240761

Lambert, C. E., and Bondy, S. C. (1989). Effects of MPTP, MPPþ and paraquat on mitochondrial potential and oxidative stress. *Life Sci.* 44, 1277–1284. doi: 10.1016/0024-3205(89)90365-2

Lehmann, M., Schwarzländer, M., Obata, T., Sirikantaramas, S., Burow, M., Olsen, C. E., et al. (2009). The metabolic response of Arabidopsis roots to oxidative stress is distinct from that of Heterotrophic cells in culture and highlights a complex relationship between the levels of transcripts, metabolites, and flux. *Mol. Plant* 2 (3), 390–406. doi: 10.1093/mp/ssn080

Li, J., Mu, J., Bai, J., Fu, F., Zou, T., An, F., et al. (2013). PARAQUAT RESISTANT1, a Golgi-localized putative transporter protein, is involved in intracellular transport of paraquat. *Plant Physiol.* 162, 470–483. doi: 10.1104/pp.113.213892

Li, W., Zhang, F., Chang, Y., Zhao, T., Schranz, M. E., and Wang, G. (2015). Nicotinate O-Glucosylation is an evolutionary metabolic trait important for seed germination under stress conditions in *Arabidopsis thaliana*. *Plant Cell* 27, 1907–1924. doi: 10.1105/tpc.15.00223

Linka, N., and Weber, A. P. M. (2010). Intracellular metabolite transporters in plants. *Mol. Plant* 3 (1), 21–53. doi: 10.1093/mp/ssp108

Ma, X., Wang, W., Bittner, F., Schmidt, N., Berkey, R., Zhang, L., et al. (2016). Dual and opposing roles of Xanthine dehydrogenase in defense-associated reactive oxygen species metabolism in Arabidopsis. *Plant Cell* 28, 1108–1126. doi: 10.1105/tpc.15.00880

Mainguet, S. E., Gakiére, B., Majira, A., Pelletier, S., Bringel, F., Guérard, F., et al. (2009). Uracil salvage is necessary for early *Arabidopsis* development. *Plant J.* 60, 280–291. doi: 10.1111/j.1365-313X.2009.03963.x

McIntosh, C. A., and Oliver, D. J. (1992). NAD^+-linked isocitrate dehydrogenase: Isolation, purification, and characterization of the protein from pea mitochondria. *Plant Physiol.* 100, 69–75. doi: 10.1104/pp.100.1.69

Mhamdi, A., and Noctor, G. (2015). Analysis of the roles of the Arabidopsis peroxisomal isocitrate dehydrogenase in leaf metabolism and oxidative stress. *Environ. Exp. Bot.* 114, 22–29. doi: 10.1016/j.envexpbot.2014.07.002

Mhamdi, A., Mauve, C., Gouia, H., Saindrenan, P., Hodges, M., and Noctor, G. (2010). Cytosolic NADP-dependent isocitrate dehydrogenase contributes to redox homeostasis and the regulation of pathogen responses in *Arabidopsis* leaves. *Plant Cell Environ.* 33, 1112–1123. doi: 10.1111/j.1365-3040.2010.02133.x

Mittler, R. (2017). ROS are good. *Trends In Plant Sci.* 22 (1), 11–19. doi: 10.1016/j.tplants.2016.08.002

Munné-Bosch, S., Queval, G., and Foyer, C. H. (2013). The impact of global change factors on redox signaling underpinning stress tolerance. *Plant Phys.* 161, 5–19. doi: 10.1104/pp.112.205690

Návarová, H., Bernsdorff, F., Döring, A.-C., and Zeier, J. (2012). Pipecolic acid, an endogenous mediator of defense amplification and priming, is a critical regulator of inducible plant immunity. *Plant Cell* 24, 5123–5141. doi: 10.1105/tpc.112.103564

Noctor, G., and Mhamdi, A. (2017). Climate change, CO_2, and defense: the metabolic, redox, and signaling perspectives. *Trends In Plant Sci.* 22 (10), 857–870. doi: 10.1016/j.tplants.2017.07.007

Noctor, G., Lelarge-Trouverie, C., and Mhamdi, A. (2015). The metabolomics of oxidative stress. *Phytochemistry* 112, 33–53. doi: 10.1016/j.phytochem.2014.09.002

Noctor, G. (2006). Metabolic signaling in defense and stress: the central roles of soluble redox couples. *Plant Cell Environ.* 29, 409–425. doi: 10.1111/j.1365-3040.2005.01476.x

Noguchi, K., and Yoshida, K. (2008). Interaction between photosynthesis and respiration in illuminated leaves. *Mitochondrion* 8, 87–99. doi: 10.1016/j.mito.2007.09.003

Ogawa, T., Ueda, Y., Yoshimura, K., and Shigeoka, S. (2005). Comprehensive analysis of cytosolic Nudix hydrolases in Arabidopsis thaliana. *J. Biol. Chem.* 280, 25277–25283. doi: 10.1074/jbc.M503536200

Ogawa, T., Ishikawa, K., Harada, K., Fukusaki, E., Yoshimura, K., and Shigeoka, S. (2009). Overexpression of an ADP-ribose pyrophosphatase, AtNUDX2, confers enhanced tolerance to oxidative stress in Arabidopsis plants. *Plant J.* 57, 289–230. doi: 10.1111/j.1365-313X.2008.03686.x

Ogawa, T., Muramoto, K., Takada, R., Nakagawa, S., Shigeoka, S., and Yoshimura, K. (2016). Modulation of NADH levels by Arabidopsis Nudix Hydrolases, AtNUDX6 and 7, and the Respective proteins themselves play distinct roles in the regulation of various cellular responses involved in biotic/abiotic stresses. *Plant Cell Physiol.* 57 (6), 1295–1308. doi: 10.1093/pcp/pcw078

Oliver, D. A., and McIntosh, C. A. (1995). "The biochemistry of mitochondrial matrix," in *The Molecular Biology of Plant Mitochondria*. Eds. Ch, C. Levings and I. K. Vasil (The Netherlands: Kluwer Academic Publishers), 237–280.

Overmyer, K., Tuominen, H., Kettunen, R., Betz, C., Langebartels, C., Sandermann, H., et al. (2000). Ozone-sensitive *Arabidopsis rcd1* mutant reveals opposite roles for ethylene and jasmonate signaling pathways in regulating superoxide-dependent cell death. *Plant Cell* 12, 1849–1862. doi: 10.1105/tpc.12.10.1849

Puisac, B., Arnedo, M., Casale, C. H., Ribate, M. P., Castiella, T., Ramos, F. J., et al. (2010). Differential HMG-CoA lyase expression in human tissues provides clues about 3-hydroxy-3-methylglutaric aciduria. *J. Inherit Metab. Dis.* 33, 405–410. doi: 10.1007/s10545-010-9097-3

Rissel, D., Heym, P. P., Thor, K., Brandt, W., Wessjohann, L. A., and Peiter, E. (2017). No silver bullet – Canonical Poly(ADP-Ribose) Polymerases (PARPs) are no universal factors of abiotic and biotic stress resistance of *Arabidopsis thaliana*. *Front. Plant Sci.* 8, 59. doi: 10.3389/fpls.2017.00059

Roessner, U., Wagner, C., Kopka, J., Trethewey, R. N., and Willmitzer, L. (2000). Simultaneous analysis of metabolites in potato tuber by gas chromatography–mass spectrometry. *Plant J.* 23, 131–142. doi: 10.1046/j.1365-313x.2000.00774.x

Saito, K. (2004). Sulfur assimilatory metabolism: the long and smelling road. *Plant Physiol.* 136, 2443–2450. doi: 10.1104/pp.104.046755

Scarpeci, T. E., and Valle, E. M. (2008). Rearrangement of carbon metabolism in *Arabidopsis thaliana* subjected to oxidative stress condition: an emergency survival strategy. *Plant Growth Regul.* 54, 133–142. doi: 10.1007/s10725-007-9236-5

Schertl, P., and Braun, H.-P. (2014). Respiratory electron transfer pathways in plant mitochondria. *Front. Plant Sci.* 5, 163. doi: 10.3389/fpls.2014.00163

Schneider, M., Knuesting, J., Birkholz, O., Heinisch, J., and Scheibe, R. (2018). Cytosolic GAPDH as a redox-dependent regulator of energy metabolism. *BMC Plant Biol.* 18, 184. doi: 10.1186/s12870-018-1390-6

Schultz, C. J., Hsu, M., Miesak, B., and Coruzzi, G. M. (1998). Arabidopsis mutants define an in vivo role for Isoenzymes of Aspartate Aminotransferase in plant nitrogen assimilation. *Genetics* 149, 491–499.

Selinski, J., and Scheibe, R. (2019). Malate valves: old shuttles with new perspectives. *Plant Biol. (Stuttg)* 21 Suppl 1 (Suppl Suppl 1), 21–30. doi: 10.1111/plb.12869

Selinski, J., Hartmann, A., Deckers-Hebestreit, G., Day, D. A., Whelan, J., and Scheibe, R. (2018). Alternative oxidase isoforms are differentially activated by Tricarboxylic acid cycle intermediates. *Plant Phys.* 176, 1423–1432. doi: 10.1104/pp.17.01331

Shapiguzov, A., Vainonen, J., Hunter, K., Tossavainen, H., Tiwari, A., Järvi, S., et al. (2019). Arabidopsis RCD1 coordinates chloroplast and mitochondrial functions through interaction with ANAC transcription factors. *elife*. 8, e43284 doi: 10.7554/eLife.43284

Slocum, R. D. (2005). Genes, enzymes and regulation of arginine biosynthesis in plants. *Plant Physiol. Biochem.* 43, 729–745. doi: 10.1016/j.plaphy.2005.06.007

Smith, A. M., and Zeeman, S. C. (2006). Quantification of starch in plant tissues. *Nat. Protoc.* 1 (3), 1342. doi: 10.1038/nprot.2006.232

Struecker da Rosa, M., Seminotti, B., Ribeiro, C. A. J., Parmeggiani, B., Grings, M., Wajner, M., et al. (2016). 3-Hydroxy-3-methylglutaric and 3-methylglutaric acids impair redox status and energy production and transfer in rat heart: relevance for the pathophysiology of cardiac dysfunction in 3-hydroxy-3 methylglutaryl-Coenzyme A lyase deficiency. *Free Radical Res.* 50 (9), 997–1010. doi: 10.1080/10715762.2016.1214952

Studart-Guimarães, C., Fait, A., Nunes-Nesi, A., Carrari, F., Usadel, B., and Fernie, A. R. (2007). Reduced expression of the succinyl-coenzyme A ligase can be compensated for by up-regulation of the gamma-aminobutyrate shunt in illuminated tomato leaves. *Plant Physiol.* 145, 626–639. doi: 10.1104/pp.107.103101

Sweetlove, L. J., Heazlewood, J. L., Herald, V., Holtzapffel, R., Day, D. A., Leaver, C. J., et al. (2002). The impact of oxidative stress on *Arabidopsis* mitochondria. *Plant J.* 32, 891–904. doi: 10.1046/j.1365-313X.2002.01474.x

Taylor, N. L., Day, D. A., and Millar, A. H. (2002). Environmental stress causes oxidative damage to plant mitochondria leading to inhibition of glycine

decarboxylase. *J. Biol. Chem.* 277 (45), 42663–42668. doi: 10.1074/jbc.M204761200

Torres, M. A., and Dangl, J. L. (2005). Functions of the respiratory burst oxidase in biotic interactions, abiotic stress and development. *Curr. Opin. In Plant Biol.* 8, 397–403. doi: 10.1016/j.pbi.2005.05.014

Tsugane, K., Kobayashi, K., Niwa, Y., Ohba, Y., and Wada K. and Kobayashi, H. (1999). A recessive Arabidopsis mutant that grows photoautotrophically under salt stress shows enhanced active oxygen detoxification. *Plant Cell* 11, 1195–1206. doi: 10.1105/tpc.11.7.1195

Verniquet, F., Gaillard, J., Neuburger, M., and Douce, R. (1991). Rapid inactivation of plant aconitase by hydrogen peroxide. *Biochem. J.* 276, 643–648. doi: 10.1042/bj2760643

Vorbach, C., Harrison, R., and Capecchi, M. R. (2003). Xanthine oxidoreductase is central to the evolution and function of the innate immune system. *Trends Immunol.* 24, 512–517. doi: 10.1016/S1471-4906(03)00237-0

Waszczak, C., Carmody, M., and Kangasjärvi, J. (2018). Reactive oxygen species in plant signaling. *Annu. Rev. Plant Biol.* 69, 209–236. doi: 10.1146/annurev-arplant-042817-040322

Watanabe, M., Balazadeh, S., Tohge, T., Erban, A., Giavalisco, P., Kopka, J., et al. (2013). Comprehensive dissection of spatiotemporal metabolic shifts in primary, secondary, and lipid metabolism during developmental senescence in Arabidopsis. *Plant Physiol.* 162, 1290–1310. doi: 10.1104/pp.113.217380

Watanabe, C. K. A., Yamori, W., Takahashi, S., Terashima, I., and Noguchi, K. (2016). Mitochondrial alternative pathway-associated photoprotection of photosystem II is related to the photorespiratory pathway. *Plant Cell Physiol.* 57 (7), 1426–1431. doi: 10.1093/pcp/pcw036

Wilkie, S. E., and Warren, M. J. (1998). Recombinant expression, purification and characterization of three Isoenzymes of Aspartate Aminotransferase from Arabidopsis thaliana. *Protein Expression Purification* 12, 381–389. doi: 10.1006/prep.1997.0845

Wingler, A., Ann, V. J., Lea, P. J., and Leegood, R. C. (1999). Serine:glyoxylate aminotransferase exerts no control on photosynthesis. *J. Exp. Bot.* 50, 719–722. doi: 10.1093/jxb/50.334.719

Wingler, A., Lea, P. J., Quick, W. P., and Leegood, R. C. (2000). Photorespiration: metabolic pathways and their role in stress protection. *Philos. Trans. R Soc. Lond. B Biol. Sci.* 355, 1517–1529. doi: 10.1098/rstb.2000.0712

Xi, J., Xu, P., and Xiang, C.-B. (2012). Loss of AtPDR11, a plasma membrane localized ABC transporter, confers paraquat tolerance in *Arabidopsis thaliana*. *Plant J.* 69, 782–791. doi: 10.1111/j.1365-313X.2011.04830.x

Xia, J., and Wishart, D. S. (2016). Using MetaboAnalyst 3.0 for comprehensive metabolomics data analysis. *Curr. Protoc. In Bioinf.* 55 (1), 14–10. doi: 10.1002/cpbi.11

Ye, D., Guan, K.-L., and Xiong, Y. (2018). Metabolism, Activity, and Targeting of D- and L-2-Hydroxyglutarates. *Trends Cancer* 4 (2), P151–P165. doi: 10.1016/j.trecan.2017.12.005

Zaffagnini, M., Fermani, S., Costa, A., Lemaire, S. D., and Trost, P. (2013). Plant cytoplasmic GAPDH: redox post-translational modifications and moonlighting properties. *Front. Plant Sci.* 4, 450. doi: 10.3389/fpls.2013.00450

Zhu, Y., Baijuan, D., Qian, J., Zou, B., and Hua, J. (2013). Disease resistance gene-induced growth inhibition is enhanced by *rcd1* independent of defense activation in Arabidopsis. *Plant Physiol.* 161, 2005–2013. doi: 10.1104/pp.112.213363

Conflict of Interest: The authors declare that the research was conducted in the absence of any commercial or financial relationships that could be construed as a potential conflict of interest.

frontiers in Plant Science

MINI REVIEW
published: 13 March 2020
doi: 10.3389/fpls.2020.00211

Minimizing an Electron Flow to Molecular Oxygen in Photosynthetic Electron Transfer Chain: An Evolutionary View

Marina A. Kozuleva, Boris N. Ivanov, Daria V. Vetoshkina and Maria M. Borisova-Mubarakshina**

Institute of Basic Biological Problems (RAS), Pushchino, Russia

OPEN ACCESS

Edited by:
Chikahiro Miyake, Kobe University, Japan

Reviewed by:
Yoshitaka Nishiyama, Saitama University, Japan
Christine Helen Foyer, University of Leeds, United Kingdom

***Correspondence:**
Marina A. Kozuleva
kozuleva@gmail.com
Maria M. Borisova-Mubarakshina
mubarakshinamm@gmail.com

Specialty section:
This article was submitted to Plant Physiology, a section of the journal Frontiers in Plant Science

Received: *30 September 2019*
Accepted: *11 February 2020*
Published: *13 March 2020*

Citation:
Kozuleva MA, Ivanov BN, Vetoshkina DV and Borisova-Mubarakshina MM (2020) Minimizing an Electron Flow to Molecular Oxygen in Photosynthetic Electron Transfer Chain: An Evolutionary View. Front. Plant Sci. 11:211. doi: 10.3389/fpls.2020.00211

Recruitment of H_2O as the final donor of electrons for light-governed reactions in photosynthesis has been an utmost breakthrough, bursting the evolution of life and leading to the accumulation of O_2 molecules in the atmosphere. O_2 molecule has a great potential to accept electrons from the components of the photosynthetic electron transfer chain (PETC) (so-called the Mehler reaction). Here we overview the Mehler reaction mechanisms, specifying the changes in the structure of the PETC of oxygenic phototrophs that probably had occurred as the result of evolutionary pressure to minimize the electron flow to O_2. These changes are warranted by the fact that the efficient electron flow to O_2 would decrease the quantum yield of photosynthesis. Moreover, the reduction of O_2 leads to the formation of reactive oxygen species (ROS), namely, the superoxide anion radical and hydrogen peroxide, which cause oxidative stress to plant cells if they are accumulated at a significant amount. From another side, hydrogen peroxide acts as a signaling molecule. We particularly zoom in into the role of photosystem I (PSI) and the plastoquinone (PQ) pool in the Mehler reaction.

Keywords: photosystems, evolution, plastoquinone, phylloquinone, oxygen, reactive oxygen species

INTRODUCTION

Mehler reaction is the major source of reactive oxygen species (ROS), such as $O_2^{\bullet -}$ and H_2O_2, in chloroplasts. During the Mehler reaction, O_2 molecules serve as an alternative electron acceptor from the photosynthetic electron transfer chain (PETC), being a safety valve to release surplus electrons and thus alleviating the PETC over-reduction. This reaction also contributes to building up of ΔpH across the thylakoid membrane and produces a signaling messenger, H_2O_2, which is capable of initiating various signaling pathways (Ivanov et al., 2012). However, an efficient electron flow to O_2 would decrease the photosynthetic quantum yield. Moreover, ROS, if not neutralized efficiently, lead to oxidative damage. Thus, the PETC evolution could have been guided toward minimizing and/or taking strong control over the Mehler reaction.

Most of the PETC components were proposed as sites of $O_2^{\bullet-}$ photoproduction, the first step of the Mehler reaction. Among them, there are water-soluble and water-exposed components (**Figure 1**, open circles) and the components situated in hydrophobic zones (**Figure 1**, closed circles). The former produce $O_2^{\bullet-}$ in water bulk phases, e.g., stroma, while the latter produce $O_2^{\bullet-}$, which can be detected outside the membrane when diffused there or can be detected within the thylakoid membranes (Kozuleva et al., 2011). The value of E_m ($O_2/O_2^{\bullet-}$) in water is −160 mV, while in hydrophobic zones of proteins and membranes it is more negative, approximately −550 mV (Wardman, 1990). Only few components in PETC possess enough negative E_m for O_2 reduction within a thylakoid membrane. Numerous experiments unambiguously demonstrated that photosystem I (PSI) is the major site of $O_2^{\bullet-}$ photoproduction (Kozuleva and Ivanov, 2016). $O_2^{\bullet-}$ generation by other components was shown under the disturbed PETC function. The second step of the Mehler reaction is H_2O_2 production via $O_2^{\bullet-}$ dismutation in stroma as catalyzed by superoxide dismutase. Apart from $O_2^{\bullet-}$ dismutation, another mechanism was shown to operate in the thylakoid membranes (Mubarakshina et al., 2006). It involves $O_2^{\bullet-}$ reduction by the plastoquinone (PQ) pool, namely, by plastoquinol (PQH_2) (Borisova-Mubarakshina et al., 2019). Thus, the Mehler reaction proceeds at a variety of sites, still leading to $O_2^{\bullet-}$ and subsequent H_2O_2 production.

The evolution of various photosynthetic complexes has been a subject of several recent reviews (Jagannathan et al., 2012; Rutherford et al., 2012; Pierella Karlusich and Carrillo, 2017; Orf et al., 2018). Here, we briefly summarize the structural changes which could have happened in PETC to control and minimize an electron flow to O_2. The general evolutionary trends could include: (i) kinetic control, making the forward reactions faster than the competing electron flow to O_2, (ii) redox tuning of cofactors, disabling spontaneous exergonic reactions with O_2, and (iii) shielding of cofactors with protein environment, restricting O_2 accessibility (Rutherford et al., 2012).

PHOTOSYSTEM I

All secondary electron acceptor cofactors of PSI were proposed as the sites of O_2 photoreduction. The terminal FeS clusters F_A/F_B are inevitably oxidized by O_2 in the absence of ferredoxin (Fd). The role of intermediate cofactor FeS cluster F_X was claimed in Takahashi and Asada (1988) based on experiments showing that the primary H_2O_2 photoproduction site was a PsaA/PsaB heterodimer, which harbors F_X. However, the PsaA/PsaB heterodimer also binds two phylloquinone (PhQ) molecules at the A_1 sites and they could also contribute to H_2O_2 photoproduction. For the first time, the role of PhQs was proposed by Kruk with coauthors (Kruk et al., 2003) since adding PhQ to quinone-depleted thylakoid membranes re-established the O_2 uptake at a single light flash. This result still does not rule out that FeS clusters reduce O_2 by electrons from P_{700} *via* PhQ re-incorporated to the A_1 sites. The PhQ involvement in O_2 photoreduction in intact PSI under steady-state illumination was

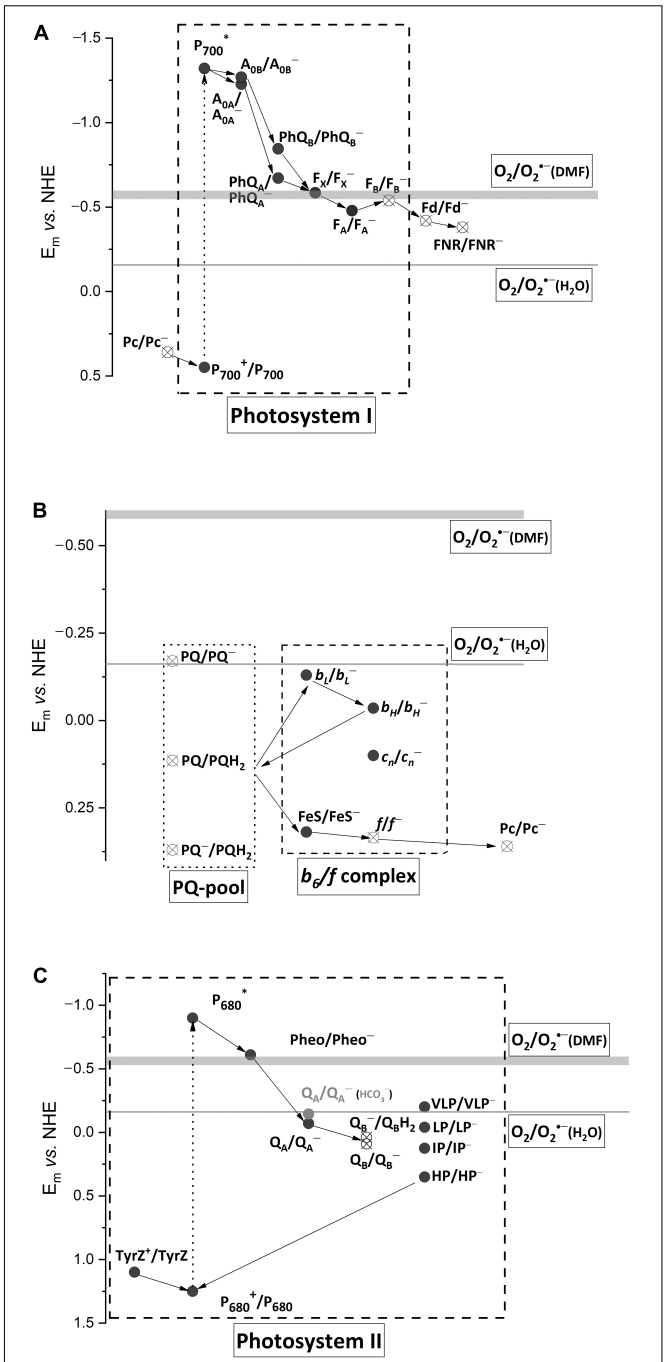

FIGURE 1 | Schematic diagram of forward electron transfer in PSI **(A)**, PQ-pool and cytochrome b_6/f complex **(B)**, and PSII **(C)**, with E_m values of the cofactors. The E_m values of ($O_2/O_2^{\bullet-}$) in water, –160 mV, and dimethylformamide (DMF), from –550 to –600 mV, are shown by thin and thick horizontal lines, respectively. Pc, plastocyanin; P_{700}, the dimer of Chl *a* molecules in PSI; A_0, the primary electron acceptor in PSI; PhQ, phylloquinone, a secondary electron acceptor in PSI; F_X, a 4Fe–4S cluster, a secondary electron acceptor in PSI; F_A and F_B, 4Fe–4S clusters, the terminal electron acceptors in PSI; Fd, ferredoxin, the mobile electron acceptor; FNR, ferredoxin/NADP$^+$ reductase; PQ, PQ$^{\bullet-}$, and PQH_2, plastoquinone, plastosemiquinone, and plastoquinol; FeS, a 2Fe-2S cluster of Rieske protein; *f*, cytochrome f; b_L and b_H, the low- and high-potential forms of cytochrome *(Continued)*

FIGURE 1 | Continued
b_6; c_n, the heme covalently bound to cytochrome b_6; TyrZ, the redox active tyrosine residue; P_{680}, the dimer of Chl *a* molecules in PSII; Pheo, pheophytin, a primary electron acceptor in PSII; Q_A, the tightly bound plastoquinone in PSII, the secondary electron acceptor in PSII; Q_B, the loosely bound plastoquinone in PSII, the terminal electron acceptor in PSII; VLP, LP, IP, and HP, the very low-, low-, intermediate-, and high-potential forms of cytochrome b_{559} in PSII. The E_m-values for PSI cofactors are according to Ptushenko et al. (2008), those for b_6/f complex are according to Alric et al. (2005), those for PSII are according to Brinkert et al. (2016) and Causmaecker et al. (2019), except cytochrome b_{559} (Khorobrykh, 2019). Closed circles, components situated in hydrophobic zones; open circles, water bulk phases exposed components.

proposed based on comparing O_2 photoreduction as a function of irradiance in the wild-type PSI with that in the mutant PQ-containing PSI (Kozuleva et al., 2014). The authors concluded that the PhQs at the A_1 sites are the major contributor to $O_2^{\bullet-}$ generation.

From an evolutionary point of view, the terminal cofactor F_B can be one of the sites where the Mehler reaction should have been taken under control. This cofactor possesses negative E_m, allowing for the efficient reduction of both Fd and O_2. However, Fd is a mobile protein, diffusing to and out of PSI and leaving F_B^- transiently open to O_2. If F_B^- is oxidized by O_2 efficiently, it would be insufficient in a steady-state reduction of Fd. However, the electron lives mostly on F_A, not F_B, because of a positive shift of E_m (F_A/F_A^-) relative to (F_B/F_B^-) (**Figure 1A**; Fischer et al., 1997; Shinkarev et al., 2000). F_A is embedded deeper in the protein, which shields it from O_2. This feature allows keeping of electrons for Fd and avoiding any wasteful electron leakage to O_2.

The PsaC protein carrying F_A and F_B is homologous to mobile ferredoxins in anoxigenic phototrophs (Jagannathan and Golbeck, 2009). It is widely accepted that, during evolution, the ancestral mobile Fd was tightly bound to the ancestral homodimeric reaction center (RC). This binding resulted in an elongation of the ET chain in the RC that could have aimed at stabilizing the charge separation state and minimizing the charge recombination, which could lead to $^3P_{700}$ and, hence, $^1O_2$ formation (Orf et al., 2018). However, that binding probably provided an additional protein shielding for F_X, which was the terminal cofactor in the ancestral RC, and for F_A, limiting O_2 diffusion and preventing unproductive electron leakage (Jagannathan et al., 2012). The protein shielding of these FeS clusters, being potentially capable of catalyzing H_2O_2 decomposition into a highly reactive $HO^{\bullet}$ (Šnyrychová et al., 2006), could have additionally protected the PSI acceptor side from $HO^{\bullet}$ formation.

Binding of the ancestral Fd to the ancestral homodimeric RC resulted in RC asymmetry through locating the F_A cluster closer to one of the quinones (PhQ_B), bringing about a negative shift in E_m ($PhQ_B/PhQ_B^{\bullet-}$) (Rutherford et al., 2012). The difference in E_m between PhQ_A and PhQ_B is up to 170 mV (Ptushenko et al., 2008). Rutherford with coauthors presented an elegant hypothesis explaining the benefit of this asymmetry as it eliminates $^3P_{700}$ (and hence $^1O_2$) formation under the conditions of the Fd pool over-reduction (Rutherford et al., 2012). In line with this hypothesis, $PhQ^{\bullet-}$ oxidation by O_2 sustains a forward ET and contributes to both alleviating PETC over-reduction and preventing charge recombination (Kozuleva and Ivanov, 2016). Both PhQs in PSI have one of the most negative E_m in the PETC (−671 and −840 mV for PhQ_A and PhQ_B, respectively; **Figure 1A**), which allows phyllosemiquinones to reduce O_2 even in the hydrophobic zones of the thylakoid membranes, where E_m ($O_2/O_2^{\bullet-}$) is close to −550 mV (see above). Due to a longer lifetime, $PhQ_A^{\bullet-}$ gets higher chances to react with O_2, although the more negative E_m of $PhQ_B/PhQ_B^{\bullet-}$ provides a larger $-\Delta G$ in reaction with O_2. However, the particular impact of each PhQ as well as clarifying the F_X role is still open questions.

FERREDOXIN AND FNR

In bacterial type Fd, two 4Fe-4S clusters are partially exposed to solvent and accessible for O_2 attacks (Jagannathan et al., 2012). After binding the ancestral Fd to RC, the organisms recruited another Fd, where a single 2Fe–2S cluster is shielded by a protein.

A long-lasting controversy on the role of Fd in the Mehler reaction was solved nearly a decade ago. In the absence of $NADP^+$, which is the major electron sink for Fd, O_2 inevitably oxidizes the reduced Fd (Fd^-). In the presence of $NADP^+$, simultaneously with its photoreduction, the electron flow to O_2 was shown to be significant in high light; however, the contribution of Fd was almost negligible relative to that of the membrane-bound PETC components (Kozuleva and Ivanov, 2010). These results reveal a low reactivity of Fd^- toward O_2, which enables Fd to fulfill the function of stromal hub-donating electrons to multiple enzymes and proteins, including ferredoxin-$NADP^+$ reductase (FNR) (Hanke and Mulo, 2013).

The Fd affinity to its redox partners, i.e., PSI acceptor side, was also raised to ensure the competition with O_2 for electrons. However, this is not entirely the case of FNR. Although a semiquinone form of FAD prosthetic group in FNR can react with O_2 (Massey, 1994), so far there are no reliable experimental data demonstrating that FNR is involved in O_2 photoreduction in the thylakoid membranes (Kozuleva and Ivanov, 2016). The FNR of oxygenic phototrophs possesses ∼10 times higher catalytic activity than the bacterial FNR (Pierella Karlusich and Carrillo, 2017), with affinity remaining roughly the same. The high catalytic activity is likely achieved through conformational changes caused by $NADP^+$ binding to FNR, which greatly facilitate both the Fd^- oxidation (Batie and Kamin, 1984) and the liberation of the oxidized Fd from the complex (Mulo and Medina, 2017). This enhancement in the FNR catalytic activity most possibly decreased the chances for both the FAD semiquinone ($Q^{\bullet-}$) oxidation by O_2 and the formation of $Fd:FNR^{\bullet-}$ complex in the absence of $NADP^+$.

PLASTOQUINONE POOL

$O_2^{\bullet-}$ photoproduction by $PQ^{\bullet-}$ in the PQ pool was demonstrated (Khorobrykh and Ivanov, 2002; Vetoshkina et al., 2017). However, the maximal $O_2^{\bullet-}$ production rates observed in the pool were 10 times lower than in the PSI.

While anoxygenic phototrophs use menaquinone (MQ) and ubiquinone (UQ), the oxygenic ones recruited PQ, a representative of a "more recent" group of quinones (Schoepp-Cothenet et al., 2009). MQ was probably the first quinone in ancient photosynthetic membranes. The rationale for replacing MQ with PQ is clear: the E_m values of ($Q/Q^{\bullet-}$) and (Q/QH_2) are ∼100 mV (Kishi et al., 2017) and ∼180 mV (Bergdoll et al., 2016), more negative for MQ than for PQ (**Figure 1B**). This means that $PQ^{\bullet-}$ and the PQ pool itself in the reduced state are more stable in the presence of O_2. Furthermore, pK_a ($Q^{\bullet-}/QH$) for PQ is higher than for MQ, providing an easier protonation and, hence, a higher stability of plastosemiquinone (Hasegawa et al., 2017).

A possible rationale for choosing PQ instead of UQ in the PETC of oxygenic phototrophs is still vague. Firstly, the $O_2^{\bullet-}$ generation by free $UQ^{\bullet-}$ in the mitochondria was discovered as early as in 80-s (Turrens et al., 1985). This reaction has long been considered as an important source of $O_2^{\bullet-}$ in animal cells. On the contrary, $PQ^{\bullet-}$ in photosynthetic cells has little impact on $O_2^{\bullet-}$ production, as stated above. Secondly, PQH_2 is more efficient as an antioxidant than UQH_2 (Borisova-Mubarakshina et al., 2019), e.g., in lipid peroxidation prevention (Kruk et al., 1997). A consequence of higher antioxidant activity of PQH_2 is its higher ability to reduce $O_2^{\bullet-}$ to H_2O_2. It was shown that the PQ pool in the thylakoid membranes (presumably PQH_2) is indeed oxidized by $O_2^{\bullet-}$ (Borisova-Mubarakshina et al., 2018). Therefore, despite the low $O_2^{\bullet-}$-generating activity, the contribution of the PQ pool to the Mehler reaction can be essential due to the production of H_2O_2 from $O_2^{\bullet-}$. We hypothesize that ensuring the efficient transformation of $O_2^{\bullet-}$, which is generated by PSI, to H_2O_2 could be one of the evolutionary driving forces for the choice of PQ.

Replacing MQ with PQ as a mobile pool in the thylakoid membrane inevitably affected all of the complexes interacting with quinone. All cofactors in photosystem II (PSII) and cytochrome b_6/f complexes have 110–150 mV more positive E_m values than in their MQ-based analogs (Schoepp-Cothenet et al., 2009; Bergdoll et al., 2016).

CYTOCHROME b_6/f COMPLEX

The cytochrome b_6/f complex is also considered to be an O_2 photoreduction site (Taylor et al., 2018). The high E_m values of the b_6f complex cofactors are a consequence of MQ replacement with PQ (Bergdoll et al., 2016). Among its ET cofactors, the b_L heme possesses one of the lowest E_m, −130 mV (Alric et al., 2005). Thermodynamically, this heme can hardly reduce O_2 since E_m ($O_2/O_2^{\bullet-}$) in the membrane is close to −550 mV (**Figure 1B**, see above). The fast ET from b_L to b_H decreases the possibility of a b_L reaction with O_2.

In several studies, $PQ^{\bullet-}$ at the quinol-oxidizing (Q_o) site of the complex is considered as the electron donor to O_2. However, the concerted oxidation of PQH_2 diminishes the $PQ^{\bullet-}$ lifetime. If semiquinone is produced, it is either quickly oxidized by b_L heme or reduced by it, if the heme is pre-reduced. The dimer organization of the b_6/f complex was proposed to lower the chances of $O_2^{\bullet-}$ generation at the Q_o site (Rutherford et al., 2012). In the bc_1 complex, a spin–spin complex state between the semiquinone and the Rieske cluster was shown to suppress $O_2^{\bullet-}$ generation (Bujnowicz et al., 2019). This keeps up well with the experimental observations that $PQ^{\bullet-}$ can reduce O_2 once it leaves the Q_o pocket (Forquer et al., 2006), becoming a part of the pool (see above). It was demonstrated that $O_2^{\bullet-}$ production by the isolated b_6/f complexes was 10 times higher than the one by the isolated bc_1 complexes (Baniulis et al., 2013). This can be explained by an easier liberation of semiquinone from the Q_o site in the former case. It is important that, *in vivo*, such $PQ^{\bullet-}$ would appear at the luminal side of the thylakoid membrane. The lumen pH determines the protonation of $PQ^{\bullet-}$. Since $PQH^{\bullet}$ has a lower chance to reduce O_2, the lumen pH can regulate the $O_2^{\bullet-}$ production there.

The appearance of semiquinone at the quinone-reducing site (Q_r) of the bc_1 complex from purple bacteria was shown (Drachev et al., 1989). There are still no reliable data on semiquinone formation at the Q_r site of the b_6/f complex. The double reduction of PQ occurs there when the second electron is transferred to the b_H heme (Ivanov, 1993). The residence of the first electron at the b_H heme can be a result of the c_n heme situated in close vicinity to the b_H in the b_6/f complex.

PHOTOSYSTEM II

Three major tasks could have been solved during the evolution of PSII: (i) the existence of highly oxidizing $P680^+$, (ii) dealing with charge recombination leading to $^1O_2$ production, and (iii) stabilization of Q_B^- waiting for the second electron (Rutherford et al., 2012). $O_2^{\bullet-}$ production in PSII was shown many times (Pospíšil, 2012). Pheophytin (Pheo), Q_A, Q_B, and cytochrome b_{559} were suggested as the sites of O_2 reduction to $O_2^{\bullet-}$, based presumably on the experiments with PSII complexes with disrupted function, e.g., after modifications of the water-oxidizing complex.

Although $Pheo^-$ possesses E_m, −610 mV (Rappaport et al., 2002), negative enough to reduce O_2 even in hydrophobic media (**Figure 1C**), its lifetime is rather short (300 ps) such that it prevents the electron leakage to O_2. This reaction with Q_A^- (Ivanov and Khorobrykh, 2003; Pospíšil, 2012) is thermodynamically unfavorable due to a more positive E_m (Q_A/Q_A^-), −70 mV (Brinkert et al., 2016), than E_m ($O_2/O_2^{\bullet-}$). However, the binding of HCO_3^- to non-heme Fe situated between the Q_A and the Q_B shifts E_m (Q_A/Q_A^-) to −145 mV, making the electron leakage from Q_A^- to O_2 more probable. In contrast to Q_A, Q_B undergoes two sequential reduction steps, meaning that Q_B^- lives for a longer time waiting for the second electron. However, Q_B^- is thermodynamically stable due to the positive E_m potentials (Causmaecker et al., 2019).

The role of a very low potential form of cytochrome b_{559} (E_m is −150 to −200 mV) in O_2 reduction was also proposed (Khorobrykh, 2019). However, the fraction of this form is extremely small under normal conditions and increases only when the PSII functioning is severely perturbed. The b_{559} heme is embedded in the hydrophobic zone of the membrane; therefore, O_2 photoreduction by b_{559} heme is thermodynamically unfavorable.

DISCUSSION

In this review, we briefly summarize some features of the modern PETC, which have evolved at the background of the Mehler reaction. The main site of $O_2^{\bullet-}$ generation is PSI. Several experiments revealed that PhQ could be the major contributor to this process (Kruk et al., 2003; Kozuleva et al., 2011, 2014). The reactivity of the FeS components with O_2, especially F_B and Fd, was diminished by redox tuning and protein shielding. The recruitment of a high-potential PQ to the membrane quinone pool instead of a low-potential MQ was driven by the necessity to keep the pool in the reduced state under illumination in the presence of O_2. Replacing MQ with PQ triggered a redox tuning of PSII and cytochrome b_6/f complex cofactors, disabling, among other things, efficient $O_2^{\bullet-}$ generation in these complexes. The only MQ-based cofactor preserved in the modern PETC is PhQ, which is likely to be the main site of $O_2^{\bullet-}$ generation.

The stromal production of $O_2^{\bullet-}$ *via* Fd greatly increases if the $NADP^+$ recovering in the Calvin–Benson–Bassham cycle is retarded, e.g., due to closed stomata. In the stroma, H_2O_2 is produced from $O_2^{\bullet-}$ under catalysis by superoxide dismutase. O_2 reduction by $PhQ^{\bullet-}$ can account for $O_2^{\bullet-}$ appearance within the thylakoid membrane (Kozuleva et al., 2011); however, a significant part of $O_2^{\bullet-}$ formed by $PhQ^{\bullet-}$ still likely diffuses outside the membrane. Nevertheless, the increasing irradiance resulted in both a larger $O_2^{\bullet-}$ production just within the thylakoid membrane and a larger H_2O_2 production *via* $O_2^{\bullet-}$ reduction by PQH_2, i.e., by the mechanism different from dismutation (Borisova-Mubarakshina et al., 2012).

Thus, in chloroplasts, H_2O_2 is produced *via* two distinct reactions in two distinct chloroplast compartments. We believe that this observation may be important for the understanding of H_2O_2-mediated signal transduction. The stromal H_2O_2, which might be considered as a messenger of $NADP^+$/NADPH status, can oxidize thioredoxins (Hofmann, 2010; Netto and Antunes, 2016). Therefore, a temporary H_2O_2 accumulation in the stroma can affect the expression of chloroplast genes and/or the translation aimed at the fast adaptation of photosynthetic apparatus. H_2O_2 formed by the membrane PQ pool might be considered as a messenger of PETC status. It is important in terms of the PQ pool function as a central hub, of which the redox state represents a signal for both the chloroplast gene expression (Pfannschmidt et al., 2009) and the retrograde signaling pathways from the chloroplast to the nucleus (Pfannschmidt et al., 2003). For example, the PQ pool redox state initiates the changes in the PSII light-harvesting antenna size as a long-term acclimation to light conditions (Escoubas et al., 1995; Frigerio et al., 2007). We demonstrated that it is H_2O_2 rather than the PQ pool reduction state itself that is responsible for the antenna size reduction in high light (Borisova-Mubarakshina et al., 2015, 2019). Therefore, we suppose that a high potential of the PQ pool to form H_2O_2 in high light and under stress conditions could serve as evolutionarily set to signal about the PETC redox state to adjust to the ever-changing environmental conditions.

AUTHOR CONTRIBUTIONS

MK and MB-M designed the concept of the article. All authors contributed to the writing of the first draft and manuscript revision, and approved the submitted version. MK incorporated all inputs from the coauthors, reviewers, and editor.

FUNDING

This work was funded by the Russian Science Foundation, project 17-14-01371 and by The Ministry of Science and Higher Education of the Russian Federation, State Scientific Program, theme no. AAAA-A17-117030110135-1.

REFERENCES

Alric, J., Pierre, Y., Picot, D., Lavergne, J., and Rappaport, F. (2005). Spectral and redox characterization of the heme ci of the cytochrome b6f complex. *Proc. Natl. Acad. Sci. U.S.A.* 102, 15860–15865. doi: 10.1073/pnas.0508102102

Baniulis, D., Hasan, S. S., Stofleth, J. T., and Cramer, W. A. (2013). Mechanism of enhanced superoxide production in the cytochrome b6f complex of oxygenic photosynthesis. *Biochemistry* 52, 8975–8983. doi: 10.1021/bi4013534

Batie, C. J., and Kamin, H. (1984). Ferredoxin:NADP (oxidoreductase. Equilibria in binary and ternary complexes with NADP (and ferredoxin. *J. Biol. Chem.* 259, 8832–8839.

Bergdoll, L., ten Brink, F., Nitschke, W., Picot, D., and Baymann, F. (2016). From low- to high-potential bioenergetic chains: Thermodynamic constraints of Q-cycle function. *Biochim. Biophys. Acta* 1857, 1569–1579. doi: 10.1016/j.bbabio.2016.06.006

Borisova-Mubarakshina, M. M., Ivanov, B. N., Vetoshkina, D. V., Lubimov, V. Y., Fedorchuk, T. P., Naydov, I. A., et al. (2015). Long-term acclimatory response to excess excitation energy: evidence for a role of hydrogen peroxide in the regulation of photosystem II antenna size. *J. Exp. Bot.* 66, 7151–7164. doi: 10.1093/jxb/erv410

Borisova-Mubarakshina, M. M., Kozuleva, M. A., Rudenko, N. N., Naydov, I. A., Klenina, I. B., and Ivanov, B. N. (2012). Photosynthetic electron flow to oxygen and diffusion of hydrogen peroxide through the chloroplast envelope via aquaporins. *Biochim. Biophys. Acta* 1817, 1314–1321. doi: 10.1016/j.bbabio.2012.02.036

Borisova-Mubarakshina, M. M., Naydov, I. A., and Ivanov, B. N. (2018). Oxidation of the plastoquinone pool in chloroplast thylakoid membranes by superoxide anion radicals. *FEBS Lett.* 592, 3221–3228. doi: 10.1002/1873-3468.13237

Borisova-Mubarakshina, M. M., Vetoshkina, D. V., and Ivanov, B. N. (2019). Antioxidant and signaling functions of the plastoquinone pool in higher plants. *Physiol. Plant.* 166, 181–198. doi: 10.1111/ppl.12936

Brinkert, K., Causmaecker, S. D., Krieger-Liszkay, A., Fantuzzi, A., and Rutherford, A. W. (2016). Bicarbonate-induced redox tuning in Photosystem II for regulation and protection. *PNAS* 113, 12144–12149. doi: 10.1073/pnas.1608862113

Bujnowicz, Ł, Borek, A., Kuleta, P., Sarewicz, M., and Osyczka, A. (2019). Suppression of superoxide production by a spin-spin coupling between semiquinone and the Rieske cluster in cytochrome bc1. *FEBS Lett.* 593, 3–12. doi: 10.1002/1873-3468.13296

Causmaecker, S. D., Douglass, J. S., Fantuzzi, A., Nitschke, W., and Rutherford, A. W. (2019). Energetics of the exchangeable quinone, QB, in Photosystem II. *PNAS* 116, 19458–19463. doi: 10.1073/pnas.1910675116

Drachev, L. A., Kaurov, B. S., Mamedov, M. D., Mulkidjanian, A. Y., Semenov, A. Yu, Shinkarev, V. P., et al. (1989). Flash-induced electrogenic events in the photosynthetic reaction center and bc1 complexes of Rhodobacter sphaeroides chromatophores. *Biochim. Biophys. Acta* 973, 189–197. doi: 10.1016/S0005-2728(89)80421-9

Escoubas, J. M., Lomas, M., LaRoche, J., and Falkowski, P. G. (1995). Light intensity regulation of cab gene transcription is signaled by the redox state of the plastoquinone pool. *PNAS* 92, 10237–10241. doi: 10.1073/pnas.92.22.10237

Fischer, N., Sétif, P., and Rochaix, J.-D. (1997). Targeted mutations in the psac gene of *Chlamydomonas reinhardtii*: preferential reduction of FB at low temperature is not accompanied by altered electron flow from Photosystem I to Ferredoxin. *Biochemistry* 36, 93–102. doi: 10.1021/bi962244v

Forquer, I., Covian, R., Bowman, M. K., Trumpower, B. L., and Kramer, D. M. (2006). Similar transition states mediate the Q-cycle and superoxide production by the cytochrome bc1 complex. *J. Biol. Chem.* 281, 38459–38465. doi: 10.1074/jbc.M605119200

Frigerio, S., Campoli, C., Zorzan, S., Fantoni, L. I., Crosatti, C., Drepper, F., et al. (2007). Photosynthetic antenna size in higher plants is controlled by the plastoquinone redox state at the post-transcriptional rather than transcriptional level. *J. Biol. Chem.* 282, 29457–29469. doi: 10.1074/jbc.M705132200

Hanke, G., and Mulo, P. (2013). Plant type ferredoxins and ferredoxin-dependent metabolism. *Plant Cell Environ.* 36, 1071–1084. doi: 10.1111/pce.12046

Hasegawa, R., Saito, K., Takaoka, T., and Ishikita, H. (2017). pKa of ubiquinone, menaquinone, phylloquinone, plastoquinone, and rhodoquinone in aqueous solution. *Photosynth. Res.* 133, 297–304. doi: 10.1007/s11120-017-0382-y

Hofmann, N. R. (2010). A new thioredoxin is involved in plastid gene expression. *Plant Cell* 22:1423. doi: 10.1105/tpc.110.220512

Ivanov, B., and Khorobrykh, S. (2003). Participation of photosynthetic electron transport in production and scavenging of reactive oxygen species. *Antioxid. Redox Signal.* 5, 43–53. doi: 10.1089/152308603321223531

Ivanov, B., Kozuleva, M., and Mubarakshina, M. (2012). "Oxygen metabolism in chloroplast," in *Cell Metabolism-Cell Homeostasis and Stress Response*, ed. P. Bubulya (London: InTech).

Ivanov, B. N. (1993). "Stoichiometry of proton uptake by thylakoids during electron transport in chloroplasts," in *Photosynthesis: Photoreactions to Plant Productivity*, eds Y. P. Abrol and P. Mohanty (Dordrecht: Springer Netherlands), 109–128. doi: 10.1007/978-94-011-2708-0_4

Jagannathan, B., and Golbeck, J. H. (2009). Understanding of the binding interface between PsaC and the PsaA/PsaB heterodimer in Photosystem I. *Biochemistry* 48, 5405–5416. doi: 10.1021/bi900243f

Jagannathan, B., Shen, G., and Golbeck, J. H. (2012). "The evolution of type i reaction centers: the response to oxygenic photosynthesis," in *Functional Genomics and Evolution of Photosynthetic Systems Advances in Photosynthesis and Respiration*, (Dordrecht: Springer), 285–316. doi: 10.1007/978-94-007-1533-2_12

Khorobrykh, A. (2019). Hydrogen peroxide and superoxide anion radical photoproduction in PSII preparations at various modifications of the water-oxidizing complex. *Plants* 8:329. doi: 10.3390/plants8090329

Khorobrykh, S. A., and Ivanov, B. N. (2002). Oxygen reduction in a plastoquinone pool of isolated pea thylakoids. *Photosynth. Res.* 71, 209–219. doi: 10.1023/A:1015583502345

Kishi, S., Saito, K., Kato, Y., and Ishikita, H. (2017). Redox potentials of ubiquinone, menaquinone, phylloquinone, and plastoquinone in aqueous solution. *Photosynth. Res.* 134, 193–200. doi: 10.1007/s11120-017-0433-4

Kozuleva, M., Klenina, I., Proskuryakov, I., Kirilyuk, I., and Ivanov, B. (2011). Production of superoxide in chloroplast thylakoid membranes: ESR study with cyclic hydroxylamines of different lipophilicity. *FEBS Lett.* 585, 1067–1071. doi: 10.1016/j.febslet.2011.03.004

Kozuleva, M. A., and Ivanov, B. N. (2010). Evaluation of the participation of ferredoxin in oxygen reduction in the photosynthetic electron transport chain of isolated pea thylakoids. *Photosynth. Res.* 105, 51–61. doi: 10.1007/s11120-010-9565-5

Kozuleva, M. A., and Ivanov, B. N. (2016). The mechanisms of oxygen reduction in the terminal reducing segment of the chloroplast photosynthetic electron transport chain. *Plant Cell Physiol.* 57, 1397–1404. doi: 10.1093/pcp/pcw035

Kozuleva, M. A., Petrova, A. A., Mamedov, M. D., Semenov, A. Y., and Ivanov, B. N. (2014). O2 reduction by photosystem I involves phylloquinone under steady-state illumination. *FEBS Lett.* 588, 4364–4368. doi: 10.1016/j.febslet.2014.10.003

Kruk, J., Jemioła-Rzemiłska, M., Burda, K., Schmid, G. H., and Strzałka, K. (2003). scavenging of superoxide generated in Photosystem I by Plastoquinol and other Prenyllipids in Thylakoid membranes. *Biochemistry* 42, 8501–8505. doi: 10.1021/bi034036q

Kruk, J., Jemioła-Rzemińska, M., and Strzałka, K. (1997). Plastoquinol and (-tocopherol quinol are more active than ubiquinol and (-tocopherol in inhibition of lipid peroxidation. *Chem. Phys. Lipids* 87, 73–80. doi: 10.1016/S0009-3084(97)00027-3

Massey, V. (1994). Activation of molecular oxygen by flavins and flavoproteins. *J. Biol. Chem.* 269, 22459–22462.

Mubarakshina, M., Khorobrykh, S., and Ivanov, B. (2006). Oxygen reduction in chloroplast thylakoids results in production of hydrogen peroxide inside the membrane. *Biochim. Biophys. Acta* 1757, 1496–1503. doi: 10.1016/j.bbabio.2006.09.004

Mulo, P., and Medina, M. (2017). Interaction and electron transfer between ferredoxin–NADP (oxidoreductase and its partners: structural, functional, and physiological implications. *Photosynth. Res.* 134, 265–280. doi: 10.1007/s11120-017-0372-0

Netto, L. E. S., and Antunes, F. (2016). The roles of peroxiredoxin and thioredoxin in hydrogen peroxide sensing and in signal transduction. *Mol. Cells* 39, 65–71. doi: 10.14348/molcells.2016.2349

Orf, G. S., Gisriel, C., and Redding, K. E. (2018). Evolution of photosynthetic reaction centers: insights from the structure of the heliobacterial reaction center. *Photosynth. Res.* 138, 11–37. doi: 10.1007/s11120-018-0503-2

Pfannschmidt, T., Bräutigam, K., Wagner, R., Dietzel, L., Schröter, Y., Steiner, S., et al. (2009). Potential regulation of gene expression in photosynthetic cells by redox and energy state: approaches towards better understanding. *Ann. Bot.* 103, 599–607. doi: 10.1093/aob/mcn081

Pfannschmidt, T., Schütze, K., Fey, V., Sherameti, I., and Oelmüller, R. (2003). Chloroplast redox control of nuclear gene expression—a new class of plastid signals in interorganellar communication. *Antioxid. Redox Signal.* 5, 95–101. doi: 10.1089/152308603321223586

Pierella Karlusich, J. J., and Carrillo, N. (2017). Evolution of the acceptor side of photosystem I: ferredoxin, flavodoxin, and ferredoxin-NADP (oxidoreductase. *Photosyn. Res.* 134, 235–250. doi: 10.1007/s11120-017-0338-2

Pospíšil, P. (2012). Molecular mechanisms of production and scavenging of reactive oxygen species by photosystem II. *Biochim. Biophys. Acta* 1817, 218–231. doi: 10.1016/j.bbabio.2011.05.017

Ptushenko, V. V., Cherepanov, D. A., Krishtalik, L. I., and Semenov, A. Y. (2008). Semi-continuum electrostatic calculations of redox potentials in photosystem I. *Photosynth. Res.* 97:55. doi: 10.1007/s11120-008-9309-y

Rappaport, F., Guergova-Kuras, M., Nixon, P. J., Diner, B. A., and Lavergne, J. (2002). Kinetics and Pathways of Charge Recombination in Photosystem II. *Biochemistry* 41, 8518–8527. doi: 10.1021/bi025725p

Rutherford, A. W., Osyczka, A., and Rappaport, F. (2012). Back-reactions, short-circuits, leaks and other energy wasteful reactions in biological electron transfer: redox tuning to survive life in O2. *FEBS Lett.* 586, 603–616. doi: 10.1016/j.febslet.2011.12.039

Schoepp-Cothenet, B., Lieutaud, C., Baymann, F., Verméglio, A., Friedrich, T., Kramer, D. M., et al. (2009). Menaquinone as pool quinone in a purple bacterium. *PNAS* 106, 8549–8554. doi: 10.1073/pnas.0813173106

Shinkarev, V. P., Vassiliev, I. R., and Golbeck, J. H. (2000). A kinetic assessment of the sequence of electron transfer from F(X) to F(A) and further to F(B) in photosystem I: the value of the equilibrium constant between F(X) and F(A). *Biophys. J.* 78, 363–372. doi: 10.1016/S0006-3495(00)76599-4

Šnyrychová, I., Pospíšil, P., and Nauš, J. (2006). Reaction pathways involved in the production of hydroxyl radicals in thylakoid membrane: EPR spin-trapping study. *Photochem. Photobiol. Sci.* 5, 472–476. doi: 10.1039/B514394B

Takahashi, M., and Asada, K. (1988). Superoxide production in aprotic interior of chloroplast thylakoids. *Arch. Biochem. Biophys.* 267, 714–722. doi: 10.1016/0003-9861(88)90080-X

Taylor, R. M., Sallans, L., Frankel, L. K., and Bricker, T. M. (2018). Natively oxidized amino acid residues in the spinach cytochrome b6f complex. *Photosynth. Res.* 137, 141–151. doi: 10.1007/s11120-018-0485-0

Turrens, J. F., Alexandre, A., and Lehninger, A. L. (1985). Ubisemiquinone is the electron donor for superoxide formation by complex III of heart mitochondria. *Arch. Biochem. Biophys.* 237, 408–414. doi: 10.1016/0003-9861(85)90293-0

Vetoshkina, D. V., Ivanov, B. N., Khorobrykh, S. A., Proskuryakov, I. I, and Borisova-Mubarakshina, M. M. (2017). Involvement of the chloroplast plastoquinone pool in the Mehler reaction. *Physiol. Plant.* 161, 45–55. doi: 10.1111/ppl.12560

Wardman, P. (1990). Bioreductive activation of quinones: redox properties and Thiol reactivity. *Free Radic. Res. Commun.* 8, 219–229. doi: 10.3109/10715769009053355

Conflict of Interest: The authors declare that the research was conducted in the absence of any commercial or financial relationships that could be construed as a potential conflict of interest.

frontiers in Plant Science

ORIGINAL RESEARCH
published: 15 April 2020
doi: 10.3389/fpls.2020.00382

A Commonly Used Photosynthetic Inhibitor Fails to Block Electron Flow to Photosystem I in Intact Systems

*Duncan Fitzpatrick, Eva-Mari Aro and Arjun Tiwari**

Molecular Plant Biology Unit, Department of Biochemistry, University of Turku, Turku, Finland

In plant science, 2,4-dinitrophenylether of iodonitrothymol (DNP-INT) is frequently used as an alternative to 2,5-dibromo-6-isopropyl-3-methyl-1,4-benzoquinone (DBMIB) to examine the capacity of plastoquinol and semiquinone to reduce O_2. DNP-INT is considered to be an effective inhibitor of the photosynthetic electron transfer chain (PETC) through its binding at the Q_0 site of Cyt-*b6f*. The binding and action of DNP-INT has been previously characterized spectroscopically in purified Cyt-*b6f* complex reconstituted with Plastocyanin, PSII membranes and plastoquinone, as well as in isolated thylakoids based on its property to block MV-mediated O_2 consumption. Contrary to the conclusions obtained from these experiments, we observed clear reduction of $P700^+$ in samples incubated with DNP-INT during our recent investigation into the sites of oxygen consumption in isolated thylakoids. Therefore, we carried out an extensive investigation of DNP-INT's chemical efficacy in isolated thylakoids and intact leaves. This included examination of its capacity to block the PETC before PSI, and therefore its inhibition of CO_2 fixation. P700 redox kinetics were measured using Dual-PAM whilst Membrane Inlet Mass Spectrometry (MIMS) was used for simultaneous determination of the rates of O_2 evolution and O_2 consumption in isolated thylakoids and CO_2 fixation in intact leaves, using two stable isotopes of oxygen ($^{16}O_2$, $^{18}O_2$) and CO_2 (^{12}C, ^{13}C), respectively. Based on these investigations we confirmed that DNP-INT is unable to completely block the PETC and CO_2 fixation, therefore its use may produce artifacts if applied to isolated thylakoids or intact cells, especially when determining the locations of reactive oxygen species formation in the photosynthetic apparatus.

Keywords: DNP-INT, superoxide, P700 spectroscopy, MIMS, photosynthetic electron transfer chain, reactive oxygen species, stable-isotopes

OPEN ACCESS

Edited by:
Anja Liszkay,
Centre National de la Recherche Scientifique (CNRS), France

Reviewed by:
Yuji Suzuki,
Tohoku University, Japan
Toru Hisabori,
Tokyo Institute of Technology, Japan

***Correspondence:**
Arjun Tiwari
arjun.tiwari@utu.fi

Specialty section:
This article was submitted to Plant Physiology, a section of the journal Frontiers in Plant Science

Received: *14 November 2019*
Accepted: *17 March 2020*
Published: *15 April 2020*

Citation:
Fitzpatrick D, Aro E-M and Tiwari A (2020) A Commonly Used Photosynthetic Inhibitor Fails to Block Electron Flow to Photosystem I in Intact Systems. Front. Plant Sci. 11:382. doi: 10.3389/fpls.2020.00382

INTRODUCTION

Life in all three domains is sustained by membrane protein complexes participating in circuits that couple redox reactions and proton pumping, with the generation of ATP and NAD(P)H. The strategic application of chemical inhibitors, in isolation and in concert, has proven invaluable to study the roles, components and mechanisms of electron transport chains. In studies of photosynthetic systems, 3-(3,4-dichlorophenyl)-1,1-dimethylurea (DCMU), inhibitor of plastoquinone (PQ) reduction by PSII (Trebst, 2007; see **Figure 1**) and 2,5-Dibromo-6-isopropyl-3-methyl-1,4-benzoquinone (DBMIB), inhibitor of PQ-oxidation by cytochrome

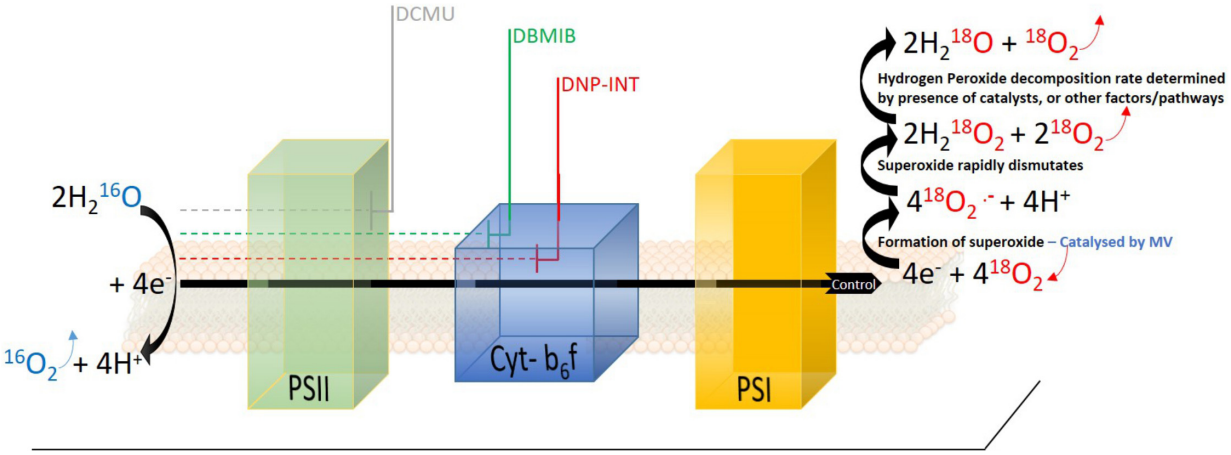

FIGURE 1 | Schematic diagram of photosynthetic electron transport chain in isolated thylakoid samples when natural $^{16}O_2$ isotope (Blue) was diminished significantly from the measuring chamber and enriched with the heavy $^{18}O_2$ isotope (Red). One molecule of $^{16}O_2$ (Blue) and four electrons are produced through oxidation of two water molecules at PSII. Electrons are transferred to four molecules of $^{18}O_2$ at the acceptor side of PSI (potentially also within PQ pool), forming four superoxide molecules (step catalyzed by methyl viologen, MV). The superoxide dismutates rapidly into two hydrogen peroxide molecules, releasing two molecules of $^{18}O_2$. Further decomposition of H_2O_2 to H_2O and O_2 is the final step in the electron transfer pathway of the water-water cycle. Approximate locations of inhibition of electron transport targeted by DCMU, DBMIB, and DNP-INT are indicated in the figure.

(Cyt)-*b6f* complex (Trebst, 2007; see **Figure 1**) have been the most regularly used and commercially available inhibitors. A drawback of the quinol base of DBMIB is that it possesses intrinsic redox functionality that in excess concentrations provides endogenous electron transport capacity able to bypass Cyt-*b6f* (Chain and Malkin, 1979). To counter this, 2,4-dinitrophenylether of iodonitrothymol (DNP-INT) was synthesized as a redox inert surrogate with characteristics otherwise similar to DBMIB (Trebst et al., 1978).

Significant effort has been committed to characterize the inhibitory action of DNP-INT in the photosynthetic electron transfer chain (PETC). Absorption spectroscopy measurements of purified Cyt-*b6f* complex reconstituted with plastocyanine (PC), PQ, photosystem (PS)I and PSII in the reaction medium (Lam and Malkin, 1983; O'Keefe, 1983), along with low temperature electron paramagnetic resonance (EPR) spectroscopy of purified Cyt-*b6f* complex (Malkin, 1986; Roberts and Kramer, 2001) have shown that DNP-INT blocks oxidation of plastoquinol and reduction of PC by binding at the Q_0 site of Cyt-*b6f*. Furthermore, functional measurements have been used to demonstrate the effectiveness of DNP-INT in blocking linear electron transfer in more complex samples, such as isolated thylakoids. To this end, the oxygen (O_2) consumption rate upon exposure of thylakoid samples to light was measured with a Clarke type O_2 electrode in the absence of artificial electron acceptors (Khorobrykh and Ivanov, 2002). These experiments demonstrated similar O_2 uptake rates between untreated and DNP-INT incubated thylakoid samples, yet the addition of methyl viologen (MV), a strong catalyst of O_2 reduction at PSI acceptor side (see **Figure 1**), increased Net O_2 uptake rates only in samples lacking DNP-INT. This was interpreted as strong evidence that DNP-INT blocks electron flow via PSI to MV, and therefore the chemical effectively truncates PSI from the PETC. Furthermore, similarity in O_2 uptake rates observed between untreated and DNP-INT treated samples suggested the presence of superoxide forming pathways, similar to that in PSI, also associated with the reduced PQ pool and Cyt-*b6f* complex (Khorobrykh and Ivanov, 2002; Mubarakshina and Ivanov, 2010; Borisova-Mubarakshina et al., 2018).

The results from O_2 electrode measurements with isolated thylakoids were interpreted as the ability of DNP-INT to allow semiquinone formation, whilst simultaneously blocking Cyt-*f* reduction (Mubarakshina and Ivanov, 2010), which made DNP-INT a critical tool in truncating the PETC at Cyt-*b6f*. It has resulted in the wide use of DNP-INT as an alternative to DBMIB for truncation of PSI from the PETC, particularly in works to explore reactive oxygen species (ROS) formation and scavenging pathways involving both reduced PQ-pool and semiquinones (Khorobrykh and Ivanov, 2002; Heyno et al., 2009; Mubarakshina and Ivanov, 2010; Borisova-Mubarakshina et al., 2018). Based on these characterizations, use of DNP-INT has provided a range of significant findings in plant (Stepien and Johnson, 2009) and algal physiology (Barbagallo et al., 1999), bioenergetics (Malnoe et al., 2011), bio-fuel applications (Mus et al., 2005), biochemical characterizations of PETC components (Krieger-Liszkay et al., 2000) and efforts to determine sites and activity of ROS formation/quenching (Khorobrykh and Ivanov, 2002; Heyno et al., 2009; Mubarakshina and Ivanov, 2010; Vetoshkina et al., 2017; Borisova-Mubarakshina et al., 2018).

In our current work, we attempted to determine the contribution of PSI in overall light-induced O_2 reduction from isolated thylakoids and intact leaf discs. For this, we planned to truncate the PETC with inhibitors such as DBMIB and DNP-INT. As a control for successful and complete truncation of PSI from the PETC under our specific experimental conditions, we measured both isolated thylakoid and intact leaf samples with

a Dual PAM to record the redox kinetics of P700. However, DNP-INT failed to block linear electron transport to PSI in both sample types. After controlling for the chemical structure of our commercially procured DNP-INT with ^{1}HNMR spectroscopy, and following our successful reproduction of the frequently published O_2 electrode results (Khorobrykh and Ivanov, 2002; Vetoshkina et al., 2017) described above, we embarked on a thorough investigation of PSI redox kinetics and photosynthetic gas exchange in DNP-INT treated samples. To confirm whether DNP-INT truly truncates PSI from the PETC, we compared the redox kinetics of P700 measurements incubated with DNP-INT and other well characterized PETC inhibitors. MIMS was used to distinguish the O_2 consuming and O_2 producing reactions occurring simultaneously in isolated thylakoid samples to test conclusions drawn from O_2 electrode data, and was used then to measure rates of CO_2 fixation in leaf discs infiltrated with DNP-INT.

MATERIALS AND METHODS

Leaf Samples and Isolation of Thylakoids

Thylakoids were isolated from 6 week old *Arabidopsis thaliana* plants, grown at 16/8 h dark/light cycle at 120 μmol photons m^2 s^1 at atmospheric CO_2. Thylakoids were isolated as described earlier (Tiwari et al., 2016) except all measurements were performed with freshly isolated thylakoids in buffer containing: 330 mM Sorbitol, 5 mM $MgCl_2$, 10 mM NaCl, 5 mM NH_4Cl, 50 mM Hepes (pH 7.6). Leaf measurements in MIMS and Dual-PAM were taken from the same plants.

Inhibitor Stocks

The inhibitors DCMU (Sigma, United States), DBMIB (Sigma, United States) were prepared as standard in ethanol. We purchased two separate stocks of DNP-INT (caymann chemicals batch no. 0468094-2, 0468093-2, 0524164-2) with the second being sent for analytical analysis to confirm purity via ^{1}HNMR. In addition we received another DNP-INT stock from the original Trebst preparation (donated by Anja Krieger). All DNP-INT stock solutions were prepared in dimethyl sulfoxide and used separately to repeat experiments as stated in the text. For conducting each experiment, all stock solutions used were freshly prepared and the concentrations of all inhibitors used were based on those experimentally demonstrated in literature to completely block electron transfer process.

MIMS Measurements of Isolated Thylakoid Membranes

Freshly isolated thylakoid samples of known chlorophyll concentration were stored on ice in darkness. A Sentinel-PRO magnetic sector mass spectrometer (Thermo Fisher Scientific, United States) was employed to collect masses 32 and 36 with a total cycle time of approximately 4.5 s. For each run sufficient measurement buffer (containing: 330 mM Sorbitol, 5 mM $MgCl_2$, 10 mM NaCl, 5 mM NH_4Cl, 50 mM Hepes pH 7.6) was loaded into the cuvette equilibrated and calibrated to 25°C, thylakoids were added (equivalent to approximately 50 μg chlorophyll) to a final volume of 1000 μl. In darkness the sample was briefly purged with N_2 to reduce the background $^{16}O_2$ signal before a bubble of $^{18}O_2$ (Cambridge Isotope Laboratories Inc., United Kingdom) was loaded into the stirring liquid, bringing the concentration of the heavier isotope up to approximately 150 nmol ml^1. The bubble was removed and inhibitors were injected at this moment (either 10 μM DCMU, 10 μM MV, 10 μM DBMIB, 10 μM DNP-INT) and samples equilibrated in darkness for 5 min before data acquisition was started. Samples were illuminated via halogen lamp (Dolan Jenner, United States) at 120 μmol photons m^2 s^1. At the end of each run, the Chl concentration of the sample was determined in triplicate using the Porra Method (Porra et al., 1989) in 90% MeOH to ensure accurate normalization of rates between samples. The cuvette was washed thoroughly with multiple rinses of 70% Ethanol followed by MQ H_2O when changing between inhibitors to avoid cross contamination. This was checked by running controls. All data was analyzed and fluxes calculated with equations described in Beckmann et al. (2009).

MIMS Measurements of Leaf Discs

Leaf discs (14 mm) were cut from detached leaves and floated in darkness in either H_2O (control) or H_2O + 10 μM DBMIB or H_2O + 10 μM DNP-INT. Samples were incubated overnight in darkness at 25°C. For measurements, all excess water from leaf surface was removed and a smaller 12.5 mm disc was cut from the larger disc to remove the old edge. This was loaded into an in-house built stainless steel cuvette of 1000 μl volume, equilibrated and calibrated at 25°C, using Teflon (Hansatech) membrane to separate the sample space from the high vacuum line of the Mass Spectrometer. With the disc maintained in darkness, the cuvette was purged with N_2 to remove atmospheric $^{16}O_2$ and $^{12}CO_2$ before $^{18}O_2$ (as above) and $^{13}CO_2$ (Sigma-Aldrich, United States) were injected to approximately 3 and 2% by volume, respectively. Discs were kept for approximately 5 min in darkness inside the cuvette to ensure isotopic equilibrium in the system before the measurement started. The instrument recorded *m*/*z* 32, 36, 44, and 46 with a time resolution of approximately 6.5 s. After 4 min dark a halogen light directed via a liquid light guide illuminated the samples at 120 then 520 μmol photons m^{-2} s^{-1}. All data was analyzed and fluxes calculated with equations described in Beckmann et al. (2009). Leaf discs are often used as a surrogate for intact leaf measurements. Although experimental limitations relating to altered physiological responses do exist between a leaf disc and an intact leaf, for the purposes of demonstrating functional PSI activity via CO_2 fixation, these limitations do not apply to this set of experiments.

P700 Redox Kinetics Measurements

P700 redox kinetics were measured with detached leaves and isolated thylakoids using Dual-PAM-100 or Dual-Klass NIR (Walz, Germany). Isolated thylakoids in Dual Pam were measured at 100 μg Chl ml^{-1} using liquid sample holder. The P700 was oxidized under continuous far red (FR) light. Activating two short pulses of saturating actinic light i.e., single turnover (ST) (50 μs) and multiple turnover (MT) (50 ms) pulses, over

the FR light oxidized P700, induced partial P700 re-reduction by electrons from PSII (Tiwari et al., 2016). Infiltration of inhibitors was conducted in the same manner as described for MIMS, however, the incubation time for leaves was only 1 h.

O_2 Electrode Measurements

Thylakoid membranes prepared for MIMS measurements were also submitted to the Clark-type O_2 electrode (Hansatech, United Kingdom) measurements according to the methods described (Khorobrykh and Ivanov, 2002). 15 μg Chlorophyll ml^{-1} of sample was injected to 1000 μl of the same measurement buffer used in MIMS measurements. Inhibitors were added as described in the text. Samples were loaded in darkness and after one minute of dark data acquisition the halogen lamp was turned on (800 μmol photons m^{-2} s^{-1}) for 4 min (total 5 min).

RESULTS AND DISCUSSION

P700 Redox Kinetics Suggested DNP-INT Does Not Truncate PSI From the PETC

In attempts to differentiate rates of O_2 reduction between the acceptor side of PSI and the reduced PQ pool/Cyt-*b6f* complex, we have tested the efficacy of DBMIB and DNP-INT, two well characterized chemicals used to truncate PSI from the PETC, to validate that PSI was not reduced during our measurements. To examine this question we used a Dual PAM to measure the redox kinetics of P700 from both intact leaf and isolated thylakoid samples incubated with these inhibitors, and further compared them with DCMU as an unambiguous control for the inhibition of all intersystem electron transport between PSII and PSI (**Figures 2A,B**).

Following a dark period, addition of a constant FR light oxidized P700 to $P700^+$ in all samples (**Figures 2A,B**). Transient re-reduction of $P700^+$ to P700 by PSII derived electrons was achieved in inhibitor-free controls (Black lines, **Figures 2A,B**) via superimposition of saturating ST and MT actinic light pulses over the oxidizing FR light. Such transient re-reduction requires, and therefore tested, the function of the entire intersystem PETC (Fan et al., 2016; Tiwari et al., 2016). Extinguishing the FR light allowed $P700^+$ to re-reduce to P700, at varying rates, in all samples. In a clear demonstration of successful PSI truncation from the rest of the PETC, the level of $P700^+$ was largely unaffected following the ST and MT actinic pulses in both leaf and thylakoid samples treated with 10 μM DCMU (Blue lines) and 10 μM DBMIB (Pink lines). Unexpectedly, leaf and thylakoid samples treated with 10 μM DNP-INT (Orange lines) behaved in a manner resembling untreated controls. Although smaller in amplitude as compared to the controls, these dips (re-reduction of $P700^+$) produced by ST and MT actinic pulses in the $P700^+$ curves of DNP-INT treated leaf and thylakoid samples were undeniably present.

This suggested that electrons liberated by PSII were able to transiently reduce $P700^+$ to P700, whilst the smaller amplitude of the dips suggested that the number of electrons transferred to $P700^+$ in DNP-INT treated samples was impaired, compared to untreated samples. We also used a Dual Klass NIR to measure the redox kinetics of PC (**Supplementary Figure S1**), which accepts electrons exclusively from Cyt-*f*.

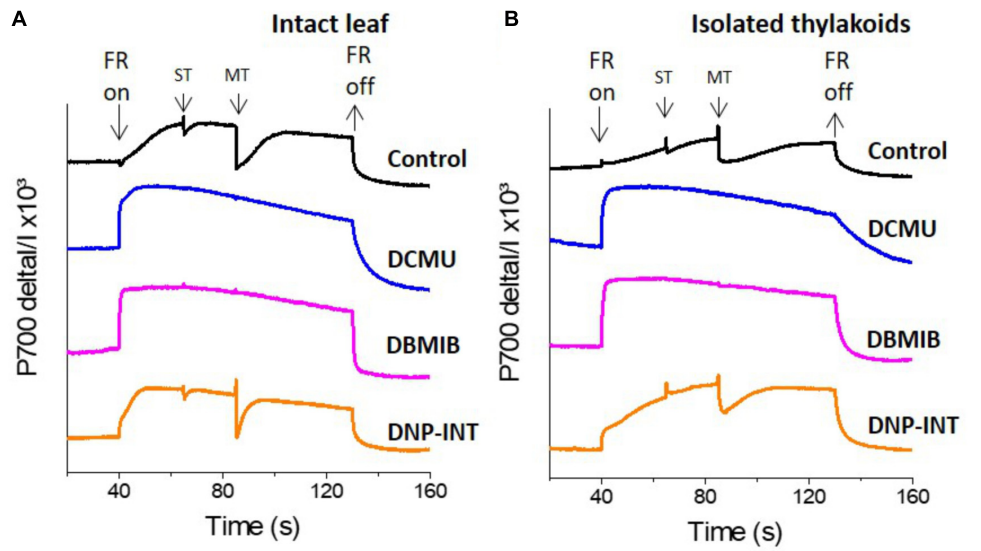

FIGURE 2 | Comparison of P700 redox kinetics from DCMU, DBMIB and DNP-INT infiltrated intact leaf and isolated thylakoid samples, measured with Dual Pam. **(A)** P700 redox kinetics of intact leaves; **(B)** P700 redox kinetics of isolated thylakoids. Uncoupled thylakoid samples were measured in liquid sample holder cuvette of Dual Pam at a chl concentration of 100 μg Chl ml^{-1} in buffer containing only 330 mM Sorbitol, 5 mM $MgCl_2$, 10 mM NaCl, 5 mM NH_4Cl, 50 mM Hepes pH 7.6 or with each chemical modulator at 10 μM as indicated in figure. Leaves were infiltrated in darkness using water for the control sample and all inhibitors were used at 10 μM concentration. Representative curves are average of minimum n = 5 samples. FR = P700 oxidizing Far Red light. ST = Single turnover (50 μs) actinic light pulse, MT = multiple turnover (50 ms) saturating light pulse.

For all treatments, the PC kinetics essentially matched with those discussed for the P700 data. This suggests that use of DNP-INT at 10 μM in isolated thylakoid samples did not block reduction of Cyt-*f*, and therefore P700 was still actively coupled to PSII, as opposed to the clear inhibition of PC and $P700^+$ re-reduction produced by the treatment of samples with DCMU and DBMIB.

Our DNP-INT Stocks and Isolated Thylakoids Reproduce Published Data

The concentration, quality and activity of our DNP-INT stocks were checked before making further investigations into the results of the Dual PAM data. Although the 10 μM DNP-INT concentration used in our protocol was at the high end of published protocols, and five times the "minimum concentration required for complete inhibition" of 2 μM (Trebst et al., 1978), we tested the possibility that we had under-dosed the DNP-INT samples by conducting a concentration response curve (see **Supplementary Figure S1**). In this experiment, DNP-INT failed to block the transient re-reduction of P700 caused by actinic light pulses in both the leaf and thylakoid samples from 2 to 500 μM concentration. That is 1000× the published minimum concentration required and 100× the concentration generally reported when DNP-INT is used to truncate PSI from the PETC (Krieger-Liszkay et al., 2000; Khorobrykh and Ivanov, 2002; Borisova-Mubarakshina et al., 2018). Another important question was to assure the purity of the DNP-INT we had procured. Historically DNP-INT has only been available to researchers through collaboration with its creator, Prof Achim Trebst. However, companies have recently started to synthesize and market this chemical as an inhibitor of PQ oxidation. Although our supplier, Cayman Chemicals, provided a full analytical analysis of their product to validate its purity, we repeated our experiments with a second stock purchased from a separate batch and independently verified the structure of the product. The Turku University Instrumentation Center conducted ^{1}H NMR on our DNP-INT stock, confirming the chemical's structure and that the two benzene rings were connected (see **Supplementary Figure S2**). Additionally, we have repeated the P700 redox kinetics experiment with a sample of the original DNP-INT stock synthesized by Prof Achim Trebst, kindly donated to us by Anja Krieger. Significantly, the original stock of DNP-INT did not block electron flow to PSI in isolated thylakoids or intact leaves (see **Supplementary Figure S3**), validating the conclusions we have based on the commercially procured chemical.

To further test the reliability of our DNP-INT samples, and to confirm the proper functionality of the isolated thylakoid preparations, we decided to replicate published measurements that purportedly demonstrate effectiveness of DNP-INT in truncating PSI from the PETC (Trebst et al., 1978; Khorobrykh and Ivanov, 2002).

In this measurement, a Clark-type O_2 electrode was used to compare Net O_2 fluxes from isolated thylakoid samples (**Figure 3**), initially in the absence of artificial electron acceptors

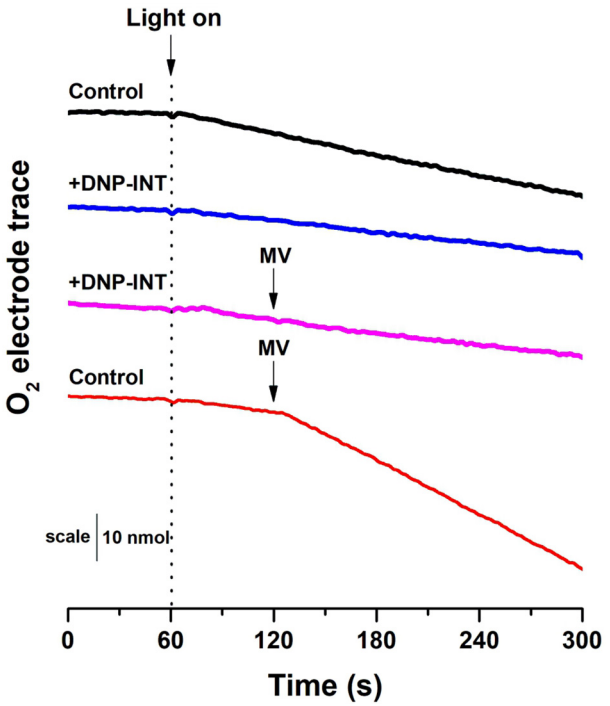

FIGURE 3 | Raw traces from O_2 electrode to demonstrate that our materials and methods can reproduce O_2 electrode data historically used to show the efficacy in DNP-INT. Raw [O_2] vs time traces were generated with thylakoids isolated from *Arabidopsis thaliana*. All measurements were conducted at a starting [O_2] of approximately 250 nmol ml^{-1}. Light intensity was 800 μmol photons m^{-2} s^{-1}, Thylakoids equivalent to 15 μg Chl ml^1. Each curve is an average of n = 6 replicate measurements.

but with and without DNP-INT. The experiment was repeated with similar samples but MV was injected after one minute of illumination to observe its capacity to increase Net O_2 uptake fluxes. The results (**Figure 3F**) faithfully reproduce the published outcome (Trebst et al., 1978; Khorobrykh and Ivanov, 2002). Compared to the untreated control (Black line), addition of DNP-INT (10 μM) to isolated thylakoid samples decreased rates of illuminated Net O_2 uptake (Blue line). The addition of MV to the DNP-INT treated samples had no effect on this impaired flux (Pink line), in stark contrast to MV's large effect of increasing the net O_2 flux of untreated control samples (Red line). The fact that MV cannot increase O_2 uptake rates in the presence of DNP-INT is traditionally interpreted as functional evidence for truncation of PSI from the PETC by 10 μM DNP-INT. Based on the following conclusions: (a) our independent ^{1}H NMR analysis of the commercially procured DNP-INT stock (b) that we could faithfully re-produce the published O_2 electrode result with the commercially procured DNP-INT stock and our preparation of thylakoid material, and (c) the successful reproduction of our initial P700 experiments using an original DNP-INT stock synthesized by Prof Trebst, we concluded that redox kinetics of PSI presented in **Figure 2** were not the result of any artifacts and warranted an in-depth investigation.

MIMS Data Showed That O_2 Electrode Assumptions Are Not Always Correct

Interpretation of data in **Figure 2** surprised us by suggesting that DNP-INT did not fully inhibit the re-reduction of $P700^+$ by actinic light pulses, as was expected and observed in samples incubated with DBMIB and DCMU (**Figure 2**). At the same time, the O_2 electrode data in **Figure 3** has been interpreted to imply that DNP-INT effectively blocks electron donation to MV (**Figure 3**) and therefore PSI is effectively truncated from the PETC by DNP-INT. We inferred the best explanation for this discrepancy to rest with the inherent limitations of the Clark-type O_2 electrode, which can only measure Net O_2 fluxes. This is particularly problematic when the stoichiometry of O_2 production and consumption is not clearly known, as is the case when O_2 is both produced and consumed in the same sample, at unknown relative rates depending on the characteristics of the O_2 reduction pathways active under different conditions (see **Figure 1**). To investigate whether this limitation of O_2 electrodes has potentially contributed to miscalculate/misinterpret the efficacy of DNP-INT's activity in isolated thylakoid samples, we employed the resolving power of MIMS. MIMS is able to discriminate between O_2 isotopologues to independently and simultaneously measure activity of PSII, and concomitant reduction of O_2 in isolated thylakoids (Furbank and Badger, 1983). By independently measuring the activity of PSII it was possible to unambiguously judge whether MV added to the DNP-INT inhibited samples could increase the rate of O_2 evolution or not, providing a clear test of whether or not PSI is truncated from the PETC in isolated thylakoids. As a final test of the capacity for DNP-INT to impair electron donation to PSI in intact leaves, we used the MIMS to measure whether or not leaf discs infiltrated with DNP-INT could still fix CO_2 in comparison to those infiltrated with DBMIB.

In both isolated thylakoid and leaf disc samples, PSII activity was measured as the Gross O_2 evolution rate, [or production of $^{16}O_2$ derived from PSII splitting of $H_2{}^{16}O$ (see **Figure 1**)]. The reduction of O_2 was measured directly through enrichment of the samples with the stable $^{18}O_2$ isotope, which following an N_2 purge to reduce $^{16}O_2$ became the primary electron acceptor in the isolated thylakoid samples. Leaf disc samples were purged with N_2 gas before being enriched to approximately 2% with $^{13}CO_2$, used as the terminal electron acceptor, and 3% $^{18}O_2$ to monitor O_2 reduction rates. Photorespiration in leaf discs was minimized by maintaining an elevated CO_2 partial pressure, which left mitochondrial respiration and potentially the Mehler reaction as primary O_2 uptake pathways. Monitoring $^{12}CO_2$ efflux rates derived from mitochondrial respiration enabled an estimate of illuminated respiration rates, minus any CO_2 re-fixation (Busch et al., 2013; Busch, 2018) to offset its contribution

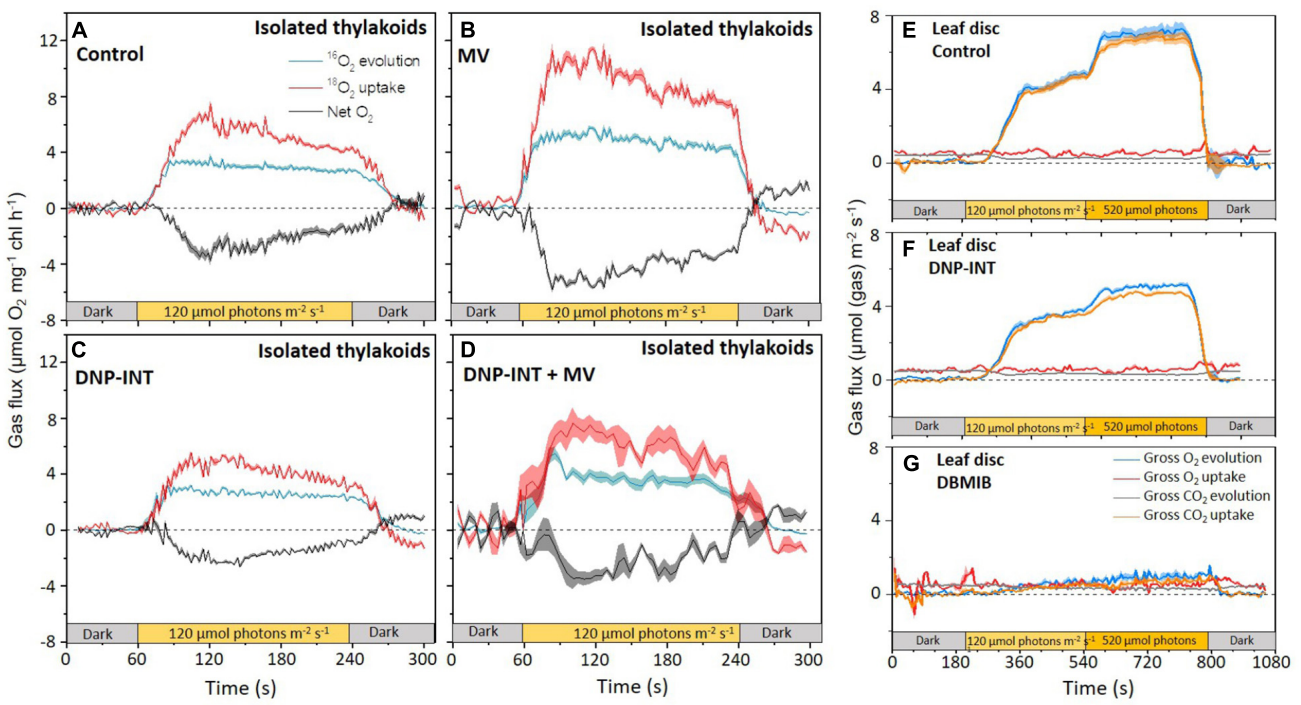

FIGURE 4 | Integrated gas flux versus time plots of isolated thylakoid and intact leaf disc samples (±SE) Simultaneously measured rates of O_2 Evolution and Consumption from isolated thylakoids (50 µg chlorophyll ml^{-1}) **(A–D)**, with the addition of CO_2 consumption and production rates from intact 12.5 mm leaf discs **(E–G)** measured with MIMS. Thylakoid samples measured under similar conditions used in Dual-PAM, see **Figure 2**. Leaf discs were floated overnight in water, or water containing 10 µM DNP-INT or 10 µM DBMIB in darkness. The rates of all isolated thylakoids were offset to zero in pre-illuminated darkness. Isolated thylakoid curves comprise averaged data from n = 7 (Control), n = 8 (DNP-INT), n = 8 (MV) and n = 4 (DNP-INT + MV) independent replicates. Leaf disc curves comprise the averaged data of n = 4 (control), n = 4 (DNP-INT) n = 3 (DBMIB) independent replicates.

to $^{18}O_2$ consumption, whilst the latter was minimized through low O_2 partial pressure.

MIMS data from isolated thylakoid samples are presented in **Figures 4A–D**. When illuminated at 120 μmol photons m^{-2} s^{-2} little difference in PSII activity (Blue lines, **Figure 4**) could be observed between control and DNP-INT treated thylakoids (**Figures 4A,C**). However, Gross O_2 uptake rates (Red Lines, **Figure 4**) were slightly lower in the latter, resulting in Net O_2 fluxes (Gray Lines, **Figure 4**), calculated from the difference between the two Gross O_2 rates, being smaller (less negative) in the DNP-INT samples. The difference in Net O_2 fluxes matches the results from the Clark-type O_2 electrode in **Figure 3**. However, the observation that O_2 evolution rates were actually very similar between the two conditions was unexpected. The smaller O_2 uptake rates in DNP-INT treated samples (**Figure 4C**) suggests that less H_2O_2 accumulated in the presence of this chemical, potentially due to unknown complexities of ROS scavenging pathways within the thylakoid membrane.

Addition of MV to thylakoids (**Figure 4B**) resulted in a large increase to rates of PSII O_2 evolution and Gross O_2 uptake, compared to the control, demonstrating that PSII activity is dictated by the strength of the acceptors in isolated thylakoid samples. The proportionate increase in both O_2 fluxes resulted in an increased difference between them, producing a larger negative Net O_2 flux, which also strongly reflected the Clark-type O_2 electrode data in **Figure 3**. Whilst it was clear that DNP-INT impeded rates of MV photoreduction (**Figure 4D**), it was also clear that MV increased rates of PSII activity in the DNP-INT inhibited samples (for a direct comparison refer to **Supplementary Figure S4** where we plot the Gross O_2 evolution rates measured under the four conditions on the same axis). This suggests that in-spite of the presence of DNP-INT, MV was able to increase the acceptor side capacity, which strongly supports the conclusions from P700 data in **Figure 2**, implying that DNP-INT does not truncate PSI from the PETC. In addition, the data shows that O_2 uptake rates did not increase proportionately with the increased PSII activity. This resulted in a smaller increase in the negative Net O_2 flux than would be predicted from a measure of PSII O_2 evolution alone, which again fits the O_2 electrode data in **Figure 3** and suggests that DNP-INT treated samples seem to generate less stable H_2O_2 than samples lacking this compound. Overall, deconvolution of O_2 generation and uptake afforded by MIMS has revealed that the Net O_2 fluxes observed do not necessarily correlate to the activity of PSII for a given condition. This suggests that the Net rates reported by Clark-type O_2 electrodes are unable to provide sufficient information to accurately interpret the site-specific complexities of ROS formation and scavenging in isolated thylakoid membrane samples lacking artificial donors and acceptors.

The final experiment to test the efficacy of DNP-INT to block electron transport to PSI in infiltrated leaves was to measure the capacity of intact leaves, infiltrated with 10 μM DNP-INT, to fix CO_2 during illumination using MIMS. Again, DBMIB was used as a comparison when electron transport at the Cyt-*b6f* complex was significantly inhibited. After 5 min darkness, leaf discs were illuminated 5 min at 120 μmol photons m^{-2} s^{-1}, then 5 min at 520 μmol photons m^{-2} s^{-1} before extinguishing the actinic light. As expected, photosynthetic activity was severely impaired by infiltration with DBMIB (**Figure 4G**) compared to untreated controls (incubated in water, **Figure 4E**). However, samples incubated with DNP-INT (**Figure 4F**) exhibited only a small reduction, of approximately 30%, in CO_2 fixation rates during illumination at both irradiances. In all samples, rates of mitochondrial respiration (CO_2 efflux, gray lines **Figures 4E–G**) were similar.

CONCLUSION

In efforts to assess the contribution of PSI-independent O_2 reduction pathways operating during illumination within the PETC, it is necessary to disconnect PSI completely from the rest of the PETC with effective inhibitors. Whilst DCMU and DBMIB functioned as expected in this regard, we were surprised when our initial results suggested that DNP-INT failed to block re-reduction of $P700^+$ at concentrations up to 1000× the published minimum concentration required. To verify that our materials were not producing an artifact, we confirmed the structure of our commercially procured DNP-INT stocks through ^1H NMR and we successfully reproduced a published O_2 electrode experiment used historically to support the contention that DNP-INT effectively truncates PSI from the PETC in isolated thylakoid samples. Then we again compared the rates of $P700^+$ re-reduction measured with a Dual-PAM between untreated controls, the inhibitors DCMU, DBMIB and both the commercially procured and original stocks of DNP-INT. Whilst DBMIB and DCMU clearly blocked complete re-reduction of $P700^+$ in both isolated thylakoid and leaf disc samples, neither stock of DNP-INT was able to replicate this result. This suggests that DNP-INT can only slow electron transfer through the PETC. The implication of this conclusion is that DNP-INT fails to block the Mehler reaction during *in vitro* experiments, or the carbon reduction cycle in intact samples. Using MIMS to independently and simultaneously measure the rates of O_2 production and consumption in isolated thylakoids, we demonstrated that MV added to DNP-INT treated samples was able to increase rates of PSII activity. However, the O_2 uptake rate did not increase commensurately, potentially due to unknown complexities of ROS scavenging within thylakoid membranes. As such, the Net O_2 flux did not appear to be different from the DNP-INT treated samples lacking MV. Through these experiments, we demonstrated that measurements of Net O_2 fluxes with an O_2 electrode are insufficient for measurements of the site-specific O_2 reduction pathways operating within thylakoid membranes, due to the complexities of the competing routes of superoxide formation and quenching that potentially invalidate some assumptions underpinning the interpretation of Net O_2 fluxes. Finally, we showed that leaf discs incubated with DNP-INT could still fix CO_2 at rates impaired by approximately 30%, whereas DBMIB severely impaired all photosynthetic fluxes from similar samples. We suggest that DNP-INT should no longer be used as an inhibitor of PSI reduction and that results reliant on the

assumption that DNP-INT had effectively inhibited the activity of PSI must be revisited. Nonetheless, the chemical may still find use for its apparent ability to slow electron transport between the PQ pool and PSI. This could be useful as a tool to artificially replicate the induction of photosynthetic control, imparted by the Cyt-*b6f* complex by an acidified lumen, potentially in the absence of NPQ or state transitions. It may also find use with researchers trying to modulate electron transfer rates in biophotovoltaic applications (Tschörtner et al., 2019). Finally, the disagreement in results between characterization studies of DNP-INT in purified complexes and our findings from intact samples may point to currently unknown aspects of Cyt-*b6f* function. Perhaps DNP-INT only partially blocks Cyt-*b6f* due to competitive inhibition with some other substrate that may now be studied with DNP-INT. Or perhaps the results reflect a sub-population of DNP-INT sensitive Cyt-*b6f* which may correlate to some spatial distribution in the thylakoid membrane, or its participation in super or mega complexes. Further work to explain the apparent discrepancies of DNP-INT function between spectroscopic measurements in highly purified samples and our results obtained with isolated thylakoids and intact leaf discs may yield significant information about photosynthesis in the future.

DATA AVAILABILITY STATEMENT

The datasets generated for this study are available on request to the corresponding author.

AUTHOR CONTRIBUTIONS

AT, DF, and E-MA conceptualized and designed the work. DF and AT carried out the experimental work, the data analysis and interpretation of the data. DF drafted the manuscript. AT and E-MA revised the content for final submission.

FUNDING

Research was funded by the Center of Excellence program of the Academy of Finland (project no 307335) and by the Jane and Aatos Erkko Foundation.

ACKNOWLEDGMENTS

Thanks to Tuomas Karskela at the Turku instrument Center for ^{1}H NMR measurement and analysis. We thank Dr. Anja Krieger-Liszkay for providing original DNP-INT synthesized by Prof. Achim Trebst.

SUPPLEMENTARY MATERIAL

The Supplementary Material for this article can be found online at: https://www.frontiersin.org/articles/10.3389/fpls.2020.00382/full#supplementary-material

REFERENCES

Barbagallo, R. P., Finazzi, G., and Forti, G. (1999). Effects of inhibitors on the activity of the cytochrome b(6)f complex: evidence for the existence of two binding pockets in the lumenal site. *Biochemistry* 38, 12814–12821. doi: 10.1021/bi990424+

Beckmann, K., Messinger, J., Badger, M. R., Wydrzynski, T., and Hillier, W. (2009). On-line mass spectrometry: membrane inlet sampling. *Photosynthesis Res.* 102, 511–522. doi: 10.1007/s11120-009-9474-7

Borisova-Mubarakshina, M. M., Naydov, placeI. A., and Ivanov, B. N. (2018). Oxidation of the plastoquinone pool in chloroplast thylakoid membranes by superoxide anion radicals. *FEBS Lett.* 592, 3221–3228. doi: 10.1002/1873-3468.13237

Busch, F. A. (2018). Photosynthetic gas exchange in land plants at the leaf level. *Methods Mol. Biol.* 1770, 25–44. doi: 10.1007/978-1-4939-7786-4_2

Busch, F. A., Sage, T. L., Cousins, A. B., and Sage, R. F. (2013). C3 plants enhance rates of photosynthesis by reassimilating photorespired and respired CO2. *Plant Cell Environ.* 36, 200–212. doi: 10.1111/j.1365-3040.2012.02567.x

Chain, R. K., and Malkin, R. (1979). On the interaction of 2,5-dibromo-3-methyl-6-isopropylbenzoquinone (DBMIB) with bound electron carriers in spinach chloroplasts. *Arch. Biochem. Biophys.* 197, 52–56. doi: 10.1016/0003-9861(79)90217-0

Fan, D. Y., Fitzpatrick, D., Oguchi, R., Ma, W., Kou, J., and Chow, W. S. (2016). Obstacles in the quantification of the cyclic electron flux around Photosystem I in leaves of C3 plants. *Photosynth Res.* 129, 239–251. doi: 10.1007/s11120-016-0223-4

Furbank, R. T., and Badger, M. R. (1983). Oxygen exchange associated with electron transport and photophosphorylation in spinach thylakoids. *Biochim. Biophys. Acta* 723, 400–409. doi: 10.1016/0005-2728(83)90047-6

Heyno, E., Gross, C. M., Laureau, C., Culcasi, M., Pietri, S., and Krieger-Liszkay, A. (2009). Plastid alternative oxidase (PTOX) promotes oxidative stress when overexpressed in tobacco. *J. Biol. Chem.* 284, 31174–31180. doi: 10.1074/jbc.M109.021667

Khorobrykh, S. A., and Ivanov, B. N. (2002). Oxygen reduction in a plastoquinone pool of isolated pea thylakoids. *Photosynth Res.* 71, 209–219.

Krieger-Liszkay, A., Kienzler, K., and Johnson, G. N. (2000). Inhibition of electron transport at the cytochrome b(6)f complex protects photosystem II from photoinhibition. *FEBS Lett.* 486, 191–194. doi: 10.1016/s0014-5793(00)02250-x

Lam, E., and Malkin, R. (1983). Characterization of electron transfer from water to plastocyanin catalyzed by resolved electron transfer complexes from chloroplasts. *Arch. Biochem. Biophys.* 224, 456–463. doi: 10.1016/0003-9861(83)90232-1

Malkin, R. (1986). Interaction of stigmatellin and DNP-INT with the Rieske iron-sulfur center of the chloroplast cytochrome b6-f complex. *FEBS Lett.* 208, 317–320. doi: 10.1016/0014-5793(86)81041-9

Malnoe, A., Wollman, F. A., de Vitry, C., and Rappaport, F. (2011). Photosynthetic growth despite a broken Q-cycle. *Nat. Commun.* 2:301. doi: 10.1038/ncomms1299

Mubarakshina, M. M., and Ivanov, B. N. (2010). The production and scavenging of reactive oxygen species in the plastoquinone pool of chloroplast thylakoid membranes. *Physiol. Plant.* 140, 103–110. doi: 10.1111/j.1399-3054.2010.01391.x

Mus, F., Cournac, L., Cardettini, V., Caruana, A., and Peltier, G. (2005). Inhibitor studies on non-photochemical plastoquinone reduction and H(2) photoproduction in *Chlamydomonas reinhardtii*. *Biochim. Biophys. Acta* 1708, 322–332. doi: 10.1016/j.bbabio.2005.05.003

O'Keefe, D. P. (1983). Sites of cytochrome b-563 reduction, and the mode of action of DNP-INT and DBMIB in the chloroplast cytochrome b-563/f complex. *FEBS Lett.* 162, 349–354. doi: 10.1016/0014-5793(83)80786-8

Porra, R. J., Thompson, W. A., and Kriedemann, P. E. (1989). Determination of accurate extinction coefficients and simultaneous equations for assaying

chlorophylls a and b extracted with four different solvents: verification of the concentration of chlorophyll standards by atomic absorption spectroscopy. *Biochim. Biophys. Acta* 975, 384–394. doi: 10.1016/s0005-2728(89)80347-0

Roberts, A. G., and Kramer, D. M. (2001). Inhibitor "double occupancy" in the Q(o) pocket of the chloroplast cytochrome b6f complex. *Biochemistry* 40, 13407–13412. doi: 10.1021/bi015774m

Stepien, P., and Johnson, G. N. (2009). Contrasting responses of photosynthesis to salt stress in the glycophyte *Arabidopsis* and the halophyte thellungiella: role of the plastid terminal oxidase as an alternative electron sink. *Plant Physiol.* 149, 1154–1165. doi: 10.1104/pp.108.132407

Tiwari, A., Mamedov, F., Grieco, M., Suorsa, M., Jajoo, A., Styring, S., et al. (2016). Photodamage of iron-sulphur clusters in photosystem I induces non-photochemical energy dissipation. *Nat. Plants* 2:16035. doi: 10.1038/nplants.2016.35

Trebst, A. (2007). Inhibitors in the functional dissection of the photosynthetic electron transport system. *Photosynth Res.* 92, 217–224. doi: 10.1007/s11120-007-9213-x

Trebst, A., Wietoska, H., Draber, W., and Knops, H. (1978). The inhibition of photosynthetic electron flow in chloroplasts by the dinitrophenylether of bromo- or iodo-nitrothymol. *Z Naturforsch* 33c, 919–927. doi: 10.1515/znc-1978-11-1220

Tschörtner, J., Lai, B., and Krömer, J. O. (2019). Biophotovoltaics: green power generation from sunlight and water. *Front. Microbiol.* 10:866. doi: 10.3389/fmicb.2019.00866

Vetoshkina, D. V., Ivanov, B. N., Khorobrykh, S. A., Proskuryakov, I. I., and Borisova-Mubarakshina, M. M. (2017). Involvement of the chloroplast plastoquinone pool in the Mehler reaction. *Physiol. Plant.* 161, 45–55. doi: 10.1111/ppl.12560

Conflict of Interest: The authors declare that the research was conducted in the absence of any commercial or financial relationships that could be construed as a potential conflict of interest.

frontiers in Plant Science

ORIGINAL RESEARCH
published: 15 May 2020
doi: 10.3389/fpls.2020.00505

Identification of the Optimal Light Harvesting Antenna Size for High-Light Stress Mitigation in Plants

Guangxi Wu[1,2,3], Lin Ma[1,2,3], Richard T. Sayre[2,3] and Choon-Hwan Lee[1,2,3]**

[1] Department of Molecular Biology, Pusan National University, Busan, South Korea, [2] Pebble Labs, Los Alamos, NM, United States, [3] New Mexico Consortium, Los Alamos, NM, United States

One of the major constraints limiting biomass production in autotrophs is the low thermodynamic efficiency of photosynthesis, ranging from 1 to 4%. Given the absorption spectrum of photosynthetic pigments and the spectral distribution of sunlight, photosynthetic efficiencies as high as 11% are possible. It is well-recognized that the greatest thermodynamic inefficiencies in photosynthesis are associated with light absorption and conversion of excited states into chemical energy. This is due to the fact that photosynthesis light saturates at one quarter full sunlight intensity in plants resulting in the dissipation of excess energy as heat, fluorescence and through the production of damaging reactive oxygen species. Recently, it has been demonstrated that it is possible to adjust the size of the light harvesting antenna over a broad range of optical cross sections through targeted reductions in chlorophyll *b* content, selectively resulting in reductions of the peripheral light harvesting antenna size, especially in the content of Lhcb3 and Lhcb6. We have examined the impact of alterations in light harvesting antenna size on the amplitude of photoprotective activity and the evolutionary fitness or seed production in Camelina grown at super-saturating and sub-saturating light intensities to gain an understanding of the driving forces that lead to the selection for light harvesting antenna sizes best fit for a range of light intensities. We demonstrate that plants having light harvesting antenna sizes engineered for the greatest photosynthetic efficiency also have the greatest capacity to mitigate high light stress through non-photochemical quenching and reduction of reactive oxygen associated damage. Under sub-saturating growth light intensities, we demonstrate that the optimal light harvesting antenna size for photosynthesis and seed production is larger than that for plants grown at super-saturating light intensities and is more similar to the antenna size of wild-type plants. These results suggest that the light harvesting antenna size of plants is designed to maximize fitness under low light conditions such as occurs in shaded environments and in light competition with other plants.

Keywords: antenna size, biomass yield, chlorophyll *b*, photosynthesis, reactive oxygen species, stress

OPEN ACCESS

Edited by:
Mikko Tikkanen, University of Turku, Finland

Reviewed by:
Michael Hippler, University of Münster, Germany
Erica Belgio, Centrum Algatech, Czechia

****Correspondence:***
Richard T. Sayre
rsayre@newmexicoconsortium.org
Choon-Hwan Lee
chlee@pusan.ac.kr

Specialty section:
This article was submitted to Plant Physiology, a section of the journal Frontiers in Plant Science

Received: *20 September 2019*
Accepted: *03 April 2020*
Published: *15 May 2020*

Citation:
Wu G, Ma L, Sayre RT and Lee C-H (2020) Identification of the Optimal Light Harvesting Antenna Size for High-Light Stress Mitigation in Plants. Front. Plant Sci. 11:505. doi: 10.3389/fpls.2020.00505

INTRODUCTION

In nature, photosynthetic organisms grow under constantly varying light intensities ranging from full sunlight intensities to sub-saturating light intensities. In addition, leaves at the top of the canopy experience higher light intensities than those at the bottom of the canopy. This raises the question why do virtually all plants have light harvesting antenna sizes that capture photons at rates

nearly 10-fold greater than they can be converted into chemical energy at full sunlight conditions. Having large light harvesting antenna sizes incurs damage to the photosynthetic apparatus at light intensities greater than those that saturate electron transfer processes. Plants mitigate high light (HL) stress through non-productive energy dissipation pathways including heat and fluorescence and the production of damaging reactive oxygen species (Perrine et al., 2012; Friedland et al., 2019). This raises the question why have plants evolved large fixed size light harvesting antenna sizes that light saturate at one quarter full sunlight intensity.

In low light environments and in stratified plant canopies having a large wasteful light harvesting antenna may provide a selective advantage by excluding light from competing species. In monoculture or agricultural environments, however, having large wasteful light harvesting complexes (LHCs) may not be advantageous for biomass production (Ort et al., 2011). For example, it has been shown in green algal and plant monocultures that organisms which have slightly reduced light harvesting apparatus grow more efficiently than wild-type (WT) strains having larger, more wasteful light harvesting antenna (Perrine et al., 2012; Friedland et al., 2019). Chlamydomonas lines having smaller optimized light harvesting antenna sizes were shown to have growth rates 40% greater than WT algae when grown in simulated pond environments (Perrine et al., 2012). Similar effects of antenna size reduction on enhanced crop biomass production have been observed in Camelina engineered to have optimal light harvesting antenna sizes (Friedland et al., 2019).

Chlorophyll (Chl) *b* accounts for approximately half of the chlorophyll in the peripheral LHC and is not present in photosynthetic reaction centers. The LHC apoproteins which bind Chl *b* and other pigments are made in the cytoplasm, imported into chloroplasts, and folded in the presence of the photosynthetic pigments. As a result, a reduction or absence of Chl *b* can reduce the stability of the LHC proteins resulting in their degradation and graded reductions in the apparent optical cross section of the light harvesting antenna (Hoober et al., 2007; Friedland et al., 2019). As previously demonstrated, small reductions in Chl *b* synthesis (Chl *a/b* ratio = 5) leads to a reduction in the number of trimeric LHCII complexes. Reductions in Chl *b* levels leading to Chl *a/b* ratios > 6.5, however, result in additional losses in photochemical efficiency and the ability to dissipate excess excited states at saturating light intensities (Perrine et al., 2012; Friedland et al., 2019). Thus, there is an optimal light harvesting antenna size for plants corresponding to a Chl *a/b* ratio of 5.

The fact that smaller light harvesting antenna are more susceptible to photodamage than larger antenna is counter-intuitive since reductions in light harvesting antenna size would inherently be expected to reduce HL stress damage as a result of the decrease in light capture efficiency. Thus, it is hypothesized that there is likely a trade-off between reductions in photosynthetic efficiency and reductions in HL stress induced damage associated with alterations in light harvesting antenna size. To determine the optimal light harvesting antenna size for biomass production and fitness (seed production) under low and high light conditions, we characterized the photosynthetic performance and light stress responses of Camelina plants having altered levels of Chl *b* accumulation and associated light harvesting antenna sizes. These plants had Chl *a/b* ratios ranging from 3 to 14 and corresponding alterations in light harvesting antenna size (Friedland et al., 2019).

We demonstrate that for plants having an optimal antenna size for photosynthetic efficiency, the photo-protective mechanisms are fully operational resulting in the best overall photosynthetic performance. In contrast, plants having reduced light harvesting antenna sizes (Chl *a/b* ratios > 6.5) are more susceptible to HL damage. Thus, there is a tipping point in light harvesting antenna size at which reductions in light harvesting antenna size leads to both reductions in photosynthetic efficiency and reductions in photoprotective mechanisms against HL leading to reductions in both electron transport and high light stress protection efficiency (Friedland et al., 2019). In contrast, the optimal light harvesting antenna size for photosynthesis and seed production for plants grown at low light intensities is much larger and more similar in size to the light harvesting antenna of WT plants. These results suggest that for Camelina light harvesting antenna sizes in wild-type plants have been selected for best performance under low light intensities as occurs during competition for light.

MATERIALS AND METHODS

Plants and Growth Condition

Wild-type *Camelina sativa* plants and T4 generation back-crossed transgenic plants expressing RNAi molecules targeting the silencing of the chlorophyllide *a* oxygenase (CAO) gene previously described by Friedland et al. (2019) were grown in the greenhouse at 24°C/26°C with a 14 h/10 h day/night photoperiod. The average moderate light intensity (ML) at mid-morning in the green house was 850 μmol photons m^{-2} s^{-1} (400–700 nm, photosynthetic active radiation, PAR), while for shaded low light (LL) plants the growth light intensity was sub-saturating (200 μmol photons m^{-2} s^{-1}, PAR). Fully expanded leaves from the top of WT and CAO RNAi (CR) plants were assessed using 3- to 5-weeks old plants for all experiments. The Chl concentration was determined in aqueous 80% acetone as described by Porra et al. (1989). The transgenic plants were assigned to three different groups according to their Chl *a/b* ratios or apparent light harvesting antenna sizes at 3–5 weeks of age including: a low-intermediate Chl *a/b* ratio group (CR L-I) having Chl *a/b* ratios ranging from 4.5 to 6.5, a high-intermediate Chl *a/b* ratio group (CR H-I) group having Chl *a/b* ratios ranging from 6.5 to 8.5, and a very-high Chl *a/b* ratio group (CR V-H) having Chl *a/b* ratios greater than 8.5 having the smallest light harvesting antenna size. Significantly, the Chl *a/b* ratios of top fully expanded leaves from a given plant line did not significantly change during growth from 3 to 5 weeks, indicating antenna sizes were stable in a given transgenic line (**Supplementary Figure S1**).

Light Stress Treatment

Leaves were detached from dark-adapted (overnight) plants and floated on water to avoid water stress for all subsequent treatments. Leaves were then exposed to different light

intensities ranging from 200, 600, 1,000, 1,400 and 1,800 μmol photons m^{-2} s^{-1} PAR using a white light-emitting diode (LED) lamp for 3 h at 26°C. For HL treatments, plants were dark-adapted overnight and treated at 1,000 μmol photons m^{-2} s^{-1} PAR using the LED lamp for 24 h at 26°C.

Chlorophyll Fluorescence Measurements

In vivo chlorophyll fluorescence kinetics were measured using detached leaves using a Handy FluorCam FC 1000-H (Photon Systems Instruments, Drásov, Czechia) after dark-adaptation for 30 min at room temperature. The photosystem II (PSII) photochemical efficiency (Fv/Fm) was calculated according to the equation of Fv/Fm = (Fm – Fo)/Fm, where Fo is the minimum fluorescence determined using low-intensity measuring light pulses at 620 nm, and Fm is the maximum fluorescence determined after a 0.8 s saturating pulse of white light at 4,000 μmol photons m^{-2} s^{-1}. Non-photochemical quenching (NPQ) was calculated according to the equation of NPQ = (Fm – Fm′)/Fm′, where Fm' is the maximum fluorescence measured using a light-adapted leaf. For the measurement of NPQ development kinetics, leaves were exposed to actinic light (100 μmol photons m^{-2} s^{-1}) for 60 s and were then kept in darkness for 60 s before measurement of NPQ decay kinetics. To determine the impact of high light stress on NPQ kinetics and its long-term recovery, plants were exposed to high light (1,000 μmol photons m^{-2} s^{-1}) for 3, 6, 9 and 24 h. After dark-adaptation for 30 min NPQ kinetics were determined as described above.

Reactive Oxygen Species (ROS) Measurements

A qualitative or histochemical assay for superoxide oxygen detection was performed using detached leaf segments as previously described by Fryer et al. (2002) and Zulfugarov et al. (2011). Briefly, leaf samples from overnight dark-adapted plants were immersed in 6 mM nitroblue tetrazolium (NBT) solution containing 50 mM HEPES buffer (pH 7.5) for 2 h in the dark. After the treatment at the corresponding growth light conditions (ML and LL) for 4 h, pigments were extracted from leaf segments using absolute ethanol at 65°C by shaking in a water bath. Quantitative levels of NBT reactive superoxide radicals produced were then analyzed from the image in the gray scale value using Image J[1].

Measurement of Light Stress Induced Lipid Peroxidation

Malondialdehyde (MDA) is a product of lipid peroxidation and an indirect indicator of ROS-mediated membrane lipid damage. MDA production was determined using the thiobarbituric acid reaction according to Peever and Higgins (1989) with slight modifications. Leaves were detached from overnight dark-adapted plants, floated on water, and dark-adapted as controls or illuminated at the corresponding growth light intensity for 4 h. Leaf material (100 mg) was then homogenized in 1 mL 0.1% (w/v) trichloroacetic acid in a blender at 4°C. The homogenate was centrifuged at 10,000 *g* for 10 min. After adding 1 mL of 20% trichloroacetic acid containing 0.6% (w/v) thiobarbituric acid to the supernatant, the mixture was incubated at 95°C for 25 min and then centrifuged at 10,000 *g* for 10 min. The absorbance was measured from the supernatant at 440, 532, and 600 nm. MDA contents were calculated as described by Hodges et al. (1999).

Sodium Dodecyl Sulfate-Polyacrylamide Gel Electrophoreses and Immunoblotting

Sodium dodecyl sulfate (SDS)-polyacrylamide gel electrophoreses (PAGE) and immunoblotting were performed as described by Towbin et al. (1979). Thylakoid membrane containing 2 μg Chl was solubilized with SDS sample buffer containing 40 mM Tris-HCl (pH 6.8), 10% (v/v) glycerol, 0.1% (w/v) bromophenol blue, 0.1M dithiothreitol and 2% (w/v) SDS for 30 min at room temperature. Polypeptides were separated by SDS-PAGE using 12% (w/v) acrylamide gel with 3M urea and electro-transferred into polyvinylidene fluoride membrane (Immobilon-P, Merck, Darmstadt, Germany). Photosystem I (PSI), PSII and LHC proteins were detected using antibodies raised against the PsbA or D1 protein, PsbS, PsaA, Lhcb1-Lhcb6, and Lhca1-Lhca4 (Agrisera AB, Vännäs, Sweden). After incubating with anti-rabbit IgG HRP conjugated secondary antibody (Agrisera, Vännäs, Sweden) for 2 h at room temperature, antibody-specific signals were imaged using a Clarity Western ECL substrate (Bio-Rad Laboratories, Berkeley, CA, United States).

Pigments Analysis

Xanthophyll cycle pigment were determined according to Gilmore and Yamamoto (1991) with slight modifications. Pigments were extracted with 100% cold acetone from overnight dark-adapted leaves after treatment with HL (1,000 μmol photons m^{-2} s^{-1}) for 0, 1, and 2 h. The pigment extracts were filtered through a 0.2-μm membrane filter. Pigment separation was performed in a high performance liquid chromatography system (HP 1100 series, Hewlett-Packard, Waldbronn, Germany) on a Spherisorb ODS-1 column (Waters, Milford, MA, United States) using a solvent mixture of acetonitrile:methanol:0.1M Tris-HCl pH 8.0 (72:12:7, v/v/v) for 6 min followed by a 10 min linear gradient to methanol:hexane (4:1, v/v). The eluted pigments were monitored at 445 nm. Concentrations of the pigments were estimated by using the conversion factors for peak area normalized to 100% Chl *a* molecule (Chen et al., 2012).

Statistical Analysis

All experiments were repeated at least three times ($n \geq 3$). Values are expressed as mean ± SD. The significance of differences between experimental groups was analyzed using the unequal

[1] rsb.info.nih.gov/ij

variance two-tailed Student's *t*-tests. Statistically significant are considered as $^{*}P < 0.05$ or $^{**}P < 0.01$.

RESULTS

Sensitivity of NPQ and PSII to HL Stress Damage as a Function of Light Harvesting Antenna Size

To determine the sensitivity of plants having different light harvesting antenna sizes to HL stress, we analyzed the impact of HL stress (1,000 μmol photons m^{-2} s^{-1} for 24 h) on PSII photochemical efficiency as determined by the Chl fluorescence Fv/Fm ratio (**Figure 1A**). In contrast to plants with substantially reduced light harvesting antenna sizes (Chl *a/b* > 6.5), plants with optimal light harvesting antenna sizes (CR L-I) had lower reductions in photochemical efficiency following light stress treatment. In fact, the lowest reductions in photochemical efficiency following HL stress treatment were observed in CR L-1 plants and not in wild-type plants with larger light harvesting antenna complexes.

To gain greater insights into the biophysical basis for these differences in light stress sensitivity associated with different light harvesting antenna sizes, we compared the relative levels of dark-adapted non-photochemical quenching (NPQ) activity of plants having a range of light harvesting antenna sizes (**Figure 1B**). NPQ is one of the mechanisms by which excess Chl excited

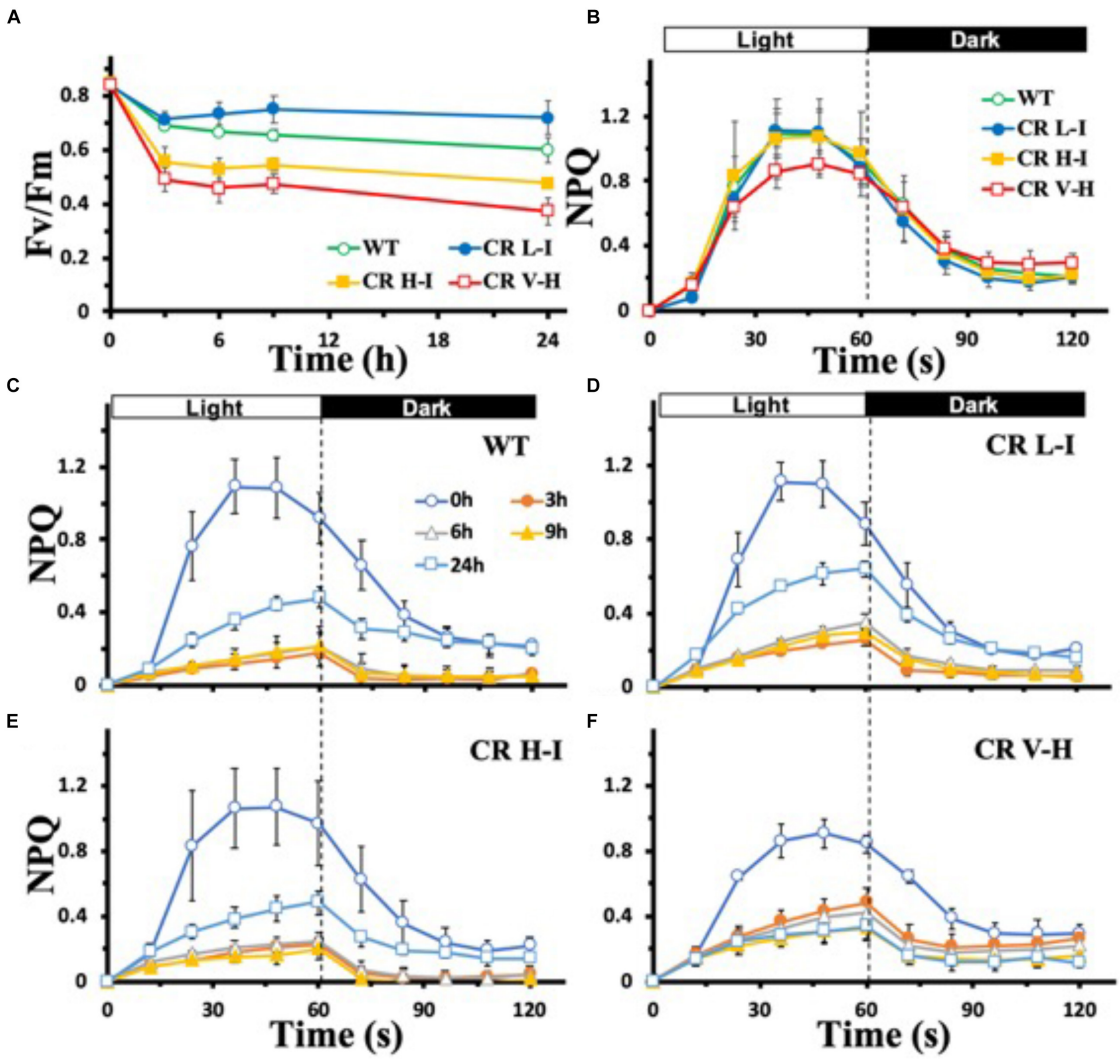

FIGURE 1 | Comparison of Fv/Fm and NPQ development and relaxation kinetics in wild-type and CAO RNAi transgenic lines under high light stress. Wild-type (WT), CR L-I (Chl *a/b* = 4.5–6.5), CR H-I (Chl *a/b* = 6.5–8.5), and CR V-H (Chl *a/b* 8.5 or above) plant leaves were dark-adapted for 30 min before the measurement of Fv/Fm **(A)** and NPQ **(B–F)**. Leaves were exposed to high light (HL) stress at 1,000 μmol photons m^{-2} s^{-1} for 24 h. For the measurement of NPQ development and relaxation kinetics, leaves were exposed to actinic light (100 mmol photons m^{-2} s^{-1}) for 60 s and were then kept in darkness for 60 s. The effects of HL stress on the NPQ development and relaxation kinetics were tested for 24 h in WT **(C)**, CR L-I **(D)**, CR H-I **(E)**, and CR V-H **(F)** lines. All experiments were done using fully expanded leaves from the top of 4–5 weeks old plants. Results represent the average and SD of three independent measurements.

states are dissipated non-destructively (Zulfugarov et al., 2014). In overnight dark-adapted leaves, NPQ rise kinetics in all of the CAO RNAi lines were similar to that of WT, except for the CR V-H lines having the smallest light harvesting antenna size (**Figure 1B**). In addition, the maximum level of NPQ was reduced by 20% in the CR V-H lines and NPQ decay kinetics were slower than WT, CR L-I and CR H-I lines. Following high light exposure ranging from 3 to 9 h, NPQ development was repressed in all plants (**Figures 1C–F**). Recovery of NPQ after high light stress for 24 h also varied as a function of antenna size. In WT plants, the NPQ level reached after actinic light exposure for 60 s was 44% of the control level (**Figure 1C**). In CR L-I lines the NPQ level reached was 58% of the control level (**Figure 1D**), whereas the maximum NPQ level reached in CR H-I lines was only 45% of the control level (**Figure 1E**). The NPQ level reached in CR L-I lines was significantly higher than the levels reached both in WT and in CR H-I lines at $P < 0.5$. We observed that plants having the smallest antenna sizes (CR V-H lines) had no NPQ recovery after HL treatment for 24 h (**Figure 1F**). Thus, there was a tipping point in antenna size relative to NPQ recovery after HL stress with maximum recovery occurring in plants with Chl *a/b* ratios near 5, the Chl *a/b* ratio that is also optimal for photosynthetic efficiency (Friedland et al., 2019).

Due to the light-induced production of a strong oxidant, $P680^+$, photosystem II is the most susceptible electron transport complex to damage under HL stress (Huang et al., 2018). To determine the impact of varying light intensities on PSII stability, we exposed plants to various light intensities for 3 h and then determined their PSII efficiency after a dark adaptation period. As shown in **Figure 2**, both ML and LL grown plants having Chl *a/b* ratios of approximately 5 (CR L-I) had statistically significantly lower losses in PSII efficiency than WT or transgenic plants having Chl *a/b* ratios > 6.5, when exposed to light intensities ≥ 1,000 μmol photons m^{-2} s^{-1}. Furthermore, plants having the smallest antenna size had the greatest PSII sensitivity to light stress.

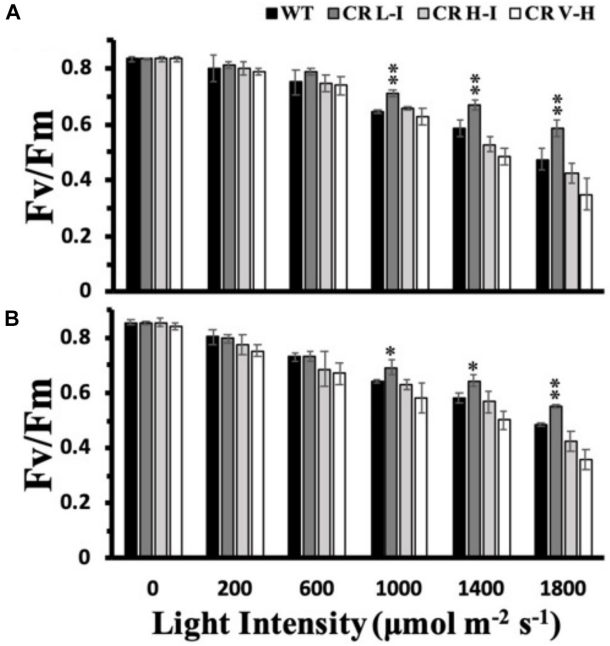

FIGURE 2 | Comparison of growth light intensity-dependent changes in Fv/Fm in wild-type and CAO RNAi transgenic lines. Wild-type (WT), CR L-I (Chl *a/b* = 4.5–6.5), CR H-I (Chl *a/b* = 6.5–8.5), and CR V-H (Chl *a/b* 8.5 or above) plants grown either in moderate light (ML) (850 μmol photons m^{-2} s^{-1}) **(A)** or in low light (LL) (200 μmol photons m^{-2} s^{-1}) **(B)** were exposed to light of various intensities for 3 h. All experiments were done using fully expanded leaves from the top of 4–5 weeks old plants. Before the measurement of Fv/Fm, leaves were dark-adapted for 30 min. Results represent the average and SD of three independent measurements. ∗, values are significantly different at $P < 0.05$ and ∗∗, values are significantly different at $P < 0.01$ between experimental groups.

Changes in Various Factors Affecting NPQ

The LHCII is expected to be one of the major quenching site for NPQ (Horton et al., 1991). In our previous paper (Friedland et al., 2019), we observed that the reduction of LHCII trimer abundance was directly associated with reduced Chl *b* contents in CAO RNAi lines. To determine the impact of Chl b reduction on the specific levels of other LHC protein subunits we assessed the relative abundance of individual LHC proteins by immunoblotting (**Figure 3**). We observed a gradual reduction in major LHCII polypeptides (Lhcb1, Lhcb2, and Lhcb3) and especially Lhcb3 with reductions in Chl *b* levels. In contrast there was little impact on Lhcb4 and Lhcb5 and LHCI polypeptide (Lhca1, Lhca2, Lhca3, and Lhca4) levels as Chl *b* levels were reduced. The content of Lhcb6, a minor LHCII was also reduced in CR H-I and CR V-H lines, with no noticeable changes in the PSII and PSI core polypeptides, D1 and PsaA, respectively. Overall, it is apparent that Lhcb3 is most sensitive to reductions in Chl *b*. This is not surprising since it is the least abundant subunit in the LHCII complex. Given that Lhcb3 apparently evolved as plants adapted to land environments and is not found in algae, a role for this protein in NPQ mechanisms has been implied (Alboresi et al., 2008). Furthermore, the Lhcb3 protein is part of the M-trimer of LHCII family members (Crepin and Caffarri, 2018). Reductions in Lhcb3 content have been shown to be correlated with the loss of moderately bound LHCII M-trimers and alterations in the orientation of the M-trimers. Thus, Lhcb3 plays a critical role in regulating energy transfer from the LHC to the reaction center core in higher plants. While the greatest losses in LHCII protein subunit family member abundance were observed for Lhcb3 in low Chl *b* CAO RNAi lines, we also observed reductions in the abundance of Lhcb1 associated with reductions in Chl *b* content. Lhcb1 is predominantly found in the loosely bound LHCII L-trimers as well as in LHCII M-trimers. The reduction in Lhcb1 levels are consistent with previous descriptions demonstrating the loss of loosely bound LHCII trimers associated with the loss of Chl *b* (Friedland et al., 2019) as well as losses in Lhcb6 content involved in binding the LHCII M-trimer with PCII core. Overall, these results indicate that loosely bound LHCII L-trimers are most impacted by reductions in Chl *b* content followed by the LHCII M-trimers.

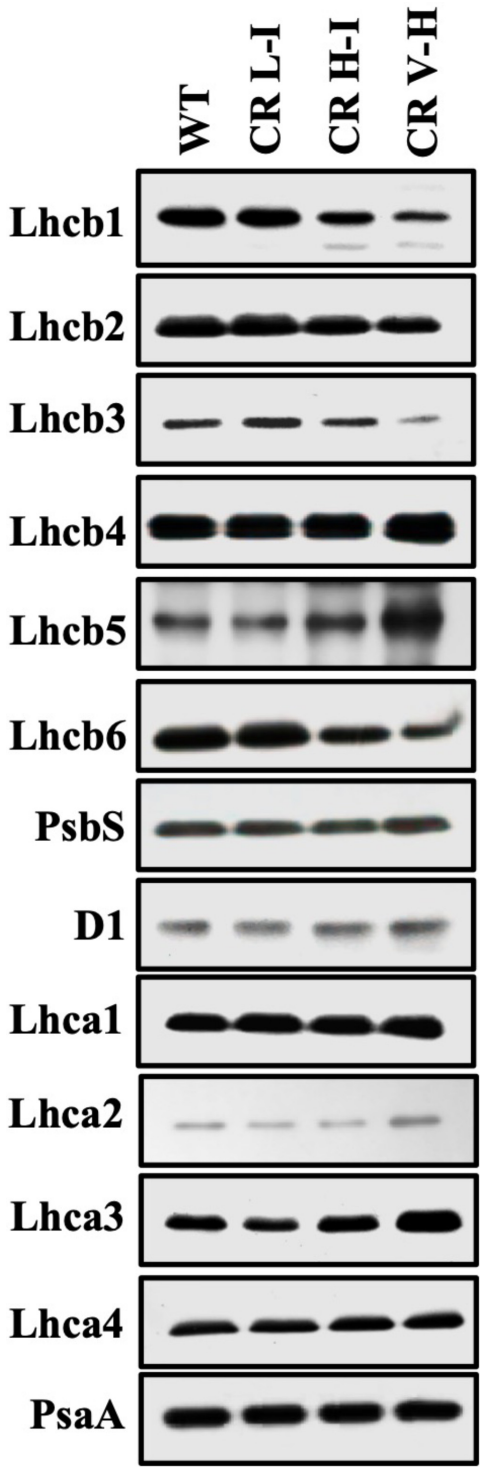

FIGURE 3 | Comparison of thylakoid protein contents in wild-type and CAO RNAi transgenic lines. Thylakoid membranes were isolated from overnight dark-adapted wild-type (WT), CR L-I (Chl *a/b* = 4.5–6.5), CR H-I (Chl *a/b* = 6.5–8.5), and CR V-H (Chl *a/b* 8.5 or above) transgenic plant leaves. Thylakoid membrane contents 2 μg Chl were separated by the sodium dodecyl sulfate-polyacrylamide gel electrophoresis (SDS-PAGE) and immunoblotted using specific antibodies raised against Lhcb1, Lhcb2, Lhcb3, Lhcb4, Lhcb5, Lhcb6, Lhca1, Lhca2, Lhca3, Lhca4, D1, PsbS, and PsaA.

To determine the impact of Chl *b* reduction on NPQ levels, we measured PsbS and xanthophyll cycle carotenoid levels in the various CAO RNAi lines. The PsbS protein has been implicated in the regulation of NPQ (Li et al., 2002) and the xanthophyll cycle carotenoids participate in energy quenching (Niyogi et al., 1998). Significantly, there were no noticeable differences in the level of PsbS protein among the different CAO RNAi lines (**Figure 3**). This is surprising given the differential responses in NPQ levels among the different CAO RNAi lines to reductions in Chl *b* levels, thus implying that the observed perturbations in NPQ responses are not associated with changes in PsbS levels. Just as surprising, we observed that both zeaxanthin content per Chl *a* and the carotenoid de-epoxidation state increased in CAO RNAi lines with lower Chl *b* content (**Table 1**), indicating that steady state levels of zeaxanthin and the de-epoxidation state were also not correlated with NPQ (**Figure 1**). Overall, we observed about a 10 to 20% drop in the total xanthophyll cycle pigment content (violaxanthin + antheraxanthin + zeaxanthin) in all the CAO RNAi lines compared to WT plants. As antenna size became smaller neoxanthin and lutein content per Chl *a* also decreased, while the relative content of β-carotene per Chl *a* increased.

Relative Accumulation of Reactive Oxygen Species During Growth at Low and High Light Intensities as a Function of Antenna Size

To assess the relative production of ROS during growth as a function of antenna size and light stress, we exposed plants grown at ML and LL to the corresponding light for 4 h followed by analysis of ROS accumulation (Asada, 1999; Bondarava et al., 2010; Zulfugarov et al., 2014). Fully expanded leaves were detached from overnight dark-adapted plants and chemical-infiltrated with ROS detection agents by floating on a 6 mM NBT solution in darkness for 2 h. We observed that NBT-detectable superoxide levels were lowest in the CR L-I line and greatest in WT and transgenic lines (CR H-I and CR V-H) having Chl *a/b* ratios > 6.5 following exposure of leaves from ML grown plants when to ML at 850 μmol photons m^{-2} s^{-1} for 4 h (**Figure 4**). In the rates of oxygen evolution with ferricyanide as a whole chain electron acceptor, we did not observe any significant differences among WT and all three transgenic lines (**Supplementary Figure S2**). In the case of the leaves from LL grown plants, exposed to LL at 200 μmol photons m^{-2} s^{-1}, superoxide production in CR L-I lines was similar to that of WT but increased in CR H-I and CR V-H lines. As expected, plants grown under LL conditions had lower levels of ROS production than those grown under ML conditions suggesting ML grown plants are more predisposed to ROS production than LL grown plants. Thus, CAO RNAi lines having smaller antenna sizes were more prone to photodamage by ROS at both low and high light intensities.

Lipid Peroxidation

One of the potential outcomes of high light stress induced ROS production is lipid peroxidation leading to the production of malondialdehyde (MDA) and damaged membranes. We measured lipid peroxidation levels in plants with different light

TABLE 1 | Comparison of pigment compositions in wild-type and CAO RNAi transgenic lines under darkness and high light stress.

	Neo	Vio	Ant	Lut	Zea	Chl *b*	β-Car	Vio + Ant + Zea	AZ/VAZ
WT dark	2.92 ± 0.78	10.95 ± 0.28	**ND**	20.12 ± 0.69	**ND**	27.67 ± 0.27	12.98 ± 0.30	10.95 ± 0.28	0
WT HL 1 h	2.79 ± 0.35	4.02 ± 0.01	2.19 ± 0.03	19.34 ± 0.33	4.07 ± 0.08	27.62 ± 0.16	12.43 ± 0.37	10.29 ± 0.05	0.50 ± 0.004
WT HL 2 h	3.34 ± 0.45	3.60 ± 0.01	2.43 ± 0.03	19.94 ± 0.56	5.40 ± 0.12	27.52 ± 0.36	13.06 ± 0.34	11.44 ± 0.10	0.58 ± 0.005
CR L-I dark	2.23 ± 0.25	9.32 ± 0.16	**ND**	18.04 ± 0.75	**ND**	16.83 ± 0.14	13.96 ± 0.22	9.32 ± 0.16	0
CR L-I HL 1 h	1.76 ± 0.23	2.62 ± 0.22	1.56 ± 0.07	17.23 ± 0.96	4.39 ± 0.27	16.45 ± 0.15	13.90 ± 0.33	8.57 ± 0.12	0.60 ± 0.028
CR L-I HL 2 h	2.00 ± 0.18	2.56 ± 0.30	1.45 ± 0.09	18.18 ± 0.71	5.15 ± 0.24	16.76 ± 0.31	14.55 ± 0.40	9.16 ± 0.17	0.64 ± 0.031
CR H-I dark	1.75 ± 0.09	8.57 ± 0.15	**ND**	16.69 ± 0.48	**ND**	13.34 ± 0.09	14.95 ± 0.25	8.57 ± 0.15	0
CR H-I HL 1 h	1.37 ± 0.26	2.23 ± 0.18	1.38 ± 0.07	15.90 ± 0.72	4.92 ± 0.18	13.29 ± 0.15	14.71 ± 0.41	8.53 ± 0.31	0.66 ± 0.010
CR H-I HL 2 h	1.35 ± 0.08	1.99 ± 0.10	1.35 ± 0.05	16.93 ± 0.67	5.98 ± 0.34	13.57 ± 0.19	15.33 ± 0.34	9.32 ± 0.25	0.71 ± 0.017
CR V-H dark	0.85 ± 0.11	9.91 ± 0.17	**ND**	14.07 ± 0.38	**ND**	6.91 ± 0.07	15.70 ± 0.68	9.91 ± 0.17	0
CR V-H HL 1 h	0.96 ± 0.12	2.08 ± 0.03	1.07 ± 0.17	15.82 ± 0.60	6.76 ± 0.35	7.29 ± 0.11	15.55 ± 0.87	9.91 ± 0.51	0.74 ± 0.007
CR V-H HL 2 h	0.94 ± 0.10	1.87 ± 0.14	0.72 ± 0.20	15.70 ± 0.35	7.12 ± 0.26	7.50 ± 0.09	15.82 ± 0.37	9.72 ± 0.19	0.77 ± 0.015

Wild-type (WT), CR L-I (Chl a/b = 4.5–6.5), CR H-I (Chl a/b = 6.5–8.5) and CR V-H (Chl a/b 8.5 or above) plants were used, and overnight dark-adapted (dark) leaves from 4-week old Camelina plants were treated with high light (HL 1,000 μmol photons m^{-2} s^{-1}) for 1 or 2 h. Pigments were subjected to high performance liquid chromatography analysis after extraction with 100% cooled acetone. Pigment content was normalized to 100 chlorophyll (Chl) a molecules. Ant, antheraxanthin; β-car, β-carotene; Lut, lutein; ND, not detectable; Neo, neoxanthin; Vio, violaxanthin; Zea, zeaxanthin. AZ/VAZ, de-epoxidation state was calculated from (0.5 Ant + Zea)/(Vio + Ant + Zea).

harvesting antenna sizes as a function of light treatment by quantifying MDA content (Masia, 2003). As show in **Figure 5**, MDA levels in LL grown plants did not vary between WT, CR L-I and CR H-I lines when they were either dark-adapted or exposed to low light intensities for 4 h. In contrast, plants grown in medium light intensities and then exposed to the dark had twofold greater MDA levels then LL grown plants, suggesting that growth at higher light predisposes the plants to increased sustained MDA production. When dark-adapted, medium light grown plants were subsequently exposed to medium growth light for 4 h, MDA levels increased most substantially in WT plants (>60%) but to a lesser extent in the CR L-I and CR H-I lines (>20%). Increased MDA production in CR H-I plants was consistent with the elevated ROS production relative to the CR L-I transgenics as observed in **Figure 4**. These results indicate that WT plants exposed to greater than light saturating growth conditions generated substantially more ROS and MDA than the CR transgenics with smaller light harvesting antenna sizes. As expected, CAO RNAi plants having a range of light harvesting antenna sizes had lower MDA and ROS production levels when grown under sub-saturating light conditions (LL).

Growth Light Intensity-Dependent Changes in the Seed Yield

Previously, we have demonstrated that Camelina plants having an upper canopy leaf Chl *a/b* ratio of 5 had the highest photosynthetic and biomass production yields (Friedland et al., 2019). To determine whether there was a relationship between light harvesting antenna size, growth light intensity and maximum seed yield, we compared the number of seed pods, total pod weight/plant and plant height between WT, CR L-I, CR H-I, and CR V-H plants grown either under ML or LL conditions (**Figure 6**). Previously, we had demonstrated that total harvestable seed yield in Camelina plants was largely determined by the number of seed pods and not seed mass or numbers of seeds per pod (Friedland et al., 2019). In the current study, the only observable statistically significant difference in yield was for number of pods and total pod yield/plant for the CR L-I plants versus WT when grown under ML growth conditions (**Figure 6**). Under ML conditions, both the number of seed pods and the total weight of pods were about 24% greater for the CR L-I line relative to WT. All plant lines grown at ML had greater pod numbers and yield than plants grown at LL but had identical plant height at both light intensities (**Figure 6**). Compared to WT, seed pod number, pod mass and plant height were all slightly reduced in CR H-I lines and further reduced in CR V-H lines when grown in LL conditions. These results demonstrate the impact of sink (pod) strength on determining the distribution of biomass allocation. Furthermore, it is apparent that WT light harvesting antenna sizes are most fit at low light intensities, and CAO RNAi plants having smaller light harvesting antenna sizes had reduced fitness compared to WT and the CR L-1 line.

Relationship Between Chl *a/b* Ratios and Seed Yield

To investigate the dependency of plant light harvesting antenna size on seed yield as a function of growth light intensities, we measured the number of seed pods/plant for WT and CAO RNAi plants across a range of Chl *a/b* ratios (measured at top fully expanded leaf) for ML and LL grown plants (**Figures 7A,B**). When the ML grown data were fit with a second order polynomial function, the peak seed pod yield was correlated with plants having a Chl *a/b* ratio of 5.0 (**Figure 7A**). However, when plants were grown under LL conditions, the peak seed pod yield was correlated with plants having a Chl *a/b* ratio of 4.3, more similar to WT plants (**Figure 7B**). In addition to the shift in optimal Chl *a/b* ratio or antenna size for plants grown under LL vs. ML conditions, there was a broadening in the distribution of seed yield vs. Chl *a/b* ratio for LL grown plants. Thus, more wild-type like Chl *a/b* ratios were associated with enhanced seed yield under low and medium light conditions while plants having Chl *a/b* ratios less than 5 had reduced seed yield or fitness.

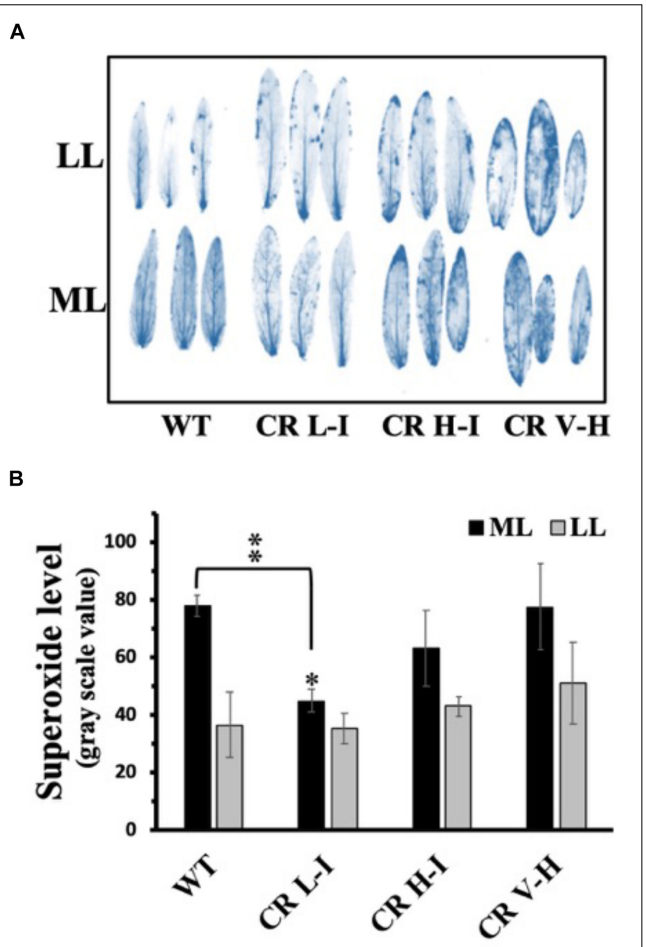

FIGURE 4 | Comparison of superoxide anion radical production in wild-type and CAO RNAi transgenic lines. Moderate light (ML) (850 μmol photons m^{-2} s^{-1}) and low light (LL) (200 μmol photons m^{-2} s^{-1}) grown wild-type (WT), CR L-I (Chl *a/b* = 4.5–6.5), CR H-I (Chl *a/b* = 6.5–8.5) and CR V-H (Chl *a/b* 8.5 or above) transgenic plant leaves were treated with nitroblue tetrazolium (NBT) for histochemical staining for superoxide production during illumination at ML or LL for 4 h **(A)**. Quantitative levels of the superoxide produced were analyzed from the image in grayscale value using Image J (rsb.info.nih.gov/ij) **(B)**. All experiments were done using fully expanded leaves from the top of 4–5 weeks old plants. Results represent the average and SD of three independent measurements. ∗, values are significantly different at $P < 0.05$ and ∗∗, values are significantly different at $P < 0.01$ between experimental groups.

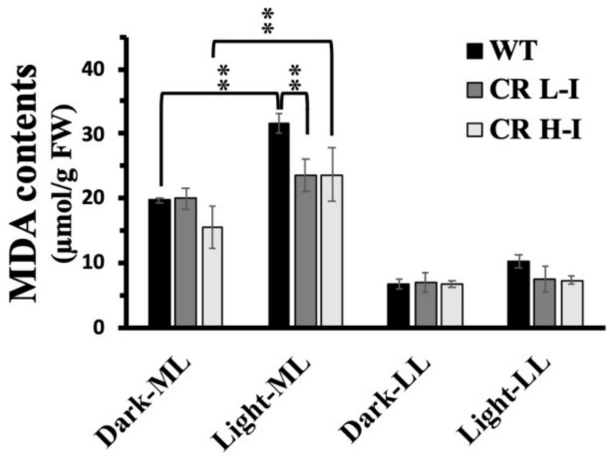

FIGURE 5 | Comparison of malondialdehyde (MDA) content in wild-type and CAO RNAi transgenic lines. Moderate light (ML) (850 μmol photons m^{-2} s^{-1}) and low light (LL) (200 μmol photons m^{-2} s^{-1}) grown wild-type (WT), CR L-I (Chl *a/b* = 4.5–6.5), CR H-I (Chl *a/b* = 6.5–8.5), and CR V-H (Chl *a/b* 8.5 or above) transgenic plant leaves were exposed to growth light for 4 h. The MDA content was measured before the light illumination (Dark-ML or Dark-LL) and after the light illumination (Light-ML or Light-LL). All experiments were done using fully expanded leaves from the top of 4–5 weeks old plants. Results represent the average and SD of three independent measurements.∗∗, values are significantly different at $P < 0.05$ between experimental groups.

DISCUSSION

Previously, it has been demonstrated that optimizing light harvesting antenna size enhances light utilization efficiency leading up to a 40% increase in algal biomass yield relative to WT green algae (Mussgnug et al., 2007; Perrine et al., 2012). Similar yield enhancement results were observed for transgenic Camelina having slightly reduced light harvesting antenna sizes (Friedland et al., 2019). It was observed both in green algae and plants that there is a tipping point in light harvesting antenna size (Chl *a/b* ratio = 5) where even a small change in Chl *a/b* values can result in significant differences in thylakoid membrane architecture, sensitivity to photoinhibition, and optimal biomass and seed yield (Perrine et al., 2012; Friedland et al., 2019). Interestingly, the transition point or the optimal Chl *a/b* ratio for photosynthetic performance for both green algae (Perrine et al., 2012) and Camelina (Friedland et al., 2019) is similar and more pronounced when grown under high light conditions.

In this study, we compared the light stress performance of Camelina CAO RNAi plants grown under ML and LL conditions to determine; (1) whether plants with different Chl *a/b* ratios and grown under different light intensities had altered sensitivity to photoinhibition associated with ROS production and lipid peroxidation; and (2) whether the optimal light harvesting antenna size for seed yield depends on the growth light intensities. Our results suggest that the optimal Chl *a/b* ratio for photosynthetic performance increases from that of wild-type plants as the growth light intensity increases. We observed that high-light induced photoinhibition, ROS and MDA production were lowest in ML grown plants having Chl *a/b* ratios (5) optimal for biomass production. In contrast, under low light growth conditions there were no significant differences in sensitivity to photoinhibition, ROS or MDA production between plants having Chl *a/b* ratios ranging from 3.2 (WT) to 10. As previously reported (Bruch and Thayer, 1983), high lipid peroxidation results in reduction in membrane fluidity by lipid peroxidation. Thus, plants with increased ROS production are likely to have more damaged membranes as observed in higher light grown plants (**Figure 5**).

The reason for the higher sensitivity to HL stress in plants having antenna sizes corresponding to Chl *a/b* ratios

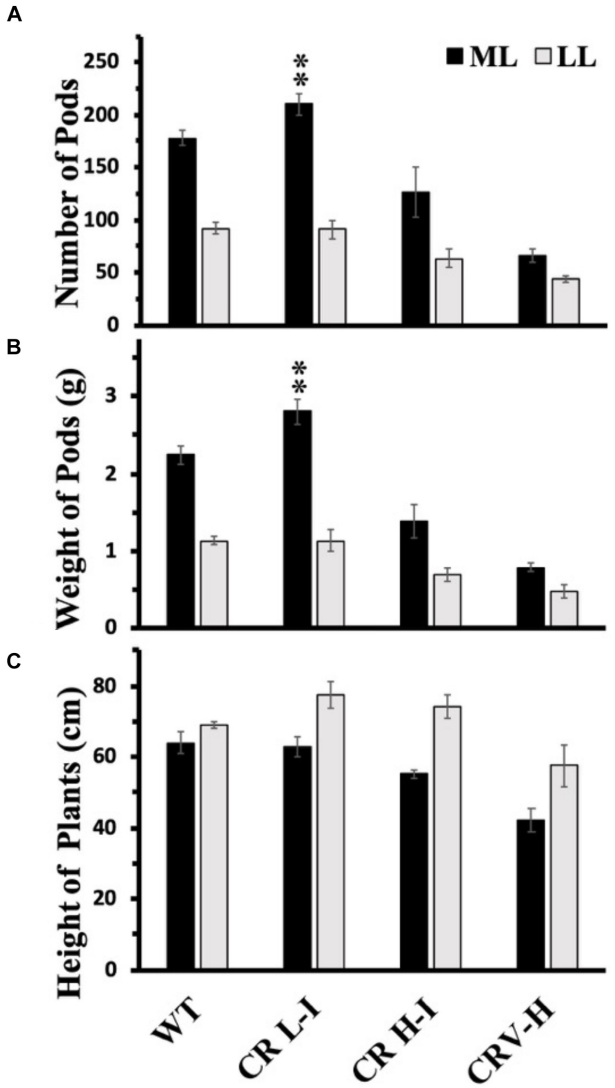

FIGURE 6 | Comparison of number of seed pods **(A)**, weight of seed pods **(B)** and height of plants **(C)** in wild-type and CAO RNAi transgenic lines. Wild-type (WT), CR L-I (Chl *a/b* = 4.5–6.5), CR H-I (Chl *a/b* = 6.5–8.5), and CR V-H (Chl *a/b* 8.5 or above) transgenic lines grown in moderate light (ML) (850 μmol photons m^{-2} s^{-1}) or in low light (LL) (200 μmol photons m^{-2} s^{-1}). Grouping of transgenic lines was made using fully expanded leaves from the top of 4–5 weeks old plants. Results represent the average and SD of three independent measurements. **, values are significantly different at $P < 0.05$ between experimental groups.

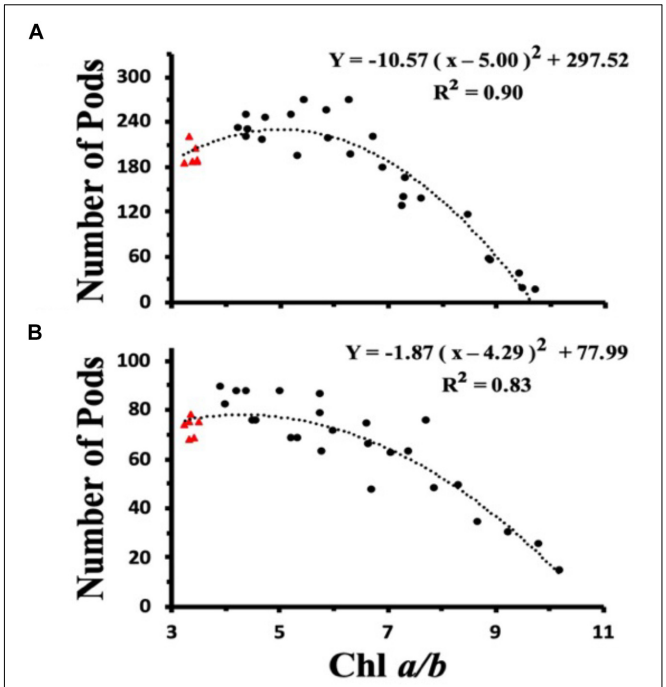

FIGURE 7 | Chl *a/b* ratio dependent changes in seed pod number in wild-type (triangles) and CAO RNAi transgenic lines (circles) grown in moderate light (ML) (850 μmol photons m^{-2} s^{-1}) **(A)** or in low light (LL) (200 μmol photons m^{-2} s^{-1}) **(B)**. The data were fit with a second order polynomial function. Chl content was determined according to Porra et al. (1989).

less than 5 may in part be due to the role of Chl *b* in stabilizing antennae pigment-protein complexes that mediate NPQ processes. The cbs3 *Chlamydomonas* lines lacking all Chl *b* showed impaired photo-autotropic growth and failed to carry out normal photoprotective processes including; state transitions and NPQ relative to WT plants (Perrine et al., 2012). Re-arrangement of PSII-LHCII supercomplexes is observed in HL-acclimated *Arabidopsis* plants, which is accompanied by reductions in Lhcb3 and Lhcb6 levels (Kouřil et al., 2013). In this study, we also report noticeable decreases in major LHCII polypeptides, especially Lhcb3 and Lhcb1 as well as a minor LHCII polypeptide, Lhcb6 (**Figure 3**). Lhcb3 is a major component of LHCII M-trimer, and Lhcb6 is involved in connecting the M-trimer to PSII core to form higher-order PSII-LHCII supercomplexes together with Lhcb4 (Kouřil et al., 2012). Lhcb1 levels were also reduced with increasing reductions in Chl *b*. Based on previous studies assessing the relative abundance of LHCII supercomplexes and LHCII loosely bound trimers (Friedland et al., 2019) we conclude that the LHCII L-trimers are most sensitive to reductions in Chl *b* followed by the LHCII M-trimers (Friedland et al., 2019). There is no direct evidence to prove whether missing Chl *b* was replaced by Chl *a,* however, during pigment assembly with LHC apoproteins, but we speculate that the pigment composition of LHCII is likely to have changed, because the ratio of Chl *a/b* in isolated LHCII-L trimer complexes was significantly increased [from 1.56 (WT) to 2.2 and 4.5] with decreased Chl levels (38 and 54%) in CR H-I and CR V-H lines (Friedland et al., 2019).

To determine the impact of Chl *b* and antenna size reduction on high-light induced photoprotective systems, we assessed the impact of varied Chl *b* reduction on NPQ associated factors. NPQ is enhanced by the presence of PsbS and zeaxanthin as well as by low pH (Li et al., 2002). Thus, we quantified the impact of Chl *b* reduction on PsbS and xanthophyll cycle carotenoid levels. The level of zeaxanthin per Chl *a* and the de-epoxidation state increased in the CR H-I and CR V-H lines (**Table 1**) inconsistent with the reduction in NPQ levels (**Figure 1**) and increased production of ROS in the low Chl *b* CAO RNAi lines

(**Figure 4**). However, total xanthophyll pigment contents were lower than WT in CAO RNAi lines (**Table 1**) consistent with reductions in NPQ and increased ROS production. In contrast, there was no apparent reduction in PsbS levels in Camelina plants having wild-type to very low levels of Chl *b* (**Figure 3**). These results are surprising given that adjustments in PsbS levels in response to light stress are correlated with NPQ levels (Ballottari et al., 2007; Albanese et al., 2016). However, in other studies altering antenna size in *Arabidopsis* Lhcb1 and Lhcb2 knock-down mutants, no reduction in PsbS levels were observed (Nicol et al., 2019). We also observed reductions in Lhcb1 levels in the low Chl *b* CAO RNAi lines. Thus, it can be inferred that alterations in the loosely bound LHCII complex levels have little or no impact on PsbS levels or NPQ. Regardless, ROS production increased with reductions in Chl *b* levels without changes in NPQ levels. Collectively, these results suggest that ROS production and NPQ are not directly correlated and that alternate de-excitation pathways for NPQ and ROS production exist in plants (Berman et al., 2015). Overall, the lowest levels of ROS production were observed in WT and the CR L-1 lines and increased in very low Chl *b* lines. Consistent with earlier observations these results indicate the optimal light harvesting antenna size is a Chl *a/b* ratio of 5 (Friedland et al., 2019).

An additional factor that may determine the optimal light harvesting antenna size is the ability to recover from photoinhibitory light treatment. Under prolonged HL stress (24 h) the CR V-H lines failed to show even partial restoration of HL-repressed NPQ compared with WT, CR L-I and CR H-I lines (**Figure 1**). In fact, the CR L-I lines exhibited the greatest ability to recover NPQ activity following high light stress followed by WT, CR H-I and CR V-H. For high light grown plants, plants having a Chl *a/b* ratio of 5 had the greatest ability to recover NPQ following light stress, and the lowest yields of ROS, MDA and photoinhibition. Earlier studies had also shown that algae and plants with self-adjusting antenna sizes or Chl *a/b* ratio of 5, had the highest biomass productivity and seed production, respectively (Friedland et al., 2019; Negi et al., 2020). In this study, we compared seed production (fitness) across a broad range of plants having altered Chl *a/b* ratios grown at low and high light intensities. The assessment of various photosynthetic performance characteristics indicates that plants with Chl *a/b* ratios > 5 have reductions in multiple photosynthetic parameters leading to reduced fitness (seed yield).

In summary, CAO RNAi lines with slightly reduced antenna (Chl *a/b* ratio = 5) compared to WT showed improved tolerance to HL stress and recovered well following HL stress when grown at greater than saturating light intensities. These more efficient plants also accumulated lower levels of damaging ROS and demonstrated less damage (reduced MDA, reduced photoinhibition and greater NPQ recovery) than WT plants or plants with smaller antenna. The effects of small reductions in antenna size on excess light mediated stress response were not as pronounced for plants grown under LL conditions. In addition, there was a more pronounced tipping point in seed production (fitness) associated with slight antenna size reduction under high light than low light growth conditions. The fact that wild-type plants and algae have less than optimal antenna sizes, suggests that the driver for antenna size was to perform well under low light conditions rather than high light conditions.

DATA AVAILABILITY STATEMENT

All datasets generated for this study are included in the article/**Supplementary Material**.

AUTHOR CONTRIBUTIONS

GW contributed to the design of light stress experiments, and measurements of leaf chlorophyll content, MDA, superoxide and biomass yield, and substantially to drafting the manuscript. LM carried out light stress and leaf chlorophyll fluorescence measurement. RS provided transgenic plant materials and contributed to the experimental design, financial support, writing and editing of the manuscript. C-HL contributed to the design of the experimental system, provided research oversight and financial support, and manuscript editing.

FUNDING

This research was also supported by Bayer Crop Sciences.

ACKNOWLEDGMENTS

C-HL acknowledges support from the Next-Generation Biogreen 21 Program (SSAC, Grant No. PJ013155012019), Rural Development Administration; the Basic Science Research Program of the National Foundation of Korea (NRF), by the Ministry of Science, ICT and Future Planning (Grant No. NRF-2017R1A2A2A05001287).

SUPPLEMENTARY MATERIAL

The Supplementary Material for this article can be found online at: https://www.frontiersin.org/articles/10.3389/fpls.2020.00505/full#supplementary-material

REFERENCES

Albanese, P., Manfredi, M., Meneghesso, A., Marengo, E., Saracco, G., Barber, J., et al. (2016). Dynamic reorganization of photosystem II supercomplexes in response to variations in light intensities. *Biochim. Biophys. Acta* 1857, 1651–1660. doi: 10.1016/j.bbabio.2016.06.011

Alboresi, A., Caffarri, S., Nogue, F., Bassi, R., and Morosinotto, T. (2008). In silico and biochemical analysis of Physcomitrella patens photosynthetic antenna: identification of subunits which evolved upon land adaptation. *PLoS One* 3:e0002033. doi: 10.1371/journal.pone.0002033

Asada, K. (1999). The water-water cycle in chloroplasts: scavenging of active oxygens and dissipation of excess photons. *Annu. Rev. Plant Biol.* 50, 601–639. doi: 10.1146/annurev.arplant.50.1.601

Ballottari, M., Dall'Osto, L., Morosinotto, T., and Bassi, R. (2007). Contrasting behavior of higher plant photosystem I and II antenna systems during acclimation. *J. Biol. Chem.* 282, 8947–8958. doi: 10.1074/jbc.M606417200

Berman, G. P., Nesterov, A. I., López, G. V., and Sayre, R. T. (2015). Superradiance transition and nonphotochemical quenching in photosynthetic complexes. *J. Phys. Chem. C* 119, 22289–22296. doi: 10.1021/acs.jpcc.5b04455

Bondarava, N., Gross, C. M., Mubarakshina, M., Golecki, J. R., Johnson, G. N., and Krieger-Liszkay, A. (2010). Putative function of cytochrome b559 as a plastoquinol oxidase. *Physiol. Plant.* 138, 463–473. doi: 10.1111/j.1399-3054.2009.01312.x

Bruch, R. C., and Thayer, W. S. (1983). Differential effect of lipid peroxidation on membrane fluidity as determined by electron spin resonance probes. *Biochim. Biophys. Acta* 733, 216–222. doi: 10.1016/0005-2736(83)90525-4

Chen, M., Li, Y., Birch, D., and Willows, R. D. (2012). A cyanobacterium that contains chlorophyll f–a red-absorbing photopigment. *FEBS Lett.* 586, 3249–3254. doi: 10.1016/j.febslet.2012.06.045

Crepin, A., and Caffarri, S. (2018). Functions and evolution of Lhcb isoforms composing LHCII, the major light harvesting complex of photosystem II of green eukaryotic organisms. *Curr. Protein Pept. Sci.* 19, 699–713. doi: 10.2174/1389203719666180222101534

Friedland, N., Negi, S., Wu, G., Ma, L., Flynn, S., Kummsa, T., et al. (2019). Fine-tuning the photosynthetic light harvesting apparatus for improved photosynthetic efficiency and biomass yield. *Sci. Rep.* 9, 1–12. doi: 10.1038/s41598-019-49545-8

Fryer, M. J., Oxborough, K., Mullineaux, P. M., and Baker, N. R. (2002). Imaging of photo-oxidative stress responses in leaves. *J. Exp. Bot.* 53, 1249–1254. doi: 10.1093/jexbot/53.372.1249

Gilmore, A. M., and Yamamoto, H. Y. (1991). Zeaxanthin formation and energy-dependent fluorescence quenching in pea chloroplasts under artificially mediated linear and cyclic electron transport. *Plant Physiol.* 96, 635–643. doi: 10.1104/pp.96.2.635

Hodges, D. M., Delong, J. M., Forney, C. F., and Prange, R. K. (1999). Improving the thiobarbituric acid-reactive-substances assay for estimating lipid peroxidation in plant tissues containing anthocyanin and other interfering compounds. *Planta* 207, 604–611. doi: 10.1007/s004250050524

Hoober, J. K., Eggink, L. L., and Chen, M. (2007). Chlorophylls, ligands and assembly of light-harvesting complexes in chloroplasts. *Photosynth. Res.* 94, 387–400. doi: 10.1007/s11120-007-9181-1

Horton, P., Ruban, A. V., Rees, D., Pascal, A. A., Noctor, G., and Young, A. J. (1991). Control of the light-harvesting function of chloroplast membranes by aggregation of the LHCII chlorophyll—protein complex. *FEBS Lett.* 292, 1–4. doi: 10.1016/0014-5793(91)80819-o

Huang, W., Zhang, S.-B., and Liu, T. (2018). Moderate photoinhibition of photosystem II significantly affects linear electron flow in the shade-demanding plant Panax notoginseng. *Front. Plant Sci.* 9:637. doi: 10.3389/fpls.2018.00637

Kouřil, R., Dekker, J. P., and Boekema, E. J. (2012). Supramolecular organization of photosystem II in green plants. *Biochim. Biophys. Acta* 1817, 2–12. doi: 10.1016/j.bbabio.2011.05.024

Kouřil, R., Wientjes, E., Bultema, J. B., Croce, R., and Boekema, E. J. (2013). High-light vs. low-light: effect of light acclimation on photosystem II composition and organization in *Arabidopsis thaliana*. *Biochim. Biophys. Acta* 1827, 411–419. doi: 10.1016/j.bbabio.2012.12.003

Li, X. P., Müller-Moulé, P., Gilmore, A. M., and Niyogi, K. K. (2002). PsbS-dependent enhancement of feedback de-excitation protects photosystem II from photoinhibition. *Proc. Natl. Acad. Sci. U.S.A.* 99, 15222–15227. doi: 10.1073/pnas.232447699

Masia, A. (2003). "Physiological effects of oxidative stress in relation to ethylene in postharvest produce," in *Postharvest Oxidative Stress in Horticultural Crops*, ed. D. M. Hodges, (New York, NY: Food Products Press), 165–197.

Mussgnug, J. H., Thomas-Hall, S., Rupprecht, J., Foo, A., Klassen, V., Mcdowall, A., et al. (2007). Engineering photosynthetic light capture: impacts on improved solar energy to biomass conversion. *Plant Biotechnol. J.* 5, 802–814. doi: 10.1111/j.1467-7652.2007.00285.x

Negi, S., Perrine, Z., Friedland, N., Kumar, A., Tokutsu, R., Minagawa, J., et al. (2020). Light-regulation of light harvesting antenna size substantially enhances photosynthetic efficiency and biomass yield in green algae. *Plant J.* doi: 10.1111/TPJ.14751

Nicol, L., Nawrocki, W. J., and Croce, R. (2019). Disentangling the sites of non-photochemical quenching in vascular plants. *Nat. Plants* 5, 1177–1183. doi: 10.1038/s41477-019-0526-5

Niyogi, K. K., Grossman, A. R., and Björkman, O. (1998). Arabidopsis mutants define a central role for the xanthophyll cycle in the regulation of photosynthetic energy conversion. *Plant Cell* 10, 1121–1134. doi: 10.1105/tpc.10.7.1121

Ort, D. R., Zhu, X., and Melis, A. (2011). Optimizing antenna size to maximize photosynthetic efficiency. *Plant Physiol.* 155, 79–85. doi: 10.1104/pp.110.165886

Peever, T. L., and Higgins, V. J. (1989). Electrolyte leakage, lipoxygenase, and lipid peroxidation induced in tomato leaf tissue by specific and nonspecific elicitors from Cladosporium fulvum. *Plant Physiol.* 90, 867–875. doi: 10.1104/pp.90.3.867

Perrine, Z., Negi, S., and Sayre, R. T. (2012). Optimization of photosynthetic light energy utilization by microalgae. *Algal Res.* 1, 134–142. doi: 10.1016/j.algal.2012.07.002

Porra, R., Thompson, W., and Kriedemann, P. (1989). Determination of accurate extinction coefficients and simultaneous equations for assaying chlorophylls a and b extracted with four different solvents: verification of the concentration of chlorophyll standards by atomic absorption spectroscopy. *Biochim. Biophys. Acta* 975, 384–394. doi: 10.1016/s0005-2728(89)80347-0

Towbin, H., Staehelin, T., and Gordon, J. (1979). Electrophoretic transfer of proteins from polyacrylamide gels to nitrocellulose sheets: procedure and some applications. *Proc. Natl. Acad. Sci. U.S.A.* 76, 4350–4354. doi: 10.1073/pnas.76.9.4350

Zulfugarov, I. S., Tovuu, A., Eu, Y.-J., Dogsom, B., Poudyal, R. S., Nath, K., et al. (2014). Production of superoxide from Photosystem II in a rice (*Oryza sativa* L.) mutant lacking PsbS. *BMC Plant Biol.* 14:242. doi: 10.1186/s12870-014-0242-2

Zulfugarov, I. S., Tovuu, A., Kim, J.-H., and Lee, C.-H. (2011). Detection of reactive oxygen species in higher plants. *J. Plant Biol.* 54, 351–357. doi: 10.1007/s12374-011-9177-4

Conflict of Interest: The authors declare that the research was conducted in the absence of any commercial or financial relationships that could be construed as a potential conflict of interest.

frontiers in Plant Science

ORIGINAL RESEARCH
published: 09 June 2020
doi: 10.3389/fpls.2020.00786

Atmospheric CO_2 Concentration and N Availability Affect the Balance of the Two Photosystems in Mature Leaves of Rice Plants Grown at a Free-Air CO_2 Enrichment Site

*Hiroshi Ozaki[1], Takeshi Tokida[2], Hirofumi Nakamura[3], Hidemitsu Sakai[4], Toshihiro Hasegawa[5] and Ko Noguchi[1]**

[1] School of Life Sciences, Tokyo University of Pharmacy and Life Sciences, Hachioji, Japan, [2] Division of Biogeochemical Cycles, Institute for Agro-Environmental Sciences, Tsukuba, Japan, [3] Taiyo Keiki Co., Ltd., Toda, Japan, [4] Division of Climate Change, Institute for Agro-Environmental Sciences, Tsukuba, Japan, [5] Division of Agro-Environmental Research, Tohoku Agricultural Research Center, Morioka, Japan

OPEN ACCESS

Edited by:
Stefano Santabarbara, National Research Council (CNR), Italy

Reviewed by:
Kintake Sonoike, Waseda University, Japan
Yuji Suzuki, Iwate University, Japan

***Correspondence:**
Ko Noguchi
knoguchi@toyaku.ac.jp

Specialty section:
This article was submitted to Plant Physiology, a section of the journal Frontiers in Plant Science

Received: *13 January 2020*
Accepted: *18 May 2020*
Published: *09 June 2020*

Citation:
Ozaki H, Tokida T, Nakamura H, Sakai H, Hasegawa T and Noguchi K (2020) Atmospheric CO_2 Concentration and N Availability Affect the Balance of the Two Photosystems in Mature Leaves of Rice Plants Grown at a Free-Air CO_2 Enrichment Site. Front. Plant Sci. 11:786. doi: 10.3389/fpls.2020.00786

Atmospheric CO_2 concentration ($[CO_2]$) has been substantially increasing. Responses of leaf photosynthesis to elevated $[CO_2]$ have been intensively investigated because leaf photosynthesis is one of the most important determinants of crop yield. The responses of photosynthesis to elevated $[CO_2]$ can depend on nitrogen (N) availability. Here, we aimed to investigate the significance of the appropriate balance between two photosystems [photosystem I (PSI) and photosystem II (PSII)] under various $[CO_2]$ and N levels, and thus to clarify if responses of photosynthetic electron transport rates (ETRs) of the two photosystems to elevated $[CO_2]$ are altered by N availability. Thus, we examined parameters of the two photosystems in mature leaves of rice plants grown under two $[CO_2]$ levels (ambient and 200 μmol mol^{-1} above ambient) and three N fertilization levels at the Tsukuba free-air CO_2 enrichment experimental facility in Japan. Responses of ETR of PSII (ETRII) and ETR of PSI (ETRI) to $[CO_2]$ levels differed among N levels. When moderate levels of N were applied (MN), ETRI was higher under elevated $[CO_2]$, whereas at high levels of N were applied (HN), both ETRII and ETRI were lower under elevated $[CO_2]$ compared with ambient $[CO_2]$. Under HN, the decreases in ETRII and ETRI under elevated $[CO_2]$ were due to increases in the non-photochemical quenching of PSII [Y(NPQ)] and the donor side limitation of PSI [Y(ND)], respectively. The relationship between the effective quantum yields of PSI [Y(I)] and PSII [Y(II)] changed under elevated $[CO_2]$ and low levels of N (LN). Under both conditions, the ratio of Y(I) to Y(II) was higher than under other conditions. The elevated $[CO_2]$ and low N changed the balance of the two photosystems. This change may be important because it can induce the cyclic electron flow around PSI, leading to induction of non-photochemical quenching to avoid photoinhibition.

Keywords: CO_2 enrichment, FACE, nitrogen, photosystem I, photosystem II, rice (*Oryza sativa*)

INTRODUCTION

Atmospheric CO_2 concentration ($[CO_2]$) has increased substantially since the Industrial Revolution. Since leaf photosynthesis is one of the most important determinants of crop yield, responses of photosynthesis to elevated $[CO_2]$ have been intensively examined (Long et al., 2004; Ainsworth and Long, 2005; Ainsworth and Rogers, 2007; Leakey et al., 2009a; Xu et al., 2015). For example, long-term elevated $[CO_2]$ by free-air CO_2 enrichment (FACE) experiments have been used to stimulate leaf photosynthesis in C_3 plants (Long et al., 2004; Leakey et al., 2009a). In the case of rice, a meta-analysis revealed that biomass and yield increase by approximately 20% under long-term elevated $[CO_2]$ (Ainsworth, 2008). However, plants that acclimate to long-term elevated $[CO_2]$ conditions show lower increases in photosynthesis and yield than expected (Long et al., 2004). In C_3 species, photosynthesis is usually considered to be limited by the carboxylation capacity of Rubisco (V_{cmax}), and/or ribulose-1,5-bisphosphate (RuBP) regeneration rate (J_{max}) (Farquhar et al., 1980). In many plant species, including rice, V_{cmax} and J_{max} are decreased by elevated $[CO_2]$ (Bernacchi et al., 2005; Chen et al., 2005, 2014; Zhang et al., 2008; Hasegawa et al., 2016). Although plants grown under elevated $[CO_2]$ often show a larger decrease in V_{cmax} compared with J_{max}, the limitation of photosynthetic rates under elevated $[CO_2]$ will shift from V_{cmax} to J_{max}. The long-term responses of V_{cmax} and J_{max} to elevated $[CO_2]$, analyzed in soybean plants at FACE site, showed a shift of the limitation from V_{cmax} to J_{max} (Bernacchi et al., 2005). In a durum wheat cultivar that has a low harvest index, both V_{cmax} and J_{max} decreased, but the degree of decreases in V_{cmax} was larger than that in J_{max}, leading to an increase in the ratio of J_{max} to V_{cmax} under elevated $[CO_2]$ (Aranjuelo et al., 2013). The decreases in V_{cmax} and J_{max} occurred not only at FACE sites but also at a natural CO_2 spring where $[CO_2]$ is consistently high (Saban et al., 2019). Plants grown at the CO_2 spring exhibited a larger decrease in V_{cmax} compared to J_{max} (Saban et al., 2019).

J_{max} is related to the whole photosynthetic electron transport system. Several studies examined the effective quantum yield of photosystem II (PSII) [Y(II)] and/or electron transport rate of PSII (ETRII) in leaves grown under long-term elevated $[CO_2]$ using chlorophyll (Chl) fluorescence measurements. Habash et al. (1995) reported that wheat plants grown under elevated $[CO_2]$ showed higher Y(II) than those grown under ambient $[CO_2]$. Cousins et al. (2001) examined responses of Y(II) to long-term $[CO_2]$ in *Sorghum bicolor* grown at FACE sites. A small decrease in Y(II) was observed under low measurement CO_2 condition in *Sorghum* plants grown at FACE sites. In contrasts, responses of photosystem I (PSI) to long-term elevated $[CO_2]$ have rarely been examined. Pan et al. (2018) examined effects of elevated $[CO_2]$ and heat stress to Y(II) and the effective quantum yields of PSI [Y(I)] in tomato plants. They showed that long-term elevated $[CO_2]$ ameliorated the decrease in both Y(II) and Y(I) by heat stress.

The photosynthetic electron transport through both PSII and PSI supplies ATP and NADPH. This supply should be matched to their demands in downstream metabolism such as the Calvin cycle and the photorespiratory pathway (Noctor and Foyer, 2000). The cyclic electron transport around PSI (CEF-PSI) in terrestrial plants consists of two partially redundant pathways, the ferredoxin (Fd)-dependent CEF-PSI and the NAD(P)H dehydrogenase (NDH)-dependent pathways, and can balance the ratio of ATP to NADPH production (Shikanai, 2014). Therefore, the response of CEF-PSI to elevated $[CO_2]$ is important for balancing supply and demand. Also, the balance between two photosystems, PSII and PSI, is important to suppress the generation of reactive oxygen species (ROS) in the photosynthetic electron transport. However, few studies have examined the balance between the two photosystems in leaves grown under elevated $[CO_2]$.

Nitrogen (N) availability intensely affects responses of leaf photosynthesis to elevated $[CO_2]$ (Xu et al., 2015). Significant decreases in V_{cmax} and J_{max} under elevated $[CO_2]$ were observed in wheat leaves under low N fertilization (Miglietta et al., 1996). In leaves of *Arabidopsis thaliana* under elevated $[CO_2]$, the carbohydrate accumulation and down regulation of photosynthetic genes were observed (Cheng et al., 1998). When plants with low sink capacity are grown under low N and elevated $[CO_2]$, carbohydrates accumulate in leaves, and the sugar repression leads to the down regulation of photosynthetic gene expression (Drake et al., 1997; Rogers et al., 1998; Long et al., 2004). The decrease in photosynthesis under low N and elevated $[CO_2]$ is also attributed to decreased concentrations of leaf N (Nakano et al., 1997; Seneweera et al., 2011). Since plants invest a large quantity of N into photosynthetic enzymes, the decrease in leaf N under elevated $[CO_2]$ can directly lead to decreased photosynthetic rates. However, while many studies have examined the responses of ribulose 1,5-bisphosphatecarboxylase/oxygenase (Rubisco) and V_{cmax} to low N and elevated $[CO_2]$, few studies have examined the response of photosynthetic electron transport to low N and elevated $[CO_2]$. Therefore, it is important to clarify the responses of photosynthetic electron flow through the two photosystems to elevated $[CO_2]$, and how these responses differ depending on N availability. This is because the appropriate balance between the two photosystems and the response of CEF-PSI are important not only for relevant supply of NADPH and ATP but also for suppression of ROS production under various environmental conditions.

In this study, we aimed to investigate the significance of the appropriate balance between two photosystems under various $[CO_2]$ and N levels, and thus addressed two following hypotheses. (i) The linear electron transport rate (ETR) responds to elevated $[CO_2]$, and its response depends on N availability. (ii) The response of PSI to elevated $[CO_2]$ and N availability is different from the response of PSII, and the balance between the two photosystems differs depending on $[CO_2]$ or N availability. To address the above hypotheses, we examined the two photosystems in mature leaves of a *japonica* rice variety (Koshihikari) grown under two $[CO_2]$ levels (ambient and 200 μmol mol^{-1} above ambient) and three N fertilization levels at the Tsukuba FACE experimental site in central Japan. At this FACE site, growth, photosynthesis and yield have been examined for many rice varieties including Koshihikari (Hasegawa et al.,

2013; Chen et al., 2014; Usui et al., 2014; Ikawa et al., 2018; Sakai et al., 2019). Koshihikari is one of the standard *japonica* varieties and the most widely planted variety in Japan. We measured the photochemical parameters of the two photosystems in Koshihikari leaves at a vegetative growth stage, and determined the N and carbon (C) contents of the leaves. The results indicated that the balance between the two photosystems changed under elevated [CO_2] and low levels of N (LN). Under both conditions, the ratio of Y(I) to Y(II) was higher than under other conditions.

MATERIALS AND METHODS

Site Description

The study was conducted at the Tsukuba FACE experimental facility in Tsukubamirai, Ibaraki, Japan (35°58′ N, 139°60′ E) in 2017. There were four pairs of ambient and elevated [CO_2] plots at the site. We used two of the four pairs of plots. The average ambient [CO_2] at the site across the entire growing season (June–September) and day-to-day SD was 391 ± 12.8 μmol mol^{-1}. The CO_2 enrichment was performed only in the daytime. The target concentration of the elevated [CO_2] treatment was 200 μmol mol^{-1} above ambient [CO_2], and the actual season-long mean [CO_2] and day-to-day SD in the FACE plots was 585 ± 16.3 μmol mol^{-1}. Previously published articles have provided further details of the experimental site set-up and CO_2 control performance (Nakamura et al., 2012) and soil chemical properties (Hasegawa et al., 2013).

Plant Materials

We used a *japonica* rice (*Oryza sativa* L.; variety, Koshihikari). Three-week-old seedlings were transplanted into the experimental plots on May 24 and 25 in 2017. Plants received fertilizers prior to planting at a rate of 4.36 g m^{-2} of P and 8.3 g m^{-2} of K, as described in Hasegawa et al. (2013). Under the moderate (standard) N treatment (MN), 8 g m^{-2} of N was applied. For the low and high N treatments (LN and HN), 0 and 12 g m^{-2} were applied, respectively. Further details of N fertilization can be found in Hasegawa et al. (2019). We sampled the uppermost fully expanded leaves at the vegetative stage (from June 19 to July 6). Four biological replications were used for each experiment.

Measurement of Chlorophyll Fluorescence and P700 Absorption Using a Dual-PAM-100 Measuring System

Leaves were sampled in each plot, and measured in the cabin at the site. Measurements were taken on detached leaves at a room temperature and ambient CO_2 concentration. Chl fluorescence and absorption changes at 830 nm were simultaneously measured using a Dual-PAM-100 (Walz, Effeltrich, Germany). The Chl fluorescence parameters were calculated according to the methods developed by Genty et al. (1989); Baker et al. (2007), and Kono et al. (2014). The Y(II) was calculated as $(F_m' - F_s)/F_m'$, where F_m' and F_s are the maximum fluorescence level and the steady-state fluorescence level under actinic light (AL), respectively. Two other PSII quantum yields, Y(NPQ) and Y(NO), which represent the regulated and non-regulated energy dissipation at PSII centers, were calculated as $F_s/F_m' - F_s/F_m$ and F_s/F_m, respectively. F_m is the maximum fluorescence level in the dark-adapted state. The fraction of PSII centers that are in the open state, qL, was calculated as $(F_m' - F_s)(F_o'/F_s)/(F_m' - F_o')$. Additionally, F_o', the minimal fluorescence yield under AL, was estimated as described by Oxborough and Baker (1997) [i.e., $F_o/(F_v/F_m + F_o/F_m')$]. The ETR through PSII was calculated as ETRII = Y(II) × PPFD × 0.84 × 0.5, where 0.84 and 0.5 were based on the assumption that leaves absorb 84% of incident photons and that 50% of these photons are absorbed by PSII.

In the Dual-PAM-100, $P700^+$ was monitored as the difference between the absorptions at 830 and 875 nm in the transmission mode. We estimated PSI parameters, including photochemical quantum yield [Y(I)], non-photochemical quantum yield due to donor side limitations [Y(ND)], non-photochemical quantum yield due to acceptor side limitations [Y(NA)], and the PSI electron transport rate (ETRI), as described by Baker et al. (2007) and Kono et al. (2014). We estimated ETRI based on the assumption that leaves absorb 84% of incident photons and that 50% of these photons are absorbed by PSI. The steady-state rate of CEF-PSI was estimated by subtracting ETRII from ETRI, when each rate was simultaneously estimated (Dahal et al., 2014; Yamada et al., 2020).

The minimum fluorescence level in the dark-adapted state (F_o), F_m, and the maximum P700 signal (fully oxidized P700) in darkness (P_m) were measured after a 30-min incubation in darkness. Subsequently, we illuminated leaves at the strong AL (1599 μmol photons m^{-2} s^{-1}) to activate the photosynthesis for 28 min, and then measured Chl fluorescence and P700 absorption at 978, 602, 356, and 131 μmol photons m^{-2} s^{-1} of AL to generate photosynthetic light-response curves.

Determinations of Leaf Dry Weight, and Contents of Carbon and Nitrogen

After the Chl fluorescence and P700 absorption change were measured, leaf segments were dried at 80°C for more than 48 h and then weighed to measure leaf mass per area (LMA). After the LMA was determined, C and N contents of the samples were measured with an MT-700 Mark 2 CN analyzer (Yanaco, Kyoto, Japan).

Statistical Analyses

An analysis of variance, Tukey–Kramer multiple comparison test, analysis of covariance (ANCOVA) and correlation analysis were conducted using the statistical software R (R Core Team, 2016). The analyzed data in **Figures 1–5** and **Supplementary Figures S1–S6** are summarized in **Supplementary Table S1**. Statistical significance was noted if $p < 0.1$.

RESULTS

Leaf Characteristics

There were no significant differences in LMA and leaf C content between the two [CO_2] levels and among the three N levels,

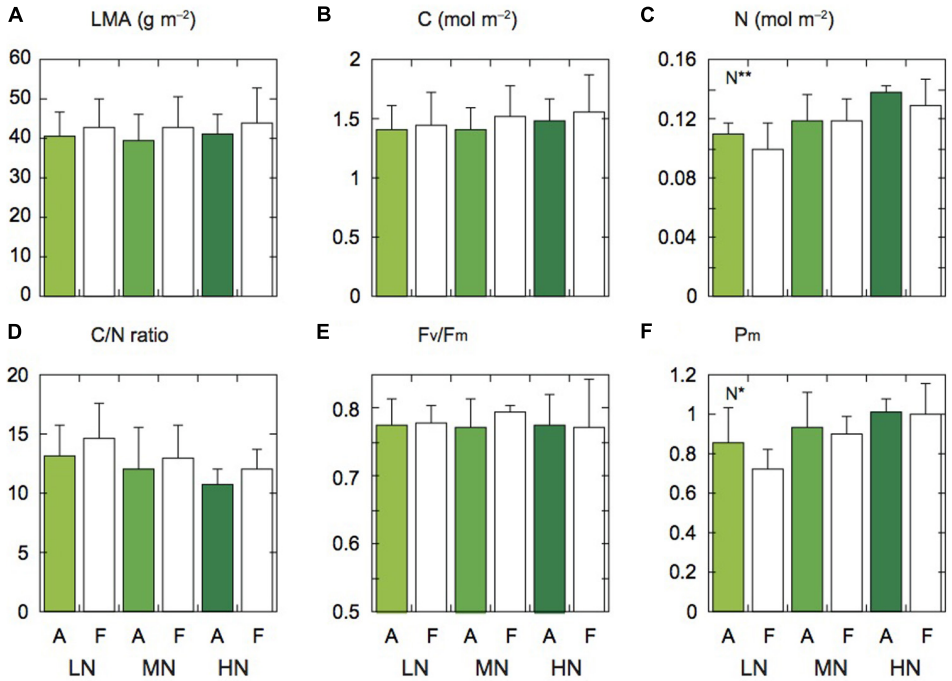

FIGURE 1 | Leaf characteristics of rice plants. Leaf mass per area (LMA; **A**), carbon content (C; **B**), nitrogen content (N; **C**), ratio of carbon to nitrogen contents (C/N; **D**), F_v/F_m **(E)**, and P_m **(F)** under low (LN), moderate (MN) and high nitrogen levels (HN). Panels **(A,F)** denote the data of leaves under ambient and elevated [CO_2] levels. Data are presented as the mean ± standard deviation ($n = 4$). Statistical results are also shown (*$p < 0.05$, **$p < 0.01$).

but these parameters under elevated [CO_2] tended to be lower compared with those under ambient [CO_2] (**Figures 1A,B**). Leaf N content significantly differed among the three N levels (**Figure 1C**). The N content under elevated [CO_2] was lower than under ambient [CO_2], but the difference was insignificant. In our previous study at the same FACE site, the ratio of C to N (C/N ratio) of Koshihikari leaves was higher under elevated [CO_2] compared with under ambient [CO_2] (Noguchi et al., 2018). In this study, this ratio tended to be high under elevated [CO_2] (**Figure 1D**). This ratio was also different among the N levels, but the difference was insignificant.

Since low N often induces PSII photoinhibition in leaves (Noguchi and Terashima, 2006; Kumagai et al., 2009), we measured the maximum photochemical quantum yield of PSII (F_v/F_m). The F_v/F_m values were not different between the two [CO_2] levels and among the three N levels (**Figure 1E**). In Koshihikari leaves, PSII photoinhibition was not observed under low N (LN). We also measured the maximum fully oxidized P700 in darkness (P_m). The P_m value of LN leaves was significantly lower than that of the other N levels (**Figure 1F**). The PSI contents may be lower in LN leaves. The P_m values were not different between the two [CO_2] levels.

Photosynthetic Electron Transport Rates Through PSII and PSI Were Decreased by Elevated [CO_2] Under the HN Condition

Since the N contents and P_m values were different among the N levels, we compared the light response curves of ETRII and ETRI between the two [CO_2] levels within each N level (**Figure 2**). Under MN, ETRII were not different between the two [CO_2] levels, but ETRI of leaves under elevated [CO_2] was significantly higher than that under ambient [CO_2]. Under LN, ETRII of leaves under elevated [CO_2] tended to be lower than that under ambient [CO_2], but the difference was insignificant. ETRI of leaves under LN were similar between the two [CO_2] levels. In contrast, under HN, both ETRII and ETRI were significantly lower in leaves under elevated [CO_2] compared with those under ambient [CO_2]. Previous studies reported that photosynthetic rates were decreased by elevated [CO_2] in leaves under low N fertilization (e.g., Miglietta et al., 1996). However, in this study, both ETRs were decreased by elevated [CO_2] only under HN.

We also compared ETRs at the highest AL intensity among the N levels (**Supplementary Figures S1A,B**). ETRI was different among the N levels ($p < 0.1$), and the interaction between N and [CO_2] levels was significant.

Under the High N Condition, the Decrease in Y(II) Is Related to the Increase in Y(NPQ) Under Elevated [CO_2]

Since the responses of ETRII to elevated [CO_2] were different among the N levels, we examined the light-dependence of the PSII parameters, Y(II), Y(NPQ), and Y(NO), based on the Chl fluorescence data. The decrease in Y(II) is due to increases in Y(NPQ) and/or Y(NO) (Baker et al., 2007). Under LN and MN, Y(II) did not differ between the [CO_2] levels, but under HN, Y(II) was lower under elevated [CO_2] (**Figure 3A**

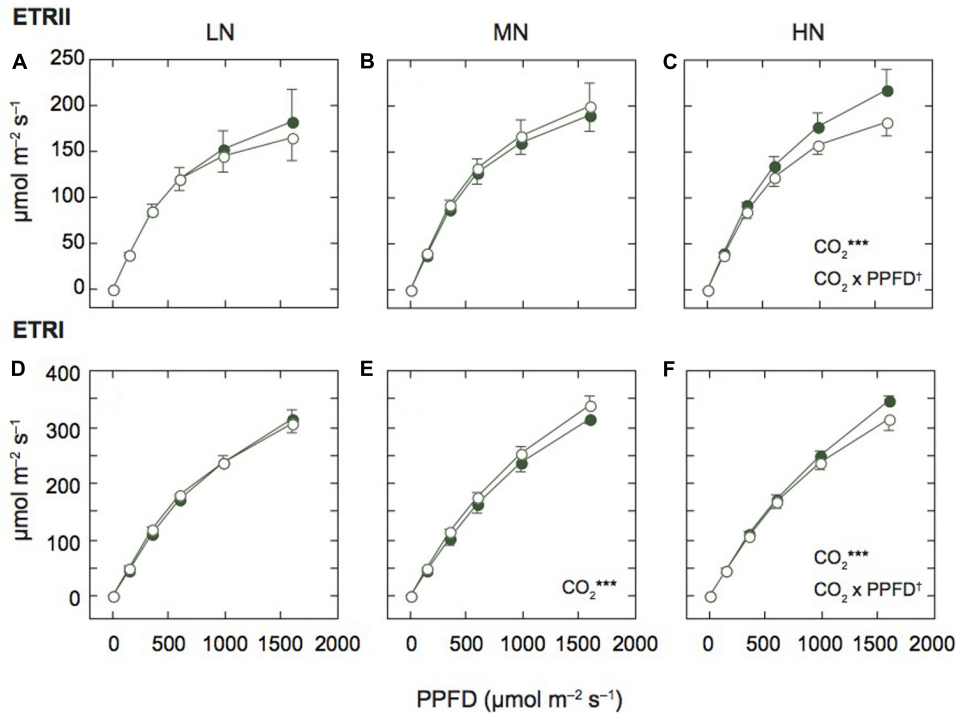

FIGURE 2 | Light-response curves of photosynthetic electron transport in mature leaves of rice plants. The electron transport rate in PSII (ETRII; **A–C**) and PSI (ETRI; **D–F**) under low (LN; **A,D**), moderate (MN; **B,E**) and high nitrogen levels (HN; **C,F**). Closed and open symbols denote the data of leaves under ambient and elevated [CO_2] levels. Data are presented as the mean ± standard deviation ($n = 4$). Statistical results are also shown ($^{\dagger}p < 0.1$, $^{*}p < 0.05$, $^{**}p < 0.01$, $^{***}p < 0.001$). CO_2 and CO_2 × PPFD denote the effects of CO_2 concentration and interaction between CO_2 and PPFD, respectively. Statistical results of effects of PPFD were less than 0.001 under all N levels.

and **Supplementary Figures S2A,B**). This decrease in Y(II) was related to the increase in Y(NPQ), the regulated energy dissipation at PSII centers, under elevated [CO_2] (**Figure 3B**). Under the other N conditions, Y(NPQ) was not significantly different between the two [CO_2] levels (**Supplementary Figures S2C,D**). On the other hand, the difference in Y(NO) between the two [CO_2] levels was small under all N levels, although Y(NO) was significantly different between the two [CO_2] levels only under MN (**Figure 3C** and **Supplementary Figures S2E,F**). The relationship between Y(II) and Y(NO) was not well correlated (**Supplementary Figures S3D–F**). In contrast, the relationship between Y(II) and Y(NPQ) was well correlated irrespective of N level (**Supplementary Figures S3A–C**). This good correlation suggests that the dependence of Y(II) on measurement light intensity is mainly determined by that of Y(NPQ).

The qL, the fraction of PSII centers that are in the open state, was not different between the two [CO_2] levels under any N level (data not shown). The decrease in ETRII under elevated [CO_2] and HN may not be determined by the limited electron flow downstream of PSII. The decrease in ETRII under elevated [CO_2] and HN is mainly determined by the increase in non-photochemical quenching.

We compared the PSII parameters among N levels (**Supplementary Figures S1D–F**). Under the ambient [CO_2], Y(II) under LN was lower than that under HN, but the difference was insignificant. The other parameters, Y(NPQ) and Y(NO), were similar among the N levels.

Under the High N Condition, the Decrease in Y(I) Is Related to the Increase in Donor-Side Limitation Under Elevated [CO_2]

Next, we examined the light-dependence of the PSI parameters based on the P700 absorption data. The decrease in Y(I) is caused by increases in non-photochemical quantum yield due to donor side limitations [Y(ND)] and/or non-photochemical quantum yield due to acceptor side limitations [Y(NA)] (Baker et al., 2007). Under MN and HN, Y(I) was significantly different between the two [CO_2] levels, although the responses to elevated [CO_2] were different between the two N levels (**Figure 3D** and **Supplementary Figure S4B**). Under MN, the difference in Y(I) between the two [CO_2] levels was mainly dependent on that in Y(NA) (**Supplementary Figure S4D**). Under MN, the decrease in Y(NA) under elevated [CO_2] determined the increase in Y(I). Under MN, elevated [CO_2] may increase the components downstream of PSI, leading to a decrease in Y(NA). Under LN, the difference in Y(NA) was small but significant (**Supplementary Figure S4E**). The decrease in Y(NA) under elevated [CO_2] determined the increase in Y(I) under LN. In contrasts, under HN, Y(NA) was not different between the two

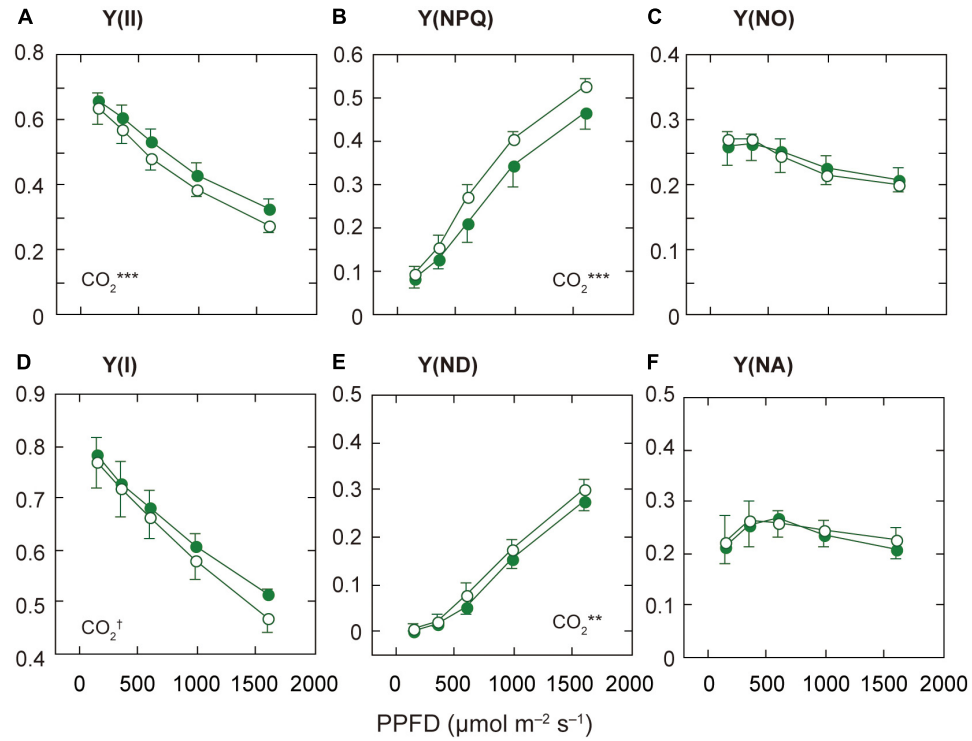

FIGURE 3 | Light-response curves of PSII and PSI parameters in mature leaves of rice plants grown under a high nitrogen level (HN). The effective quantum yield of PSII [Y(II); **A**], the quantum yield of regulated [Y(NPQ); **B**] and non-regulated [Y(NO); **C**] energy dissipation in PSII. The effective quantum yield of PSI [Y(I); **D**], the non-photochemical quantum yield due to donor side limitations [Y(ND); **E**], and the non-photochemical quantum yield due to acceptor side limitations [Y(NA); **F**]. Statistical results of effects of PPFD are less than 0.05. For other details, see the legend of **Figure 2**.

$[CO_2]$ levels (**Figure 3F**). Under HN, the acceptor side limitations of PSI may be similar between the two $[CO_2]$ levels, but elevated $[CO_2]$ may lead to H^+ accumulation in the thylakoid lumen. This H^+ accumulation may affect the increase in Y(ND) in leaves under elevated $[CO_2]$ and HN (**Figure 3E**). We examined the relationships between Y(I) and Y(ND) and between Y(I) and Y(NA) (**Supplementary Figure S5**). Y(I) and Y(ND) were well correlated irrespective of N level (**Supplementary Figures S5A–C**). This good correlation suggests that the dependence of Y(I) on measurement light intensity is mainly determined by that of Y(ND).

We investigated the PSI parameters at the highest AL intensity among N levels (**Supplementary Figures S1G–I**). Y(I) differed among the N levels ($p < 0.1$). The Y(ND) significantly differed among the N levels, and was highest under LN (**Supplementary Figure S1H**). The low N availability induced the donor-side limitation of PSI.

The Relationship Between PSII and PSI Changed Under LN and Elevated $[CO_2]$

We assumed that ETRII equals the linear ETR, and estimated the rate of CEF-PSI by subtracting ETRII from ETRI. Under all N levels, CEF-PSI increased with the increase in measurement light intensity (**Figures 4A–C**). Under HN, CEF-PSI was similar between the two $[CO_2]$ levels. On the other hand, under MN and LN, CEF-PSI under elevated $[CO_2]$ was higher than that under ambient $[CO_2]$ ($p < 0.1$). We also examined the ratio of Y(I) to Y(II) [Y(I)/Y(II)], similar parameter to CEF-PSI. The Y(I)/Y(II) value increased with the increase in measurement light intensity (**Figures 4D–F**). Under LN and HN, Y(I)/Y(II) under elevated $[CO_2]$ was higher than that under ambient $[CO_2]$ ($p = 0.0715$ for LN and $p = 0.0482$ for HN). Both parameters suggested that the activity of PSI is higher than that of PSII under elevated $[CO_2]$.

Next, to compare the balance between PSI and PSII under the two $[CO_2]$ levels and the three N levels, we examined the relationship between Y(I) and Y(II) (**Figure 5**). The data were divided into different N levels (**Figure 5A**) and different $[CO_2]$ levels (**Figure 5B**). We analyzed the statistical significance between slopes and y-intercepts using ANCOVA. There were no significant differences in slopes between the $[CO_2]$ levels and among the N levels. However, significant differences in the y-intercepts between the $[CO_2]$ levels and among the N levels were observed (**Supplementary Table S1**). The y-intercept of the regression line under LN and elevated $[CO_2]$ were higher than the other conditions, that is Y(I) was higher than Y(II) under LN and elevated $[CO_2]$. Under low N and elevated $[CO_2]$, ETRII is suppressed compared with ETRI, leading to increases in Y(I)/Y(II). The Y(NPQ) was increased, but not Y(NO) under conditions where ETRII was suppressed (**Figure 3**), suggesting that excess energy may be safely dissipated by non-photochemical quenching. Under LN and elevated $[CO_2]$,

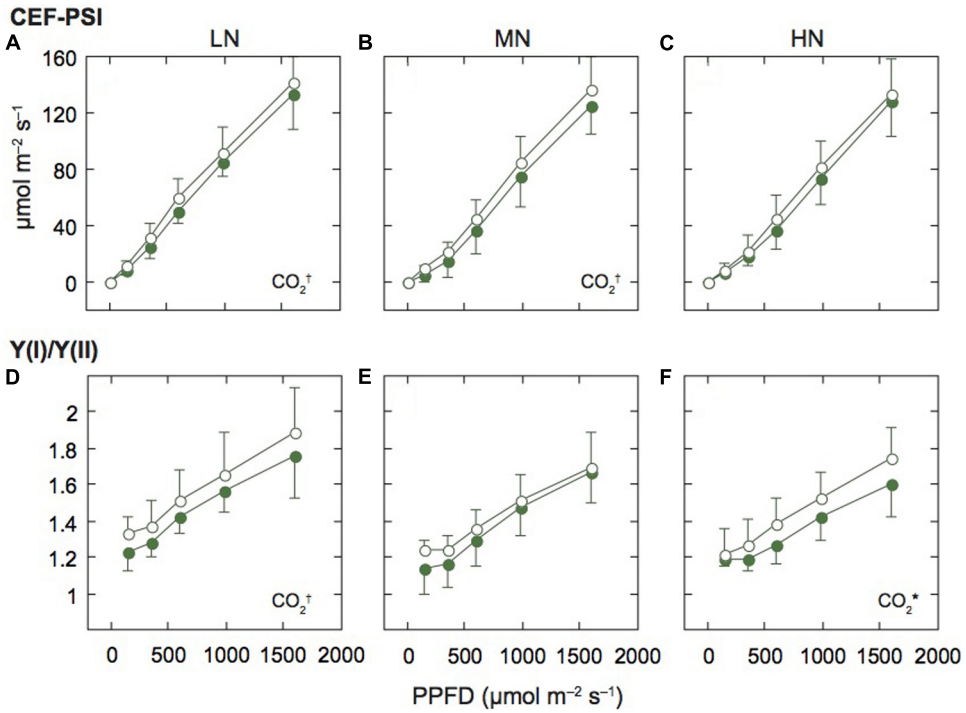

FIGURE 4 | Light-response curves of the rate of cyclic electron flow around PSI and the ratio of PSI to PSII activities in mature leaves of rice plants. The rate of the cyclic electron flow around PSI (CEF-PSI; **A–C**), and the ratio of effective quantum yield of PSI [Y(I)] to effective quantum yield of PSII [Y(II)] [Y(I)/Y(II); **D–F**] under low (LN; **A,D**), moderate (MN; **B,E**) and high nitrogen levels (HN; **C,F**). For other details, see the legend of **Figure 2**.

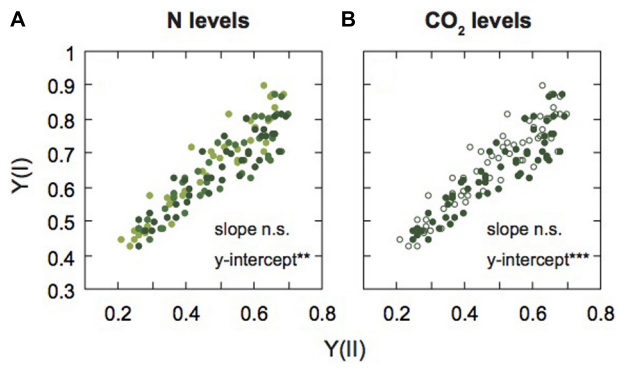

FIGURE 5 | Relationship between PSI and PSII activities in mature leaves of rice plants. The relationship between effective quantum yield of PSI [Y(I)] and effective quantum yield of PSII [Y(II)] are shown under each N level **(A)** and each $[CO_2]$ level **(B)**. Light green, medium green, and dark green symbols denote low (LN), moderate (MN), and high nitrogen levels (HN), respectively **(A)**. Closed and open symbols denote the data of leaves under ambient and elevated $[CO_2]$ levels **(B)**. Statistical significance in slopes and y-intercepts using ANCOVA are also shown (**$p < 0.01$, ***$p < 0.001$).

CEF-PSI was up-regulated, leading to the suppression of the increase in Y(NA). An increase in Y(NA) can induce the production of ROS in PSI (Sejima et al., 2014). The changes in balance between the two photosystems may suppress ROS production under LN and elevated $[CO_2]$.

DISCUSSION

In this study, we aimed to clarify the responses of ETRs to elevated $[CO_2]$ and if these responses change depending on N availability. We found that the responses of linear ETR of Koshihikari leaves to elevated $[CO_2]$ changed among different N levels. Under HN, the linear ETR was lower under elevated $[CO_2]$ than ambient $[CO_2]$. Under HN, ETRI was also lower under elevated $[CO_2]$. The decreases in both ETRs were due to the increases in non-photochemical quenching in PSII and the donor side limitation of PSI, respectively. We also found that the degree of the decrease under elevated $[CO_2]$ was different for both ETRII and ETRI, and thereby the relationship between Y(I) and Y(II) changed under elevated $[CO_2]$. The increases in the Y(I)/Y(II) ratio imply the induction of CEF-PSI, leading to H^+ accumulation in the lumen of the thylakoid membrane and induction of non-photochemical quenching (Miyake, 2010).

The Response of Photosynthetic Linear Electron Transport Rate to Elevated $[CO_2]$ Differed Depending on N Availability

In this study, we assumed that the linear ETR equals ETRII. The responses of ETRII to elevated $[CO_2]$ were different depending on N level (**Figure 2**). The photosynthetic electron transport affects the J_{max} value that is estimated from the A-Ci curve. In soybean leaves in a FACE experiment, J_{max} did not show any

difference between two [CO_2] levels (Bernacchi et al., 2005). Under MN in the same FACE site as this study, J_{max} was significantly decreased in rice leaves at the booting and grain-filling stages under elevated [CO_2] (Chen et al., 2014). The previous experiments including the same FACE site showed that J_{max} is strongly related to leaf N content in rice leaves (Hasegawa et al., 2016). In this study, both ETRs were significantly correlated with leaf N (**Supplementary Figure S6**). Even under HN, the decrease in leaf N may affect the decrease in ETR under elevated [CO_2]. In an experiments where seven C_3 grassland species were exposed to elevated [CO_2] at a FACE site, three forb species exhibited a decrease in both V_{cmax} and J_{max} in response to elevated [CO_2], especially under high N condition, whereas four C_3 grasses did not (Crous et al., 2010). In their study, the grasses had higher root biomass and allocated more biomass to roots under elevated [CO_2] but the forbs did not. The rice variety used in our study, Koshihikari, was shown to have a larger decrease in J_{max} than an *indica* variety, Takanari (Chen et al., 2014). Takanari had more below-ground biomass than Koshihikari, and had higher yield in response to elevated [CO_2] (Hasegawa et al., 2013). Even under HN, elevated [CO_2] may induce the sink limitation, leading to the down regulation of photosynthesis and decreases in leaf N in some plant species including the Koshihikari variety.

Previous studies have reported that the transcripts of genes related to photosynthetic electron transport components are down-regulated under elevated [CO_2]. Leakey et al. (2009b) showed the down-regulation of these genes in leaves of soybean plants grown under elevated [CO_2]. Genes related to the RuBP regeneration process were also down-regulated in leaves of *A. thaliana* and rice plants under elevated [CO_2] compared with under ambient [CO_2] (Li et al., 2008; Fukayama et al., 2011). In rice leaves under elevated [CO_2] in a FACE experiment, the amount of cytochrome f protein, the photosynthetic ETR, and J_{max} were lower compared with in leaves under ambient [CO_2] (Zhang et al., 2008). In this study, we did not examine whether the changes in ETR were related to those in transcripts related to photosynthetic electron transport components, but the degree of down regulation of these transcripts could differ depending on N availability. The responses of P_m value to elevated [CO_2] were different among the N levels (**Figure 1F**), suggesting that the degree of changes in PSI content may be different among the N levels.

Responses of the Balance Between PSII and PSI to Elevated [CO_2]

The response of Y(I) to elevated [CO_2] differed depending on N level (**Figure 3** and **Supplementary Figure S4**). Under HN, elevated [CO_2] decreased Y(I) due to the increase in Y(ND). In some cases, a decrease in Y(I) is related to a decrease in P700 content, which can be estimated from P_m (Sejima et al., 2014). In this study, because Y(I) was not correlated with P_m (r = 0.239, p = 0.261), the decrease in Y(I) may be determined by the increase in Y(ND), but not the decrease in P_m. Under MN, elevated [CO_2] increased Y(I) due to the decrease in Y(NA). This suggests the decrease in the limitation downstream of PSI under this condition. An increase in Y(NA) can induce the generation of hydroxyl radical, one type of ROS, in PSI (Sejima et al., 2014; Shimakawa and Miyake, 2018). In this study, the ROS production in PSI may be lower because Y(NA) was low under all condition. We cannot explain how Y(NA) value was lower under MN and elevated [CO_2], but the increase in CEF-PSI under elevated [CO_2] may be related to the decrease in Y(NA). The mutant of Fd-dependent CEF-PSI, *pgr5*, had higher Y(NA) than a wild-type even under the low measurement light intensity (Kono et al., 2014).

Under HN, Y(II) was lower under elevated [CO_2] due to the increased in Y(NPQ). Y(NO) did not change under elevated [CO_2] regardless of N level, and it was consistently low (**Figure 3**). When Y(NO) is increased, charge recombination reactions in PSII are expected to lead to the triplet state of Chl (Telfer, 2014). The triplet Chl can react with O_2 to produce harmful singlet oxygen in PSII (Müller et al., 2001). In the present study, the decrease in Y(II) was coupled with an increase in Y(NPQ), which effectively resulted in low Y(NO). Under HN, the donor-side limitation in PSI, Y(ND), was higher under elevated [CO_2]. The increase in the limitation may be induced by H^+ accumulation in the thylakoid lumen. The acidification of the lumen suppresses the electron flow through the cytochrome b_6f complex (Tikhonov, 2014), and induces energy-dependent non-photochemical quenching (Baker et al., 2007). In this study, the underlying mechanisms in H^+ accumulation under HN and elevated [CO_2] are still unknown. Under these conditions, the decreases in consumption of ATP and NADPH due to the decreased flux in the Calvin cycle may limit photosynthetic electron transport.

Elevated [CO_2] induces an increase in carboxylase activity and suppression of the oxygenase activity of Rubisco, leading to increases in CO_2 fixation rates compared with photorespiratory rates (Long et al., 2004). The photorespiratory pathway requires a higher ratio of ATP to NADPH compared with the Calvin cycle (Kramer and Evans, 2011). Since CEF-PSI can supply ATP relative to NADPH, the requirement of CEF-PSI may be lower under elevated [CO_2] than ambient [CO_2]. In a study with tobacco plants grown in a growth cabinet, the rate of CEF-PSI was lower under 1000 μmol mol^{-1} [CO_2] than under 400 μmol mol^{-1} [CO_2] (Dahal and Vanlerberghe, 2018). In contrast, in this study, the Y(I)/Y(II) and CEF-PSI were higher under elevated [CO_2] than ambient [CO_2]. We cannot explain the different responses of CEF-PSI to elevated [CO_2] between the two studies, but in our study, plants grew under lower [CO_2] and more fluctuating light environments than the plants in their experiments in a growth cabinet. Under the fluctuating light environments, CEF-PSI may be important to avoid overreduction of photosynthetic electron transport (Kono et al., 2014; Yamori and Shikanai, 2016; Yamori et al., 2016). In the FACE site, the induction of CEF-PSI may be more important because the H^+ accumulation in the lumen by high CEF-PSI can induce the photosynthetic control and the induction of non-photochemical quenching, leading to avoidance of photoinhibition.

Effect of N Availability on the Photosystems

The ETRI was lower under low N. The decrease in Y(I) was accompanied by an increase in Y(ND). Also, ETRII tented to be lower under low N and ambient [CO_2] (**Supplementary Figure S1**). A similar decrease in ETRII has been shown in many plant species including rice (de Groot et al., 2003; Ushio et al., 2003; Miyake et al., 2005). In tomato leaves, both Y(I) and Y(II) were lower under low N, and the ratio between the two parameters was not affected by N level (de Groot et al., 2003). A similar result was shown in the leaves of tobacco that were grown under two levels of N fertilizations (Miyake et al., 2005). Our results showed the balance between the two photosystems was altered by N availability (**Figure 5A**). We cannot explain this discrepancy, but in the previous studies mentioned, plants were cultivated in growth cabinets. The fluctuating light environment in the FACE system may affect the balance between the two photosystems under different N availabilities.

DATA AVAILABILITY STATEMENT

The datasets generated for this study are available on request to the corresponding author.

AUTHOR CONTRIBUTIONS

HO, HS, and KN designed the research. HO and KN performed the experiments and analyzed the data. TT, HN, HS, and TH controlled and regulated paddy field conditions and plant qualities. HO, TT, HN, HS, TH, and KN wrote the manuscript.

FUNDING

This study was supported by the JSPS KAKENHI (Grant Number JP17H05729), CREST, JST (JPMJCR15O3), and the Ministry of Agriculture, Forestry and Fisheries, Japan, through the research project "Development of Technologies for Mitigation and Adaptation to Climate Change in Agriculture, Forestry and Fisheries."

ACKNOWLEDGMENTS

We are grateful to Drs. Tomomi Inoue, Ayumi Kawanishi, Ichiro Terashima, Chikahiro Miyake, Masaru Kono, and Daisuke Takagi, as well as our laboratory members for technical support, advice, and encouragement. We would like to thank Editage (www.editage.com) for English language editing.

SUPPLEMENTARY MATERIAL

The Supplementary Material for this article can be found online at: https://www.frontiersin.org/articles/10.3389/fpls.2020.00786/full#supplementary-material

REFERENCES

Ainsworth, E. A. (2008). Rice production in a changing climate: a meta-analysis of responses to elevated carbon dioxide and elevated ozone concentration. *Glob. Change Biol.* 14, 1642–1650. doi: 10.1111/j.1365-2486.2008.01594.x

Ainsworth, E. A., and Long, S. P. (2005). What have we learned from 15 years of free air CO_2 enrichment (FACE)? A meta-analytic review of the responses of photosynthesis, canopy properties and plant production to rising CO_2. *New Phytol.* 165, 351–372. doi: 10.1111/j.1469-8137.2004.01224.x

Ainsworth, E. A., and Rogers, A. (2007). The response of photosynthesis and stomatal conductance to rising [CO_2]: mechanisms and environmental interactions. *Plant Cell Environ.* 30, 258–270. doi: 10.1111/j.1365-3040.2007.01641.x

Aranjuelo, I., Sanz-Sáez, A., Jáuregui, I., Irigoyen, J. J., Araus, J. L., Sánchez-Díaz, M., et al. (2013). Harvest index, a parameter conditioning responsiveness of wheat plants to elevated CO_2. *J. Exp. Bot.* 64, 1879–1892. doi: 10.1093/jxb/ert081

Baker, N. R., Harbinson, J., and Kramer, D. M. (2007). Determining the limitations and regulation of photosynthetic energy transduction in leaves. *Plant Cell Environ.* 30, 1107–1125. doi: 10.1111/j.1365-3040.2007.01680.x

Bernacchi, C. J., Morgan, P. B., Ort, D. R., and Long, S. P. (2005). The growth of soybean under free air [CO_2] enrichment (FACE) stimulates photosynthesis while decreasing in vivo Rubisco capacity. *Planta* 220, 434–446. doi: 10.1007/s00425-004-1320-8

Chen, C. P., Sakai, H., Tokida, T., Usui, Y., Nakamura, H., and Hasegawa, T. (2014). Do the rich always become richer? Characterizing the leaf physiological response of the high-yielding rice cultivar Takanari to free-air CO_2 enrichment. *Plant Cell Physiol.* 55, 381–391. doi: 10.1093/pcp/pcu009

Chen, G.-Y., Yong, Z.-H., Liao, Y., Zhang, D.-Y., Chen, Y., Zhang, H.-B., et al. (2005). Photosynthetic acclimation in rice leaves to free-air CO_2 enrichment related to both ribulose-1,5-bisphosphate carboxylation limitation and ribulose-1,5-bisphosphate regeneration limitation. *Plant Cell Physiol.* 46, 1036–1045. doi: 10.1093/pcp/pci113

Cheng, S.-H., Moore, B. D., and Seemann, J. R. (1998). Effects of short- and long-term elevated CO_2 on the expression of ribulose-1,5-bisphosphate carboxylase/oxygenase genes and carbohydrate accumulation in leaves of *Arabidopsis thaliana* (L.) Heynh. *Plant Physiol.* 116, 715–723. doi: 10.1104/pp.116.2.715

Cousins, A. B., Adam, N. R., Wall, G. W., Kimball, B. A., Pinter, P. J. Jr., Leavitt, S. W., et al. (2001). Reduced photorespiration and increased energy-use efficiency in young CO_2-enriched sorghum leaves. *New Phytol.* 150, 275–284. doi: 10.1046/j.1469-8137.2001.00112.x

Crous, K. Y., Reich, P. B., Hunter, M. D., and Ellsworth, D. S. (2010). Maintenance of leaf N controls the photosynthetic CO_2 response of grassland species exposed to 9 years of free-air CO_2 enrichment. *Glob. Change Biol.* 16, 2076–2088. doi: 10.1111/j.1365-2486.2009.02058.x

Dahal, K., and Vanlerberghe, G. C. (2018). Growth at elevated CO_2 requires acclimation of the respiratory chain to support photosynthesis. *Plant Physiol.* 178, 82–100. doi: 10.1104/pp.18.00712

Dahal, K., Wang, J., Martyn, G. D., Rahimy, F., and Vanlerberghe, G. C. (2014). Mitochondrial alternative oxidase maintains respiration and preserves photosynthetic capacity during moderate drought in *Nicotiana tabacum*. *Plant Physiol.* 166, 1560–1574. doi: 10.1104/pp.114.247866

de Groot, C. C., van den Boogaard, R., Marcelis, L. F. M., Harbinson, J., and Lambers, H. (2003). Contrasting effects of N and P deprivation on the regulation of photosynthesis in tomato plants in relation to feedback limitation. *J. Exp. Bot.* 54, 1957–1967. doi: 10.1093/jxb/erg193

Drake, B. G., Gonzalez-Meler, M. A., and Long, S. P. (1997). More efficient plants: a consequence of rising atmospheric CO_2? *Annu. Rev. Plant Physiol. Plant Mol. Biol.* 48, 609–639. doi: 10.1146/annurev.arplant.48.1.609

Farquhar, G. D., von Caemmerer, S., and Berry, J. A. (1980). A biochemical model of photosynthetic CO_2 assimilation in leaves of C_3 species. *Planta* 149, 78–90. doi: 10.1007/BF00386231

Fukayama, H., Sugino, M., Fukuda, T., Masumoto, C., Taniguchi, Y., Okada, M., et al. (2011). Gene expression profiling of rice grown in free air CO_2 enrichment (FACE) and elevated soil temperature. *Field Crops Res.* 121, 195–199. doi: 10.1016/j.fcr.2010.11.018

Genty, B. E., Briantais, J. M., and Baker, N. R. (1989). The relationship between the quantum yield of photosynthesis electron transport and quenching of chlorophyll fluorescence. *Biochim. Biophys. Acta* 990, 87–92. doi: 10.1016/S0304-4165(89)80016-9

Habash, D. Z., Paul, M. J., Parry, M. A. J., Keys, A. J., and Lawlor, D. W. (1995). Increased capacity for photosynthesis in wheat grown at elevated CO_2: the relationship between electron transport and carbon metabolism. *Planta* 197, 482–489. doi: 10.1007/BF00196670

Hasegawa, T., Sakai, H., Tokida, T., Nakamura, H., Zhu, C., Usui, Y., et al. (2013). Rice cultivar responses to elevated CO_2 at two free-air CO_2 enrichment (FACE) sites in Japan. *Funct. Plant Biol.* 40, 148–159. doi: 10.1071/FP12357

Hasegawa, T., Sakai, H., Tokida, T., Usui, Y., Nakamura, H., Wakatsuki, H., et al. (2019). A high-yielding rice cultivar "Takanari" shows no N constraints on CO_2 fertilization. *Front. Plant Sci.* 10:361. doi: 10.3389/fpls.2019.00361

Hasegawa, T., Sakai, H., Tokida, T., Usui, Y., Yoshimoto, M., Fukuoka, M., et al. (2016). "Rice free-air carbon dioxide enrichment studies to improve assessment of climate change effects on rice agriculture," in *Improving Modeling Tools to Assess Climate Change Effects on Crop Response, Adv. Agric. Syst. Model. 7*, eds J. L. Hatfield and D. Fleisher (Madison: ASA, CSSA, and SSSA), 45–68.

Ikawa, H., Chen, C. P., Sikma, M., Yoshimoto, M., Sakai, H., Tokida, T., et al. (2018). Increasing canopy photosynthesis in rice can be achieved without a large increase in water use–a model based on free-air CO_2 enrichment. *Glob. Change Biol.* 24, 1321–1341. doi: 10.1111/gcb.13981

Kono, M., Noguchi, K., and Terashima, I. (2014). Roles of the cyclic electron flow around PSI (CEF-PSI) and O2-dependent alternative pathways in regulation of the photosynthetic electron flow in short-term fluctuating light in *Arabidopsis thaliana*. *Plant Cell Physiol.* 55, 990–1004. doi: 10.1093/pcp/pcu033

Kramer, D. M., and Evans, J. R. (2011). The importance of energy balance in improving photosynthetic productivity. *Plant Physiol.* 155, 70–78. doi: 10.1104/pp.110.166652

Kumagai, E., Araki, T., and Ueno, O. (2009). Effect of nitrogen-deficiency on midday photoinhibition in flag leaves of different rice (*Oryza sativa* L.) cultivars. *Photosynthetica* 47, 241–246. doi: 10.1007/s11099-009-0038-z

Leakey, A. D., Ainsworth, E. A., Bernacchi, C. J., Rogers, A., Long, S. P., and Ort, D. R. (2009a). Elevated CO_2 effects on plant carbon, nitrogen, and water relations: six important lessons from FACE. *J. Exp. Bot.* 60, 2859–2876. doi: 10.1093/jxb/erp096

Leakey, A. D., Xu, F., Gillespie, K. M., McGrath, J. M., Ainsworth, E. A., and Ort, D. R. (2009b). Genomic basis for stimulated respiration by plants growing under elevated carbon dioxide. *Proc. Natl. Acad. Sci. U.S.A.* 106, 3597–3602. doi: 10.1073/pnas.0810955106

Li, P., Ainsworth, E. A., Leakey, A. D. B., Ulanov, A., Lozovoya, V., Ort, D. R., et al. (2008). Arabidopsis transcript and metabolite profiles: ecotype-specific responses to open-air elevated [CO_2]. *Plant Cell Env.* 31, 1673–1687. doi: 10.1111/j.1365-3040.2008.01874.x

Long, S. P., Ainsworth, E. A., Rogers, A., and Ort, D. R. (2004). Rising atmospheric carbon dioxide: plants FACE the future. *Annu. Rev. Plant Biol.* 55, 591–628. doi: 10.1146/annurev.arplant.55.031903.141610

Miglietta, F., Giuntoli, A., and Bindi, M. (1996). The effect of free air carbon dioxide enrichment (FACE) and soil nitrogen availability on the photosynthetic capacity of wheat. *Photosynth. Res.* 47, 281–290. doi: 10.1007/BF02184288

Miyake, C. (2010). Alternative electron flows (water-water cycle and cyclic electron flow around PSI) in photosynthesis: molecular mechanisms and physiological functions. *Plant Cell Physiol.* 51, 1951–1963. doi: 10.1093/pcp/pcq173

Miyake, C., Horiguchi, S., Makino, A., Shinzaki, Y., Yamamoto, H., and Tomizawa, K. (2005). Effects of light intensity on cyclic electron flow around PSI and its relationship to non-photochemical quenching of Chl fluorescence in tobacco leaves. *Plant Cell Physiol.* 46, 1819–1830. doi: 10.1093/pcp/pci197

Müller, P., Li, X. P., and Niyogi, K. K. (2001). Non-photochemical quenching. A response to excess light energy. *Plant Physiol.* 125, 1558–1566. doi: 10.1104/pp.125.4.1558

Nakamura, H., Tokida, T., Yoshimoto, M., Sakai, H., Fukuoka, M., and Hasegawa, T. (2012). Performance of the enlarged Rice-FACE system using pure CO_2 installed in Tsukuba, Japan. *J. Agric. Meteorol.* 68, 15–23. doi: 10.2480/agrmet.68.1.2

Nakano, H., Makino, A., and Mae, T. (1997). The effect of elevated partial pressures of CO_2 on the relationship between photosynthetic capacity and N content in rice leaves. *Plant Physiol.* 115, 191–198. doi: 10.1104/pp.115.1.191

Noctor, G., and Foyer, C. H. (2000). Homeostasis of adenylate status during photosynthesis in a fluctuating environment. *J. Exp. Bot.* 51, 347–356. doi: 10.1093/jexbot/51.suppl_1.347

Noguchi, K., and Terashima, I. (2006). Responses of spinach leaf mitochondria to low N availability. *Plant Cell Environ.* 29, 710–719. doi: 10.1111/j.1365-3040.2005.01457.x

Noguchi, K., Tsunoda, T., Miyagi, A., Kawai-Yamada, M., Sugiura, D., Miyazawa, S. I., et al. (2018). Effects of elevated atmospheric CO_2 on respiratory rates in mature leaves of two rice cultivars grown at a free-air CO_2 enrichment site and analyses of the underlying mechanisms. *Plant Cell Physiol.* 59, 637–649. doi: 10.1093/pcp/pcy017

Oxborough, K., and Baker, N. R. (1997). Resolving chlorophyll a fluorescence images of photosynthetic efficiency into photochemical and non-photochemical components - calculation of qP and Fv' /Fm' without measuring Fo'. *Photosynth. Res.* 54, 135–142. doi: 10.1023/A:1005936823310

Pan, C., Ahammed, G. J., Li, X., and Shi, K. (2018). Elevated CO_2 improves photosynthesis under high temperature by attenuating the functional limitations to energy fluxes, electron transport and redox homeostasis in tomato leaves. *Front. Plant Sci.* 9:1739. doi: 10.3389/fpls.2018.01739

R Core Team (2016). *R: A Language and Environment for Statistical Computing*. Vienna: R Foundation for Statistical Computing.

Rogers, A., Fischer, B. U., Bryant, J., Frehner, M., Blum, H., Raines, C. A., et al. (1998). Acclimation of photosynthesis to elevated CO_2 under low-nitrogen nutrition is affected by the capacity for assimilate utilization. Perennial ryegrass under free-Air CO_2 enrichment. *Plant Physiol.* 118, 683–689. doi: 10.1104/pp.118.2.683

Saban, J. M., Chapman, M. A., and Taylor, G. (2019). FACE facts hold for multiple generations; Evidence from natural CO_2 springs. *Glob. Change Biol.* 25, 1–11. doi: 10.1111/gcb.14437

Sakai, H., Tokida, T., Usui, Y., Nakamura, H., and Hasegawa, T. (2019). Yield responses to elevated CO_2 concentration among Japanese rice cultivars released since 1882. *Plant Prod. Sci.* 22, 352–366. doi: 10.1080/1343943X.2019.1626255

Sejima, T., Takagi, D., Fukayama, H., Makino, A., and Miyake, C. (2014). Repetitive short-pulse light mainly inactivates photosystem I in sunflower leaves. *Plant Cell Physiol.* 55, 1184–1193. doi: 10.1093/pcp/pcu061

Seneweera, S., Makino, A., Hirotsu, N., Norton, R., and Suzuki, Y. (2011). New insight into photosynthetic acclimation to elevated CO_2: The role of leaf nitrogen and ribulose-1,5-bisphosphate carboxylase/oxygenase content in rice leaves. *Environ. Exp. Bot.* 71, 128–136. doi: 10.1016/j.envexpbot.2010.11.002

Shikanai, T. (2014). Central role of cyclic electron transport around photosystem I in the regulation of photosynthesis. *Curr. Opin. Biotech.* 26, 25–30. doi: 10.1016/j.copbio.2013.08.012

Shimakawa, G., and Miyake, C. (2018). Oxidation of P700 ensures robust photosynthesis. *Front. Plant Sci.* 9:1617. doi: 10.3389/fpls.2018.01617

Telfer, A. (2014). Singlet oxygen production by PSII under light stress: mechanism, detection and the protective role of β-carotene. *Plant Cell Physiol.* 55, 1216–1223. doi: 10.1093/pcp/pcu040

Tikhonov, A. N. (2014). The cytochrome b_6f complex at the crossroad of photosynthetic electron transport pathways. *Plant Physiol. Biochem.* 81, 163–183. doi: 10.1016/j.plaphy.2013.12.011

Ushio, A., Makino, A., Yokota, S., Hirotsu, N., and Mae, T. (2003). Xanthophyll cycle pigments and water-water cycle in transgenic rice with decreased amounts of ribulose-1,5-bisphosphate carboxylase and the wild-type rice grown under different N levels. *Soil Sci. Plant Nutr.* 49, 77–83. doi: 10.1080/00380768.2003.10409982

Usui, Y., Sakai, H., Tokida, T., Nakamura, H., Nakagawa, H., and Hasegawa, T. (2014). Heat-tolerant rice cultivars retain grain appearance quality under free-air CO_2 enrichment. *Rice* 7:6. doi: 10.1186/s12284-014-0006-5

Xu, Z., Jiang, Y., and Zhou, G. (2015). Response and adaptation of photosynthesis, respiration, and antioxidant systems to elevated CO_2 with environmental stress in plants. *Front. Plant Sci.* 6:701. doi: 10.3389/fpls.2015.00701

Yamada, S., Ozaki, H., and Noguchi, K. (2020). The mitochondrial respiratory chain maintains the photosynthetic electron flow in *Arabidopsis thaliana* leaves under high-light stress. *Plant Cell Physiol.* 61, 283–295. doi: 10.1093/pcp/pcz193

Yamori, W., Makino, A., and Shikanai, T. (2016). A physiological role of cyclic electron transport around photosystem I in sustaining photosynthesis under fluctuating light in rice. *Sci. Rep.* 6:20147. doi: 10.1038/srep20147

Yamori, W., and Shikanai, T. (2016). Physiological functions of cyclic electron transport around photosystem I in sustaining photosynthesis and plant growth. *Annu. Rev. Plant Biol.* 67, 81–106. doi: 10.1146/annurev-arplant-043015-112002

Zhang, D. Y., Chen, G. Y., Gong, Z. Y., Chen, J., Yong, Z. H., Zhu, J. G., et al. (2008). Ribulose-1,5-bisphosphate regeneration limitation in rice leaf photosynthetic acclimation to elevated CO_2. *Plant Sci.* 175, 348–353. doi: 10.1016/j.plantsci.2008.05.008

Conflict of Interest: HN was employed by the company Taiyo Keiki Co., Ltd.

The remaining authors declare that the research was conducted in the absence of any commercial or financial relationships that could be construed as a potential conflict of interest.

frontiers in Plant Science

ORIGINAL RESEARCH
published: 24 July 2020
doi: 10.3389/fpls.2020.01121

Photorespiration Coupled With CO_2 Assimilation Protects Photosystem I From Photoinhibition Under Moderate Poly(Ethylene Glycol)-Induced Osmotic Stress in Rice

Shinya Wada[1,2], *Chikahiro Miyake*[2], *Amane Makino*[3] *and Yuji Suzuki*[1]*

[1] Faculty of Agriculture, Iwate University, Morioka, Japan, [2] Graduate School of Agricultural Science, Kobe University, Nada-ku, Japan, [3] Graduate School of Agricultural Science, Tohoku University, Aoba-ku, Japan

OPEN ACCESS

Edited by:
Adriano Nunes-Nesi, Universidade Federal de Viçosa, Brazil

Reviewed by:
Xenie Johnson, Commissariat à l'Energie Atomique et aux Energies Alternatives (CEA), France
Xinguang Zhu, Chinese Academy of Sciences (CAS), China

***Correspondence:**
Yuji Suzuki
ysuzuki@iwate-u.ac.jp

Specialty section:
This article was submitted to Plant Physiology, a section of the journal Frontiers in Plant Science

Received: *01 October 2019*
Accepted: *07 July 2020*
Published: *24 July 2020*

Citation:
Wada S, Miyake C, Makino A and Suzuki Y (2020) Photorespiration Coupled With CO_2 Assimilation Protects Photosystem I From Photoinhibition Under Moderate Poly (Ethylene Glycol)-Induced Osmotic Stress in Rice. Front. Plant Sci. 11:1121. doi: 10.3389/fpls.2020.01121

Photorespiration coupled with CO_2 assimilation is thought to act as a defense system against photoinhibition caused by osmotic stress. In the present study, we examined whether such a mechanism is operative for the protection of photosystem I (PSI) in rice (*Oryza sativa* L.) including transgenic plants with decreased and increased Rubisco content (*RBCS*-antisense and *RBCS*-sense plants, respectively). All plants were hydroponically grown and moderate osmotic stress was imposed using hydroponic culture solutions containing poly(ethylene glycol) (PEG) at 16% or 20% (w/v) for 2 d. In wild-type plants, the rates of CO_2 assimilation (*A*) were significantly decreased by the PEG treatment, whereas the photorespiration activity estimated from the rates of electron transport in photosystem II (PSII) and *A* were not affected. The maximal quantum efficiency of PSII (F_v/F_m) and the maximal activity of PSI (P_m) were also not affected. In *RBCS*-antisense plants, *A* and the estimated photorespiration activity were considerably lower than those in wild-type plants in the presence or absence of the PEG treatment. P_m and both F_v/F_m and P_m decreased in the 16% PEG-treated and 20% PEG-treated *RBCS*-antisense plants, respectively. Thus, the decrease in Rubisco content led to the photoinhibition of PSI and PSII, indicating the importance of photorespiration coupled with CO_2 assimilation for the protection of PSI from moderate PEG-induced osmotic stress. It was also shown that PSI was more sensitive to osmotic stress than PSII. In the PEG-treated wild-type and *RBCS*-antisense plants, osmotic-stress responses of the photosynthetic electron transport reactions upstream of PSI led to the oxidation of P700, which is thought to prevent PSI from over-reduction. Although such a defense system operated, it was not sufficient for the protection of PSI in *RBCS*-antisense plants. In addition, there were no large differences in the parameters measured between wild-type and *RBCS*-sense plants, as overproduction of Rubisco did not increase photorespiration activity.

Keywords: osmotic stress, Rubisco, photorespiration, CO_2 assimilation, photosystem I, photosystem II, rice

INTRODUCTION

Drought stress is one of the most harmful environmental stresses on plant productivity. Stomatal closure in response to drought stress prevents water loss *via* transpiration but decreases CO_2 availability within a leaf and energy consumption by the Calvin-Benson cycle (Lawlor and Tezara, 2009). The resulting excess light energy can over-reduce the photosynthetic electron transport (PET) chain (Cruz de Carvalho, 2008; Xu et al., 2010) and generate reactive oxygen species (ROS) around photosystem II and I (PSII and PSI, respectively) (Asada, 1999; Müller et al., 2001; Krieger-Liszkay, 2005), leading to photoinhibition of these photosystems. PSI photoinhibition requires a long period of recovery and severely decreases photosynthesis and plant growth (Kudoh and Sonoike, 2002; Sonoike, 2011), whereas PSII photoinhibition is repaired efficiently in a short period of time (Demmig-Adams and Adams, 1992; Murata et al., 2007). It has been observed that PSI suffered from photoinhibition under severe drought stress, whereas PSII was not largely affected in some tropical tree species (Huang et al., 2013). Similar phenomena were observed when rice plants were subjected PEG-induced osmotic stress, which are widely used to mimic drought stress (Wada et al., 2019). These results show that PSI is more sensitive to drought or osmotic stress than PSII. Therefore, PSI photoinhibition would be harmful under such stress conditions.

It has been reported that the PET reactions responded to drought or osmotic stress in a manner that limits the electron flow toward PSI. Such responses include the non-photochemical quenching (NPQ) of light energy at PSII (Golding and Johnson, 2003; Zhou et al., 2007; Lawlor and Tezara, 2009; Huang et al., 2012; Zivcak et al., 2013; Zivcak et al., 2014; Wada et al., 2019) and limitation of the electron flow at the cytochrome b_6/f complex (Kohzuma et al., 2009). These events were accompanied by the oxidation of the reaction center chlorophyll of PSI, P700 (Golding and Johnson, 2003; Huang et al., 2012; Zivcak et al., 2013; Zivcak et al., 2014; Wada et al., 2019), which was suggested to suppress the production of ROS in PSI (Sejima et al., 2014; Takagi et al., 2017a). These results strongly suggest that these drought- or osmotic-stress responses of the PET reactions protect PSI from over-reduction and photoinhibition by ROS.

In addition to these responses of the PET reactions, processes downstream of PSI can also contribute to the protection of PSI under drought stress. One such process is photorespiration, a large and energy-consuming pathway that salvages byproducts of the reaction of Rubisco in the Calvin-Benson cycle (Ogren, 1984). Rubisco catalyzes not only the carboxylation of ribulose 1,5-bisphosphate, which generates two molecules of 3-phosphoglycerate for CO_2 assimilation, but also its oxygenation, which generates one molecule each of 2-phosphoglycolate and 3-phosphoglycerate. The photorespiratory pathway converts 2-phosphoglycolate to 3-phosphoglycerate while consuming reducing equivalents and ATP. Rubisco oxygenase activity and photorespiration are relatively active under CO_2-limited conditions according to the C3 photosynthesis model of Farquhar and co-workers (Farquhar et al., 1980; von Caemmerer, 2000). It was suggested that the rate of CO_2 and O_2 uptake by carboxylation and oxygenation reactions, respectively, is at the ratio of 1:2 under the CO_2 compensation point, and that the Calvin-Benson cycle and the photorespiratory pathway operate in a balanced state. Photorespiration was estimated to consume a large portion of light energy under such conditions (Sejima et al., 2016; Hanawa et al., 2017). The rates of energy consumption by photorespiration were reported to increase in response to drought or osmotic stress (Cornic and Briantais, 1991; Wingler et al., 1999; Haupt-Herting and Fock, 2002; Galmés et al., 2007; Zivcak et al., 2013; Chastain et al., 2014; Wada et al., 2019). It was also found that drought-stress induced NPQ, and that NPQ was further stimulated in barley mutants with decreased activity of a photorespiratory enzyme, suggesting that photorespiration consumes excess light energy under drought stress (Wingler et al., 1999).

However, it remains unclear whether photorespiration coupled with CO_2 assimilation protects PSI under drought or osmotic stress. In the present study, this was explored in transgenic rice (*Oryza sativa* L.) plants with decreased Rubisco content (*RBCS*-antisense plants; Makino et al., 2000). We have recently reported that the PET chain was over-reduced in *RBCS*-antisense plants under the combination of high irradiance and CO_2-compensated conditions (Wada et al., 2018). PSI also became susceptible to excess light energy imposed by repetitive illumination of saturated pulse-light, which is thought to generate ROS in PSI (Sejima et al., 2014; Zivcak et al., 2015). Transgenic rice plants with increased Rubisco content (*RBCS*-8sense plants; Suzuki et al., 2007) were also used as control plants. We have previously observed that the activities of photorespiration and CO_2 assimilation were not substantially enhanced in *RBCS*-sense plants (Makino and Sage, 2007; Suzuki et al., 2007; Suzuki et al., 2009; Wada et al., 2018). Plants were exposed to moderate osmotic-stress treatments using poly (ethylene glycol) (PEG)-containing culture solutions. The maximal quantum efficiency of PSII (F_v/F_m) and the maximal P700 signal of PSI (P_m) were determined as indices of photoinhibition and are discussed in relation to the activities of photorespiration and CO_2 assimilation. In addition, osmotic-stress responses of the PET reactions were also examined by measuring chlorophyll fluorescence and P700 absorbance and its relationship with the activities of photorespiration and CO_2 assimilation are discussed.

Abbreviations: A, the rate of CO_2 assimilation; ETRII, the rate of electron trasnport; g_s, stomatal conductance; J_{PR}, the rate of electron flow donated for photorespiration; NPQ, non-photochemical quenching; P700, the reaction center chlorophyll of photosystem I; *pCi*, an intercellular CO_2 partial pressure PEG, poly (ethylene glycol); PET, photosynthetic electron transport; PSII, photosystem II; PSI, photosystem I; Q_A, the primary quinone electron acceptor of photosystem II; $1-q_L$, the fraction of photosystem II centers in closed states; R_d, the rate of respiration under illumination; ROS, reactive oxygen species; Y(II), the quantum efficiency of photosystem II; Y(NO), the quantum yield of non-regulated and non-photochemical energy dissipation at photosystem II; Y(NPQ), the quantum yield of non-photochemical quenching at photosystem II; Y(I), the quantum efficiency of photosystem I; Y(NA), the quantum yield of the acceptor side limitation of photosystem I; Y(ND), the quantum yield of the donor side limitation of photosystem I.

MATERIALS AND METHODS

Plant Culture

Rice (*Oryza sativa* L. "Notohikari") plants were used as wild-type plants and the background cultivar for the previously generated Rubisco-transgenic plants. T_4 progenies of *RBCS*-antisense plants (line AS-71; Makino et al., 2000) and BC_2 progenies of *RBCS*-sense plants (line Sr-26-8; Suzuki et al., 2007) were used. Each plant was grown hydroponically in a growth chamber (NC-441HC, NKsystem, Osaka, Japan) operated under the conditions of photon flux density of 400–500 μmol photon m^{-2} s^{-1}, a photoperiod of 14 h, and day/night temperature regime of 27/22°C. Pre-soaked seeds were sown and germinated on a net floating on tap water, whose pH was adjusted to 5.3–5.5 with 1 M HCl. After 2 weeks, seedlings were transplanted into 1.1 L plastic pots filled with the culture solution. The composition of the culture solution is described in Makino et al. (1988). The culture solution was renewed once a week. The concentration of the culture solution was increased depending on plant growth.

Osmotic-Stress Treatments Using PEG

Plants grown for approximately 60 d after sowing were subjected to osmotic stress treatments using PEG with an average molecular weight of 6,000 (PEG, Sigma-Aldrich, St. Louis, MO, USA). The culture solution containing PEG at the concentration of 16 or 20% (w/v) was supplied instead of the regular culture solution for 2 d in the growth chamber described above. After the treatments, the uppermost, fully expanded leaves were used for the measurement of photosynthesis and biochemical assays.

Measurements of Photosynthesis

The rate of CO_2 assimilation (A), chlorophyll fluorescence, and P700 absorbance were simultaneously measured using the combination system of GFS-3000 and DUAL-PAM-100 (Heinz Walz GmbH, Effeltrich, Germany). The detailed conditions are described in Wada et al. (2019). Briefly, F_v/F_m and P_m were measured after the leaves were dark-adapted, followed by the measurements of chlorophyll fluorescence and P700 absorbance under the conditions of an actinic light intensity of 1,200 μmol photon m^{-2} s^{-1}, an ambient CO_2 partial pressure of 40 Pa, a leaf temperature of 27°C, and a relative humidity of 60–70%. The quantum efficiency of PSII [Y(II)], the quantum yields of the NPQ [Y(NPQ)] and of the non-regulated and non-photochemical energy dissipation [Y(NO)], and the index for the reduction of the primary plastoquinone electron acceptor in PSII (Q_A) (1-q_L) were calculated following the methods described by Kramer et al. (2004) and Baker (2008). Three complementary quantum yields were defined: Y(II) + Y(NO) + Y(NPQ) = 1. The rate of electron transport in PSII (ETRII) was calculated as Y(II) × photon flux density × α × 0.5. The absorptance (α) was adopted to be 0.84 in this study. The quantum efficiency of PSI [Y(I)] and the quantum yields of the donor side limitation of PSI [Y(ND)] and of the acceptor side limitation of PSI [Y(NA)] were calculated according to the methods described by Klughammer and Schreiber (1994) and Schreiber and Klughammer (2008). Three complementary quantum yields were defined: Y(I) + Y(NA) + Y(ND) = 1. The rate of electron flow donated for photorespiration (J_{PR}) was evaluated using the equation of $J_{PR} = 2/3 \times [\text{ETRII} - 4\ (A + R_d)]$ (Valentini et al., 1995; Zivcak et al., 2013). R_d was the rate of respiration under illumination and was assumed to be 1 μmol m^{-2} s^{-1} as in our previous study (Suzuki et al., 2007).

Measurements of the Relative Water Content of Leaves

The relative water content of the leaves (RWC) was determined after the stress treatment, following the methods of Zhou et al. (2007), as described in Wada et al. (2019), using leaf fresh weight measured just after the stress treatment, leaf weight after overnight immersion in deionized water at 4°C, and leaf dry weight.

Biochemical Assays

Leaves were collected after the measurement of photosynthesis, frozen using liquid nitrogen, and kept at −80°C until use. Total leaf-N, chlorophyll, and Rubisco content were determined as described in Makino et al. (1997). Briefly, total leaf-N content was determined using Nessler's reagent after Kjeldahl digestion. Arnon's method (Arnon, 1949) was used for chlorophyll determination. Rubisco content was determined by formamide extraction of Coomassie Brilliant Blue R-250-stained bands corresponding to the large and small subunits of Rubisco separated by SDS-PAGE (Makino et al., 1985), except that bovine serum albumin was used to prepare the calibration curves.

Statistical Analysis

Three to five biological replicates were analyzed using the Tukey-Kramer's HSD test using JMP 14 (SAS Institute Japan, Tokyo, Japan). The Pearson correlation coefficients of the measured parameters were calculated using Microsoft Excel 2013.

RESULTS

Table 1 shows the amounts of Rubisco protein, chlorophyll, and total leaf-N in leaves of the PEG-untreated wild-type, *RBCS*-sense, and *RBCS*-antisense plants. The amounts of Rubisco in *RBCS*-sense and *RBCS*-antisense plants were 120% and 43%, respectively, of the levels in the wild-type plants. The amount of

TABLE 1 | Amounts of Rubisco protein, chlorophyll, and total leaf-nitrogen in the uppermost, fully expanded leaves in wild-type, *RBCS*-sense, and *RBCS*-antisense rice plants.

	Rubisco (g m^{-2})	Chlorophyll (mmol m^{-2})	Total leaf-N (mmol m^{-2})
Wild-type	3.45 ± 0.13^{B} (100)	0.78 ± 0.04^{A}	142.3 ± 5.2^{A}
RBCS-sense	4.13 ± 0.23^{A} (120)	0.71 ± 0.03^{AB}	140.9 ± 4.6^{A}
RBCS-antisense	1.47 ± 0.03^{C} (43)	0.63 ± 0.02^{B}	104.2 ± 1.9^{B}

The relative amount of Rubisco when the wild-type level was defined as 100 is shown in parentheses. Data are presented as means ± SE (n = 4). Statistical analysis was carried out using ANOVA followed by the Tukey–Kramer's test. Columns with the same letter are not significantly different (p < 0.05).

chlorophyll in the *RBCS*-sense plants tended to be slightly lower than that in wild-type plants, whereas the amount of total leaf-N was not different. In *RBCS*-antisense plants, the amounts of chlorophyll and total leaf-N were lower than those in wild-type plants. Such trend was also observed previously (Makino and Sage, 2007; Suganami et al., 2018; Wada et al., 2018). The magnitude of these changes was smaller than that in the amount of Rubisco. Thus, the amounts of Rubisco were greatly affected by genetic manipulation.

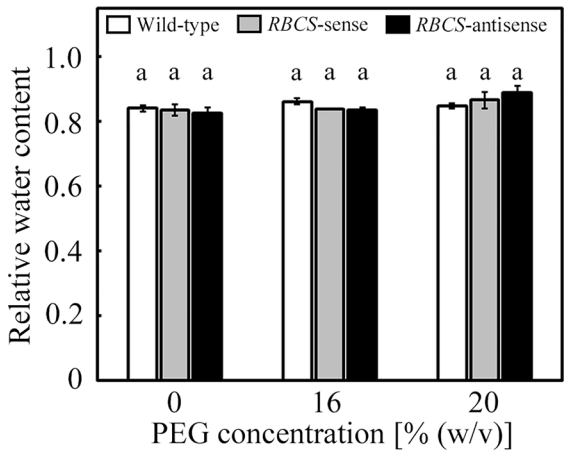

FIGURE 1 | Relative water content of leaves after water stress treatment in transgenic rice plants with an increased (*RBCS*-sense) or decreased (*RBCS*-antisense) Rubisco content. Wild-type plants were used as a control. Sixty days after germination, hydroponically grown plants were water-stressed using culture solutions containing PEG at 0, 16, and 20% (w/v) for 2 d under an irradiance of 400–500 μmol photon m^{-2} s^{-1} and day/night air-temperatures of 27/22°C, followed by the measurements of relative water content of leaves. White, gray, and black bars denote wild-type, *RBCS*-sense, and *RBCS*-antisense plants, respectively. Data are presented as average ± standard error (n = 3–4). Statistical analysis was carried out using ANOVA with a post-hoc Tukey's HSD test. Columns with the same letter are not significantly different (p < 0.05). Statistically significant differences were not observed.

The culture solutions containing PEG at concentrations of 16 and 20% (w/v) were used to impose osmotic stress to the plants. We have previously observed that values of the relative water content of leaves of wild-type rice plants only marginally decreased under these PEG treatments (Wada et al., 2019). In the present study, the relative water content of leaves was not significantly affected by the PEG treatments, and did not significantly differ among genotypes (**Figure 1**).

Effects of the PEG treatments on the fitness of the photosynthetic system were evaluated using F_v/F_m and P_m, which are the indices of the photoinhibition of PSII and PSI, respectively. It has been previously shown that F_v/F_m and P_m were not affected under these PEG treatments in wild-type rice plants. In the PEG-untreated plants, there were no differences in F_v/F_m and P_m between wild-type and *RBCS*-sense plants (**Figure 2**). There was no statistical difference between wild-type plants and *RBCS*-antisense plants, although F_v/F_m and P_m in the latter tended to be marginally lower. Similar trend has been observed in *RBCS*-antisense plants previously (Hirotsu et al., 2004). Neither F_v/F_m nor P_m changed in the PEG-treated wild-type and *RBCS*-sense plants, indicating that these genotypes did not suffer from the photoinhibition of PSII or PSI. In contrast, F_v/F_m substantially decreased to 0.59 in the 20% PEG-treated *RBCS*-antisense plants (**Figure 2A**). P_m in the 16% PEG-treated plants decreased to 78% of the level of the PEG-untreated *RBCS*-antisense plants, and further decreased to 51% in the 20% PEG-treated plants (**Figure 2B**). These results indicate that PSI and both PSII and PSI underwent photoinhibition in *RBCS*-antisense plants under the 16%- and 20%-PEG treatments, respectively. It is also indicated that PSI in *RBCS*-antisense plants was more sensitive to the PEG treatments than PSII.

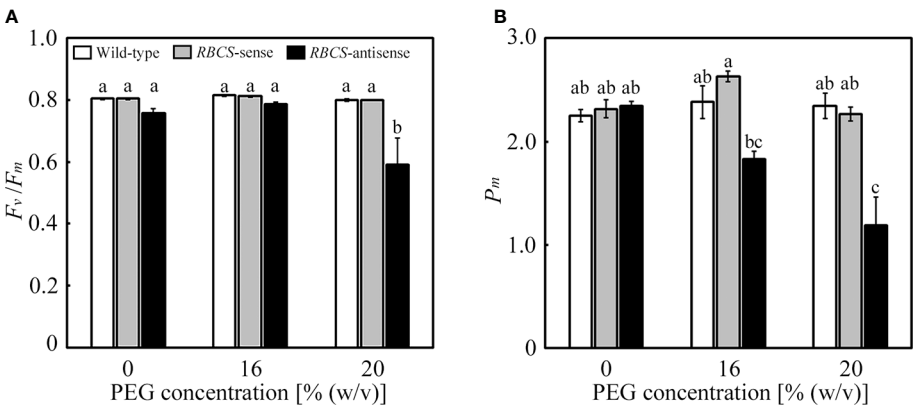

FIGURE 2 | Maximum quantum efficiency of PSII photochemistry (F_v/F_m) **(A)** and the maximal P700 signal (P_m) **(B)** after water stress treatment in transgenic rice plants with an increased (*RBCS*-sense) or decreased (*RBCS*-antisense) Rubisco content. Wild-type plants were used as a control. Sixty days after germination, hydroponically grown plants were water-stressed using culture solutions containing PEG at 0, 16, and 20% (w/v) for 2 d under an irradiance of 400–500 μmol photon m^{-2} s^{-1} and day/night air-temperatures of 27/22°C, followed by the measurements of F_v/F_m and P_m. White, gray, and black bars denote wild-type, *RBCS*-sense, and *RBCS*-antisense plants, respectively. Data are presented as average ± standard error (n = 4–5). Statistical analysis was carried out using ANOVA with a post-hoc Tukey's HSD test. Columns with the same letter are not significantly different (p < 0.05).

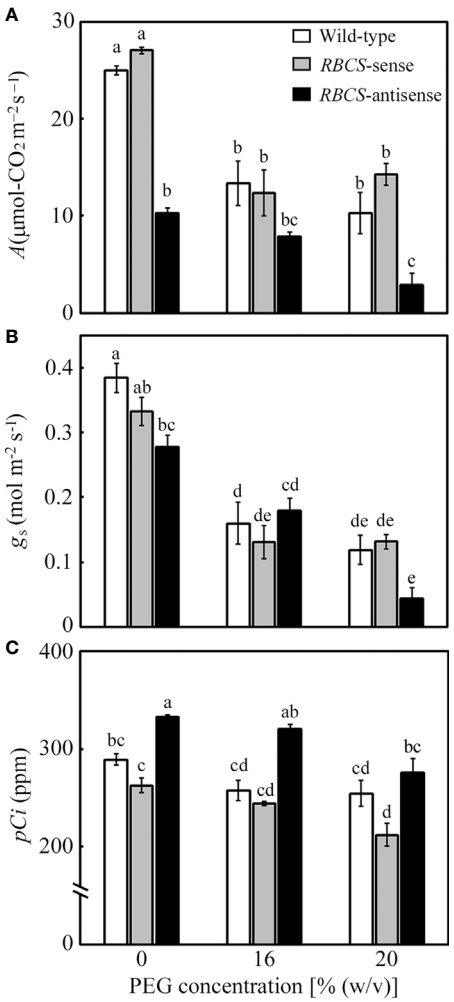

FIGURE 3 | Rate of CO_2 assimilation (*A*) **(A)**, stomatal conductance (g_s) **(B)**, and intercellular CO_2 partial pressure (*pCi*) **(C)** after water stress treatment in transgenic rice plants with an increased (*RBCS*-sense) or decreased (*RBCS*-antisense) Rubisco content. Wild-type plants were used as a control. Sixty days after germination, hydroponically grown plants were water-stressed using culture solutions containing PEG at 0, 16, and 20% (w/v) for 2 d under an irradiance of 400–500 μmol photon m^{-2} s^{-1} and day/night air-temperatures of 27/22°C. *A*, g_s, and *pCi* were measured under the conditions of an actinic light intensity of 1,200 μmol photon m^{-2} s^{-1}, an ambient CO_2 partial pressure of 40 Pa, leaf temperature of 27°C, and relative humidity of 60–70%. White, gray, and black bars denote wild-type, *RBCS*-sense, and *RBCS*-antisense plants, respectively. Data are presented as average ± standard error (n = 4–5). Statistical analysis was carried out using ANOVA followed by the Tukey–Kramer's test. Columns with the same letter are not significantly different ($p < 0.05$).

Changes in leaf gas-exchange parameters were examined (**Figure 3**). In all genotypes, *A*, stomatal conductance (g_s), and intercellular CO_2 partial pressure (*pCi*) tended to decrease in the PEG-treated plants. Although the relative water content in leaves was not affected (**Figure 1**), the PEG treatment was shown to lead to partial stomatal closure and concomitant changes in the leaf gas-exchange parameters. In wild-type plants, *A* in the PEG-treated plants decreased to 41–53% of the levels in the PEG-untreated control plants (**Figure 3A**). Similar trends were observed in g_s. The values of *pCi* decreased by more than 30 ppm in the PEG-treated wild-type plants. The decreases in *pCi* were not as much as the decrease in both *A* and g_s (**Figure 2C**; Lawlor and Tezara, 2009). The values of *A*, g_s, and *pCi* in *RBCS*-sense plants were not largely different from those in wild-type plants irrespective of (PEG) in the culture solutions, although slight decreases in g_s or *pCi* were observed in some cases (**Figures 3A–C**). In contrast, *A* in *RBCS*-antisense plants was lower than in other genotypes (**Figure 3A**). When not treated with PEG, *A* was 41% that of the wild-type level, corresponding to the magnitude of decreases in the amount of Rubisco (**Table 1**). Decreases in *A* were primarily accounted for by decreases in Rubisco content as observed in our previous studies (Hirotsu et al., 2004; Makino and Sage, 2007; Suganami et al., 2018; Wada et al., 2018). Therefore, it was unlikely that *RBCS*-antisense plants were suffering from PSII photoinhibition that affected *A* despite of decreases in chlorophyll content and marginal decreases in F_v/F_m (**Table 1** and **Figure 2**). Although the level of g_s was lower than that in the wild-type plants (**Figure 3B**), *pCi* was higher by 44 ppm owing to the greatly decreased *A* (**Figure 3C**). In the 16% and 20% PEG-treated *RBCS*-antisense plants, the values of *A* were 76% and 28%, respectively, that of the PEG-untreated *RBCS*-antisense plants. These values were 59% and 28% of those in the wild-type plants treated with the same (PEG), respectively. As g_s decreased in the PEG-treated *RBCS*-antisense plants (**Figure 3B**), the values of *pCi* decreased by 12 and 58 ppm in the 16% and 20% PEG-treated plants, respectively. The *pCi* in the PEG-treated *RBCS*-antisense plants was still higher than that in the wild-type plants treated with the same (PEG) (**Figure 3C**).

The consumption of electrons by photorespiration, J_{PR}, was calculated from *A* and ETRII (Valentini et al., 1995; Zivcak et al., 2013). The values of J_{PR} in the PEG-untreated wild-type plants and *RBCS*-sense plants were similar and did not change when treated by PEG (**Figure 4A**). In these genotypes, ratios of J_{PR} to ETRII were about 0.35 when not treated with PEG and tended to increase to 0.42–0.46 when treated with PEG (**Figure 4B**), indicating that the rate of consumption of electrons by photorespiration increased. J_{PR}/ETRII was less than 0.5, showing that CO_2 assimilation acted as a relatively greater electron sink, probably because stomata were still partially open and *pCi* was not greatly decreased under the present experimental conditions (**Figures 3B, C**). J_{PR} in *RBCS*-antisense plants was 41% of that in wild-type plants when not treated with PEG (**Figure 4A**). The magnitude of decreases in J_{PR} was similar to that in the amount of Rubisco (**Table 1**), as observed in the case of *A* (**Figure 3A**). J_{PR} further decreased in the 16% and 20% PEG treated *RBCS*-antisense plants. The values of J_{PR} in these plants corresponded to 34% and 20% of those in the wild-type plants treated with the same (PEG), respectively. These results show that the consumption of electrons by photorespiration and CO_2 assimilation was greatly restricted owing to the decreased Rubisco content in *RBCS*-antisense plants. Ratios of J_{PR} to ETRII in *RBCS*-antisense plants were

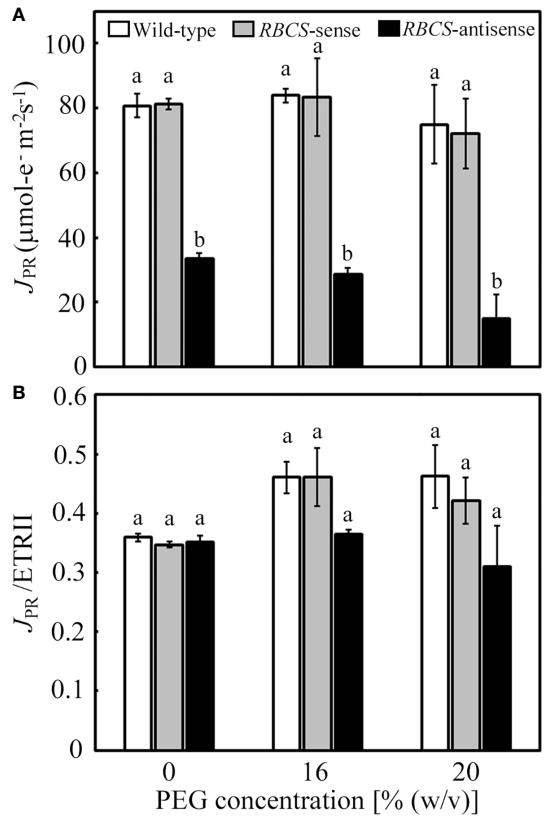

FIGURE 4 | Rate of electron flow donated for photorespiration (J_{PR}) **(A)** and its ratio to the electron transport rate in PSII (J_{PR}/ETRII) **(B)** in transgenic rice plants with an increased (*RBCS*-sense) or decreased (*RBCS*-antisense) Rubisco content. Wild-type plants were used as a control. J_{PR} was evaluated with the equation $J_{PR} = 2/3 \times [ETRII - 4 (A + R_d)]$ (Valentini et al., 1995; Zivcak et al., 2013). R_d was the rate of respiration under illumination and was assumed to be 1 μmol m^{-2} s^{-1} as in our previous study (Suzuki et al., 2007). ETRII was calculated as Y(II) × PFD × α × 0.5, where absorptance (α) was adopted to be 0.84. Data of *A* and Y(II) were taken from **Figures 3** and **5**, respectively. White, gray, and black bars denote wild-type, *RBCS*-sense, and *RBCS*-antisense plants, respectively. Data are presented as average ± standard error (n = 4–5). Statistical analysis was carried out using ANOVA followed by the Tukey–Kramer's test. Columns with the same letter are not significantly different ($p < 0.05$).

similar to those in wild-type plants when not treated with PEG (**Figure 4B**). In contrast to other genotypes, ratios of J_{PR} to ETRII in *RBCS*-antisense plants were relatively unchanged when treated with PEG, showing that the rate of consumption of electrons by photorespiration did not change.

Changes in the photochemistry of PSII were examined in response to the PEG treatments. In wild-type plants, Y(II) decreased slightly and gradually as the (PEG) in the culture solution increased (**Figure 5A**). The magnitude of the decreases was smaller than that in *A* (**Figure 3A**). Slight decreases in Y (NO), which is an index for the dissipation of light energy in a non-regulated manner (Kramer et al., 2004), were also observed (**Figure 5C**). These changes were reflected in increases in Y (NPQ) (**Figure 5B**). The $1-q_L$ indicates the fraction of PSII centers in closed states (Kramer et al., 2004), which is thought to reflect the extent of the reduction of the plastoquinone pool (Miyake et al., 2009). The $1-q_L$ is also thought to be an index for lumenal acidification, as a decrease in q_L was accompanied by lumenal acidification in transgenic or transplastomic tobacco plants with decreases in the amounts of the chloroplastic ATP synthase (Rott et al., 2011). The values of $1-q_L$ tended to slightly increase in the PEG-treated wild-type plants (**Figure 5D**), suggesting the reduction of the plastoquinone pool and/or lumenal acidification. In *RBCS*-sense plants, the values of these parameters and their response to the PEG treatments were similar to those in wild-type plants (**Figures 5A–D**). In *RBCS*-antisense plants, Y(II) decreased to 43% of that in wild-type plants when not treated with PEG, while slight decreases in Y (NO) were also observed (**Figures 5A, C**). In contrast, Y(NPQ) increased to 2.2-fold higher than that in the PEG-untreated wild-type plants (**Figure 5B**), suggesting that light energy that became excessive because of the decrease in Rubisco content was dissipated primarily by NPQ (Hirotsu et al., 2004; Wada et al., 2018). At the same time, the values of $1-q_L$ tended to be higher than in other genotypes (**Figure 5D**). Y(II) further decreased in the PEG-treated *RBCS*-antisense plants and was lower than that in the wild-type plants treated with the same (PEG) (**Figure 4A**). In the 16% PEG-treated plants, a decrease in Y(NO) and an increase in Y(NPQ) were observed as in other genotypes (**Figures 5B, C**). In the 20% PEG-treated plants, a decrease in Y(II) was not accompanied by an increase in Y(NPQ) but by a substantial increase in Y(NO). Similar phenomena were observed in severely osmotic-stressed rice plants under high temperature (Wada et al., 2019). In addition, the values of $1-q_L$ increased in the PEG-treated *RBCS*-antisense plants and were higher than those in other genotypes treated with the same (PEG), suggesting that reduction of the plastoquinone pool and/or lumenal acidification was further enhanced.

Changes in the photochemistry of PSI were examined simultaneously with those of PSII. In wild-type plants, Y(I) tended to marginally decrease in the PEG-treated plants, while slight decreases were also observed in Y(NA) (**Figures 6A, C**). These changes were reflected in increases in Y(ND) (**Figure 6B**), showing that the oxidation of P700 was stimulated by the PEG treatments. In *RBCS*-sense plants, the values of these parameters and their responses to the PEG treatments were similar to those in wild-type plants (**Figures 6A–C**). In *RBCS*-antisense plants, Y(I) and Y(NA) were lower than those in wild-type plants when not treated with PEG (**Figures 6A, C**). These changes were reflected in increases in Y(ND), being 2.0-fold higher than the level in wild-type plants (**Figure 6B**). Thus, the oxidation of P700 was stimulated in *RBCS*-antisense plants without the PEG treatments in the present study, although such a phenomenon was not observed in the previous study (Wada et al., 2018). Y(ND) gradually increased as the (PEG) in the culture solution increased, whereas Y(I) and Y(NA) gradually decreased (**Figures 6A–C**). Y(ND) in *RBCS* antisense plants was higher than that in other genotypes when treated with PEG, showing that P700 in *RBCS*-antisense plants was also in a more oxidized state by the PEG treatments.

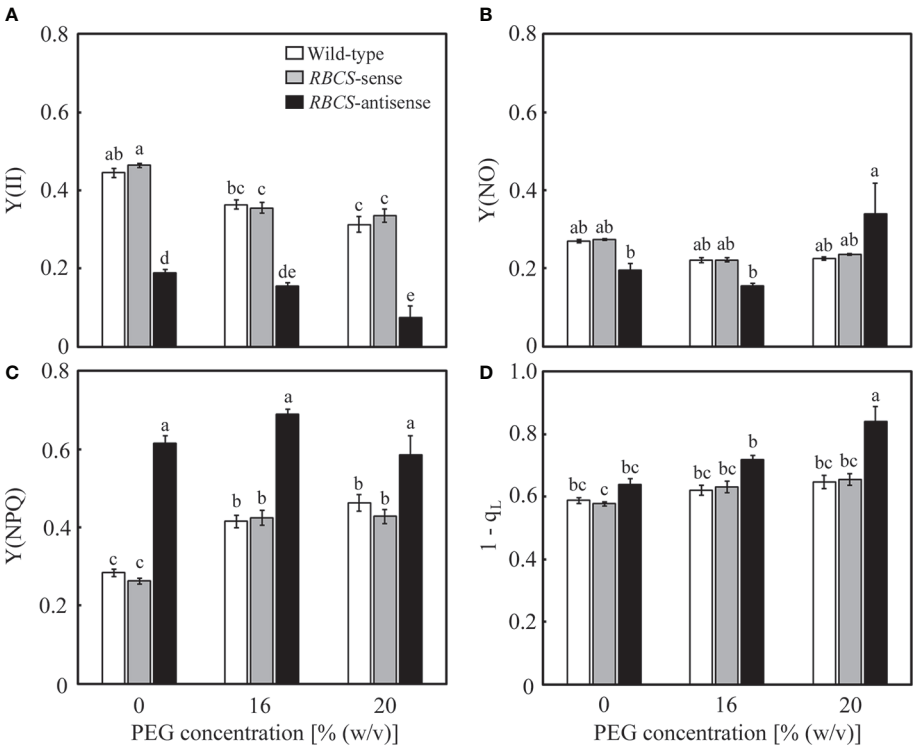

FIGURE 5 | Chlorophyll fluorescence parameters after water stress treatment in transgenic rice plants with an increased (*RBCS*-sense) or decreased (*RBCS*-antisense) Rubisco content. Wild-type plants were used as a control. Sixty days after germination, hydroponically grown plants were water-stressed using culture solutions containing PEG at 0, 16, and 20% (w/v) for 2 d under an irradiance of 400–500 μmol photon m^{-2} s^{-1} and day/night air-temperatures of 27/22°C. Y(II) **(A)**, Y(NPQ) **(B)**, Y(NO) **(C)**, and 1−q_L **(D)** were measured under the conditions of an actinic light intensity of 1,200 μmol photon m^{-2} s^{-1}, an ambient CO_2 partial pressure of 40 Pa, leaf temperature of 27°C, and relative humidity of 60–70%. Data are presented as means ± SE (n = 4–5). Statistical analysis was carried out using ANOVA followed by the Tukey–Kramer's test. Columns with the same letter are not significantly different ($p < 0.05$).

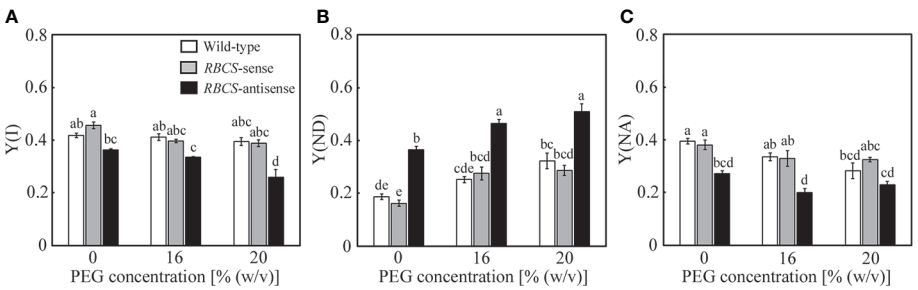

FIGURE 6 | Redox state of P700 after water stress treatment in transgenic rice plants with an increased (*RBCS*-sense) or decreased (*RBCS*-antisense) Rubisco content. Wild-type plants were used as a control. Sixty days after germination, hydroponically grown plants were water-stressed using culture solutions containing PEG at 0, 16, and 20% (w/v) for 2 d under an irradiance of 400–500 μmol photon m^{-2} s^{-1} and day/night air-temperatures of 27/22°C. Y(I) **(A)**, Y(ND) **(B)**, and Y(NA) **(C)** were measured under the conditions of an actinic light intensity of 1200 μmol photon m^{-2} s^{-1}, an ambient CO_2 partial pressure of 40 Pa, leaf temperature of 27°C, and relative humidity of 60–70%. Data are presented as means ± SE (n = 4–5). Statistical analysis was carried out using ANOVA followed by the Tukey–Kramer's test. Columns with the same letter are not significantly different ($p < 0.05$).

Relationships between the parameters of the PET reactions were analyzed (**Table 2**). Data obtained with different genotypes were analyzed together. The mutual relationships between the successive PET reactions were as follows: Y(II) was strongly, negatively correlated with 1−q_L and Y(NPQ); 1−q_L was strongly, negatively correlated with Y(I), which in turn was strongly, negatively correlated with Y(ND). 1−q_L was strongly correlated with these parameters. These results are consistent with those in osmotic-stressed rice plants

TABLE 2 | Pearson correlation coefficients among the parameters measured in the present study.

	Y(NPQ)	Y(NO)	1-q_L	Y(I)	Y(ND)	Y(NA)
Y(II)	−0.869***	−0.055	−0.830***	0.893***	−0.967***	0.831***
Y(NPQ)		−0.446**	0.534***	−0.644**	0.847***	−0.843***
Y(NO)			0.424**	−0.316*	0.040	0.196
1-q_L				−0.876***	0.830***	−0.624***
Y(I)					−0.865***	0.577***
Y(ND)						−0.909***

*Data obtained under different conditions of air temperature were analyzed together. *, **, and *** denote statistical significance at $p < 0.05$, $p < 0.01$, and $p < 0.001$, respectively.*

under normal and high temperatures (Wada et al., 2019). However, some differences were observed compared to the results reported in Wada et al. (2019). In the present study, strong, negative correlations were observed between Y(II) and Y(NPQ) and between Y(ND) and Y(NA).

The properties in leaf gas-exchange and the photochemistry of PSII and PSI in the PEG-untreated *RBCS*-sense and *RBCS*-antisense plants, and the PEG-treatment response of wild-type plants were basically consistent with those observed in our previous studies (Makino et al., 2000; Hirotsu et al., 2004; Suzuki et al., 2007; Suzuki et al., 2009; Sudo et al., 2014; Wada et al., 2018; Wada et al., 2019).

DISCUSSION

Photorespiration Coupled With CO_2 Assimilation Plays a Crucial Role in the Protection of PSI From Photoinhibition Under PEG-Induced Moderate Osmotic Stress

In the present study, we examined the role of photorespiration coupled with CO_2 assimilation in the protection of PSI from PEG-induced osmotic stress using Rubisco-transgenic rice plants. The PEG treatments did not significantly affect the relative water content of leaves in all genotypes (**Figure 1**), but substantially decreased g_s (**Figure 3B**). Stomatal closure is the earliest drought-stress response and was reported to be observed even when water status of plants was unaffected by withdrawal of water (Davies and Zhang, 1991; Chaves et al., 2003). Therefore, moderate osmotic stress was thought to be imposed to the plants by the PEG-treatments used in the present study. In *RBCS*-antisense plants, decreases in the activities of photorespiration and CO_2 assimilation led to photoinhibition of PSI and PSII under moderate osmotic stress that did not lead to photoinhibition of both photosystems in wild-type plants (**Figures 2**, **3A**, and **4A**). These results clearly indicate that photorespiration coupled with CO_2 assimilation plays a crucial role in the protection of PSI from photoinhibition under moderate osmotic stress conditions. It has been reported that PSI was more sensitive to drought or osmotic stress than PSII (Huang et al., 2013; Wada et al., 2019). Similar trends were observed in *RBCS*-antisense plants, as PSI suffered from photoinhibition in the 16% PEG-treated plants, whereas PSII did not (**Figure 2**). These results suggest that the weakness of PSI to osmotic stress can be compensated for by the operation of photorespiration coupled with CO_2 assimilation to some extent.

To examine whether photorespiration contributes the consumption of excess light energy under osmotic stress conditions, elevated CO_2 condition might be useful as it suppresses photorespiration. However, in the case of *RBCS*-antisense plants, decrease in Rubisco content affect both CO_2 assimilation and photorespiration. *A* was shown to be limited by Rubisco under elevated CO_2 conditions where *A* is not limited by Rubisco in wild-type plants (Makino et al., 2000; Suzuki et al., 2009). If osmotic-stress response in *RBCS*-antisense plants was altered under elevated (CO_2) conditions, it is very difficult to distinguish whether it sorely depended on the suppression of photorespiration.

In contrast, there were no large differences between wild-type and *RBCS*-sense plants in terms of the activities of photorespiration and CO_2 assimilation, osmotic-stress tolerance, and the photochemistry of PSII and PSI (**Figures 2**–**6**). These results are consistent with those in our previous study, in which these genotypes were exposed to the combination of high irradiance and CO_2-compensated conditions (Wada et al., 2018). We have suggested that Rubisco was not fully functional in *RBCS*-sense plants The rate of CO_2 assimilation was not increased proportionally with an increase in Rubisco content in *RBCS*-sense plants, as Rubisco was partially deactivated probably owing to imbalance between the processes of CO_2 assimilation (Makino and Sage, 2007; Suzuki et al., 2007; Suzuki et al., 2009). The same problem probably arose in the present study.

Photorespiration Is Possibly Inhibited in *RBCS*-Antisense Plants Under PEG-Induced Osmotic Stress

It has previously been observed that the absolute and/or relative rates of energy consumption by photorespiration increased under drought or osmotic stress in a number of plant species, including rice (Cornic and Briantais, 1991; Haupt-Herting and Fock, 2002; Galmés et al., 2007; Zivcak et al., 2013; Chastain et al., 2014; Wada et al., 2019), accounting for the substantial part of light energy absorbed by leaves. Therefore, it has been suggested that photorespiration plays a role in the consumption of excess light energy, at least in part, under drought or osmotic stress condition. Similar trends were observed in wild-type plants in the present study. Moderate osmotic stress by the PEG treatments tended to increase J_{PR}/ETRII simultaneously with decreases in *pCi* (**Figures 3C** and **4B**), although the magnitude of the increases were relatively small. However, such trends were not observed in *RBCS*-antisense plants even when *pCi* decreased in the PEG-treated plants. These results could mean that photorespiration was inhibited in *RBCS*-antisense plants under osmotic stress. Our previous report also suggested the inhibition of photorespiration when rice plants were severely osmotic-stressed under high temperature conditions (Wada et al., 2019). These results imply that some processes of the photorespiratory pathway were damaged when excess light energy caused by osmotic stress was far beyond the capacity of

photorespiration. As it was reported that the amounts of some photorespiratory enzymes were not affected even under severe drought stress (Wingler et al., 1999), further study is necessary to reveal whether and how photorespiration was inhibited under these osmotic stress conditions. In addition, although *pCi* was higher in *RBCS*-antisense plants than in wild-type plants when not treated with PEG (**Figure 3C**), there were no differences in J_{PR}/ETRII (**Figure 4B**), which is expected to be higher in wild-type plants owing to the nature of the carboxylase and oxygenase reactions of Rubisco. The method for the evaluation of photorespiration might also need to be improved.

P700 Oxidation Is Stimulated in Response to PEG-Induced Osmotic Stress Even When the Activities of Photorespiration and CO_2 Assimilation Are Restricted

It has been reported that the PET reactions responded to drought or osmotic stress in a manner that limits the electron flow toward PSI, leading to P700 oxidation (Golding and Johnson, 2003; Huang et al., 2012; Zivcak et al., 2013; Zivcak et al., 2014; Wada et al., 2019). Consistent with these studies, decreases in Y(II), increases in $1-q_L$, slight decreases in Y(I), and increases in Y (ND) were observed in the present study irrespective of genotype (**Figures 5A, D** and **6A, B**). Decreases in Y(II) in response to osmotic stress were accompanied by induction of NPQ in wild-type plants, *RBCS*-sense plants, and the 16% PEG-treated *RBCS*-antisense plants (**Figure 5C**), as observed in previous studies (Golding and Johnson, 2003; Zhou et al., 2007; Lawlor and Tezara, 2009; Huang et al., 2012; Zivcak et al., 2013; Zivcak et al., 2014; Wada et al., 2019). In the 20% PEG-treated *RBCS*-antisense plants, Y(NO) increased instead of Y(NPQ) (**Figures 5B, C**), as was observed in wild-type rice plants severely osmotic-stressed under high temperature conditions (Wada et al., 2019). These results indicate that the osmotic-stress responses of the PET reactions were normally operative even when the energy consumption by photorespiration and CO_2 assimilation were largely restricted. PSII photoinhibition occurred in the 20%-PEG treated *RBCS*-antisense plants as F_v/F_m substantially decreased (**Figure 2A**). This might have restricted the electron flow to PSI and led to P700 oxidation. However, Y(II) was well correlated with Y(I) and Y(ND) when data of the 20%-PEG treated *RBCS*-antisense plants were included in the correlation analysis (**Table 2**). Decreases in F_v/F_m did also not disturb the relationships among these parameters in osmotic-stressed rice plants, including severely damaged ones under high temperature conditions (Wada et al., 2019). Therefore, electron flow to PSI were likely to be limited by Y(II), not by PSII photoinhibition.

Lumenal acidification is thought to be one of the regulatory factors for the drought-stress responses of the PET reactions as it induces NPQ at PSII (Li et al., 2000; Müller et al., 2001; Huang et al., 2012) and slows down the oxidation of plastoquinol by the cytochrome b_6/f complex (Kohzuma et al., 2009; Rott et al., 2011; Tikhonov, 2013; Zivcak et al., 2014; Takagi et al., 2017b). It has also been suggested that over-reduction of the plastoquinone pool suppresses the Q cycle and electron flow at the cytochrome b_6/f complex in cyanobacteria (Shaku et al., 2016; Shimakawa et al., 2018). This system was suspected to be operative in osmotic-stressed rice plants (Wada et al., 2019). The PET reactions are thought to be regulated by such processes in response to osmotic stress even in *RBCS*-antisense plants, as $1-q_L$ was strongly correlated with Y(II), Y(NPQ), Y(I), and Y (ND) among the genotypes (**Table 2**).

In the present study, some results were different from those observed in our previous studies. P700 oxidation was not stimulated in *RBCS*-antisense plants in the absence of osmotic stress (Wada et al., 2018). P700 was over-reduced when *RBCS*-antisense plants were exposed to the combination of high irradiance and CO_2-compensated conditions (Wada et al., 2018), whereas such phenomena as indicated by increases in Y(NA) were not observed in the PEG-treated *RBCS*-antisense plants (**Figure 6C**). The latter can be accounted for, at least partly, by substantial decreases in *pCi* that led to large decreases in energy consumption by photorespiration coupled with CO_2 assimilation (Wada et al., 2018), whereas the magnitude of the decreases in *pCi* was not as much in the present study (**Figure 3C**). In addition, correlations between Y(II) and Y(NPQ) and between Y(ND) and Y(NA) were not apparent in osmotic-stressed rice plants at normal and high temperatures (Wada et al., 2019). The reason for this discrepancy is unclear. For example, growth conditions were different between these studies as different types of growth chambers were used. Such differences could lead to differences in the responses of the PET reactions, as it was shown that differences in growth irradiance affected the levels of Y(ND) in wheat (Takagi et al., 2019). Recently, Kadota et al. (2019) suggested that excess electron is dissipated by charge recombination within PSI, leading to P700 oxidation. As increases in Y(ND) was observed along with decreases in Y(NA) (**Figures 6B, C** and **Table 2**) when the activity of photorespiration coupled with CO_2 assimilation was limited (**Figures 3A** and **4A**), charge recombination in PSI might have functioned in P700 oxidation in the *RBCS*-antisense plants used in the present study.

P700 Oxidation Is Not Sufficient for the Protection of P700 in *RBCS*-Antisense Plants

We have previously reported that PSI suffered from photoinhibition even when P700 was highly oxidized under osmotic stress in rice (Wada et al., 2019). Similar trends were observed in osmotic-stressed *RBCS*-antisense plants (**Figures 2B** and **6B**). These results indicate that P700 oxidation cannot fully protect PSI from photoinhibition under osmotic stress. The reason PSI underwent photoinhibition under conditions of highly oxidized P700 still remains unknown. As PSI-specific photoinhibition has been observed under drought or osmotic stress (Huang et al., 2013; Wada et al., 2019; **Figure 2B**), it is speculated that ROS unavoidably generated within and/or near PSI led to PSI photoinhibition. In addition, P700 oxidation was shown to be gradually stimulated while PSI photoinhibition was induced in *RBCS*-antisense plants by repetitive saturated pulse-illumination under the combination of high irradiance and CO_2-compensated conditions (Wada et al., 2018), suggesting the possibility that P700 oxidation and ROS generation occurred at the same time.

CONCLUSION

In the present study, it is shown that antisense suppression of Rubisco content led to decreases in energy consumption by photorespiration coupled with CO_2 assimilation under PEG-induced osmotic stress in rice plants, leading to the photoinhibition of PSI and PSII. These results clearly indicate that photorespiration coupled with CO_2 assimilation plays a crucial role in the protection of PSI from photoinhibition caused by osmotic stress. As PSI was shown to be more sensitive to osmotic stress, photorespiration might compensate for such weakness in PSI. The PET reactions responded to osmotic stress and oxidized P700 in *RBCS*-antisense plants and in the other genotypes. Lumenal acidification and/or the redox state of the plastoquinone pool might primarily regulate the PET reactions under osmotic stress even if the activities of photorespiration and CO_2 assimilation were restricted. It is shown again that P700 oxidation was not sufficient for the protection of P700 against osmotic stress. ROS unavoidably generated in PSI might damage PSI even if P700 oxidation was stimulated. Overproduction of Rubisco, in contrast, did not alter the activities of photorespiration and CO_2 assimilation under osmotic stress. As a result, the photochemistry of PSII and PSI were not altered. These results suggest that further modifications of the metabolism of photorespiration and CO_2 assimilation is necessary to improve drought or osmotic stress tolerance and photosynthesis.

DATA AVAILABILITY STATEMENT

All datasets generated for this study are included in the article/supplementary material.

AUTHOR CONTRIBUTIONS

YS conceived the experimental design. SW performed the experiments. SW and YS analyzed the data. SW and YS wrote the manuscript. SW, CM, AM, and YS edited the manuscript.

FUNDING

This study was supported by the Core Research for Environmental Science and Technology (Scientific Research Grant No. AL65D21010 to CM) and Grants-in-Aid for Scientific Research from the Japan Society for the Promotion of Science (No. 18H02111 to YS and No. 16H06379 to AM).

ACKNOWLEDGMENTS

We would like to thank Editage (www.editage.com) for English language editing.

REFERENCES

Arnon, D. I. (1949). Copper enzymes in isolated chloroplasts. Polyphenoloxidase in *Beta vulgaris*. *Plant Physiol.* 24, 1–15. doi: 10.1104/pp.24.1.1

Asada, K. (1999). The water-water cycle in chloroplasts: scavenging of active oxygens and dissipation of excess photons. *Annu. Rev. Plant Mol. Biol.* 50, 601–639. doi: 10.1146/annurev.arplant.50.1.601

Baker, N. R. (2008). Chlorophyll fluorescence: a probe of photosynthesis *in vivo*. *Annu. Rev. Plant Biol.* 59, 89–113. doi: 10.1146/annurev.arplant.59.032607.092759

Chastain, D. R., Snider, J. L., Collins, G. D., Perry, C. D., Whitaker, J., and Byrd, S. A. (2014). Water deficit in field-grown Gossypium hirsutum primarily limits net photosynthesis by decreasing stomatal conductance, increasing photorespiration, and increasing the ratio of dark respiration to gross photosynthesis. *J. Plant Physiol.* 171, 1576–1585. doi: 10.1016/j.jplph.2014.07.014

Chaves, M. M., Maroco, J. P., and Pereira, J. S. (2003). Understanding plant responses to drought—from genes to the whole plant. *Func. Plant Biol.* 30, 239–264. doi: 10.1071/FP02076

Cornic, G., and Briantais, J.-M. (1991). Partitioning of photosynthetic electron flow between CO_2 and O_2 reduction in a C_3 leaf (*Phaseolus vulgaris* L.) at different CO_2 concentrations and during drought stress. *Planta* 183, 178–184. doi: 10.1007/BF00197786

Cruz de Carvalho, M. H. (2008). Drought stress and reactive oxygen species. *Plant Signal. Behav.* 3, 156–165. doi: 10.4161/psb.3.3.5536

Davies, W. J., and Zhang, J. (1991). Root signals and the regulation of growth and development of plants in drying soil. *Annu. Rev. Plant Physiol. Plant Mol. Biol.* 42, 55–76. doi: 10.1146/annurev.pp.42.060191.000415

Demmig-Adams, B., and Adams, W. W.II (1992). Photoprotection and other responses of plants to high light stress. *Annu. Rev. Plant Physiol. Plant Mol. Biol.* 43, 599–626. doi: 10.1146/annurev.pp.43.060192.003123

Farquhar, G. D., von Caemmerer, S., and Berry, J. A. (1980). A biochemical model of photosynthetic CO_2 assimilation in leaves of C_3 species. *Planta* 149, 78–90. doi: 10.1007/BF00386231

Galmés, J., Abadía, A., Cifre, J., Medrano, H., and Flexas, J. (2007). Photoprotection processes under water stress and recovery in Mediterranean plants with different growth forms and leaf habits. *Physiol. Plant* 130, 495–510. doi: 10.1111/j.1399-3054.2007.00919.x

Golding, A. J., and Johnson, G. N. (2003). Down-regulation of linear and activation of cyclic electron transport during drought. *Planta* 218, 107–114. doi: 10.1007/s00425-003-1077-5

Hanawa, H., Ishizaki, K., Nohira, K., Takagi, D., Shimakawa, G., Sejima, T., et al. (2017). Land plants drive photorespiration as higher electron-sink: comparative study of post-illumination transient O_2-uptake rates from liverworts to angiosperms through ferns and gymnosperms. *Physiol. Plant* 161, 138–149. doi: 10.1111/ppl.12580

Haupt-Herting, S., and Fock, H. P. (2002). Oxygen exchange in relation to carbon assimilation in water-stressed leaves during photosynthesis. *Ann. Bot.* 89, 851–859. doi: 10.1093/aob/mcf023

Hirotsu, N., Makino, A., Ushio, A., and Mae, T. (2004). Changes in the thermal dissipation and the electron flow in the water-water cycle in rice grown under conditions of physiologically low temperature. *Plant Cell Physiol.* 45, 635–644. doi: 10.1093/pcp/pch075

Huang, W., Yang, S. J., Zhang, S. B., Zhang, J. L., and Cao, K. F. (2012). Cyclic electron flow plays an important role in photoprotection for the resurrection plant *Paraboea rufescens* under drought stress. *Planta* 235, 819–828. doi: 10.1007/s00425-011-1544-3

Huang, W., Fu, P. L., Jiang, Y. J., Zhang, J. L., Zhang, S. B., Hu, H., et al. (2013). Differences in the responses of photosystem I and photosystem II of three tree species *Cleistanthus sumatranus*, *Celtis philippensis* and *Pistacia weinmannifolia* exposed to a prolonged drought in a tropical limestone forest. *Tree Physiol.* 33, 211–220. doi: 10.1093/treephys/tps132

Kadota, K., Furutani, R., Makino, A., Suzuki, Y., Wada, S., and Miyake, C. (2019). Oxidation of P700 induces alternative electron flow in photosystem I in wheat leaves. *Plants* 8:152. doi: 10.3390/plants8060152

Klughammer, C., and Schreiber, U. (1994). An improved method, using saturating light pulses, for the determination of photosystem I quantum yield via $P700^+$-absorbance changes at 830 nm. *Planta* 192, 261–268. doi: 10.1007/BF01089043

Kohzuma, K., Cruz, J. A., Akashi, K., Hoshiyasu, S., Munekage, Y. N., Yokota, A., et al. (2009). The long-term responses of the photosynthetic proton circuit to drought. *Plant Cell Environ.* 32, 209–219. doi: 10.1111/j.1365-3040.2008.01912.x

Kramer, D. M., Johnson, G., Kiirats, O., and Edwards, G. E. (2004). New fluorescence parameters for the determination of Q_A redox state and excitation energy fluxes. *Photosynth. Res.* 79, 209–218. doi: 10.1023/B:PRES.0000015391.99477.0

Krieger-Liszkay, A. (2005). Singlet oxygen production in photosynthesis. *J. Exp. Bot.* 56, 337–346. doi: 10.1093/jxb/erh237

Kudoh, H., and Sonoike, K. (2002). Irreversible damage to photosystem I by chilling in the light: cause of the degradation of chlorophyll after returning to normal growth temperature. *Planta* 215, 541–548. doi: 10.1007/s00425-002-0790-9

Lawlor, D. W., and Tezara, W. (2009). Causes of decreased photosynthetic rate and metabolic capacity in water-deficient leaf cells: a critical evaluation of mechanisms and integration of processes. *Ann. Bot.* 103, 561–579. doi: 10.1093/aob/mcn244

Li, X. P., Björkman, O., Shih, C., Grossman, A. R., Rosenquist, M., Jansson, S., et al. (2000). A pigment-binding protein essential for regulation of photosynthetic light harvesting. *Nature* 403, 391–395. doi: 10.1038/35000131

Makino, A., and Sage, R. F. (2007). Temperature response of photosynthesis in transgenic rice transformed with 'sense' or 'antisense' *rbcS*. *Plant Cell Physiol.* 48, 1472–1483. doi: 10.1093/pcp/pcm118

Makino, A., Mae, T., and Ohira, K. (1985). Enzymic properties of ribulose-1,5-bisphosphate carboxylase/oxygenase purified from rice leaves. *Plant Physiol.* 79, 57–61. doi: 10.1104/pp.79.1.57

Makino, A., Mae, T., and Ohira, K. (1988). Differences between wheat and rice in the enzyme properties of ribulose-1,5-bisphosphate carboxylase/oxygenase and their relationship to photosynthetic gas exchange. *Planta* 174, 30–38. doi: 10.1007/BF00394870

Makino, A., Shimada, T., Takumi, S., Kaneko, K., Matsuoka, M., Shimamoto, K., et al. (1997). Does decrease in ribulose-1,5-bisphosphate carboxylase by antisense *rbcS* lead to a higher N-use efficiency of photosynthesis under conditions of saturating CO_2 and light in rice plants? *Plant Physiol.* 114, 483–491. doi: 10.1104/pp.114.2.483

Makino, A., Nakano, H., Mae, T., Shimada, T., and Yamamoto, N. (2000). Photosynthesis, plant growth and N allocation in transgenic rice plants with decreased Rubisco under CO_2 enrichment. *J. Exp. Bot.* 51, 383–389. doi: 10.1093/jexbot/51.suppl_1.383

Miyake, C., Amako, K., Shiraishi, N., and Sugimoto, T. (2009). Acclimation of tobacco leaves to high light intensity drives the plastoquinone oxidation system - relationship among the fraction of open PSII centers, non-photochemical quenching of Chl fluorescence and the maximum quantum yield of PSII in the dark. *Plant Cell. Physiol.* 50, 730–743. doi: 10.1093/pcp/pcp032

Müller, P., Li, X., and Niyogi, K. K. (2001). Non-photochemical quenching. A response to excess light energy. *Plant Physiol.* 125, 1558–1566. doi: 10.1104/pp.125.4.1558

Murata, N., Takahashi, S., Nishiyama, Y., and Allakhverdiev, S. I. (2007). Photoinhibition of photosystem II under environmental stress. *Biochim. Biophys. Acta* 1767, 414–421. doi: 10.1016/j.bbabio.2006.11.019

Ogren, W. L. (1984). Photorespiration: pathways, regulation, and modification. *Annu. Rev. Plant Physiol.* 35, 415–442. doi: 10.1146/annurev.pp.35.060184.002215

Rott, M., Martins, N. F., Thiele, W., Lein, W., Bock, R., Kramer, D. M., et al. (2011). ATP synthase repression in tobacco restricts photosynthetic electron transport, CO_2 assimilation, and plant growth by overacidification of the thylakoid lumen. *Plant Cell* 23, 304–321. doi: 10.1105/tpc.110.079111

Schreiber, U., and Klughammer, C. (2008). Saturation Pulse method for assessment of energy conversion in PS I. *PAM App. Notes* 1, 11–14.

Sejima, T., Takagi, D., Fukayama, H., Makino, A., and Miyake, C. (2014). Repetitive short-pulse light mainly inactivates photosystem I in sunflower leaves. *Plant Cell Physiol.* 55, 1184–1193. doi: 10.1093/pcp/pcu061

Sejima, T., Hanawa, H., Shimakawa, G., Takagi, D., Suzuki, Y., Fukayama, H., et al. (2016). Post-illumination transient O_2-uptake is driven by photorespiration in tobacco leaves. *Physiol. Plant* 156, 227–238. doi: 10.1111/ppl.12388

Shaku, K., Shimakawa, G., Hashiguchi, M., and Miyake, C. (2016). Reduction-induced suppression of electron flow (RISE) in the photosynthetic electron transport system of *Synechococcus elongatus* PCC 7942. *Plant Cell Physiol.* 57, 1443–1453. doi: 10.1093/pcp/pcv198

Shimakawa, G., Shaku, K., and Miyake, C. (2018). Reduction-induced suppression of electron flow (RISE) is relieved by non-ATP-consuming electron flow in *Synechococcus elongatus* PCC 7942. *Front. Microbiol.* 9:886:886. doi: 10.3389/fmicb.2018.00886

Sonoike, K. (2011). Photoinhibition of photosystem I. *Physiol. Plant* 142, 56–64. doi: 10.1111/j.1399-3054.2010.01437.x

Sudo, E., Suzuki, Y., and Makino, A. (2014). Whole-plant growth and N utilization in transgenic rice plants with increased or decreased Rubisco content under different CO_2 partial pressures. *Plant Cell Physiol.* 55, 1905–1911. doi: 10.1093/pcp/pcu119

Suganami, M., Suzuki, Y., Sato, T., and Makino, A. (2018). Relationship between Rubisco activase and Rubisco contents in transgenic rice plants with overproduced or decreased Rubisco content. *Soil Sci. Plant Nutr.* 64, 352–359. doi: 10.1080/00380768.2018.1433455

Suzuki, Y., Ohkubo, M., Hatakeyama, H., Ohashi, K., Yoshizawa, R., Kojima, S., et al. (2007). Increased Rubisco content in transgenic rice transformed with the 'sense' rbcS gene. *Plant Cell Physiol.* 48, 626–637. doi: 10.1093/pcp/pcm035

Suzuki, Y., Miyamoto, T., Yoshizawa, R., Mae, T., and Makino, A. (2009). Rubisco content and photosynthesis of leaves at different positions in transgenic rice with an overexpression of *RBCS*. *Plant Cell Environ.* 32, 417–427. doi: 10.1111/j.1365-3040.2009.01937.x

Takagi, D., Ishizaki, K., Hanawa, H., Mabuchi, T., Shimakawa, G., Yamamoto, H., et al. (2017a). Diversity of strategies for escaping reactive oxygen species production within photosystem I among land plants. *Physiol. Plant* 161, 56–74. doi: 10.1111/ppl.12562

Takagi, D., Amako, K., Hashiguchi, M., Fukaki, H., Ishizaki, K., Goh, T., et al. (2017b). Chloroplastic ATP synthase builds up a proton motive force preventing production of reactive oxygen species in photosystem I. *Plant J.* 91, 306–324. doi: 10.1111/tpj.13566

Takagi, D., Ihara, H., Takumi, S., and Miyake, C. (2019). Growth light environment changes the sensitivity of photosystem I photoinhibition depending on common wheat cultivars. *Front. Plant Sci.* 10:686:686. doi: 10.3389/fpls.2019.00686

Tikhonov, A. N. (2013). pH-Dependent regulation of electron transport and ATP synthesis in chloroplasts. *Photosynth. Res.* 116, 511–534. doi: 10.1007/s11120-013-9845-y

Valentini, R., Epron, D., De Angelis, P., Matteucci, G., and Dreyer, E. (1995). In situ estimation of net CO_2 assimilation, photosynthetic electron flow and photorespiration in Turkey oak (*Q. cerris* L.) leaves: diurnal cycles under different levels of water supply. *Plant Cell Environ.* 18, 631–640. doi: 10.1111/j.1365-3040.1995.tb00564.x

von Caemmerer, S. (2000). *Biochemical Models of Photosynthesis* (Melbourne: CSIRO Publishing).

Wada, S., Suzuki, Y., Takagi, D., Miyake, C., and Makino, A. (2018). Effects of genetic manipulation of the activity of photorespiration on the redox state of photosystem I and its robustness against excess light stress under CO_2-limited conditions in rice. *Photosynth. Res.* 137, 431–441. doi: 10.1007/s11120-018-0515-y

Wada, S., Takagi, D., Miyake, C., Makino, A., and Suzuki, Y. (2019). Responses of the photosynthetic electron transport reactions stimulate the oxidation of the reaction center chlorophyll of photosystem I, P700, under drought and high temperatures in rice. *Int. J. Mol. Sci.* 20, 2068. doi: 10.3390/ijms20092068

Wingler, A., Quick, W. P., Bungard, R. A., Bailey, K. J., Lea, P. J., and Leegood, R. C. (1999). The role of photorespiration during drought stress: an analysis utilizing barley mutants with reduced activities of photorespiratory enzymes. *Plant Cell Environ.* 22, 361–373. doi: 10.1046/j.1365-3040.1999.00410.x

Xu, Z., Zhou, G., and Shimizu, H. (2010). Plant responses to drought and rewatering. *Plant Signal. Behav.* 5, 649–654. doi: 10.4161/psb.5.6.11398

Zhou, Y., Lam, H. M., and Zhang, J. (2007). Inhibition of photosynthesis and energy dissipation induced by water and high light stresses in rice. *J. Exp. Bot.* 58, 1207–1217. doi: 10.1093/jxb/erl291

Zivcak, M., Brestic, M., Balatova, Z., Drevenakova, P., Olsovska, K., Kalaji, H. M., et al. (2013). Photosynthetic electron transport and specific photoprotective

responses in wheat leaves under drought stress. *Photosynth. Res.* 117, 529–546. doi: 10.1007/s11120-013-9885-3

Zivcak, M., Kalaji, H. M., Shao, H. B., Olsovska, K., and Brestic, M. (2014). Photosynthetic proton and electron transport in wheat leaves under prolonged moderate drought stress. *J. Photochem. Photobiol. B.* 137, 107–115. doi: 10.1016/j.jphotobiol.2014.01.007

Zivcak, M., Brestic, M., Kunderlikova, K., Sytar, O., and Allakhverdiev, S. I. (2015). Repetitive light pulse-induced photoinhibition of photosystem I severely affects CO_2 assimilation and photoprotection in wheat leaves. *Photosynth. Res.* 126, 449–463. doi: 10.1007/s11120-015-0121-1

Conflict of Interest: The authors declare that this research was conducted in the absence of any commercial or financial relationships that could be construed as a potential conflict of interest.

Advantages of publishing in Frontiers

OPEN ACCESS
Articles are free to read for greatest visibility and readership

FAST PUBLICATION
Around 90 days from submission to decision

HIGH QUALITY PEER-REVIEW
Rigorous, collaborative, and constructive peer-review

TRANSPARENT PEER-REVIEW
Editors and reviewers acknowledged by name on published articles

Frontiers
Avenue du Tribunal-Fédéral 34
1005 Lausanne | Switzerland

Visit us: www.frontiersin.org
Contact us: info@frontiersin.org | +41 21 510 17 00

REPRODUCIBILITY OF RESEARCH
Support open data and methods to enhance research reproducibility

DIGITAL PUBLISHING
Articles designed for optimal readership across devices

FOLLOW US
@frontiersin

IMPACT METRICS
Advanced article metrics track visibility across digital media

EXTENSIVE PROMOTION
Marketing and promotion of impactful research

LOOP RESEARCH NETWORK
Our network increases your article's readership